Pure

Bangor University

DOCTOR OF PHILOSOPHY

Functional analysis of the cancer-associated proteins Translin and Trax reveal a novel function in genome stability control

Alahmadi, Hanadi Ahmed S

Award date:
2020

Awarding institution:
Bangor University

Link to publication

General rights
Copyright and moral rights for the publications made accessible in the public portal are retained by the authors and/or other copyright owners and it is a condition of accessing publications that users recognise and abide by the legal requirements associated with these rights.

- Users may download and print one copy of any publication from the public portal for the purpose of private study or research.
- You may not further distribute the material or use it for any profit-making activity or commercial gain
- You may freely distribute the URL identifying the publication in the public portal ?

Take down policy
If you believe that this document breaches copyright please contact us providing details, and we will remove access to the work immediately and investigate your claim.

Download date: 16. May. 2022

Functional analysis of the cancer-associated proteins Translin and Trax reveal a novel function in genome stability control

A thesis is submitted for the degree of Doctor of Philosophy
at Bangor University By

Hanadi Ahmed Saud Alahmadi

North West Cancer Research Fund Institute School of Biological Science
University of Bangor
United Kingdom

January 2020

Declaration and Consent

Details of the Work

I hereby agree to deposit the following item in the digital repository maintained by Bangor University and/or in any other repository authorized for use by Bangor University.

Author
Nam…….…….
Title: …….…….…….……
Supervisor/Department: .....
Funding body (if any): .....
Qualification/Degree obtained: …….…….…….…….

This item is a product of my own research endeavours and is covered by the agreement below in which the item is referred to as "the Work". It is identical in content to that deposited in the Library, subject to point 4 below.

Non-exclusive Rights

Rights granted to the digital repository through this agreement are entirely non-exclusive. I am free to publish the Work in its present version or future versions elsewhere.
I agree that Bangor University may electronically store, copy or translate the Work to any approved medium or format for the purpose of future preservation and accessibility. Bangor University is not under any obligation to reproduce or display the Work in the same formats or resolutions in which it was originally deposited.

Bangor University Digital Repository

I understand that work deposited in the digital repository will be accessible to a wide variety of people and institutions, including automated agents and search engines via the World Wide Web.
I understand that once the Work is deposited, the item and its metadata may be incorporated into public access catalogues or services, national databases of electronic theses and dissertations such as the British Library's EThOS or any service provided by the National Library of Wales.

Statement 1:

This work has not previously been accepted in substance for any degree and is not being concurrently submitted in candidature for any degree unless as agreed by the University for approved dual awards.

Signed ……. (candidate)
Date …….

Statement 2:

This thesis is the result of my own investigations, except where otherwise stated. Where correction services have been used, the extent and nature of the correction is clearly marked in a footnote(s).
All other sources are acknowledged by footnotes and/or a bibliography.

Signed ……. (candidate)
Date …….

Statement 3:

I hereby give consent for my thesis, if accepted, to be available for photocopying, for inter-library loan and for electronic repositories, and for the title and summary to be made available to outside organisations.

Signed ……. (candidate)
Date …….
NB: Candidates on whose behalf a bar on access has been approved by the Academic Registry should use the following version of **Statement 3:**

Statement 3 (bar):

I hereby give consent for my thesis, if accepted, to be available for photocopying, for inter-library loans and for electronic repositories after expiry of a bar on access.

Signed …… (candidate)
Date ……

Statement 4:

Choose **one** of the following options

a) I agree to deposit an electronic copy of my thesis (the Work) in the Bangor University (BU) Institutional Digital Repository, the British Library ETHOS system, and/or in any other repository authorized for use by Bangor University and where necessary have gained the required permissions for the use of third party material.	
b) I agree to deposit an electronic copy of my thesis (the Work) in the Bangor University (BU) Institutional Digital Repository, the British Library ETHOS system, and/or in any other repository authorized for use by Bangor University when the approved **bar on access** has been lifted.	
c) I agree to submit my thesis (the Work) electronically via Bangor University's e-submission system, however I **opt-out** of the electronic deposit to the Bangor University (BU) Institutional Digital Repository, the British Library ETHOS system, and/or in any other repository authorized for use by Bangor University, due to lack of permissions for use of third party material.	

Options B should only be used if a bar on access has been approved by the University.

In addition to the above I also agree to the following:

1. That I am the author or have the authority of the author(s) to make this agreement and do hereby give Bangor University the right to make available the Work in the way described above.

2. That the electronic copy of the Work deposited in the digital repository and covered by this agreement, is identical in content to the paper copy of the Work deposited in the Bangor University Library, subject to point 4 below.

3. That I have exercised reasonable care to ensure that the Work is original and, to the best of my knowledge, does not breach any laws – including those relating to defamation, libel and copyright.

4. That I have, in instances where the intellectual property of other authors or copyright holders is included in the Work, and where appropriate, gained explicit permission for the inclusion of that material in the Work, and in the electronic form of the Work as accessed through the open access digital repository, *or* that I have identified and removed that material for which adequate and appropriate permission has not been obtained and which will be inaccessible via the digital repository.

5. That Bangor University does not hold any obligation to take legal action on behalf of the Depositor, or other rights holders, in the event of a breach of intellectual property rights, or any other right, in the material deposited.

6. That I will indemnify and keep indemnified Bangor University and the National Library of Wales from and against any loss, liability, claim or damage, including without limitation any related legal fees and court costs (on a full indemnity bases), related to any breach by myself of any term of this agreement.

Signature: …… Date: ……

Abstract

Translin and its partner Trax (Translin-associated factor X) are highly conserved proteins and they have been shown to have a functional relationship in a range of biological processes including tRNA processing, degradation of microRNAs during oncogenesis, mRNA regulation in spermatogenesis, neuronal function and telomere transcript regulation. Translin was first identified in humans as a protein that binds to chromosomal translocation breakpoint junctions in lymphoid malignancies, although it remains unknown if there is a direct requirement for one, or both of these proteins in the DNA damage response and/or chromosomal translocation formation. This led us to ask whether Translin and/or Trax have any role in genome stability regulation. In the current study, the biological function(s) of Translin and Trax were investigated further using the facile fission yeast (*Schizosaccharomyces pombe*) model system (Tsn1 = Translin; Tfx1 = Trax). Previously, analysis of null mutants of *tsn1* and *tfx1* did not reveal a genome instability or DNA damage recovery phenotype. Recently, a hetero dimeric complex that influences the removal of passenger strands in the RNA interference (RNAi) pathway, termed C3PO, has been found to consist of Translin and Trax. In addition, the Dcr1 RNAi regulator was shown to have RNAi-independent functions in controlling genome stability via regulating RNA:DNA hybrid levels within the genome of *S. pombe*. Give these findings, we generated mutants defective in both Dcr1 and Tsn1 and/or Tfx1 to determine whether Tsn1 and/or Tfx1 played a redundant role in genome stability control in the absence of Dcr1. We reveal that in the absence of Dcr1, Tsn1, but not Tfx1, is required for recovery from some types of DNA damage, but not all. By analysing this response in cells without canonical telomeres, we extend this to demonstrate that this is not associated with the alterations in telomeric TERRA transcripts which have elevated levels in *tsn1Δ* cells. Furthermore, by employing an inter-molecular genetic recombination assay we demonstrate that Tsn1, but not Tfx1, is required for replication-associated recombination in a polar fashion suggestive of an association with recombination stimulated by replicative pauses caused by RNA polymerase II, not RNA polymerase III, transcription at a tRNA gene. These data led us to reveal that Tsn1 functions in an RNAse H pathway, but we could find no evidence for a direct role in

DNA double-strand break repair. Collectively, our data reveal a function for Tsn1, but not Tfx1, for prevention of genome instability associated with the replicative stresses caused by genomic RNA:DNA hybrids.

Acknowledgements

First of all, I would like to express my sincere appreciation and gratitude to my supervisor, Dr. Ramsay McFarlane, for his advice, guidance, encouragement and support from our first meeting to the final review allowed me to understand and develop the project and during the writing of this thesis. Also, I thank Dr. Natalia Escobar, for her advice throughout the laboratory work. Special thanks to, my mother Nawal and my aunt Amnah for provided the foundation of my learning character from the time I was a child, they deserve special mention for their unswerving support, prayers, gentle love and caring. Special thanks to my father, my aunties and my two sisters, Hatoon and Hala for their love and continued support. Also, I thank my close friend Alaa Afifi for her love and support. I thank all members of the D7 Lab for being helpful and for the time we spent working together. Thank you all.

List of Abbreviations

ALT: alternative lengthening of telomeres

ATM: Ataxia telangiectasia mutated

BDNF: Brain-derived neurotrophic factor

BIR: break-induced replication

bp: base pair

CDGS: Chromatin-dependent gene silencing

CDKs: cyclin-dependent kinases

CPT: Camptothecin

C3PO: component 3 promoter of RISC

DDR: DNA damage responses

dH2O: Distilled water

dHJ: double Holliday junction

D-loop: Displacement loop

DMSO: Dimethyl sulphoxide

DNA: Deoxyribonucleic acid

DNA-PK: DNA-dependent protein kinase

dNTP: deoxyribonucleotide triphosphate

DRIP: DNA:RNA immunoprecipitation

dsDNA: double-stranded DNA

dsRNA: double-stranded RNA

DSBs: double strand breaks

DSBR: double strand break repair

g: Gram

GADD: growth arrest and DNA damage

EDTA: ethylenediamine tetraacetic acid

HP1: heterochromatin protein 1

HJ: Holliday junction

HR: homologous recombination

HU: hydroxyurea

IR: ionizing radiation

kb: kilobase

kDa: kilo Dalton

L: Litre

LB: Luria-Bertani media

LiAC: lithium acetate

MCM: mini-chromosome maintenance

MEFs: mice embryotic fibroblasts

MMC: mitomycin C

MMS: methyl methane sulfonate

MRN: MRE11-RAD50-NBS1 complex

mg: Milligram

miRNA: micro-RNAs

µg: Microgram

µl: Microliter

ml: Milliliter

mM: Millimolar

mRNA: messenger RNA

ml: Milliliter

mM: Millimolar

mRNA: messenger RNA

NB: nitrogen base

NBL: nitrogen base liquid

NE: nuclear envelope

NHEJ: non-homologous end joining

ng: Nanogram

ORF: open reading frame

PCR: polymerase chain reaction

PEG: polyethylene glycol

RC: replicative complex

rDNA: ribosomal DNA

PTGS: post-transcriptional gene silencing

piRNA: PIWI-interacting RNAs

RFB: replication fork barriers

RFC: replication factor C clamp loader

rDNA: ribosomal DNA

RISC: RNA-induced silencing complex

RLC: RISC loading complex

RNAi: RNA interference

RT-PCR: Reverse transcriptase PCR

q-RT-PCR: Quantitative real-time PCR

RNA Pol: RNA polymerase

RPA: replication protein A

SDS: Sodium Dodecyl Sulfate

SDSA: synthesis-dependent strand annealing

siRNA: small interference RNA

ssDNA: single-stranded DNA

TB-RBP: testis–brain RNA-binding protein

TERRA: telomeric repeat-containing RNA

TRAX: Translin-associated factor X

tRNA: transfer RNA

TBZ: thiabendazole

UTR: untranslated region

UV: ultra-violet

YE: yeast extract

YEA: yeast extract agar

YEL: yeast extract liquid

3': Three prime end of DNA

5': Five prime end of DNA

Table of Contents

List of Figures

Chapter 1

Chapter 3

Chapter 4

Chapter 5

Chapter 6

Chapter 7

Appendecies

List of Tables

Chapter 2

Chapter 1: Introduction

1. Introduction

1.1 Genomic instability

Cancer has become the major cause of death globally with millions dying from the disease annually (Lai et al., 2012; Shanmuganathan et al., 2019). Cancer constitutes a complex array of diseases, which are defined by alteration in genome structure and sequence (Mitelman et al., 2019). Most cancers are characterised by genomic instability which can emanate from DNA repair gene mutations, thus influencing growth of cancer (Negrini et al., 2010; Choi & Lee, 2013; Tubbs & Nussenzweig, 2017). The instability of genomes constitutes deletions in chromosomes, rearrangement of chromosomes, mutations and complete chromosome loss or gain, which ultimately results in cancer development (Aguilera & Gomez-Gonzalez, 2008; León-Ortiz et al., 2018). In view of this, genome stability maintenance is essential for proper cell functioning (Yao & Dai, 2014; Felipe-Abrio et al., 2015; Aguilera & Gomez-Gonzalez, 2019). In addition to genomic DNA genes, epigenetic alterations, constitute a characteristics of many tumour cells, and play a major role in cancer in the growth and initiation of cancer (Negrini et al., 2010; Weberpals et al., 2011; Aronica et al., 2015). Instability of chromosomes can be triggered by deficient in certain essential processes, including repair of damaged DNA, telomere maintenance errors, chromosome segregation and DNA replication errors (Felipe-Abrio et al., 2015; Fragkos & Naim, 2017). Endogenous and exogenous stresses frequently put the human genomes at risk (Reinhardt & Schumacher, 2012; Tubbs & Nussenzweig 2017). Besides intracellular events aggravating the levels of DNA damage, change is attributed to exogenous source changes, for instance, ultraviolet (UV) light, X-rays (ionising radiation), and chemical carcinogens (Tubbs & Nussenzweig 2017; So et al., 2017). These genotoxic stresses necessitate efficient cell reactions to retain the stability of genomes as they could trigger several issues or DNA lesions that include double or single-strand breaks in DNA. To avert damage to eukaryotic genomes, most processes that occur during proliferation of cells should be coordinated and controlled tightly. For correction of DNA lesions, eukaryotic cells employ a set of DNA damage responses (DDRs), including DNA repair and checkpoint activation. In view of this, the absence of such defense mechanisms might lead to genetic instability that enhances cancer growth (Figure 1.1) (Choi & Lee, 2013; So et al., 2017; Ghosh et al., 2018).

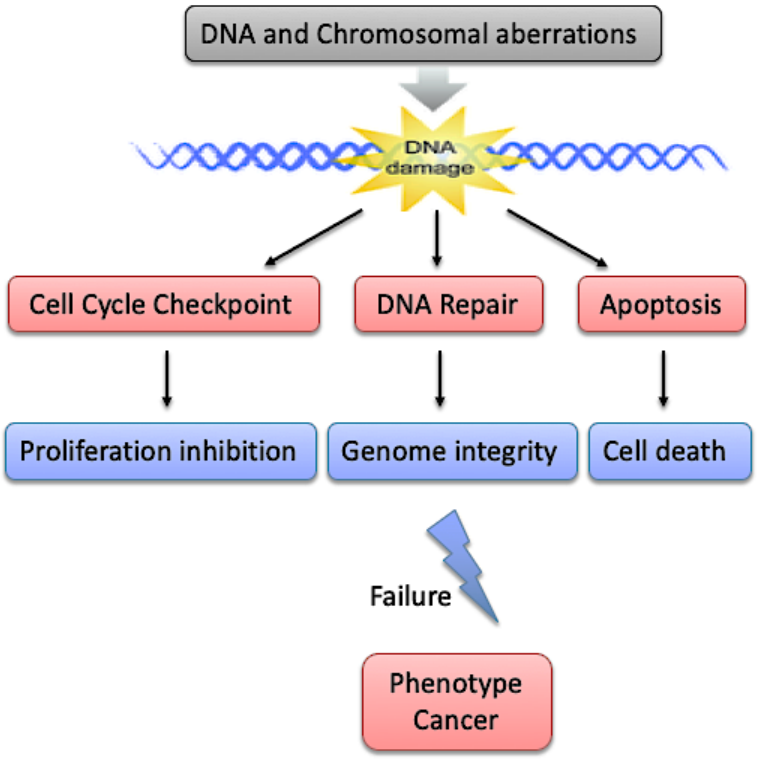

Figure 1.1 Route for genome instability to drive cancer
Inability or Failure of DNA damage response that undertake surveillance as well as checkpoints for guarding genomes trigger genome instability, which commonly characterises human cancers. In view of this, it has been suggested that the instability of genomes aggravates and influences tumour growth and initiation. Deficiencies in DNA damage response encourage tumorigenesis and cause genomic instability (adapted from Choi & Lee, 2013).

1.2 Chromosomal translocation

The presence of genetic changes in DNA repair genes, tumor suppressor genes, and proto-oncogenes could lead to cancer. Chromosomal translocations, inversions, and deletions exemplify such changes (Figure 1.2). Solid tumours, leukaemia, and lymphoma can be caused by chromosomal translocations (Nambiar & Raghavan, 2011; Harewood & Fraser, 2014). Chromosome translocations constitute well-established signs of cancer cells and usually occur non-randomly within the genomes (Burman et al., 2015; Nambiar & Raghavan, 2011). In some instances, new genes develop, generating fusion proteins, gene activation and gene separation are caused by chromosomal translocations (Willman & Hromas, 2006; Wilch et al., 2018). Chromosome translocation refers to an abnormality within chromosomes wherein chromosomes break and are attached, partially or fully to other chromosomes (Figure 1.2) (Tucker, 2010; Roukos & Misteli, 2014). Accurate linking of broken and ends could regenerate normal chromosomes. When attachment features two broken ends of one chromosome, inversions, duplications, and deletions could occur. Translocations might occur when broken ends for two non-homologous chromosomes combine. Non-homologous joining of ends is usually inaccurate; thus, some nucleotides might disappear in the process of joining (O'Connor, 2008). Non-reciprocal and reciprocal translocations are the two major translocation classes. Non-reciprocal translocations constitute one-way translocations wherein chromosomal segments are transferred to non-homologous chromosomes (O'Connor, 2008; Zhang et al., 2010; McKenna et al., 2019). In contrast, reciprocal translocations feature segment exchange from two non-homologous chromosomes. In this event there is no genetic materials lost in the exchange, and translocations are deemed balanced. In the event they are not balanced, wherein an exchange of an unequal chromosome sequence quantity occurs between the participating chromosomes, leading to genetic material loss or gain (O'Connor, 2008; Chang et al., 2013; Harewood & Fraser, 2014). A disturbance to normal chromosome replication could trigger chromosome translocation (Mirikin & Mirikin, 2007). In mice, yeast, and humans, an interruption to the process of DNA repair can cause chromosome translocation (Rabbitts & Stocks, 2003). The translocations necessitate double-strand breaks (DSBs) within DNA. The frequent nature of such DSBs is enhanced through ionizing radiation that is utilized experimentally for generating

translocations. In view of this, DSBs activate the repair machinery, which catalyses the linkage of broken ends of chromosome (Lieber et al., 2003; O'Connor, 2008). The translocation involving chromosome t(9;22) (q34;q11) that is considered the first consistent chromosomal translocation, leads to Philadelphia chromosomes. The symbols t(9;22) (q34;q11) show translocations between chromosome 9 and 22 that trigger chronic myeloid leukemia (CML) through creation of a *BCR-ABL* fusion gene (Calasanz & Cigudosa, 2008; Nambiar & Raghavan, 2011; Stefanachi, 2012; Yeung and Hughes, 2012; Zheng, 2013; Tabarestani & Movafagh, 2016).

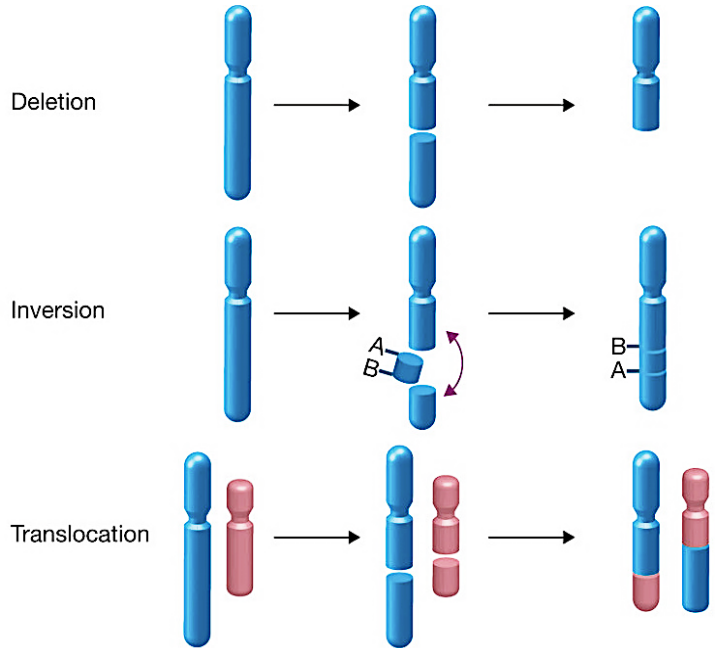

Figure 1.2 Models of the rearrangement and consequences of chromosome in the genome

Numerous forms of chromosomal rearrangement, namely translocation, inversion, and deletion. Deletion is considered chromosome breakage that results in DNA segment removal. Inversion exists when a chromosome segment is detached from it, inverted at a similar location without DNA loss. The occurrence chromosomal translocation is caused by swapping of two DNA segments from non- homologous chromosomes (adapted from Roukos & Misteli, 2014).

1.3 DNA replication

For cells to divide, all living organisms must duplicate their genetic information while shielding it from unnecessary mutations that, in humans, could result in cancer development and genetic disorders. In view of this, genomic instability is mainly caused by inaccurate DNA replication (Gadaleta & Noguchi, 2017; Cortez, 2019). In eukaryotes replication of chromosomes should be controlled to only occur once for each cell division cycle, for delivery of similar quantity of genetic information from parental cells to two daughter cells. Replication errors lead to chromosomal aberrations and mutations, which potentially trigger tumorigenesis (Preston et al., 2010; Abbas et al., 2013; Kang et al., 2018). The division cycle of eukaryotic cells features functionally unique stages: G1, S, G2, and M (Errico & Costanzo 2010; Koren et al. 2010; Kang et al., 2018). Genome replication in eukaryotes commences at different chromosome origins (Kang et al., 2018). The activation and formation of different complexes at origins are needed for DNA replication (Méchali, 2010). Initiators bind to duplicators and load replication helicases onto chromatin. Within the early G1 phase, the origins are recognised and bound by a complex called origin recognition complex (ORC). In the late G1 phase, ORC complex become a stage for proteins called pre-replicative complex (pre-RC) and another group of proteins to be loaded. DNA synthesis commences where loaded helicases are active within the S phase (Bell et al., 2002; Deegan et al., 2016; Kang et al., 2017). The pre-RC has the preserved core replicative helicases the mini-chromosome maintenance (MCM) protein complex. Besides its role in unwinding double-stranded DNA at origins, MCM prevents DNA from undergoing multiple rounds of replication in each cell cycle, and at least two MCM complexes are needed for loading at the origin of replication to create bi-directional replication forks (Figure 1.3) (Labib, 2010; Gros et al., 2015; Burgers & Kunkel, 2017; Trakselis et al., 2017). To prevent genome re-duplication, activation and loading of helicases are separated in time. Helicase loading occurs within G1 stage when Cyclin Dependent Kinase (CDK) activity is at its lowest point. High CDK activity is required in helicase activation (Figure 1.3) (Chang & Stirling, 2017; Kang et al., 2017).

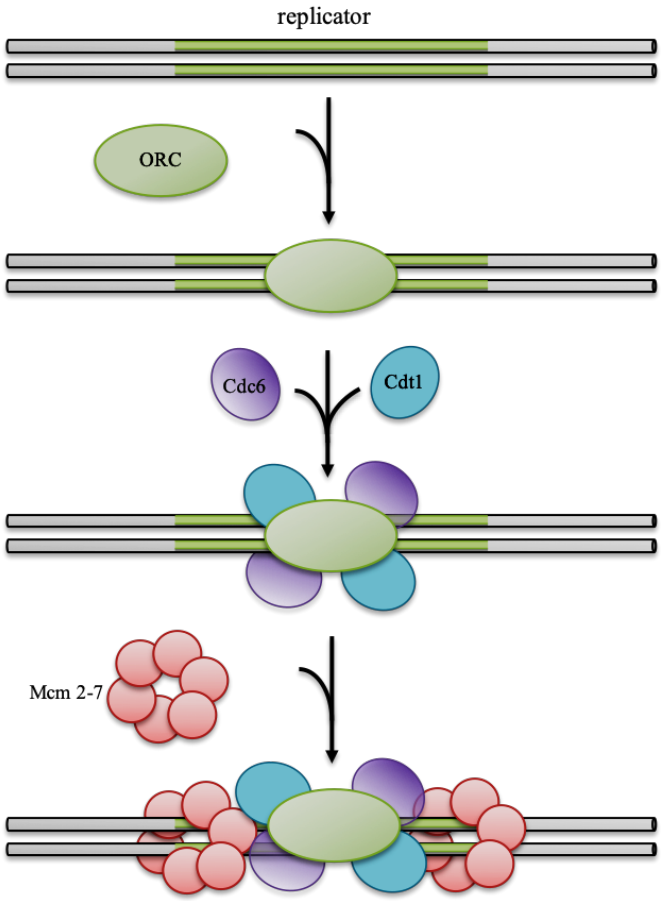

Figure 1.3 Assembly of pre-RC
The initiated of the pre-RC is when ORC binds to the origin of replication (replicator). ORC recruits the helicase loading proteins Cdc6 and Cdt1 followed by MCM helicase complex (adapted from Watson, 2004).

1.4 Replication fork (RF) progression

The RF refers to a multi-protein complex containing DNA helicase and synthesis activities. Unwinding of DNA by helicase activities occurs at forks to form single-stranded DNA (ssDNA) (Langston et al. 2009; Li & O'Donnell, 2019). During the process, the DNA helicase enzyme utilises the energy from ATP hydrolysis to break inter-strand hydrogen bounds, forming a Y-shape (see Figure 1.4). The unpaired ssDNA stability is retained by a heterotrimeric complex, replication protein A (RPA) (Stillman, 2008). Two replication forks are created at the origin of replication, and these are extended in opposite directions as replication continues. During elongation, an enzyme known as DNA polymerases add DNA nucleotides to a 3′ template end. Since DNA polymerases solely add new nucleotides to backbone ends, an RNA primes molecule offers the starting point. This RNA short piece acts as stating point of polymerase ε (epsilon) in the daughter strand synthesis (Figure 1.5). Afterwards, primers are removed, and ribonucleotides are substituted using deoxyribonucleotides. The two ssDNA strands are considered the lagging and leading strands (Figure 1.4). The leading strand is oriented in the same direction as the replication fork from, while the lagging strand is oriented away from the replication fork. As DNA replication proceeds in the 5' to 3' direction, the leading strand is able to replicated continuously, by the primase enzyme firstly creating a short RNA primer at 5' end of the nascent DNA strand which acts as the initial point of extension by DNA polymerase ε (epsilon) synthesis. The lagging strand is replicated discontinuously by creation of multiple short RNA primers at approximately 200 nucleotide intervals, creating segments termed Okazaki fragments. Hence, each Okazaki fragment needs an RNA primer to commence the synthesis and will retain this RNA primer unless removed. In the replication process, RNase H enzymes removes the RNA primer that are then substituted using DNA nucleotides, and the DNA ligase enzyme seals all the spaces between fragments (Stillman, 2008; Sabatinos, 2010 ; Leman & Noguchi, 2013; Lujan et al., 2016; Berti & Vindigni, 2016; Burgers & Kunkel, 2017 ; Li & O'Donnell, 2019; Cortez, 2019). Besides helicases, replicative DNA polymerases, and primase, the RF needs accessory proteins for progression and efficient initiation. The cooperative complexes of protein that feature within DNA replication are called replisomes. Replisome factors [that include the replication factor C clamp loader (RFC)

and fork protection complex (FPC)] are tasked with the role of controlling polymerase functions as well as coordinating the synthesis of DNA with template strand unwinding. Additionally, the replisomes associate with the checkpoint proteins as a genome integrity surveillance mechanism (Leman & Noguchi, 2013). DNA replication fork stability is important for maintaining genome integrity as collapse of forks could result in the formation of DSBs, which are toxic to cells. (Lin & Pasero, 2012; Kang et al., 2018; Pasero & Tourrière, 2019). Arrested forks could be considered recombinogenic. If they are exposed to induction of unprecedented homologous recombination, oncogenic chromosomal rearrangements might be result (Pryce et al., 2009; So et al., 2017; Son & Hasty, 2019).

DNA lesions, which originate from different exogenous and endogenous sources, affect DNA replication forks (Jones & Petermann, 2012; Berti & Vindigni, 2016). The collapse or inhibition of DNA replication forks could lead to genomic integrity alterations and cell viability loss. Lesions can accur to DNA damaging agents, for instance, active species of oxygen, alkylating chemicals, X-rays, and UV light, which inhibit elongation of DNA chains that replicative DNA polymerases catalyse, thus affecting RF progression (Cox, 2001; Lusetti & Cox 2002; Higuchi et al., 2003; Pryce et al., 2009; Gadaleta & Noguchi, 2017). High replicative inhibition levels can induce apoptosis. The response of cellular DNA damage to replication–inhibiting DNA lesions could trigger genetic changes. For instance, numerous post–replication repair pathways, including trans-lesion DNA synthesis and re-combinational repair can cause point mutations and chromosomal re-arrangements (Lusetti & Cox 2002; Higuchi et al., 2003; Aguilera & Garcia-Muse, 2013; Fragkos & Naim, 2017). Some chemicals can cause RF staling and DNA damage duplication (Calzada et al., 2005; Sabatinos, 2010). In view of this, such drug effects on RF arrest is used within model organisms to assess the impact on cell viability and DNA mutagenesis, as polymerase stalling triggers the arrest of RF complexes (Sabatinos, 2010).

Particularly, helicase-initiated unwinding activities, which precede the RF, are functionally connected to polymerisation activities. To address RF stalling, the cell might overcome or adapt to hydroxyurea (HU) inhibition that prevents synthesis of DNA by

blocking deoxyribonucleotide triphosphate (dNTP) synthesis but allows the replicative helicase to initiate the process by unwinding parental DNA duplex. The response might lead to collapse of replication forks and eventually DSB formation (Lopes et al. 2001; Mulder et al. 2005; Kurose et al. 2006; Sabatinos, 2010; Aguilera & García-Muse, 2013).

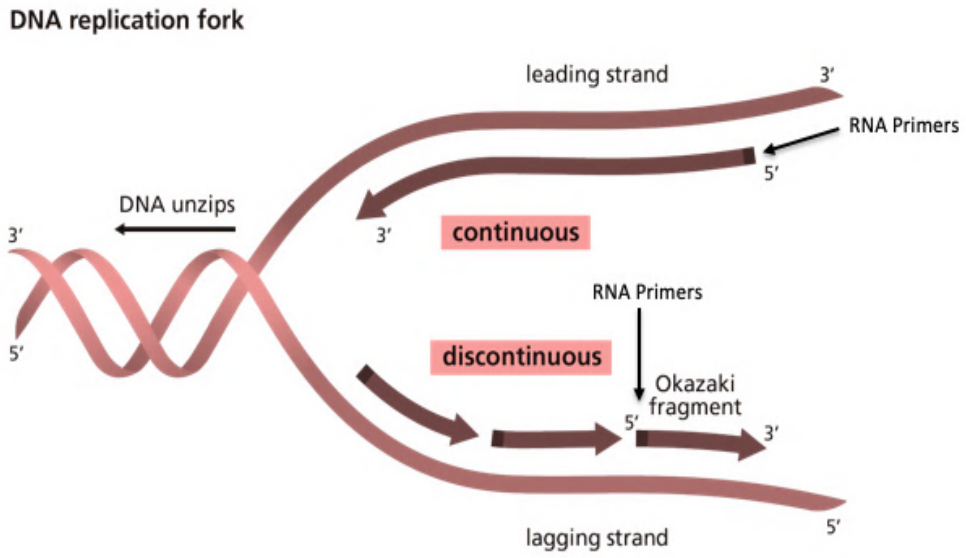

Figure 1.4 Basic diagram of the DNA replication fork
The direction of DNA replication proceeds from 5' to 3', leading to continuous duplication of leading strands alongside discontinuous replication within short lagging strand sections. The initiation of each Okazaki lagging strands, and leading strand synthesis necessitate the existence of short RNA primers (adapted from Genome Research Limited and Leman & Noguchi, 2013).

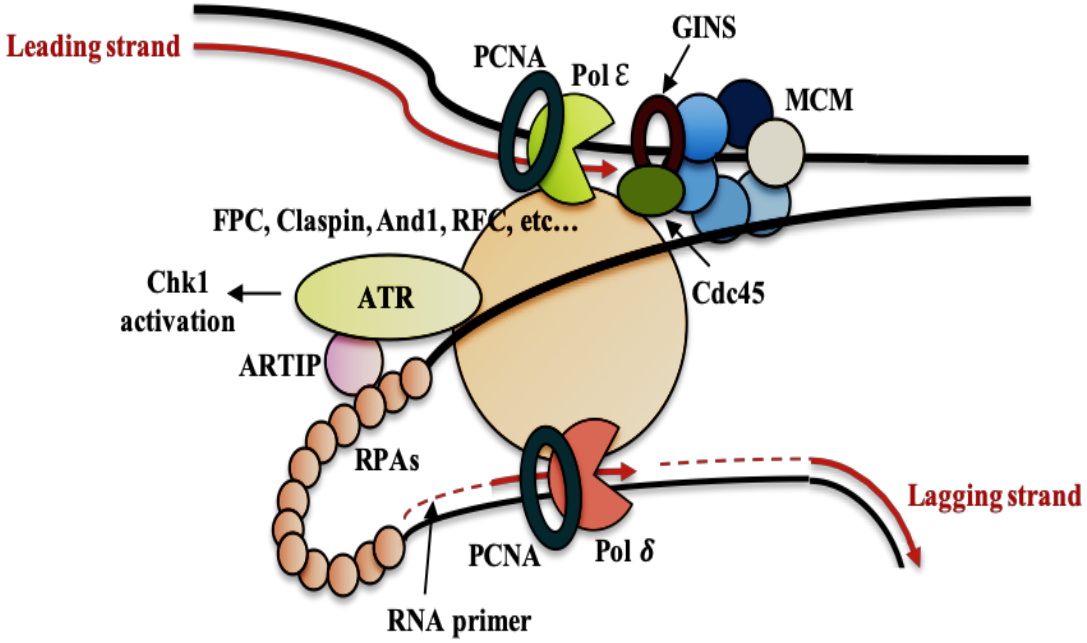

Figure 1.5 A schematic of a DNA replication complex
Pol δ and Pol ε performed replication on lagging and leading strands respectively. Coordinating DNA synthesis through template strand unwinding by Cdc45-MCM (mini-chromosome maintenance)-GINS (go-ichi-ni-san) and regulation of polymerase functions constitute the function of most replisome factors that include RFC (the replication factor C clamp loader), And1, Claspin, and the FPC (fork protection complex). Additionally, there is a correlation between replisomes and checkpoint proteins in form of genome integrity and DNA replication surveillance mechanisms (adapted from Leman & Noguchi, 2013).

1.5 DNA double-strand breaks (DSB) repair pathways

Eukaryotic cells have the ability to repair different kinds of DNA damage. Among the forms of damage, DSBs are especially detrimental because they can lead to chromosomal rearrangement such as translocations, deletions, or insertions, which are the main transforming genetic changes in many human cancers (Pannunzio et al., 2018). DSBs can emanate from exogenous (for example, reactive species of oxygen or ionizing radiation) or endogenous (for example, incidental actions by nuclear enzymes or DNA replication errors) sources (Mladenov & Iliakis, 2011; Davis & Chen, 2013; Ohle et al., 2016; Lieber, 2016; Chang et al., 2017; Pannunzio et al., 2018). In view of this, to maintain the integrity of genomes, it is imperative for cells to precisely and rapidly undertake repairs of DSBs to avoid oncogenic genomic rearrangements and mutations (Tian et al., 2015; Uckelmann & Sixma, 2017; Gomes et al., 2017). Eukaryotic cells have efficient specialised DNA repair pathways, which are largely conserved from human to yeast. These include non-homologous DNA end joining (NHEJ) and homologous recombination (HR) (Brugmans et al., 2007; Lieber, 2010; Moraes et al., 2012; Davis & Chen, 2013; Ohle et al., 2016; Zaboikin et al., 2017; Zhao et al., 2017). DSB repair mechanisms can largely be separated between those, which utilise extensive homology from sister chromatid or homologous sequence in other regions within the genome and those which utilise minimal or no homology. The two mechanisms necessitate nuclease end-processing, use of DNA polymerase and DNA strand ligation for completing broken DNA repair (Zaboikin et al., 2017; Zhao et al., 2017; Pannunzio et al., 2018).

1.5.1 The non-homologous DNA end joining repair pathway

Unlike homology direct repair, which requires a homologous template to direct repair, NHEJ is considered non-homologous as the broken ends undergo direct ligation (Mladenov & Iliakis, 2011). It is considered an error-prone repair system, as it might be linked to chromosomal rearrangement and small–scale mutations. Compared to HR, its activation is not restricted to a particular stage of the cell cycle, although the NHEJ is thought to be the main DSB repair mechanism in the G1 cell cycle stage, when there is no substantial homology from a sister chromatid (Peng & Lin, 2011; Lans et al., 2012; Davis & Chen, 2013; Ohle et al., 2016; Zaboikin et al., 2017; Chang et al., 2017). The NHEJ

pathway uses proteins, which flexibly ligate, polymerise, resect, and recognize DNA ends. Such flexibility allows NHEJ to operate on wide-ranging DNA-end configurations, with the emerging repaired DNA junctions usually containing mutations. Additionally, during the process, faults could potentially lead to alteration such as telomere fusion and translocations (Espejel et al., 2002; Chang et al., 2017; Pannunzio et al., 2018).There are many factors that feature within canonical NHEJ, for instance the Ku heterodimer (Ku70-Ku80), Artemis, X-ray repair cross-complementing protein 4 (XRCC4), DNA-dependent protein kinase catalytic subunit (DNA-PKcs), XRCC4-like factor (XLF) and DNA ligase IV (LigIV). The Ku70/Ku80 DSB-binding heterodimer forms ring-like structures especially around the broken DNA ends to avert their deterioration, where Ku70/ Ku80 DNA end binding arranges the actions of other repair factors through recruitment of the DNA phosphatidylinositol 3-kinase, DNA-PK (encoded for by the *PRKDC* gene) (Grabarz et al., 2012; Boboila et al., 2012; Jette and Lees-Miller, 2015; Li & Xu, 2016; Biehs et al., 2017; Chang et al., 2017). Therefore, the additional repair proteins undergo activation when DNA-PKcs phosphorylates ARTEMIS nuclease, then DNA ends are linked by LigIV activity alongside its cofactor XRCC4 for sealing the break. There is direct interaction between XRCC4/LigaseIV complexes with XLF (Figure 1.6) (Davis & Chen, 2013; Davis et al., 2014; Chang et al., 2017). In yeast, the NHEJ pathway is very similar to that of mammalian cells but with important differences. Whilst budding yeast has homologs of the two mammalian Ku subunits, it appears to lack a DNA-PKcs homolog. Also, there does not seem to be a clear homolog of Artemis (Jazayeri & Jackson 2002).

1.5.2 The homologous recombination repair pathway

Homologous recombination (HR) plays a significant role in accessing template genetic information, which exists as homologous chromosomes or sister chromatids when both DNA double helix strands are compromised on one duplex. Repair of impaired DNA replication forks, repair of DSBs, genomic integrity maintenance, and DNA replication support constitute essential HR biological roles. Additionally, it is involved in maintenance of telomere through repair of incomplete telomeres, for instance, cancer

cells dividing without telomerase. Moreover, HR is needed in meiosis for exchange and pairing of chromosomes, which allows reductional segregation and genetic diversity (McFarlane et al., 2011; Kasparek & Humphrey, 2011; Hustedt, & Durocher, 2017; Zhao et al., 2017; Wright et al., 2018). When chromosomes experience DSBs, the DNA damage response controls cellular pathways for genomic survival and stability that includes the pathway selection of DSB repair. Repair of DSBs could be undertaken using different HR pathways, which result in chromosome restoration, including break-induced replication (BIR), double-strand break repair (DSBR) and synthesis-dependent strand annealing (SDSA) (Sakofsky et al., 2012; Hustedt, & Durocher, 2017; Wright et al., 2018). Initiation of all three pathways is by formation of DSBs, which the Mre11-Rad50-Nbs1 (MRN complex) detect. The MRN complex begins the process of repair by locating a DSB and initiating response cascades that might result in the need the for-checkpoint kinase, Ataxia Telangiectasia Mutated (ATM). Afterwards, ATM undergoes phosphorylation, thus activating different aspects of DNA repair, including all MRN complex members, and the entire DNA damage response within the cells (Li & Heyer, 2008; Ohle et al., 2016; Harris, 2019). The MRN complex combines with Dna2-Sgs1/BLM or Exo1-nuclease, to resection the DSB end 5′ to 3′ to generate terminal 3′-OH single-stranded DNA (ssDNA) tails (Ohle et al., 2016; Zhao et al., 2017; Her & Bunting, 2018). A key conserved target for cell-cycle-dependent kinases in the end-resection machinery was identified as yeast Sae2 and its mammalian homolog CtIP. Sae2/CtIP cooperate with the Mre11/Rad50/Xrs2 (mammalian MRE11/RAD50/NBS1) complex to provide the initial resection of DSBs (Huertas et al.,2008; Wang et al.,2013). The DNA replication protein A (RPA) binds the ssDNA tails, thus preventing formation of secondary structures, which might cause interference to RAD51 at ssDNA tails (Suwaki et al., 2011; Chen & Wold, 2014; Deng et al., 2015).

BRCA2/RAD52 help in the replacement of RPA complexes by the pivotal HR protein RAD51that form nucleoprotein filaments on the single-stranded DNA (Ohle et al., 2016; Talens et al., 2017). RAD51 undergoes binding to 3′ single-stranded DNA tails and it catalyses pairing with homologous duplexes, and exchanges one duplex strand with incoming single-stranded DNA tails forming displacement loops (D-loops) (Krogh &

Symington, 2004; Li & Heyer, 2008; Suwaki et al., 2011; Grabarz et al., 2012; Deng et al., 2015; So et al., 2017). The reliance of RAD51 and RAD52 recruitment on RPA could partially be explained through their direct interactions and also by absence of suitable substrates. DNA polymerases extend the 3' invading strand ends in the D-loop. After extension of the invading strands, three proposed pathways for HR, exist (Figure 1.7) (Chen et al., 2013; Deng et al., 2015).

A double Holliday junction (dHJ) is formed when the other DSB end anneals to the D-loop within the DSBR pathway (Smith, et al., 2007; Essani et al., 2015; Lord & Ashworth, 2016; Zhao et al., 2017; Wright et al., 2018). Within the SDSA pathways, unwinding of the D-loop after DNA polymerase activity and re-annealing of the second DSB end can occur (Figure 1.7). Generation of non-crossover events only result from the SDSA pathway and this reduces the likelihood of chromosomal rearrangement from being generated; however, this is not the case for other pathways (Barber et al., 2008; Youds et al., 2010). In some instances, a single repairable end could exist in a broken DNA, particularly at telomeres (without telomerase) or collapsed DNA replication forks. To restore the integrity of chromosomes, break-induced replication (BIR) pathway can be activated (Sakofsky et al., 2012; Malkova & Ira, 2013; Mehta & Haber, 2014; Kramara et al., 2018; Cortez, 2019). Within this pathway, the D-loops formed could become replication forks capable of copying DNA sequence distal to donor molecule sites up to chromosome ends. Lagging and leading strands should be synthesised for BIR to facilitate completion of DNA replication (Figure 1.7) (Malkova & Ira, 2013; Saini et al., 2014; Sakofsky & Malkova, 2017; Kramara et al., 2018).

BIR can drive alternative lengthening of telomeres (ALT) in cancer cells where telomerase is inactive (Dilley et al., 2016; Cortez, 2019). In such case, telomere sequence replication is achieved when the BIR replisomes are induced by a damaged telomere. Tumorigenesis is facilitated when maintenance of telomere is promoted by the ALT mechanism (Sakofsky et al., 2012; Kramara et al., 2018; Cortez, 2019). Besides, findings from recent studies reveal that BIR repairs DSBs, which exist at sub-telomeric sites (Batte et al., 2017). Additionally, findings show that BIR can initiate repair when R-loops accumulate at sites of DNA damage in *S. cerevisiae* (see Section 1.5.3) (Amon &

Koshland, 2016). Even though BIR plays an important role in telomere preservation and restart of replication forks that have stalled, it can lead to induction of chromosomal instability and cause extensive loss of heterozygosity (LOH) (for instance, when DSB ends invade homologues at the expense of sister chromatid molecules), despite the important role that BIR plays in telomere preservation and restart of replication forks that have stalled. Complex rearrangement of genomes, including non-reciprocal translocations can be generated by BIR (for instance, when non-allelic chromosomal sites allow initiation of broken DNA ends) (McEachern & Haber, 2006; Malkova & Ira, 2013; Sakofsky & Malkova, 2017; Kramara et al., 2018).

1.5.3 RNA-DNA hybrids in DNA repair

Essential cellular functions such as DNA replication and transcription can form DNA:RNA strands hybrids naturally. However, they might serve as a source of genome instability, a hallmark for genetic diseases and cancer (García-Rubio, 2018). These structures that comprised of displaced single-stranded DNA (ssDNA) andwith a DNA-RNA hybrid (R loop) (Stuckey et al., 2015; Ohle et al., 2016; Oestergaard & Lisby, 2017; Aguilera & Gómez-González, 2017; García-Rubio et al, 2018). The RNA-DNA hybrid constitutes a core element which can block DNA replication forks from progression and transcription elongation that causes DSB formation and replicative stress (Bermejo et al., 2012; Lin & Pasero, 2012; Ohle et al., 2016). Furthermore, hybrids, which accumulated at replication-transcription collision sites, are potentially recombinogenic, leading to recruitment of HR factors, such as Rad52, which is an indication that R-loop misregulation could potentially aggravate cancer progression and initiation (Wahba et al., 2013; Castel et al., 2014; Stuckey et al., 2015; Brambati et al., 2015). Genomic integrity maintenance and suppression of replicated stress is achieved when eukaryotic cells prevent unscheduled RNA:DNA hybrids from being formed, so cells have develop mechanisms of degrading such hybrids, for instance, RNaseH proteins, which constitute a set of enzymes that eliminate the RNA moiety of RNA:DNA hybrids (Ohle et al., 2016; Fragkos & Naim, 2017; Aguilera & Gómez-González, 2017; Kuciński et al., 2019). RNA:DNA existing in R-loops can be degraded by two RNase H enzyme forms RNase

H1 and RNase H2 (Cerritelli & Crouch, 2009; Ohle et al., 2016). Besides degrading R-loops, the activity of RNase H2 also features in the elimination of mis-incorporated ribonucleotides and RNA primers during the process of DNA replication (Ohle et al., 2016; Aguilera & Gómez-González, 2017).

The notion that RNA:DNA hybrids only cause DNA damage and genomic instability is challenged by the recent findings in *Schizosaccharomyces. pombe.* The findings showed an unanticipated positive role that such hybrids play in the process of DNA repair, and which is important for maintaining the integrity of genomes (Ohle et al., 2016). This work indicates that HR-facilitated DSB repair can be completed proficiently in the presence of moderate quantities of RNA:DNA hybrids. The process of end resection, especially in recruitment of RPA complexes to resected DNA strands was possibly regulated by RNA:DNA hybrids. This finding showed that removal and production of both hybrids is needed, and RNase H2 (Rnh201) and RNase H1 (Rnh1) largely determine the process (Figure 1.8), and that loss of both RNase (Rnh1/Rnh201) causes sensitivity to genotoxic assays. Further studies on *S. pombe* are required to confirm this interesting finding and to locate other RNA:DNA hybrid formation factors and to examine how genome stability can be preserved through other roles that these hybrids play (Wahba et al., 2013; Aguilera & Gómez-González, 2017).

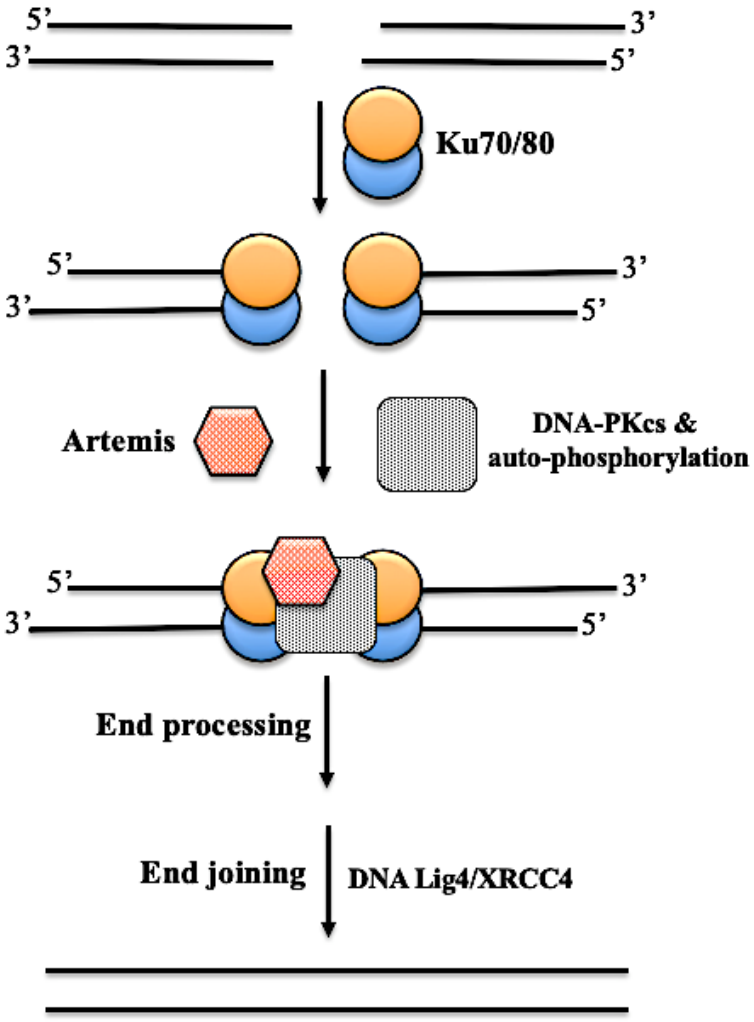

Figure 1.6 The NHEJ repair pathway stages
Ku70/80 binds to DNA due to its high affinity for DSBs ends. The Ku70/80 binding elicits conformational changes, which enable it to bind DNA-PKcs. Additionally, Ku70/80 might act as an alignment factor for NHEJ accuracy. After DNA-PK assembly on DNA breaks, the DNA repair complex activates threonine protein kinase/serine activity whereas phosphorylates target substrates, for instance, Artemis, which colocalize at broken DNA ends before events of end joining and processing (see main text for more details) (adapted from Kim et al., 2013).

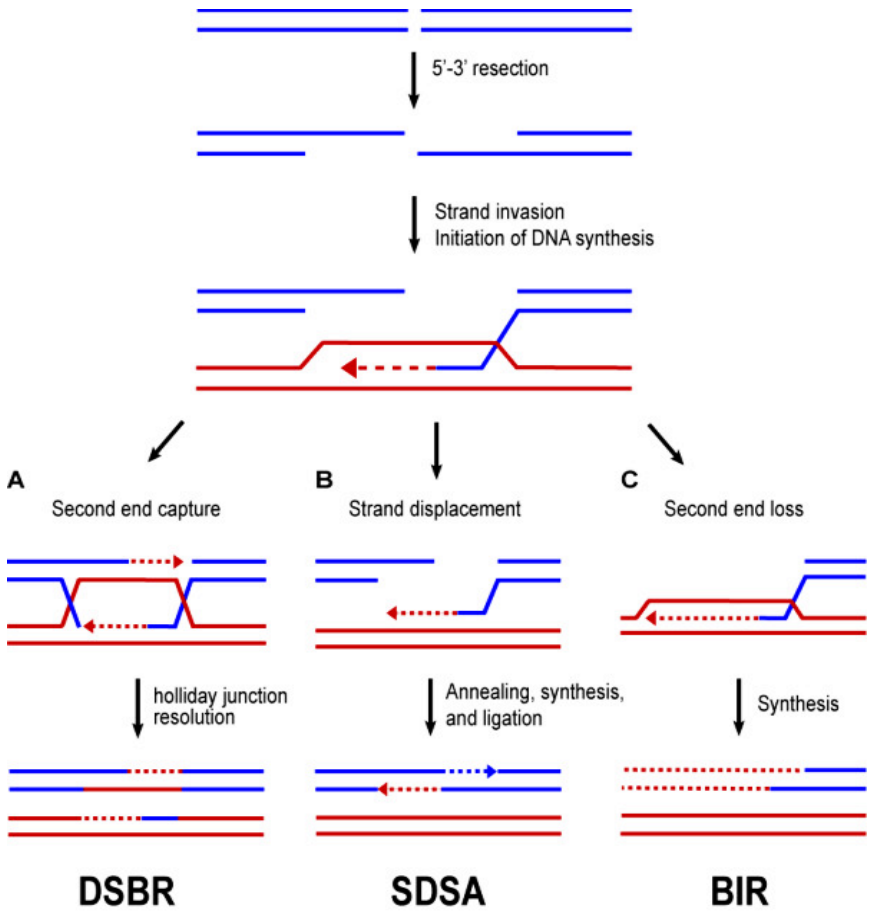

Figure 1.7 Schematic models of the HR pathways in DSB repair
Different means of repairing DSBs with homologous recombination machinery exist. In the initial phase, processing of DNA ends into 3' ssDNA tails is undertaken. The new DNA synthesis in dashed lines is primed by the tails that invade homologous templates (red). This invasion is characterised by three potential outcomes namely: **(A)** For canonical DSBR, the captured second end and the first invading strand are annealed to homologous templates and prime new DNA synthesis, leading to dHJ, which can be resolved into non-crossover products (illustration of non-crossover product) or crossover products. **(B)** From the 3' end (dashed red lines), priming of DNA synthesis occurs after the homologous template is invaded by single ssDNA tail. This D-loop gets displaced and the extended end anneals to the other end of the DSB, templates Synthesis-dependent strand annealing (SDSA). **(C)** DNA synthesis is primed by a chromosome end when one end invades the homologous template and another DSB end is lost during break-induced replication (BIR) (adapted from Rothstein & Barlow, 2010).

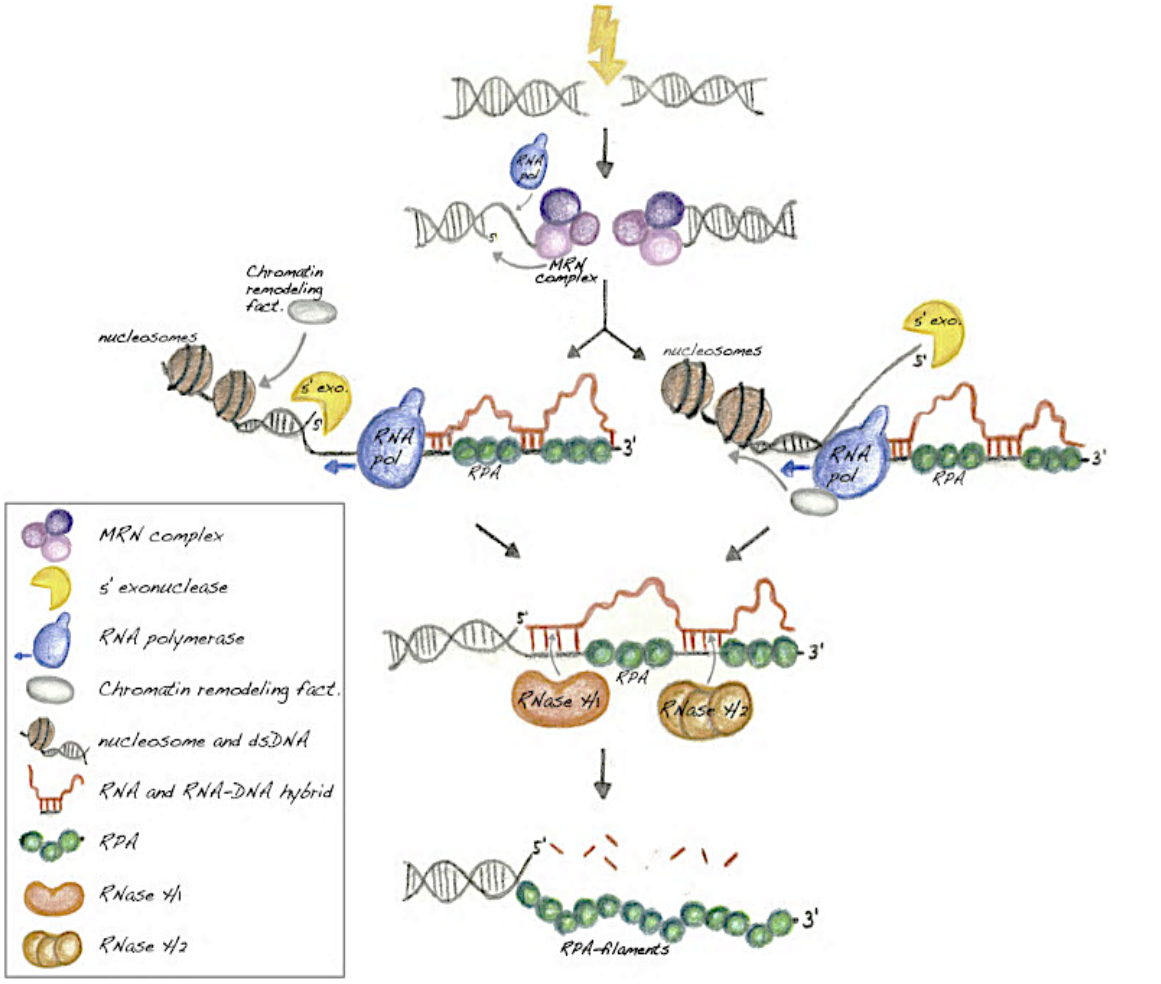

Figure 1.8 Schematic model for the role of RNA-DNA hybrids in the repair of DSBs mediated by HR

After formation of DSB, recruitment of MRN complexes to broken DNA ends occurs, and it combines with other aspects such as exonuclease Exo1 for mediation of (5'→3') resection at DSB ends, leading to formation of ssDNA overhangs containing 3' OH ends. Recruitment of RNA Pol II to overhangs of ssDNA is undertaken, thus initiating transcription. Re-annealing of nascent RNA transcripts to ssDNA is done, creating RNA-DNA hybrids that in turn might recruit ssDNA-binding RPA complex to resected DNA strands and terminate transcription of RNA Pol II as the mechanism for controlling the process of end resection. Notably, RNase H enzymes (Rnh1 and Rnh201) degrade the RNA-DNA intermediates to facilitate complete RPA loading on ssDNA overhangs and enable DSB repair process to be undertaken efficiently (Ohle et al., 2016).

1.6 Overview of Translin and TRAX

Translin is a DNA/RNA binding protein, which can create a hetero-octamer together with Translin-associated factor X (TRAX), both Translin and Trax are highly conserved proteins and are involved in RNA regulation in various biological processes such as tRNA processing, degradation of microRNAs during oncogenesis, and mRNA regulation in spermatogenesis and neuronal function (Finkenstadt et al., 2000; Jaendling & Mcfarlane, 2010; Zhang et al., 2016; Gomez-Escobar et al., 2016; Ikeuchi et al., 2018). Translin was identified as a protein with the ability to bind single-stranded DNA, but subsequent work has demonstrated it binds to both single and double stranded RNA (Finkenstadt et al., 2000). Human Translin is a protein constituting of 228 amino acids (Lluis et al., 2010; Jaendling & McFarlane, 2010). Translin was identified in human as a protein that binds to chromosomal translocation breakpoint junctions (Aoki et al., 1995; Wu et al., 1997). The association of Translin with breakpoint junction has resulted in the suggestion it is required for recombination mechanisms, although to date no direct evidence has been put forward for a role in recombination (Jaendling & McFarlane, 2010; Parizotto et al., 2013). In addition to binding to a range of cancer-associated translocation breakpoints, human Translin binds to some male meiotic recombination hot spots, but no direct evidence for a role in meiotic recombination has been found (Chalk et al., 1997; Kanoe et al., 1999; Gajecka et al., 2006). Translin-associated factor X or (Trax), was first identified by two hybrid screens as an interacting protein to Translin. It is paralogous to Translin and the Trax encoding gene is found in the species that have Translin gene. The stability of Trax is dependent on Translin in both humans and fission yeast, and this regulation is post transcriptional in nature (Aoki et al., 1995; Aoki, Ishida, & Kasai, 1997; Jaendling & Mcfarlane, 2010; Gupta & Kumar, 2012; Chern et al., 2019). A regulatory requirement for Trax to stabilize Translin is not apparent. Translin and Trax interact in a complex as an octamer made up of two Translin and Trax heterodimers and two Transiln homodimers. This signifies a close functional association between Translin and Trax (Jaendling et al., 2008; Jaendling & Mcfarlane, 2010).

Translin protein alone can create a homo-octameric ring structure, that is similar to various complexes connected to DNA recombination, repair and replication processes (Kasai et al., 1997; Fukuda et al., 2008; Jaendling et al., 2008; Jaendling & McFarlane, 2010). In this multimeric form, Translin binds single-stranded DNA (ssDNA) liner double-stranded DNA with ssDNA over hangs, but not circular double-stranded DNA (dsDNA), and it has been proposed that the Translin octameric ring structure could be responsible for DNA end recognition at the recombination hotspots in the human genome and its DNA binding activity was considered to be a sign of its requirement in recombination (Tian et al., 2011). Crystallographic analysis demonstrated that the Translin and Trax 6:2 octamer is barrel-like, with an aperture for single-stranded nucleic acid binding through the middle (Zhang et al., 2016) This complex was recently classified as C3PO (component 3 promoter of the RNA-induced silencing complex [RISC]), that functions in RNA interference (Liu et al., 2009; Joga et al., 2016; Liu et al., 2018). In the homo-octamer form, Translin is also capable of binding to double-strand and single-stranded RNA (ds/ssRNA) (Kasai et al., 1997; Eliahoo et al., 2014). The Translin and Trax hetero-octameric complex possesses an RNase activity, and this relies on Trax, with this complex having a higher affinity to bind to ssDNA sequences but a minimized potential to bind to ssRNA sequences in comparison to the Translin homo-octomer (Jaendling & McFarlane, 2010; Parizotto et al., 2013; Fu et al., 2016). Translin has no detectable DNase activity (Wang et al., 2004). Trax could bind RNA by itself in the cytoplasm, while Translin is identified in both the cytoplasmic and nuclear compartments (Chennathukuzhi et al., 2001; Cho et al., 2004; Li et al., 2008; Eliahoo et al., 2014). Early studies revealed how mouse Trax inhibits mouse Translin from binding to RNA, thereby increasing Translin binding to specific ssDNA sequences (Cho et al., 2004). Several lines of evidence have associated Trax and Translin with the mRNA control for both neuronal dynamics and spermatogenesis. For example, in testis and brain cells, mouse Translin takes part in the mRNA transport and/or stabilisation, where it binds to the 3′-UTRs (untranslated regions) of target mRNAs (Han et al., 1995). Furthermore, it was confirmed that Translin stabilises and binds a specific miRNAs in germ cells, showing a plausible functional role for Translin in gene expression posttranscriptional regulation for germ cells in males (Yu & Hecht, 2008). Besides, for

mammalian cells, the complex of Trax and Translin have been proved to mediate the directing of brain-derived neurotrophic factor (*BDNF*) mRNA to neuronal dendrites, and mutation in the Trax and Translin binding region in the *BDNF* mRNA is linked to human neurological disorders (Chiaruttini et al., 2009), showing that the Trax and Translin have a role in the function and operation of the nervous system (Jaendling & McFarlane, 2010).

During the cell cycle the *TSN* (human Translin) gene expression occurs differentially. It is activated the in G2/M phase and during the S phase where it attains its pack levels, showing a potential specific function for Translin in DNA replication and cell division (Ishida et al., 2002). Additional analysis suggested a Translin function in hastening microtubule organization and chromosome segregation during mitosis. Nonetheless, *S. pombe* Tsn1 and Tfx1 loss yielded no or limited change in the cell proliferation rate, showing that both proteins do not have an essential role in fission yeast (Jaendling et al., 2009; Jaendling & McFarlane, 2010).

1.6.1 The roles of Translin and TRAX in DNA repair

Translin and Trax proteins in various studies have implicated in the maintenance of genome stability, particularly in DNA damage response. Firstly, HeLa cells treated with etoposide or mitomycin C, resulted in Translin localizing from the cytoplasm to the nucleus, signifying a signaling approach occurring in the damaged cells (Jaendling & Mcfarlane, 2010; Wang et al., 2016). Secondly, Translin-deficient mice experience hematopoietic stem cell recovery delays following exposed to X-rays, and this signifies a possible tissue specific activity for Translin in DNA damage recovery as this was not widely observed in other tissue types (Jaendling & McFarlane, 2010). Conversely, identical studies that sought to identify the DNA repair function of Translin in MEFs did not find any dissimilarity between *Tsn*-null fibroblasts and unexposed cells (Wild type fibroblasts) concerning the quantity of DNA gaps and breaks, or in cells with survival (Cho et al., 2004; Yang et al., 2004). Also, *S. pombe tsn1*Δ and *tfx1*Δ mutants have no sensitivity to an extensive array of DNA damaging agents (Jaendling et al., 2008). However, Trax and Translin do bind to other proteins taking part in the DNA damage

response. For instance, by utilizing a yeast-two hybrid system, murine Translin seemed to bind to the apoptosis inhibitor protein GADD34, normally a DNA damage-inducible and growth arrest protein (Jaendling & McFarlane, 2010). GADD34 is implicated in the commencement of translation, this resulted in the proposal that the role of Translin, alongside GADD34, may be associated in some way with an RNA-processing/binding role instead of a direct involvement with DNA damage (Jaendling & Mcfarlane, 2010), even though postulates exist that GADD34 may take part in transporting Translin to the nucleus (from the cytoplasm) as a response to DNA damage (Hasegawa & Isobe, 1999; Hasegawa et al., 2000). Trax has been demonstrated to directly interact with the DNA-PK (DNA-dependent protein kinase) activator protein CID, which takes part in the repair of DNA in both NHEJ and HR pathways (Yavuzer et al., 1998; Erdemir et al., 2002; Li et al., 2008; Jackson et al., 2016). Nevertheless, the direct function of Trax in CID-associated DNA damage response has not been demonstrated. A vital function for murine Trax was identified in DNA damage repair as it was demonstrated to function alongside ATM-mediated pathway for MRN complex stabilization at DSBs. Trax dysfunction results in ATM inactivation, indicating that Trax is a major factor engaged in the DNA damage response (Wang et al., 2016). Nonetheless, to date, no evidence has demonstrated a direct role for Translin in DNA damage repair. Despite this lack of clear, overt evidence for a major role in DNA damage response, it is yet to be evaluated whether Trax and Translin play a redundant function in recombination and DNA repair activities, capable of accounting for the originally postulated role in translocation formation (Jaendling & McFarlane, 2010).

1.6.2 Evidence for a role for TRAX and Translin in RNAi

RNA-mediated interference (RNAi) is a mechanism of silencing gene expression in a many organism at the transcriptional or post-transcriptional stage. Gene silencing results from the guiding of ribonucleases to specific mRNAs. (Kanoh et al., 2005; Li & Zhang, 2012; Zamore et al., 2017). The process involves small, non-coding RNA molecules, around 20–30 nucleotides in length, controling the gene activity through degrading transcripts or inhibiting their translation (Zamore et al., 2017). The short RNAs control

expression of genes via two pathways. The post-transcriptional gene silencing (PTGS) is the first pathway, and it silences target mRNAs in the cytoplasm to inhibit their translation. Chromatin-dependent gene silencing (CDGS) is the second pathway, that represses specific genes at the transcription stage through heterochromatin development (Moazed, 2009; Castel & Martienssen, 2013). There are three key types of RNA pathways, which have been classified so far as: small interfering RNA (siRNA), microRNA (miRNA), and piwiRNA (piRNA) pathways (Moazed, 2009; Castel & Martienssen, 2013; Holoch & Moazed, 2015; Joga et al., 2016). The major mediators, miRNAs and siRNAs, take part in both CDGS and PTGS. However, piRNAs are associated with suppressing retro transposable element in germ line cells. These non-coding RNA molecules have a significant role as a guide for the RNAi pathway (Pushpavalli et al., 2012). In brief, the RNAi process is started with long double-stranded RNA (dsRNA) molecules, which are generated via distinct routes, including long-hairpin RNA and sense-antisense transcript annealer. The processing of exogenous dsRNA occurs through a ribonuclease III enzyme, known as Dicer, into small interference RNAs (siRNAs). The 21–24 nucleotide duplexes are then included in the RNA-induced silencing complex (RISC) where the duplex passenger strand (single strand) is removed by Argonaute (Ago) protein cutting. The guide (antisense) strand is still linked to the RISC. Subsequently, the siRNA guide strand guides the RISC and mediates the Watson-Crick base pairing with the complementary target mRNA to allow cleavage of target mRNA by Argonaute. This target mRNA degradation, initiates precise post-transcriptional gene silencing (Figure 1.9) (Agrawal et al., 2003; Kalantari et al., 2016).

The Translin/Trax complex is also referred as component 3 promoters of RISC (C3PO). C3PO has an important function in the stimulation of RISC through enhancing the unwinding and degradation of the passenger strand from the exogenous siRNAs (exo-siRNAs) on the Argonaute complex (RISC), in both human cells and *Drosophila melanogaster* (Figure 1.9) (Liu et al., 2009; Ye et al., 2011; Tian et al., 2011; Kalantari et al., 2016; Joga et al., 2016; Zhang et al., 2016; Liu et al., 2018). The C3PO function in RNAi may be restricted to particular eukaryotic species. For example, C3PO is not apparent in RNAi function in the filamentou fungus *Neurospora crassa*. *N. crassa* C3PO

has been proved to operate as a ribonuclease in tRNA processing, precisely in the pre-tRNAs maturation to tRNAs stage. After ribonuclease P (RNase P) processing of pre-tRNAs, C3PO eliminates sequences at the 5' end of the pre-tRNA. Moreover, in mouse embryonic fibroblast cells, the C3PO is also associated with the processing of tRNA (Li et al., 2012). Surprisingly, recent results have indicated that C3PO could have adverse influences on silencing activity that mediated by miRNAs and siRNAs. In *vitro,* it has been found that C3PO degrades pre-miRNAs, independently of RISC, and this has the opposite effect on silencing observed in *Drosophila* (Asada et al., 2014; Fu et al., 2016; Zhang et al., 2016; Liu et al., 2018).

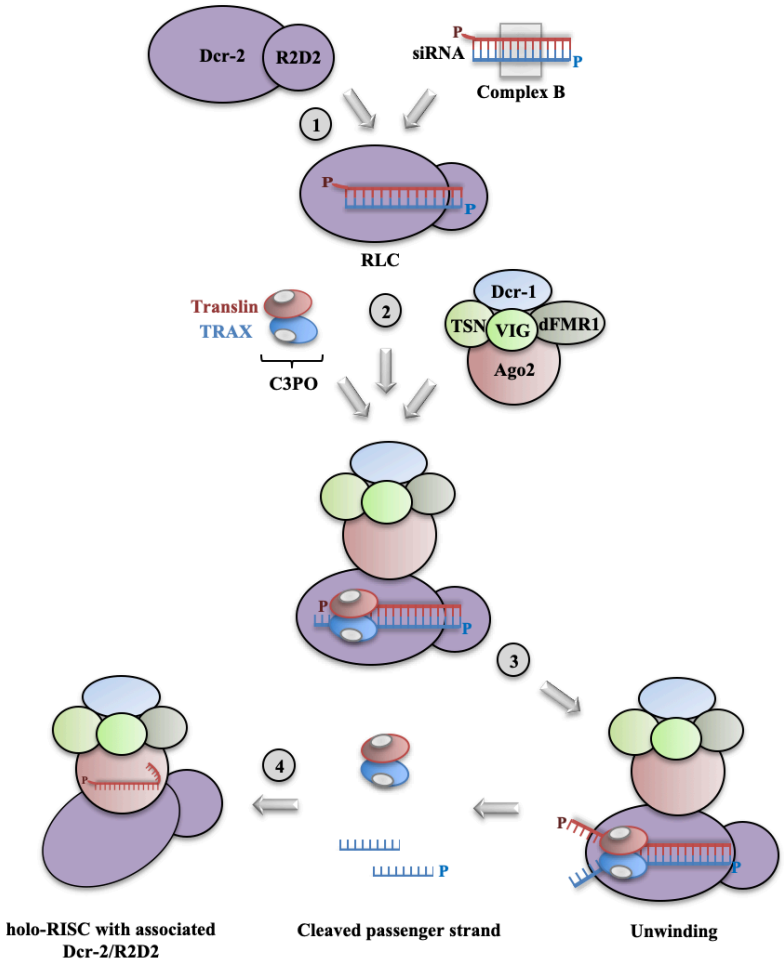

Figure 1.9 The basic diagram of the role of Translin and Trax in the *Drosophila* RNAi pathway

The above figure portrays the siRNA duplex (comprising of the guide and passenger strands) translocation from complex B to RISC loading complex (RLC), comprising of R2D2 and Dcr-2. Subsequent to this, C3PO is merged with the RLC complex, together with the RISC complex, which lead to production of holoRISC by a Drc-2–Ago2 involvement. This is followed by inducement of extraction of the passenger strand from the siRNA duplex using the endoribonuclease activity. Eventually, holoRISC complex focuses on the selected mRNA (adapted from Jaendling & McFarlane, 2010).

1.6.3 The role of Translin and TRAX as potential oncological drug targets

Dicer is riboendonuclease III enzyme and it functions to generate the small RNAs, including siRNA and miRNA. Dicer converts precursor miRNA (pre-miRNA) into mature miRNAs, which in turn direct Argonaute to selected mRNAs to mediate translational suppression (Asada et al., 2014; Gulyaeva & Kushlinskiy 2016; Baraban, et al., 2018). The expression of many human genes including tumour suppression genes, is regulated and modulated by the miRNAs, and many human cancers are characterised by deregulation of these small non-coding RNAs. miRNAs inhibit different oncogenic and tumour-suppressive mRNAs, and this has resulted in the suggestion that the miRNAs function as tumour–suppressor genes or oncogenes (Jonas & Izaurralde, 2015). In human cancer tissue, the accumulation of pre-miRNAs and the reduction of mature miRNAs has been observed in comparison to normal tissue (Gurtner et al., 2016). During the normal process to develop miRNAs, to function to control tumour suppression, pre-miRNAs get processed by Dicer to miRNAs (see Figure 1.10). When there is not enough Dicer (haploinsufficiency), this processing is limited. Therefore, pre-miRNAs potentially become the substrate for other RNase activity. Investigation was taken to place to try to identify other activates which destroy pre-miRNAs to prevent Dicer creating mature miRNAs. Translin/Trax were found to provide an RNase activity because of this, it has been hypothesis that the inhibiting of Translin/Trax would stop this degradation of the pre-miRNAs, enabling the reduced the levels of Dicer to process the pre-miRNA to mature miRNAs and re-instate tumour suppressing activity (Asada et al., 2014; Fu et al., 2016; Asada et al., 2016; Baraban, et al., 2018).

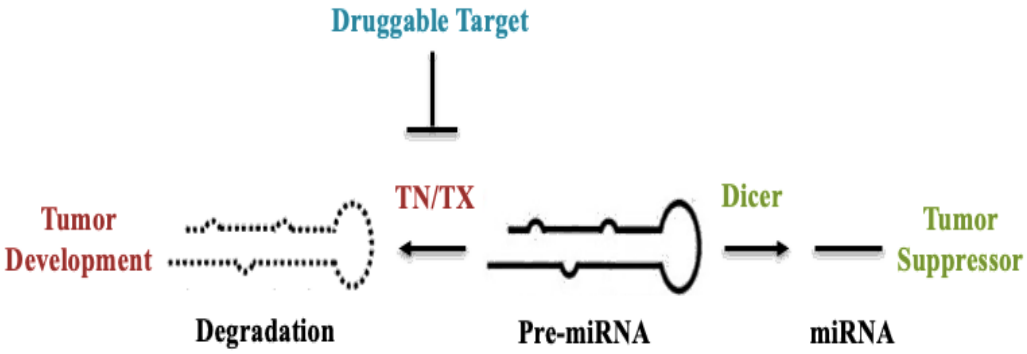

Figure 1.10 A schematic of Translin/TRAX (TN/TX) complex as a potential druggable target in tumours

Tumour suppression is maintained when a normal Dicer levels processes pre-miRNA into mature miRNA (right hand pathway, green). Nevertheless, in Dicer haploinsufficiency pre-miRNAs are degraded by the ribonuclease complex TSNAX/TSN, thus aggravating development of tumours (left hand pathway, red). During Dicer deficiency, loss of tumour and miRNA suppression would be rescued through TSNAX/TSN genetic on chemicals inhibition (blue), as right-hand pathway is destroyed (adapted from Asada et al., 2016).

1.7 *Schizosaccharomyces pombe* as a model eukaryote

Investigation of eukaryotic cellular and molecular processes over the last century has lately been based on the study of model organisms, including the fission yeast *S. pombe* (Hayles & Nurse, 2018). Saare and his colleagues were responsible for finding *S. pombe*. They isolated it from millet beer which was contaminated due to a delay in transporting it from East Africa to Germany. In the 1890s, Ziedler and Lindner managed to isolate a pure culture of *S. pombe* and provided the first detailed description of it, naming it "Pombe" which means 'beer'in Swahili. Later, in the 1950s, *S. pombe* was developed as a model for experimentation (Nurse, 2002; Forsburg, 2007; Hayles & Nurse, 2018). The genome of *S. pombe* has three chromosomes I, II, and III of approximately 5.6, 4.8, and 3.6 Mb respectively (Petrova et al., 2013). The *S. pombe* genome sequence was completed in 2002, and *S. pombe* is predicted to have approximately 5000 protein coding genes (Wood et al., 2002). Between humans and *S. pombe* there are certain genes that are conserved but are not present in other organisms such as the widely used model, the budding yeast *S. cerevisiae* (Wood et al., 2002; Koyama et al., 2017). *tsn1* (Translin) and *tfx1* (Trax) are two such genes, which have no detectable *S. cerevisiae* orthologues, but do have homo-orthologues. *S. pombe* has been used as a tool for the exploration of RNAi and cellular epigenetics as, unlike *S. cerevisiae,* it has all the RNAi components (Buhler & Gasser, 2009; Koyama et al., 2017; Hayles & Nurse, 2018). Unique heterochromatic features are displayed by the various regions of the *S. pombe* genome, including telomeres, centromere, mating-type locus, and the rDNA locus (Figure 1.11). The comparison of these regions with that of other organisms shows epigenetic regulatory similarity (Pidoux & Allshire, 2004; Reyes-Turcu & Grewal ,2012; Koyama et al., 2017; Hayles & Nurse, 2018). It is because of these characteristics that *S. pombe* is a good model for this current study.

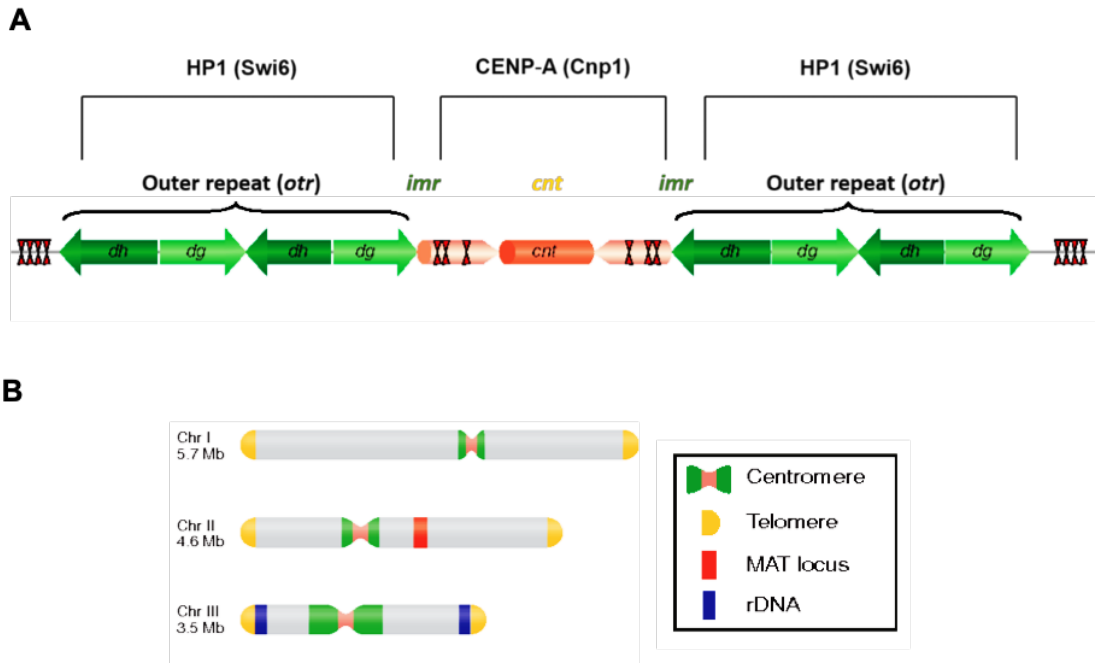

Figure 1.11 *S. pombe* centromere schematic demonstration
(A) Two main distinguishable regions characterize the centromeric region and these are *cnt* (yellow) and *imr* (green). The *otr* region surrounds *cnt* and *imr* and consists of *dg* (light green) and *dh* (dark green) sequences that are repetitive. The boundary elements, tRNA genes, are represented by the vertical lines within the *imr* regions. (**B)** The chromosomes of *S. pombe* are schematically represented here. The four regions of heterochromatin are depicted in the three chromosomes and these are telomere, centromere, *mat2/3*, and rDNA regions (adapted from Allshire & Ekwall, 2015).

1.7.1 Heterochromatin in *S. pombe*

Chromatin is principally made up of histone proteins. In eukaryotes critical functional roles are concluded by the manner in which chromatin is organised. The basic component of chromatin is the nucleosome, which consists of an octamer comprising two molecules of each of the four core histones H3, H4, H2A and H2B, surrounded by approximately 147 DNA base pairs (Harshman et al., 2013; Chen et al., 2016; Hammond et al., 2017; Koyama et al., 2017; Carlberg & Molnár, 2018; Onufriev & Schiessel, 2019). Linker DNA (20-80 bp) connects the nucleosomes. The linker DNA is associated with Histone H1 (the linker histone). For each core histone, there is a flexible N-terminal tail which protrudes into the nucleoplasm. Multiple types of enzymes can cause the modification of this tail leading to changes in its chromatin structure and thus affecting DNA accessibility. Modifications of the histone tails include acetylation and methylation, which occur post-translationally (Luger et al., 2012; Maeshima et al., 2014; Hammond et al., 2017; Timsina & Qiu, 2019). Histones H3 and H4 undergo acetylation and this reshapes the chromatin to a less-condensed euchromatin configuration, which is transcriptionally active. On the other hand, H3 also undergoes methylation and on K9, reshaping the chromatin to a compact heterochromatin form, which is transcriptionally inactive. H3K9-Me is the core of the formation of heterochromatin as it permits the binding of heterochromatin protein 1 (HP1) (Swi6 in *S. pombe*) (Moazed, 2009; Gerace et al., 2010; Olsson & Bjerling, 2011; Creamer & Partridge, 2011; Alper et al., 2012; Allshire & Ekwall, 2015; Wang et al., 2016). Acetylation of lysine 9 of histone 3 (H3K9ac) and methylation of lysine 4 of histone 3 (H3K4me) are used as markers of euchromatin. Histone protein N-terminal regions, which are altered by these epigenetic modifications, are highly conserved regions in most eukaryotic species, including humans and fission yeast (Goto and Nakayama, 2012; Nikolov & Taddei, 2016; Wang al., 2016; Kusevic et al., 2017; Carlberg & Molnár, 2018).

In the genome of *S. pombe*, the heterochromatic regions have distinct features and are epigenetically regulated to be silent (Goto & Nakayama, 2012; Bhattacharjee et al., 2019). The formation and maintenance of heterochromatin is important for control various genomic functions that include telomere functions, expression of genes, and

optimal centromere function. In lower and higher eukaryotes (such as yeast and humans), the assembly of heterochromatin has conserved features (Goto & Nakayama, 2012; Li & Zhang, 2012; Cusanelli & Chartrand, 2015; Zocco et al., 2016). The structure of heterochromatin at centromeres is significantly influenced by defects in the RNAi pathway, but at the telomeres, the impact is less clear (Volpe et al., 2002; Volpe et al., 2003; Kanoh et al., 2005; Tadeo et al., 2013; Sadeghi et al., 2015; Martienssen & Moazed, 2015). This is an indication that the formation of heterochromatin at the chromosomes ends is influenced by factors other than standard RNAi. At the telomeres, it has been shown that Tazl, a telomere associate-protein, is involved in the formation of heterochromatin. Tazl is an orthologue of mammalian telomere repeat factors. The formation of heterochromatin at the telomeres is achieved through the induction of methylation of H3 lysine 9 by the histone methyltransferase Clr4 leading to the formation of a site for the binding of Swi6. The localisation of Swi6 to the telomere is lost in a *taz1*Δ mutant, as well as the mutation of RNAi gene *dcr1*. This is an indication that Tazl and RNAi have redundant roles in the formation of heterochromatin at the telomere (Buhler & Gasser, 2009).

1.7.2 Centromeres

In eukaryotes, centromeres play a significant role in the segregation of the chromosomes during the division of cells. Most complex centromeres have highly repetitive DNA regions as well as the kinetochore proteins that are bound to it. The kinetochore is a proteinaceous structure which provides the surface onto which microtubules attach to chromosomes during meiosis and mitosis (Buhler & Gasser, 2009; Westhorpe & Straight, 2013; Westhorpe & Straight, 2015; Thakur et al., 2015; Moreno-Moreno et al., 2017; Okita et al., 2019). The structure of centromeres must be maintained, as failure can result in chromosome mis-segregation that is implicated in cancer (Ekwall et al., 1999; Lee et al., 2013; Santaguida & Amon, 2015). *S. pombe* centromeres have three regions with the centromeres of the three chromosomes differing in size from 35 kb to about 110 kb. One region is the central core (*cnt*) is where the kinetochore is assembled. It is also the location of nucleosomes containing a unique variant of histone H3 called CENP-A (Cnp1

in *S. pombe*). While *cnt* is a non-repetitive region, the other two regions are repetitive and flank the *cnt* (Figure 1.11). These regions have silent chromatin where RNAi induces Swi6 bound to H3K9me. These two flanking regions are the *otr* (outer repeats) and *imr* (inner most repeats). The *otr* is further split into two repeat sequences *dg* and *dh* (Figure 1.11) (Smirnova & McFarlane, 2002; Pidoux & Allshire, 2004; Thakur et al., 2015; Allshire & Ekwall, 2015). The functional nature of the centromere repeats remains unclear, but it has been postulated that they serve to form higher order structure (McFarlane & Humphrey, 2010). In a majority of organisms, including *S. pombe*, the mediation of the silenced formation of the heterochromatin at the centromere regions needs the RNAi machinery and thus the functions of heterochromatin at the centromere are influenced by the mutation of the central players of the RNAi pathway (Chan & Wong, 2012; Tadeo et al., 2013). The localization of Swi6 and methylation of H3K9 is prevented by the deletion of any RNAi genes (e.g., *ago1* and *dcr1*). RNA polymerase II transcribes DNA sequences *dg* and *dh* in the *otr* region resulting in the production of the nascent noncoding transcripts that are processed into dsRNAs by RNA-dependent RNA polymerase (Rdp1). These dsRNAs processed into small interference RNAs (siRNA) via the RNAs III Dcr1 (Dicer). These siRNA are then presented to the RNA induced transcription silencing (RITS) complex, which contain Ago1 (Argonaute), to mediate the siRNA dependent recruitment of the Clr4 histone methyltransferase to the nascent centromeric *otr* transcript being generated by RNA polymerase II (Figure 1.12) (Motamedi et al., 2003; Holoch & Moazed, 2015).

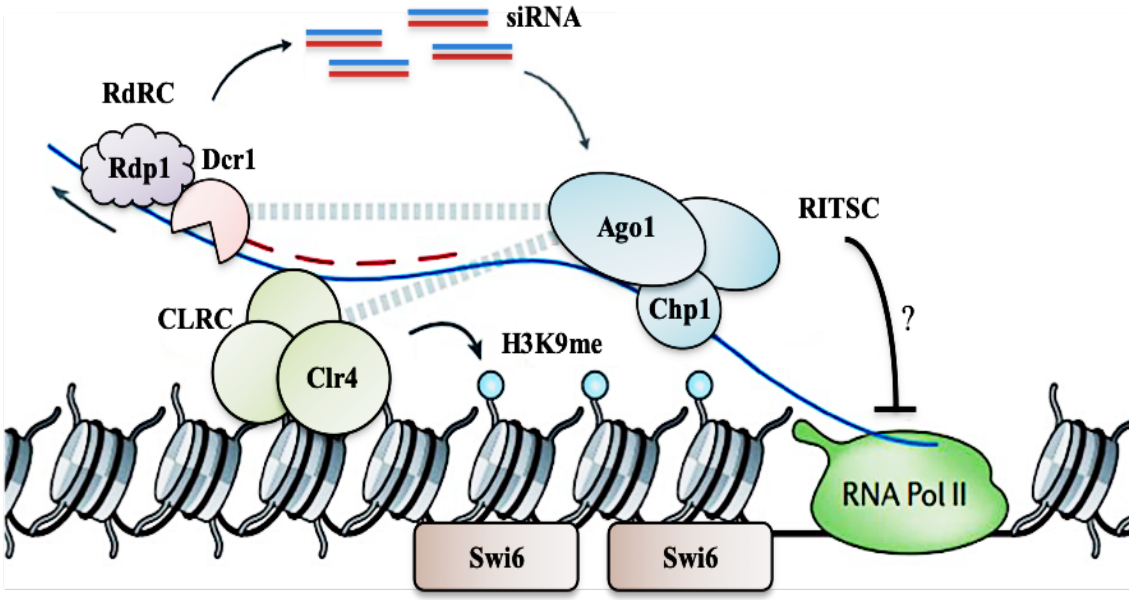

Figure 1.12 The basic diagram of the RNA interference in heterochromatin assembly
The RITS complex that features Chp1, Ago1, and siRNA targets nascent transcripts (blue lines) through siRNA base pairing leading to RNA Pol II transcription blockage by unknown mechanisms (denoted by question mark). The interaction involving H3 and Chp1 on lysine 9 results in Clr4 recruitment to methylate histone H3 at lysine 9, which in turn acts as Swi6 binding site. The RDRC complex (Rdp1) creates the new double-stranded RNA (dsRNA) that comprises nascent strands and siRNA, to produce additional dsRNAs, which Dcr1cleaves to generate siRNAs. The RITS complex connects H3k9me and RNA cycles, thus facilitating effective assembly of heterochromatin (Source: Castel & Martienssen, 2013).

1.7.3 Telomeres

In eukaryotic cells, the organization of chromatin is in structural and functional domains that are key for genome stability. G/T-rich tandem DNA repeats characterize the telomeres and provide sites for docking of the proteins that bind to telomeres for the protection of the chromosomal ends from fusion and erosion (Cooper et al., 1997; Eberhard et al., 2019; Van Emden et al., 2019; Keefe, 2019). In many cancer cells, telomerase, the enzyme required for synthesizing telomeres, is activated and plays a role in telomere maintenance that is crucial for the extension of DNA at the chromosome ends in proliferating cells (Buhler & Gasser, 2009; Ohlo et al., 2016; Hsu & Lue, 2017; Mizukoshi & Kaneko, 2019). DNA damage response (DDR) signaling pathways can be activated by chromosome ends being recognised as DSBs. To solve this problem, telomeres form structure that repress all forms of DDR signaling and DSB repair (Vancevska et al., 2017; De Lange, 2018). The Shelterin complex mediates the protection of telomere in *S. pombe* and comprises particular protein complexes that facilitate the functions of telomere including regulating the length of telomeres to avoid dysfunction at the chromosomes end (Miyoshi et al., 2008; Armstrong et al., 2014; Maestroni et al., 2017; Vancevska et al., 2017; Eberhard et al., 2019). Therefore, for many of the genome dynamics, telomeres play an important role and it is important to maintain telomere function as well as telomerase functions and integrity. Failure in maintenance is related to genetic diseases such as cancer (Armstrong et al., 2014; Sarek et al., 2015; Chatterjee, 2017; Van Emden et al., 2019).

Initially, telomeres were considered to be transcriptionally inactive due to their heterochromatin state (see Figure 1.11). (Novo & Londoño-Vallejo, 2013; Lorenzi et al., 2015). Later, it was found that telomeres are transcribed into TERRA (telomeric repeat-containing RNA) molecules that are also transcribed by RNA Pol II to the telomere from the sub-telomere (Wang et al., 2015; Feretza et al., 2017). The identification of TERRA was first done in humans and has since been associated with various telomere-related functions that include the regulation of the length of the telomere, DNA damage response, regulation of the telomerase activity, and the formation of telomeric heterochromatin (Schoeftner & Blasco, 2008; Wang et al., 2015; Bettin et al., 2019). The

stability and integrity of the genome is dependent on the regulation of the expression of TERRA (Cusanelli & Chartrand, 2015; Brieño-Enríquez et al., 2018; Bettin et al., 2019). Recent study shows that, Tsn1 and Tfx1 have a role in regulating telomeric RNA. Tfx1 functions to control sub-telomeric ARRET transcript levels in a Tsn1-dependent fashion, and in a reciprocal control mechanism, Tsn1 serves to suppress telomeric TERRA transcript levels in a Tfx1- dependent fashion. This reveals important and novel telomere-associated regulatory factors (Tsn1 and Tfx1), and identifies a novel mechanism for telomeric transcriptome regulation (Gomez-Escobar et al., 2016).

1.8 Aims of this study

Human-Translin was originally identified as a chromosome break point junction binding protein. This led to the postulate that it was a repair / recombination mediator. This was further supported by its nucleic acid binding characteristics. However, to date no direct evidence for such a role has been found. To address this, and other possible functions of Translin and its binding partner Trax, we aimed to employ the fission yeast model system to:

- Investigate if Tsn1 (Translin) and Tfx1 (Trax) function in genome stability regulation.
- Assess the relationship between Tsn1/Tfx1 and the RNAi regulator Dcr1, which has been implicated in genome control.
- Investigate if Tsn1 (Translin) and/or Tfx1 are implicate in recombination or DNA damage response.

Chapter 2: Methods and Materials

2. Methods and Materials

2.1 Media and strains used in this study

Table 2.1 details the media used in this study, while Tables 2.2 and 2.3 present the *E. coli* and *S. pombe* strains. For *S. pombe* assays protocols standard techniques were applied as described by Sabatinos and Forsburg (2010). *De novo* deletion *S. pombe* mutants were generated using the Bähler method (Bähler et al., 1998) and then PCR analysis of the genomic DNA confirmed the correct deletions. The required supplements and media were obtained from Sigma and Difco (Becton Dickinson). To the minimal media, 200 mg/L of appropriate amino acid supplements were added as required. A concentration of 100 μg/mL of all antibiotics, ampicillin (Sigma), nourseothricin (Warner BioAgents), were applied to the relative media as required.

2.2 Plasmid extraction from *E. coli*

To extract the plasmid from *E. coli*, QIAGEN Miniprep kit was used. One colony was inoculated into 5 mL of LB liquid media containing ampicillin and incubated in the shaker at 37°C overnight. The cells were centrifuged for 5 minutes at 3000 *g*, and then resuspended in 250 μL of P1 buffer containing RNase A and transferred into a sterile Eppendorf tube, before the addition of 250 μL of P2 lysis buffer to lyse the cells. For 4 to 5 times invert mixing was performed, was added adding 350 μL of N3 buffer (neutralising/binding buffer) into the same tube. Invert mixing was performed again 4-5 times to homogenise the tube contents. The Eppendorf tube was then spun for 10 minutes at a speed of 12,000 r.p.m (microcentrifuge) and the supernatant was transferred to a QIAprep tube and spun down at a similar speed for 30-60 seconds. Then, the supernatant was removed, and the pellet washed using 500 μL of PB buffer, then centrifuged for 30-60 seconds at 12,000 *g*. The supernatant was removed, and the pellet washed with 750 μL of PE buffer and then centrifuged for 30-60 seconds at 12,000 *g*. The supernatant was removed and then 50 μL of EB (elution buffer) was added to the filter to eluted plasmid DNA.

2.3 Deletions of *S. pombe* gene by using the PCR method

The Bähler approach method was used to knockout different genes of the *S. pombe* genome (Bähler et al., 1998). Briefly, pFA6a-kanMX6 and pFA6a-natMX6 plasmids were utilised as template DNAs for PCR amplification of the antibiotic-resistant marker different cassette. The PCR primers included homologous sequences from 80 to 100 bp directly to the open reading frame (upstream and downstream) of the ends of target genes to be knocked out and included homologous sequences of 20 bp of the plasmid substitutes. The oligonucleotide sequences used are shown in Table 2.4. The primers used in this study were designed using software, of the Bähler lab.

http://www.bahlerlab.info/cgi-bin/PPPP/pppp_deletion.pl

All the primers and plasmids were diluted 10-fold in 1X TE buffer (1.0 M Tris-HCl at 8.0 pH and 1.0 M of EDTA) before use. Each PCR reaction contained 50 µL of the following: 1 µL of DNA template (20 ng of plasmid DNA), 1 µL high fidelity Phusion polymerase (NEB), 1 µL of 10 x dNTPs, 10 µL 5x Phusion™ GC buffer, 1 µL of forward and reverse primers of (20 ng/µL), 2.5 µL of DMSO and 32.5 µL of sterile distilled water. The PCR programme used to amplify the chosen marker cassettes was as follows: 1 minute for 98°C (initial heating), followed by 30 seconds at 59ºC, 30 cycles of 10 seconds at 98ºC, 1 minute 50 seconds at 72ºC, and at 72ºC for 5 minutes as a final elongation step. The PCR samples were then purified utilising the phenol/chloroform strategy.

Table 2.1 Media recipes of yeast and bacteria

Media	Contents
YEA Yeast extract Glucose Agar	**Per 1 litre add:** 5 g 30 g 14 g
YEL Yeast extract Glucose	**Per 1 litre add:** 5 g 30 g
LBA Tryptone Yeast extract Sodium chloride Agar	**Per 1 litre add:** 10 g 5 g 10 g 14 g
NBA Nitrogen base Glucose $(NH_4)_2\ SO_4$ Agar	**Per 1 litre add:** 1.7 g 10 g 5 g 24 g
Drugs Methyl Methanesulfonate (MMS) (Sigma) Thiabendazole (TBZ) (Sigma) Mitomycin C (Sigma) Phleomycin (Sigma) Belomycin (Sigma) Hydroxyurea (HU) (Sigma) Camptothecin (Sigma)	**Concentrations** (0.005, 0.0075, 0.01 %) (12, 13, 14, 15,16 µg/ml) (0.15, 0.18, 2 mM) (2.5, 3, 4, 5, 6, 8, 10 µg/ml) (3, 4, 5 µg/ml) (5,6,7,8,9,10 mM) (1, 1.2, 1.4, 1.8 µg/ml)

Table 2.2 *E. coli* strain and plasmid utilised in this project

Bangor strains number	*E. coli* strain	Source
BE9	DH5α (pARC782)	McFarlane, Bangor University
BE122	DH5α (pSRS5)	McFarlane, Bangor University
BE183	DH5α (pYL16)	Hartsuiker, Bangor University

Table 2.3 Strains of *S. pombe* used in this study

Strain number	Genotype	Source
BP90	*h⁻ ade6-M26 ura4-D18 leu1-32*	McFarlane, Bangor University
BP743	*h⁻ rad3-136*	McFarlane, Bangor University
BP1079	*h⁻ ade6-M26 ura4-D18 leu1-32 tsn1::kanMX6*	McFarlane, Bangor University
BP1080	*h⁻ ade6-M26 ura4-D18 leu1-32 tsn1::kanMX6*	McFarlane, Bangor University
BP1089	*h⁻ ade6-M26 ura4 -D18 leu1-32 tfx1::kanMX6*	McFarlane, Bangor University

BP1090	*h⁻ ade6-M26 ura4 -D18 leu1-32 tfx1::kanMX6*	McFarlane, Bangor University
BP1478	*h⁻ ade6::tRNAGLU (1) his3-D1 ura4–18 lys1–37 leu1–32*	McFarlane, Bangor University
BP1508	*h⁻ ade6::tRNAGLU (2) his3-D1 ura4–18 lys1–37 leu1–32*	McFarlane, Bangor University
BP1534	*h⁻ ade6::tRNAGLU (1) his3-D1 ura4–18 lys1–37 leu1–32 (pSRS5)*	McFarlane, Bangor University
BP1535	*h⁻ ade6::tRNAGLU (2) his3-D1 ura4–18 lys1–37 leu1–32 (pSRS5)*	McFarlane, Bangor University
BP1685	*h⁻ ade6::tRNAGLU (1) his3-D1 ura4–18 lys1–37 leu1–32 swi1::ura4 (pSRS5)*	McFarlane, Bangor
BP1687	*h⁻ ade6::tRNAGLU (2) his3-D1 ura4–18 lys1–37 leu1–32 swi1::ura4 (pSRS5)*	McFarlane, Bangor University
BP2746	*h⁻ ade6-M26 ura4-D18 leu1-32 dcr1::ura4⁺*	McFarlane, Bangor University
BP2748	*h⁻ ade6-M26 ura4-D18 leu1-32 tsn1:: kanMX6 dcr1::ura4⁺*	McFarlane, Bangor University
BP2749	*h⁻ ade6-M26 ura4-D18 leu1-32 tsn1:: kanMX6 dcr1::ura4⁺*	McFarlane, Bangor University
BP2750	*h⁻ ade6-M26 ura4-D18 leu1-32 tfx1:: kanMX6 dcr1::ura4⁺*	McFarlane, Bangor University
BP3248	*h⁻ ade6-M26 ura4-D18 leu1-32 tfx1::kanMX6 tsn1::natMX6*	McFarlane, Bangor University

BP3249	*h⁻ ade6-M26 ura4-D18 leu1-32 tfx1::kanMX6 tsn1::natMX6*	McFarlane, Bangor University
BP3250	*h⁻ ade6-M26 ura4-D18 leu1-32 tsn1:: kanMX6 dcr1::ura4⁺ tfx1::natMX6*	McFarlane, Bangor University
BP3301	*h⁻ ade6-M210 ura4-D18 leu1-32 his3-D1 Otrt::his3*	J. P Cooper collection
BP3313	*h⁻ ade6::tRNAGLU (1) his3-D1 ura4–18 lys1–37 leu1–32 dcr1::natMX6*	McFarlane, Bangor University
BP3314	*h⁻ ade6::tRNAGLU (1) his3-D1 ura4–18 lys1–37 leu1–32 dcr1::natMX6 tsn1::kanMX6*	McFarlane, Bangor University
BP3322	*h⁻ ade6::tRNAGLU (1) his3-D1 ura4–18 lys1–37 leu1–32 tsn1::kanMX6 (pSRS5)*	McFarlane, Bangor University
BP3324	*h⁻ ade6::tRNAGLU (1) his3-D1 ura4–18 lys1–37 leu1–32 dcr1::natMX6 (pSRS5)*	McFarlane, Bangor University
BP3325	*h⁻ ade6::tRNAGLU (1) his3-D1 ura4–18 lys1–37 leu1–32 dcr1::natMX6 (pSRS5)*	McFarlane, Bangor University
BP3326	*h⁻ ade6::tRNAGLU (1) his3-D1 ura4–18 lys1–37 leu1–32 dcr1::natMX6 tsn1::kanMX6 (pSRS5)*	McFarlane, Bangor University
BP3327	*h⁻ ade6::tRNAGLU (1) his3-D1 ura4–18 lys1–37 leu1–32 dcr1::natMX6 tsn1::kanMX6 (pSRS5)*	McFarlane, Bangor University
BP3328	*h⁻ ade6::tRNAGLU (1) his3-D1 ura4–18 lys1–37 leu1–32 tsn1::kanMX6 (pSRS5)*	McFarlane, Bangor University

BP3335	*h⁻ ade6::tRNAGLU (1) his3-D1 ura4–18 lys1–37 leu1–32 tsn1::kanMX6*	McFarlane, Bangor University
BP3336	*h⁻ ade6::tRNAGLU (2) his3-D1 ura4–18 lys1–37 leu1–32 tsn1::kanMX6*	McFarlane, Bangor University
BP3343	*h⁻ ade6::tRNAGLU (2) his3-D1 ura4–18 lys1–37 leu1–32 dcr1::kanMX6*	McFarlane, Bangor University
BP3344	*h⁻ ade6::tRNAGLU (2) his3-D1 ura4–18 lys1–37 leu1–32 tsn1::kanMX6 (pSRS5)*	McFarlane, Bangor University
BP3345	*h⁻ ade6::tRNAGLU (2) his3-D1 ura4–18 lys1–37 leu1–32 tsn1::kanMX6 (pSRS5)*	McFarlane, Bangor University
BP3348	*h⁻ ade6::tRNAGLU (2) his3-D1 ura4–18 lys1–37 leu1–32 dcr1::kanMX6 (pSRS5)*	McFarlane, Bangor University
BP3349	*h⁻ ade6::tRNAGLU (2) his3-D1 ura4–18 lys1–37 leu1–32 dcr1::kanMX6 (pSRS5)*	McFarlane, Bangor University
BP3350	*h⁻ ade6-M210 ura4-D18 leu1-32 Mat1Msmt0 his2 tetR-tup11D70::ura4URA5::I-PpolCS-hph+ lys1::kanMX6-TATAcyc1-tetO7-spo5DSR Leu1::pDUAL-TATAcyc1-tetO7-3xFlag-I-Ppol-4xDSR*	P1807 Tamas Fisher lab, Heilderbergh
BP3355	*h⁻ ade6-M210 ura4-D18 leu1-32 Mat1Msmt0 his2 tetR-tup11D70::ura4URA5::I-PpolCS-hph+lys1::kanMX6-TATAcyc1-tetO7-spo5DSR/2Leu1::pDUAL-TetO7-TATAcyc-Flag-Ippol-4xDSR*	P2882 Tamas Fisher lab, Heilderbergh
BP3362	*h⁻ ade6::tRNAGLU (2) his3-D1 ura4–18 lys1–37 leu1–32 tsn1::kanMX6 dcr1::natMX6*	McFarlane, Bangor University

BP3364	*h¯ ade6::tRNAGLU (2) his3-D1 ura4–18 lys1–37 leu1–32 tsn1::kanMX6 dcr1::natMX6 (pSRS5)*	McFarlane, Bangor University
BP3365	*h¯ ade6::tRNAGLU (2) his3-D1 ura4–18 lys1–37 leu1–32 tsn1::kanMX6 dcr1::natMX6 (pSRS5)*	McFarlane, Bangor University
BP3377	*h¯ade6-M210 ura4-D18 leu1-32 Mat1Msmt0 his2 tetR-tup11D70::ura4ura5::I-PpolCS-hph+lys1::kanMX6-TATAcyc1-tetO7-spo5DSR Leu1::pDUAL-TATAcyc1-tetO7-3xFlag-I-Ppol-4xDSR tsn1::natMX6*	McFarlane, Bangor University
BP3380	*h¯ade6-M210 ura4-D18 leu1-32 Mat1Msmt0 his2 tetR-tup11D70::ura4 ura5::I-PpolCS-hph+ lys1::kanMX6-TATAcyc1-tetO7-spo5DSR Leu1::pDUAL-TATAcyc1-tetO7-3xFlag-I-Ppol-4xDSR tfx1::natMX6*	McFarlane, Bangor University
BP3381	*h¯ade6-M210 leu1-32his3-D1 trt1::his3+tsn1::kanMX6 iso 1*	This study
BP3382	*h¯ade6-M210 leu1-32his3-D1 trt1::his3+tsn1::kanMX6 iso2*	This study
BP3383	*h¯ade6-M210 leu1-32his3-D1 trt1::his3+tsn1::kanMX6 iso 3*	This study
BP3384	*h¯ade6-M210 leu1-32his3-D1 trt1::his3+tfx1::kanMX6 iso 1*	This study
BP3491	*h¯ ade6::tRNAGLU (2) lys1-37 tfx1::kanMX6*	This study
BP3493	*h¯ ade6::tRNAGLU (1) lys1-37 tfx1::kanMX6*	This study
BP3496	*h¯ ade6::tRNAGLU (1) lys1-37 dcr1::natMX6 tfx1::kanMX6*	This study

BP3498	*h⁻ ade6::tRNAGLU(2) lys-37 dcr1::natMX6 tfx1::kanMX6*	This study
BP3400	*h⁻ ade6::tRNAGLU (2) lys1-37 tfx1::kanMX6*	This study
BP3401	*h⁻ ade6-M26 ura4-D18 leu1-32 rnh1::kanMX6*	McFarlane, Bangor University
BP3405	*h⁻ ade6-M26 ura4-D18 leu1-32 rnh201::kanMX6*	McFarlane, Bangor University
BP3410	*h⁻ ade6-M26 ura4-D18 leu1-32 rnh1::kanMX6 rnh201::hph MX6*	McFarlane, Bangor University
BP3412	*h⁻ ade6-M26 ura4-D18 leu1-32 tfx1::natMX6 rnh1::kanMX6*	McFarlane, Bangor University
BP3414	*h⁻ ade6-M26 ura4-D18 leu1-32 tfx1::natMX6 rnh201::kanMX6*	McFarlane, Bangor University
BP3417	*h⁻ ade6-M26 ura4-D18 leu1-32 rnh201::kanMX6 tsn1::natMX6*	McFarlane, Bangor University
BP3419	*h⁻ ade6-M26 ura4-D18 leu1-32 rnh201::kanMX6 rnh1::natMX6*	McFarlane, Bangor University
BP3426	*h⁻ ade6-M26 ura4-D18 leu1-32 tsn1::kanMX6 rnh1::natMX6*	McFarlane, Bangor University
BP3429	*h⁻ ade6::tRNAGLU (1) his3-D1 ura4–18 leu1–32 lys1–37 tfx1::kanMX6 (pSRS5) iso 1*	This study

BP3430	*h¯ ade6::tRNAGLU (1) his3-D1 ura4–18 leu1–32 lys1–37 tfx1::kanMX6 (pSRS5). iso 2*	This study
BP3432	*h¯ ade6::tRNAGLU (2) his3-D1 ura4–18 leu1–32 lys1–37 tfx1::kanMX6.(pSRS5).*	This study
BP3434	*h¯ ade6::tRNAGLU (1) his3-D1 ura4–18 leu1–32 lys1–37 dcr1::natMX6 tfx1::kanMX6 (pSRS5).*	This study
BP3436	*h¯ ade6::tRNAGLU (2) his3-D1 ura4–18 leu1–32 lys1–37 dcr1::natMX6 tfx1::kanMX6. (pSRS5).*	This study
BP3450	*h¯ ade6-M26 leu1-32 trt1::his3+ tsn1::kanMX6 rnh201::natMX6*	This study
BP3451	*h¯ ade6-M26 leu1-32 trt1::his3+ tsn1::kanMX6 rnh1::natMX6 iso1*	This study
BP3452	*h¯ ade6-M26 leu1-32 trt1::his3+ tsn1::kanMX6 rnh1::natMX6 iso 2*	This study
BP3453	*h¯ ade6-M26 leu1-32 trt1::his3+ rnh201::natMX6*	This study
BP3454	*h¯ ade6-M26 leu1-32 trt1::his3+ rnh1::natMX6 iso 1*	This study
BP3455	*h¯ ade6-M26 leu1-32 trt1::his3+ rnh1::natMX6 iso 2*	This study
BP3456	*h¯ ade6-M26 leu1-32 trt1::his3+ tfx1::kanMX6 rnh201::natMX6 iso 1*	This study

BP3457	*h⁻ ade6-M26 leu1-32 trt1::his3+ tfx1::kanMX6 rnh201::natMX6 iso 2*	This study
BP3458	*h⁻ ade6-M26 leu1-32 trt1::his3+ tfx1::kanMX6 rnh1::natMX6*	This study
BP3459	*h⁻ ade6-M26 leu1-32 trt1::his3+rnh1::kanMX6 rnh201::natMX6 iso 1*	This study
BP3460	*h⁻ ade6-M26 leu1-32 trt1::his3+rnh1::kanMX6 rnh201::natMX6 iso 2*	This study
BP3461	*h⁻ ade6-M26 ura4-D18 leu1-32 rnh201::kanMX6 dcr1::natMX6 iso 1*	This study
BP3462	*h⁻ ade6-M26 ura4-D18 leu1-32 rnh201::kanMX6 dcr1::natMX6 iso 2*	This study
BP3469	*h⁻ ade6-M26 ura4-D18 leu1-32 rnh1::kanMX6 dcr1::natMX6 iso 1*	This study
BP3470	*h⁻ ade6-M26 ura4-D18 leu1-32 rnh1::kanMX6 dcr1::natMX6 iso 2*	This study
BP3471	*h⁻ ade6-M26 ura4-D18 leu1-32 rnh1::kanMX6 dcr1::natMX6 iso 3*	This study
BP3448	*h⁻ ade6-M26 ura4-D18 leu1-32 sen1::kanMX6*	McFarlane, Bangor University
BP3480	*h⁻ ade6-M26 ura4-D18 leu1-32 sen1::kanMX6 rnh201::natMX6*	This study

Table 2.4 Deletions of *S. pombe* gene by PCR method

Primer name	Sequence	Notes
Tfx1NatMX6-F	5′-TAT AGA CTT ATA CAT TTA TAC CTT CCA CAC GGC TTT GCT GAA TTG AGG ATA TTA TAA AAC TTT AAC CGA ATT TGC CAA ATC GGA TCC CCG GGT TAA TTA A -3′	Forward primer for the Nourseothricin^{R} cassette for *tfx1* replacement
Tfx1NatMX6-R	5′-ATT ATG ATT TTC AAA AGC TGC AAA ACA GAA AAA CTT TTA ATA AAC TAG TAA GGT GTC TGT CGA GAG CTG TCG ATC ATA TAT GAA TTC GAG CTC GTT TAA AC -3′	Reverse primer for the Nourseothricin^{R} cassette for *tfx1* replacement
Tsn1-Kan-F	5′-TTA TTT GCA TAC TGA AAA CATCAT TCG AAT ATC AAC ACT ACTCAA CAG CAT ACA TTA CAG ATTAAG TCG ACG GAT CCC CGG GTT AAT TAA-3′	Forward primer for the Kanamycin cassette for *tsn1* replacement
Tsn1-Kan-R	5′-ATA TTA AAA AAG CAA TTT TATCGG CTC AAT TTT AGT CAA GCGTAC AGC TGG CAA ATA AAT TGTTAG CAA TGA ATT CGA GCT CGT TTA AAC-3′	Reverse primer for the Kanamycin cassette for *tsn1* replacement
Dcr1NatMX6-F	5′-ACA TAT GCA TGT TTA TTT GAA TAG CTT AGG ATT CAT TAT TTT TTA AGA GAC AAA TTT CTC GTC AAT TGA ATG AAA CCT TCC GCC TTT ATT TTC TTT TTG ACG GAT CCC CGG GTT AAT TAA-3′	Forward primer for the Nourseothricin^{R} cassette for *dcr1* replacement
Dcr1NatMX6-R	5′-AAT ATC ACG AAA GGA TCC GTG CTT TGG AGA CCC AAA TTG AAA GTT TGA AAA GTT ACA AGG GCC GCG GTC ATA AAA AAT GAA ATA CTG TAT ATT TCA AGT CGA ATT CGA GCT CGT TTA AAC-3′	Reverse primer for the Nourseothricin^{R} cassette for *dcr1* replacement

Dcr1-Kan-F	5′-ATA GCT TAG GAT TCA TTA TTT TTT AAG AGA CAA ATT TCT CGT CAA TTG AAT GAA ACC TTC CGC CTT TAT TTT CTT TTT GA C GGA TCC CCG GGT TAA TTA A-3′	Forward primer for the Kanamycin cassette for *dcr1* replacement
Dcr1-Kan-R	5′-GCT TTG GAG ACC CAA ATT GAA AGT TTG AAA AGT TAC AAG GGC CGC GGT CAT AAA AAA TGA AAT ACT GTA TAT TTC AAG TCG AAT CGA GCT CGT TTA AAC-3′	Reverse primer for the Kanamycin cassette for *dcr1* replacement
Rnh1NatMX6-F	5′TTGCAAAGTTTTGGGAAAAACTC CCAAGTTTTACTAAGTTTTACTAT TTTAAAGCTATTTTGAATCTTCGC ATTACGAACGGATCCCCGGGTTA ATTAA-3′	Reverse primer for the Nourseothricin^{R} cassette for *rnh1* replacement
Rnh1NatMX6-R	5′GAGTAGACGAAAATTATACGGC AAATTTCAAAAGAATGTACCTATA TCCATTTTTTACAGCGCTCATCAT AGATGACCATGAATTCGAGCTCGT TTAAAC-3′	Forward primer for the Nourseothricin^{R} cassette for *rnh1*replacement
Rnh201NatMX6- F	5′TATTTTTTTATTCAGTTTTTGAGC CAAATATTAGAAGTACTCTGATAA TTCTTTAAAAGATACAAAGCAGC AATCTCAACCGGATCCCCGGGTTA ATTAA-3′	Reverse primer for the Nourseothricin^{R} cassette for *rnh201* replacement
Rnh201NatMX6- R	5′ATTTTAAGCATAAATGTAAATTC GTATCACTCTCACAATTAGTCTTA GGCAAAAGTAGTGACAGATATAG TAACTAAAGAATTCGAGCTCGTTT AAAC-3′	Forward primer for the Nourseothricin^{R} cassette for *rnh201*replacement

2.4 Phenol/chloroform purification of DNA

An equal amount of phenol and chloroform and 0.1 M of NaCl in a 1:1 ratio was added to an Eppendorf tube containing the DNA mixture. The DNA mixture in the tube was then spun down for 15 minutes at 12,000 r.p.m (microcentrifuge) and the top layer was transferred into a new sterile Eppendorf tube and 100% ethanol was added. The cells were kept at -80ºC for 1 hour to precipitate the DNA. The DNA was centrifuged for 30 minutes at 4ºC at 12,000 *g,* the supernatant was removed and the pellet was washed with 70% ethanol before centrifugation for 15 minutes at 12,000 *g*. Then, the pellet was left to air dry on the bench for 5 minutes, before being resuspended in 40 µl of 1x TE buffer and stored at -20ºC.

2.5 Transformation of *S. pombe* cells

2.5.1 Lithium acetate (LiAc) transformation of *S. pombe*

A single colony of *S. pombe* strain was inoculated into 5 ml of YEL containing 200 mg/L of adenine, and incubated overnight at 30ºC with shaking. The following day, 100-200 µL of the culture was inoculated in 100 mL of YEL and incubated overnight at 30ºC. The cells were centrifuged for 5 minutes at 3,000 *g* in a microcentrifuge at room temperature and washed with sterile distilled H_2O, before they were spun down at 3,000 *g* for 5 minutes. The cells were transferred into sterile Eppendorf tubes after resuspension in 1 mL of sterile distilled H_2O and centrifuged at 6000 r.p.m in a microcentrifuge for 1 minute. Then, the pellet was washed with 1 mL of 0.1 M lithium acetate (LiAc/1X TE). After that, the cells were resuspended in LiAC/TE to achieve a concentration of 2 x 10^9 cells/mL. Next, 100 µL of the cells was transferred to a new sterile Eppendorf tube, with 2 µL of sheared herring testis DNA and 10 to 20 µg of DNA cassette. The suspensions were incubated for 10 minutes at room temperature, and 260 µL of 40% PEG/LiAC/TE (pH 7.3) was gently added. The mixture was incubated at 30ºC in a water bath for 1 hour, and then 43 µL of DMSO was added. The cells were heat shocked at 42ºC for 5 minutes and then left at room temperature for 10 minutes to cool. The cells were washed with 1 mL sterile distilled H_2O and spun for 3 minutes at 3,000 r.p.m in a microcentrifuge. The

supernatant was resuspended in 0.5 mL sterile distilled H_2O and 100 µL of the mixture was plated onto YEA media plates before incubation at 30ºC for 18 hours. Finally, the plates were replicated onto YEA containing the appropriate antibiotic drug then incubated for 3-4 days at 30ºC.

2.5.2 Plasmid transformation

Lithium acetate (LiAC) was used for the transformation of *S. pombe* strains with plasmids as described in Section 2.5, but only using 1 µg of DNA plasmid. Cells were plated directly onto selective NBA. Then, the plates incubated at 30ºC for 2-4 days.

2.6 Extraction of *S. pombe* genomic DNA

One colony of the appropriate strain was selected and inoculated into 5 mL of YEL media containing 200 mg/L of adenine supplement, before incubation with shaking at 30ºC overnight to saturation. Cells were centrifuged for 5 minutes at 3,000 *g* and the pellet transferred into sterile Eppendorf tubes, before washing with sterile distilled water and spun at 3,000 *g* for 1 minute. Then, 200 µL of chloroform/ phenol was added, along with 200 µL of lysis buffer (containing 1 mL Triton X-100, 0.5 mL of TE100X, 5 mL of 1 M NaCl and 5 mL 10% SDS) and 0.3 g of acid washed beads. A Bead Beater (FastPrep120, ThermoSavant) disrupted the cells for 30 seconds and they were centrifuged for 15 minutes at 12,000 r.p.m (microcentrifuge). The top layer of the solution was aspirated and transferred into a new tube, before adding 1 mL of 100% ethanol. The mixture was left for 1 hour at -80ºC, and then spun for 12 minutes at 12,000 *g*. The pellets were washed with 1 mL of 70% ethanol and air dried at room temperature for 10 minutes. Finally, the pellet was resuspended in 100 µL of 1X TE buffer or water, then left overnight at room temperature.

2.7 PCR screening to confirm deletion gene

After the genomic DNA extraction of the candidate knockout strain, appropriate primers were designed for target genes and the knockout cassettes. Table 2.5 shows all the oligonucleotide sequences used in these assessments. The 25 µL PCR reaction contained

12.5 µL of MyTaq Red Mix (BioLine), 10.5 µL of sterile distilled water, 0.5 µL of 20 ng/µL of forward and reverse primers, and 1 µL of the extracted genomic DNA.

The programme for PCR was set as follows: denaturation at 96°C for 1 minute, then 35 cycles of 1 minute at 96°C, 30 seconds at X°C, and 30 seconds at 72°C, followed by a 5 minutes extension at 72°C. The annealing temperature (X) was variable according to the primer sequence. The PCR products were electrophoresed in 1% agarose gel to determine the product size.

Table 2.5 PCR primers Sequence used in this study

Primer name	Sequence	Notes
Tfx1 check-F	5′-CAAATAGTCATCTTGATTTGC-3′	Upstream of *tfx1* ORF
Tfx1 check-R	5′-TCTAACATATAGAAAGCAGCG-3′	Downstream of *tfx1* ORF
Tfx1-int-F	5′-ATAAGAGGGAGAAAATTATTC G-3′	Forward primer inside *tfx1*
Tfx1-int-R	5′-CTCCTCGGGAGGAGTTGC -3′	Reverse primer inside *tfx1*
Tsn1 check-F	5′-GAT CTAAACAACCCAAGCG-3′	Upstream of *tsn1* ORF
Tsn1 check-R	5′-GCATTCATCATAGGACTGCC-3′	Downstream of *tsn1* ORF
Tsn1-int-F	5'-AAACTGACTGCAGAGGTC G-3'	Forward primer inside *tsn1*
Tsn1-int-R	5'-GAACACAGAGATAGTACTGC- 3'	Reverse primer inside *tsn1*
NatMX6-F	5′-CATGGGTACCACTCTTGACG- 3'	Forward primer inside Nourseothricin^{R} cassette
NatMX6-R	5′-CTCAGTGGCAAATCCTAACC- 3'	Revers primer inside Nourseothricin^{R} cassette
KanMX6-F	5′-CGGATGTGATGTGAGAACTG-3′	Forward primer inside kan R cassette

KanMX6-R	5′-CAGTTCTCACATCACATCCG-3′	Reverse primer inside kan R cassette
Dcr1 check-F	5′-AGTATTCTGCTCGTGTGATTG-3	Upstream of *dcr1* ORF
Dcr1 check-R	5′-TGATTGAAACTCGAGATGCTTTG-3′	Downstream *dcr1* ORF
Dcr1-int-F	5′-ATTCGACGAATGTCATCATGC-3′	Forward primer inside *dcr1*
Dcr1-int-R	5′-AGACGATATCATCAGTCACAG-3′	Reverse primer inside *dcr1*
Act1-F	5′-TGCACCTGCCTTTTAATGTTG -3′	Forward primer inside *act1*
Act1-R	5′-TGGGAACAGTGTGGGTAACA-3′	Reverse primer inside *act1*
Trt1-F	5′-CCGAACACCATACCCCCAAA-3′	Forward primer inside *trt1*
Trt1-R	5′-CCTTTAGGAGACGTTTGGGC-3′	Reverse primer inside *trt1*
Rnh1-check-F	5′-CAGTCGCGGAGATCTAACTAGC-3′	Upstream of *rnh1*ORF
Rnh1-check-R	5′-GCATTATGCAAAACGAGAACAA-3′	Downstream of *rnh1* ORF
Rnh1-int-F	5′-AGGGATGAGGCGTCGGATCA-3′	Forward primer inside *rnh1*
Rnh1-int-R	5′-TTTGCTCTTCCCCAGCCAAC-3′	Reverse primer inside *rnh1*
Rnh201-check-F	5′-GATTGCTAGGAGATGACTCGCT-3′	Upstream of *rnh201* ORF
Rnh201-check-R	5′-AAGTCTCATGCCAGCCCATATTT-3′	Downstream of *rnh201* ORF
Rnh201-int-F	5′-CGAATCCCGCAAAATCGAAT-3′	Forward primer inside *rnh201*
Rnh201-int-R	5′-GAAGCTAAACTCACGATGGG-3′	Reverse primer inside *rnh201*

2.8 Spot tests for drug sensitivity

One single colony of the *S. pombe* strain was inoculated in 5 mL of YEL media containing 200 mg/L of adenine supplement and incubated overnight with shaking at 30°C. The following day, a light microscope (40X) was used to count the cells using a haemocytometer. The cells were resuspended with sterile distilled water to achieve a concentration of 5 x 10^6 cells/mL, and then four serial dilutions were prepared, before 10 µL of the cell suspension was added to the haemocytometer for counting. Then, 10 µL of each dilution was spotted onto YEA plates and the YEA media containing adenine with the test drug (see Table 2.1 for drug concentrations). YEA plates containing adenine and replacing the drugs with sterile dH_2O or DMSO were used as controls. Finally, the plates were incubated at different temperatures as required.

2.9 Storage of *S. pombe* strains

For long-term storage, a single colony was inoculated in 5 mL of appropriate liquid media and incubated overnight with shaking at 30°C until saturation occurred. Then, 700 µL of the cultures was added to glycerol and vortexed to a final concentration of 30%, before storage at -80ºC.

2.10 Ultraviolet (UV) irradiation of *S. pombe*

The cell serial dilutions prepared in Section 2.8 were spotted (10 µL) onto YEA plates and allowed to dry, before exposure to different doses of UV irradiation (CL-1000 UV cross linker) as: 50, 70, 80 and 100 J/m^2. Finally, plates were incubated at different temperatures as required.

2.11 Fluctuation test

The recombination frequency assay required a fluctuation test using the pSRS5 plasmid, which carries *ade6-ΔG1483,* an *ade6* mutant allele as a recombination marker, generated by removal of a guanine at 1482 position of nucleotide inside the ORF of the *ade6* gene (Pryce et al., 2009). One colony of appropriate *S. pombe* strain was inoculated into 5 mL of selective liquid medium and then incubated at 30°C overnight. A dilution of the culture was plated onto selective solid medium and incubated for 4 days at 30°C until small colonies were observed. Seven whole small, micro colonies were selected and

inoculated independently into 5 mL of selective liquid media and incubated at 30°C for 2 days. Then, serial dilutions were prepared and plated onto plates containing YE+guanine (100 g/mL final concentration of guanine 20 mg/ml from and melted in 0.35 M of NaOH/ddH_2O stock, adapted the final plate pH to 6.5 with 1 M HCl) to count the adenine prototroph. Higher concentration dilutions (10^{-3} to 10^{-5}) were added to YEA plates for cell viability counts and the plates were incubated for 3 days at 30°C before counting. The experiment was performed in triplicate, with the mean of the three independent median values used to calculate the recombination frequency of each strain.

2.12 Measurement of I-PpoI cleavage efficiency

One colony of appropriate *S. pombe* strain was inoculated into 5 mL of YEL media and incubated at 30ºC overnight. The following day, the cells were diluted to an $\mathbf{OD_{600}}$ of 0.5 in 25 mL of YEL media and incubated overnight at 30ºC. On the third day, the endonuclease I-PpoI was induced for 2 hours by addition of 20 mg/ml of ahTET (anhydrotetracycline, Sigma-Aldrich), then incubated at 30ºC. Pre- (OFF) and post- (ON) induction, aliquots were taken at indicated time points (-ahTET, 2, 4 and 8 hours) and then the pellets were frozen at -80 ºC. The total genomic DNA was extracted for qPCR and the whole cell protein extracted for western blotting.

2.13 Quantitative polymerase chain reaction (qPCR)

25 µl of qPCR reactions were as follows: 12.5 µl of GoTaq® RT-qPCR Master reagents (Promega #A6001), 0.5 µl of forward and reverse primers, 6.5 µl of dH_2O and 1 µl of DNA. They were placed in each well of plate (Bio-Rad #9655) in triplicate. The reaction amplification was programmed as follows: pre-denaturation at 95°C for 10 minutes, denaturation at 95°C for 40 cycles for 15 seconds, annealing at 60°C for 1 minute, then 60°C for 5 seconds, followed by extension for 5 seconds at 95°C. The primers used are listed in Table 2.5.

2.14 Yeast TCA whole cell protein extraction

For whole cell protein extracts, pellets of appropriate *S. pombe* strains were thawed on ice, and then 250 µl of glass beads (Sigma-G8772) were added and resuspended in 250 µl of 20% TCA. The tube was vortexed at max speed for 30 seconds in a Bead Beater to rupture the cells. After that, the bottom of the Ependroff tube was pierced carefully with a red-hot 22 needle and placed into a new sterile Ependroff tube. The tube was spun at 6,000 r.p.m (microcentrifuge) for 2 minutes at 4ºC. In this step, the bottom of the Ependroff tube should contain the lysate and precipitate, while the beads should remain at the top of the Ependroff tube. Then, 300 µl of 5% TCA was added to the top tube to wash the beads, before spinning at 6,000 r.p.m (microcentrifuge) for 2 minutes at 4ºC. The top tube was discarded, 700 µl of 5% TCA was added and the tube centrifuged at 4ºC for 10 minutes at 14.000 r.p.m (microcentrifuge). Then the supernatant was discarded, and the pellet was washed with 750 µl of 100% EtOH and spun at 14.000 r.p.m (microcentrifuge) for 10 minutes at 4ºC. Again, the supernatant was discarded, and the pellet resuspend in 40 µl of 1 M Tris CI, pH 9.4 and 80 µl of Laemmli loading buffer (Sigma-S3401). The cell lysate was stored at -80ºC until further use.

2.15 Western blot of *S. pombe* cells

The protein sample was heated for 5 minutes at 95ºC, then 20 µl of the sample was loaded in 1.0 mm X12 well BoltTM 4–12% Bis-Tris Plus Gel (Thermo Scientific #NW04122BOX) with 3 µl of the Precision Plus ProteinTM Dual Color Standard (Bio-Rad #161-0374) to estimate the protein molecular weight. The gel was run for 1 hour at 100 V. The protein was transferred to a PVDF membrane using a Trans-Blot® TurboTM RTA PVDF Transfer Kit, Mini size (7 x 8.5cm) (Cat. #170-4274 Bio-Rad). The transfer buffer was prepared by mixing 200 mL of Trans-Blot® TurboTM 5x transfer buffer (Cat. #10026938 Bio-Rad), 600 mL of sterile distilled H_2O and 200 mL of ethanol.

The membrane was activated in methanol for 5 minutes, and then placed in sterile dH_2O until used. Two sheets of filter paper were thoroughly wetted with transfer buffer and the blot sandwiched as following: one sheet of filter paper, PVDF membrane, the protein gel and another one sheet of filter paper. Then, transfer of protein to the membrane utilised

the Trans-Blot®Turbo TM transfer system and mixed MW protein transfer settings. After this, the membrane was blocked overnight on a shaker in 1X PBS containing 5% skimmed powdered milk at 4°C. Next, the membrane was probed with primary antibody (in Table 2.6) diluted 1:1000 in (1X PBS/ 5% milk / 0.1% Tween) and incubated for an hour on a shaker at room temperature, followed by three washes for 10 minutes each with (1X PBS/0.1% Tween). Then, the membranes were probed with the secondary antibody (in Table 2.6) diluted 1:3000 in (1X PBS/ 5% milk / 0.1% Tween), incubated for an hour on a shaker at room temperature, followed by three washes for 10 minutes each with (1X PBS / 0.1% Tween). The membrane was wetted in 1 ml of ECL Plus (Sigma) for 5 minutes. In a dark room, the membrane was transferred into the cassette with the film and exposed for 10 to 15 minutes, before developing the film. Finally, the membrane was stored in 1X PBS in a refrigerator. The primary and secondary antibodies used are listed in Table 2.6.

Table 2.6 Primary and secondary antibodies concentrations for western blot analyses

Antibodies	Company	CAT #	Host	Application	Dilution
Anti-Flag-DDDDK tag	Abcam	Ab49763	Mouse	WB	1:1000
Anti-Beta Actin	Abcam	Ab8224	Mouse	WB	1:3000
Anti-Mouse	Cell signalling	7076S	Mouse	WB	1:3000

Chapter 3: Results

Tsn1, but not Tfx1, suppresses genome instability in the absence of Dcr1

3.1 Introduction

3.1.1 Tsn1, but not Tfx1, has a function in the DNA damage response in the absence of Dcr1.

Chromosome translocations constitute well-established signs of cancer cells and usually occur non-randomly within genomes (Burman et al., 2015; Nambiar & Raghavan, 2011). Translocations might occur when broken ends of two non-homologous chromosomes combine (O'Connor, 2008). Translin was identified in humans as a protein that binds to chromosomal translocations breakpoint junctions and it was implicated in formation of chromosomal translocation in human leukaemia cells (Wu et al., 1997). The association of Translin with breakpoint junctions has resulted in the suggestion it is required for recombination mechanisms, although to date no direct evidence has been put forward for a role in recombination (Jaendling & McFarlane, 2010). In contrast with the proposal of a role in recombination, it has been established that there is a lack of any defects in *S. pombe* Translin-null mutants during recombination processes, including the recovery from DNA damage. Additionally, *tfx1Δ* (Trax) mutants of in *S. pombe* have been found to be similar to *tsn1Δ* (Translin) mutants, as *tfx1Δ* single mutants do not have overt defaults in recombinogenic processes (Jaendling et al., 2008). Despite lack of evidence showing a role for Translin in the control of genome stabilisation, there remains a need to further question a direct role for Translin in DNA damage recovery which could explain the association with translocation breakpoint junctions.

The recent finding that in *S. pombe,* Dcr1 has an RNAi-independent function in DNA damage recovery (Castel et al., 2014; Ran et al., 2015), and the links between human Dicer and Translin/Trax (Asada et al., 2014), led us to hypothesis a possible redundant role for Tsn1 and/or Tfx1 with Dcr1. To address this hypothesis, double mutants of *dcr1*Δ *tfx1*Δ *and dcr1*Δ *tsn1*Δ were constructed and phenotypes of these mutants were analysed to determine whether Tsn1 and/or Tfx1 have function in regulation of genome stability in the absence of Dcr1.

3.2 Results

3.2.1 Spot test sensitivity to TBZ

Microtubules mediate spindle formation and function. When microtubule function is compromised by either drugs or mutations it leads to compromising mitotic events. Thiabendazole (TBZ), a microtubule-destabilizing drug, has been found to play a role to inhibit microtubule function (Ahringer, 2003; Sadeghi et al., 2015). Mutations which causes disruption to distinct aspects of genome maintenance pathways can cause sensitivity to TBZ. In *S. pombe, dcr1*Δ cells are sensitive to the TBZ (see Figure 3.1). The sensitivity of *dcr1*Δ cells to TBZ is attributed to chromosome mis-segregation (Macrae et al., 2006). Previous work from the McFarlane group demonstrated that mutation of *tfx1Δ* (Trax), but not *tsn1Δ* (Translin), suppressed the TBZ sensitivity of an *ago1Δ* mutant, defective in RNAi (Gomez-Escobar et al., 2016). Extending this, unpublished work, the McFarlane group demonstrated that both *tfx1Δ* and *tsn1Δ* mutants increased the sensitivity of a *dcr1Δ* mutant to TBZ. These findings demonstrated a clear distinction in the biological roles of Dcr1 and Ago1 in genome maintenance and suggest a redundancy of function between Tfx1/Tsn1 and Dcr1, but not Ago1. To confirm these findings, we carried out spot tests on *dcr1*Δ *tfx1*Δ *and dcr1*Δ *tsn1*Δ double mutants on TBZ. Double mutants made in this study were constructed by sequential gene replacement (i.e. *de novo*). This approach was used rather than using genetic crosses as when Tsn1 and Tfx1 mutants undergo through meiosis, none mendelian segregation patterns are observed.

The strains employed were constructed by co-workers in the lab, but the strains used in the spot tests shown were subjected to PCR verification of mutation status (Appendix Figures 1, 2 and 3). The results showed that the *dcr1*Δ *tfx1*Δ double mutant was slightly more sensitive to TBZ compared to the *dcr1Δ* single mutant (Figure 3.1 A). The *dcr1*Δ *tsn1Δ* double mutant was considerably more sensitive to TBZ compared to both the single the *dcr1*Δ mutant and the *dcr1*Δ *tfx1*Δ double mutant, indicating a greater requirement for Tsn1, than Tfx1, and a functional distinction between Tsn1 and Tfx1 (Figure 3.1). As shown previously, *tfx1*Δ and *tsn1Δ* single mutants show no sensitivity to TBZ. These

phenotypes were observed at both 30°C and 33°C (Figure 3.1). Therefore, the results indicate that Tfx1 and Tsn1 are needed for chromosomes stability when Dcr1 is absent.

During the course of these studies it was noted that in both *dcr1Δ* single mutant and the *dcr1*Δ *tsn1Δ* double mutant colonies would grow through the spot test on TBZ. This is best illustrated by the example shown in Figure 3.1 C. This appears to show suppressor formation in these backgrounds, which was not as apparent in the *dcr1*Δ *tfx1*Δ background, the reasons for this are unclear. Identifying the genetic differences of these suppressors (e.g., by whole genome sequencing) would be highly informative and might give insight into the mechanistic roles of Tsn1. Further studies of this type, however, are beyond the scope of this current study.

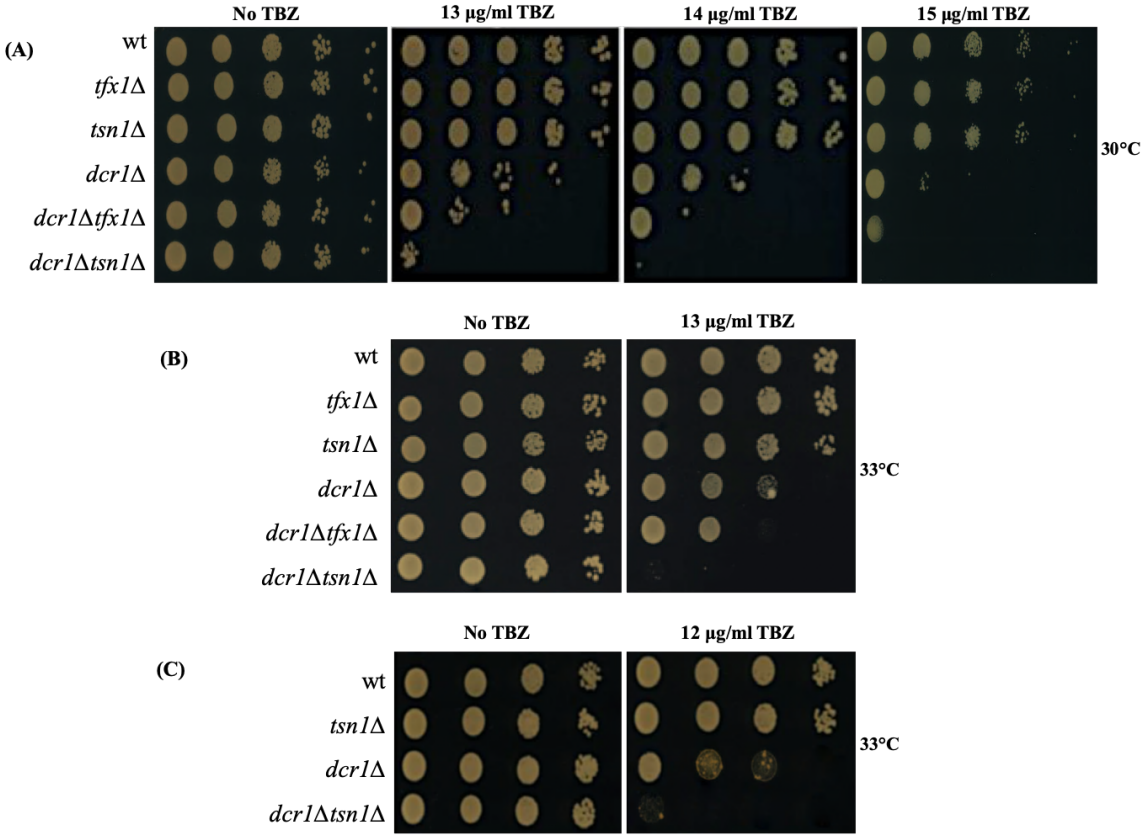

Figure 3.1 Tsn1, but not Tfx1, is required for the response to TBZ in the absence of Dcr1. *S. pombe* mutants were diluted (10-fold serial dilution left to right) and spotted onto YEA media contain different concentration of TBZ. (A) The data displayed, the single mutant *dcr1*Δ showed increased sensitivity to TBZ compared with the WT. In addition, the double mutants *dcr1Δ tfx1Δ* show increased sensitivity to TBZ compared with the single mutant *dcr1*Δ. Hypersensitivity to the TBZ was displayed by the double mutant *dcr1Δ tsn1Δ* compared with the *dcr1*Δ single mutant and the *dcr1Δ tfx1Δ* double mutant. The plates were incubated 3 days at 30°C. (B) Phenotypes are maintained at 33°C. (C) The *dcr1*Δ single mutant and the *dcr1*Δ *tsn1*Δ double mutant displayed a suppressor development at 33°C.

3.2.2 Sensitivity spot tests to investigate whether the Tsn1 and Tfx1 have roles in the DNA damage response in the absence of Dcr1.

Given that Dcr1 has been implicated in the maintenance of genome stability via an RNAi independent pathway (Castel et al., 2014), the TBZ data provoked the question of whether Tfx1 and Tsn1 function in DNA damage response in the absence of Dcr1. This prompted us to investigate the sensitivity of the *dcr1*Δ *tsn1*Δ and *dcr1*Δ *tfx1*Δ double mutants to DNA damaging agents. Spot tests were carried out using a range of DNA damage agents. The *rad3-136* mutant strain was used as a control (checkpoint defective). The DNA damage agents tested in this study included phleomycin, which is responsible for generation of DNA double-strand breaks (Figure 3.2); hydroxyurea (HU), as a DNA replication inhibitor (Figure 3.3); ultraviolet irradiation (UV), which induces multiple adducts (Figure 3.4); methyl methanesulphonate (MMS), a DNA alkylating agent (Figure 3.5); mitomycin C, a potent DNA crosslinker (Figure 3.6) and CPT, a topoisomerase inhibitor (Figure 3.7). The *dcr1*Δ single mutant showed a mild sensitivity to HU (Figure 3.3), consistent with a role in suppressing DNA replication transcription conflicts (Castel et al., 2014), but little or no notable sensitivity to other agents tested. In contrast to TBZ, the *tfx1*Δ *dcr1*Δ double mutant exhibited an almost identical phenotypic response relative to the *dcr1*Δ single mutant, with no notable increase in sensitivity in response to any agent. However, for the *tsn1*Δ *dcr1*Δ double mutant, there was a sensitivity increase relative to the *dcr1*Δ single mutant and the *tfx1*Δ *dcr1*Δ double mutant in response to HU, phleomycin and UV. The *dcr1*Δ *tsn1*Δ double mutant did not show any sensitivity increase in comparison with the *dcr1*Δ single mutant or WT in response to MMC, MMS, and CPT. These data indicate that Tsn1 but not Tfx1 is needed in the DNA damage recover response when Dcr1 is absent, for some types of DNA damage.

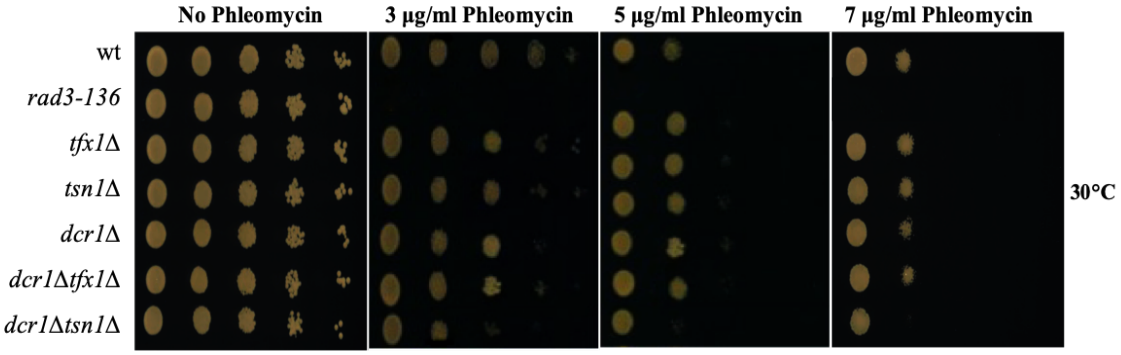

Figure 3.2 Tsn1, but not Tfx1, is required for the response to Phleomycin in the absence of Dcr1.

S. pombe mutants were diluted (10-fold serial dilution left to right) and spotted onto YEA media contain different concentration of Phleomycin. *rad3-136* was used as a positive control. The *dcr1Δ tsn1Δ* double mutant show increased sensitivity to Phleomycin compared with the *dcr1*Δ single mutant, but the *dcr1Δ tfx1Δ* double mutant show no increased sensitivity compared with the *dcr1*Δ single mutant. The plates were incubated 3 days at 30°C.

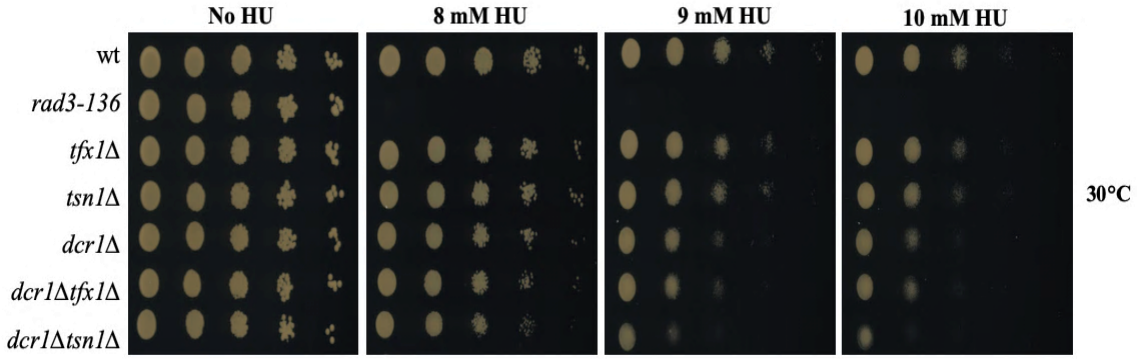

Figure 3.3 Tsn1, but not Tfx1, is required for the response to HU in the absence of Dcr1.
S. pombe mutants were diluted (10-fold serial dilution left to right) and spotted onto YEA media contain different concentration of hydroxyurea (8 mM, 9 mM and 10 mM HU). *rad3-136* was used as a positive control. The *dcr1Δ tsn1Δ* double mutant showed increased sensitivity to HU in 9 mM and 10 mM concentrations compared with the *dcr1*Δ single mutant but the *dcr1Δ tfx1Δ* double mutant show no sensitivity compared with the *dcr1*Δ single mutant. The plates were incubated 3 days at 30°C.

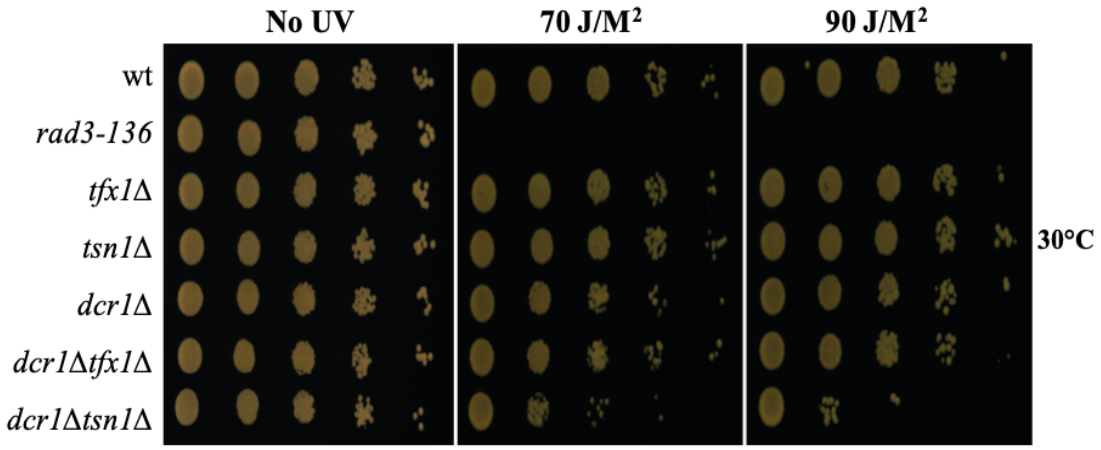

Figure 3.4 Tsn1, but not Tfx1, is required for the response to UV in the absence of Dcr1.
S. pombe mutants were diluted (10-fold serial dilution left to right) and spotted onto YEA media and then exposed to different doses of UV irradiation. *rad3-136* was used as a positive control. The *dcr1Δ tsn1Δ* but not *dcr1Δ tfx1Δ* double mutant showed increase sensitivity to the UV compared with the *dcr1*Δ single mutant and the WT. The plates were incubated 3 days at 30°C.

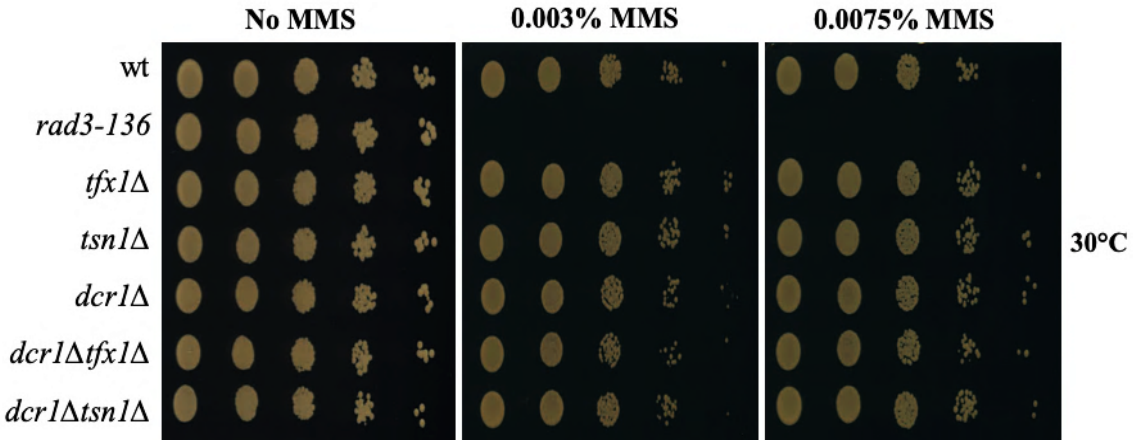

Figure 3.5 Sensitivity spot test of Methyl methane sulfonate (MMS).
S. pombe mutants were diluted (10-fold serial dilution left to right) and spotted onto YEA media contain different concentration of MMS (0.003% and 0.0075% MMS). *rad3-136* was used as a positive control. The *dcr1Δ tfx1Δ* and *dcr1Δ tsn1Δ* double mutant show no sensitivity to MMS compared with the *dcr1*Δ single mutant. The plates were incubated 3 days at 30°C.

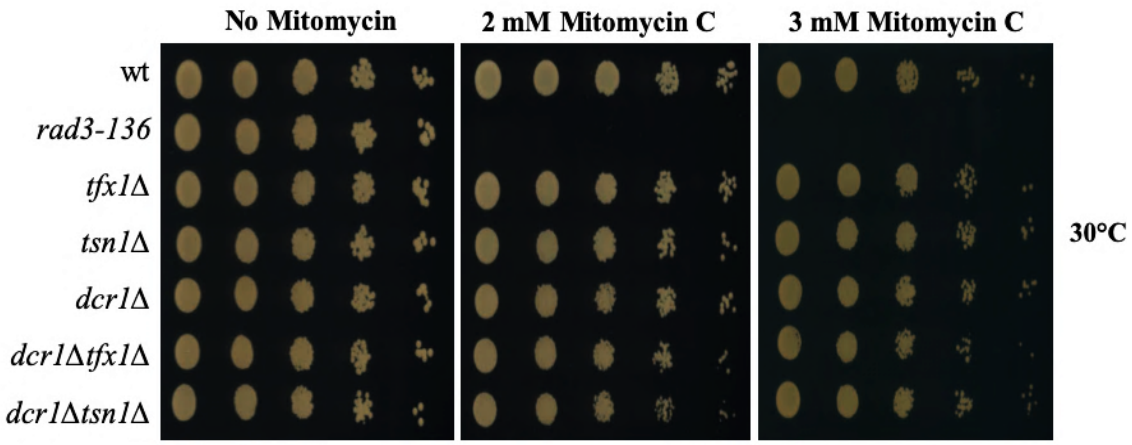

Figure 3.6 Sensitivity spot test of Mitomycin C (MMC).
S. pombe mutants were diluted (10-fold serial dilution left to right) and spotted onto YEA media contain different concentration of Mitomycin C (2mM and 3mM MMC). *rad3-136* was used as a positive control. The *dcr1Δ tfx1Δ* and *dcr1Δ tsn1Δ* double mutant show no sensitivity to Mitomycin C compared with the *dcr1*Δ single mutant. The plates were incubated 3 days at 30°C.

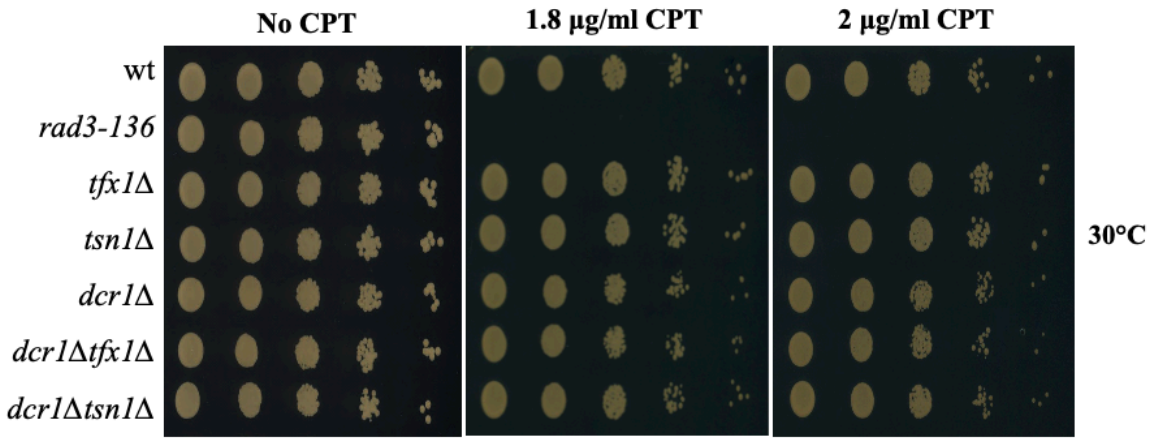

Figure 3.7 Sensitivity spot test of Camptothecin (CPT).
S. pombe mutants were diluted (10-fold serial dilution left to right) and spotted onto YEA media contain different concentration of CPT (1.8 µg/m and 2 µg/m CPT). *rad3-136* was used as a positive control. The *dcr1Δ tfx1Δ* and *dcr1Δ tsn1Δ* double mutant show no sensitivity to CPT compared with the *dcr1*Δ single mutant. The plates were incubated 3 days at 30°C.

3.2.3 A role for Tsn1 in inter-molecular recombination

The data shown in Section 3.2.2. demonstrates a role for Tsn1, but not Tfx1, in response to some DNA damaging agents in the absence of Dcr1. This was not observed for *tsn1Δ ago1Δ* double mutants (Macfarlane lab, unpublished data). This suggests the Tsn1 function potentially relates to Dcr1 RNAi-independent function in removing stalled RNA polymerase II and associated RNA: DNA hybrids from the genome to prevent transcription to replication conflicts (Castel et al., 2014). If this were the case, this would link Tsn1 function in *S. pombe* to prevention of transcription-replication conflicts, which can drive recombination initiation. This would offer an account for the link between Translin and chromosome breakpoint junctions. *S. pombe* offers a genetically tractable system in which to test recombination associated with replication-transcription conflicts. Previously, the McFarlane Group developed a recombination assay which measures recombination frequency at a specific locus, the *ade6* locus on chromosome III (Pryce et al., 2009). DNA replication occurs through the *ade6* locus largely from one direction only (Figure 3.8A). tRNA genes are known to form barriers to DNA replication and have been associated with sites of genomic rearrangements (McFarlane & Whitehall, 2009). tRNAs are transcribed by RNA pol III, but Castel and colleagues recently demonstrated that RNA pol II also transcribes the opposite strand in tRNA genes in *S. pombe*, the role of this is currently unclear, but mutation of *dcr1*Δ results in accumulation of RNA pol II (and possibly RNA:DNA hybrids) at tRNA genes (Castel et al., 2014). The recombination system developed by Pryce and co-workers involves the insertion of a tRNA gene (in this case $tRNA^{GLU}$) into the *ade6* gene open reading frame, thus generating an adenine auxotroph (Figure 3.8A). The $tRNA^{GLU}$ was inserted in *ade6* in two distinct orientations, ori1 and ori2, in independent strains, thus permitting the assessment of any replication barrier polarity influences, due to DNA replication being unidirectional through this locus. A second *ade6* allele, *ade6-ΔG1483*, carries a point mutation at a position within *ade6* that is distinct from the $tRNA^{GLU}$ insertion site, thus, recombination between the plasmid borne allele and the chromosomal tRNA gene insertion allele can generate a gene conversion event to give a wild-type *ade6* sequence, and thus prototrophy, which can be measured. The frequency of restoration of the wild-type *ade6* is a quantitative measure of recombination frequency (Figure 3.8B). Here we used this

system to assess whether Tsn1 contributes to suppressing replication-associated recombination in the absence of Dcr1.

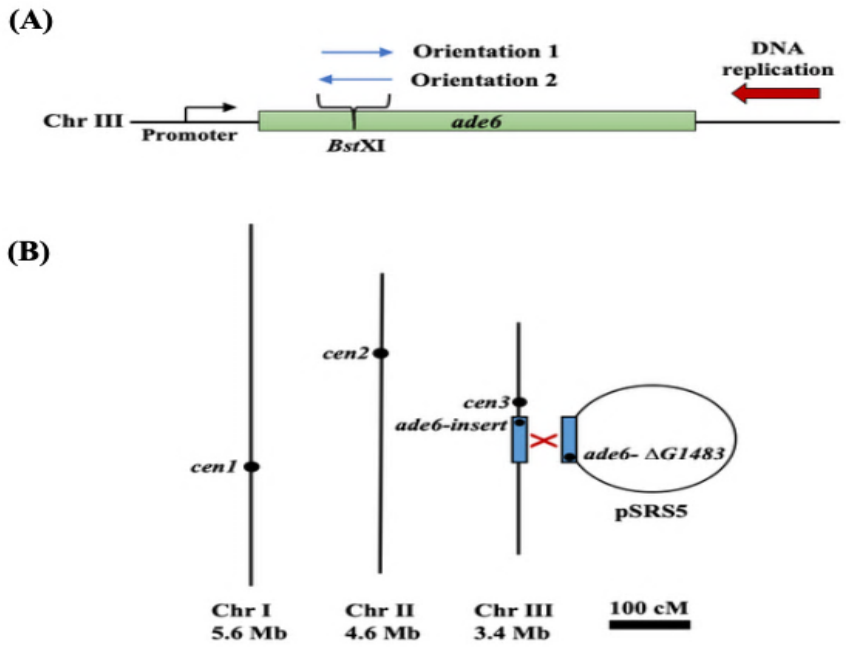

Figure 3.8 Illustration of the schematic of the plasmid-by-chromosome intermolecular recombination system which was used to measure a recombination frequency at *ade6*::*tRNA*^{GLU}

(A) An independent insertion of *tRNA*^{GLU} in orientation 1 and 2, as indicated by the blue arrows above the *Bst*XI site, into the open rectangle, *ade6* ORF at the *Bst*XI site. *ade6* is expressed from left to right with the promoter being shown by the angular arrow. The large red arrow indicates the principal direction in which the replication of DNA occurs. There is an anticipation that RNA Pol III and DNA replication collision will occur head-to-head in orientation 1. In comparison to orientation 2, which anticipates that head-to-tail collisions between the replication machinery and Pol III and will be generated. For RNA Pol II the replication fork in orientation 1, a head-to-tail collision. While in orientation 2, a head-to-head collision between RNA Pol II and the replication fork.

(B) The vertical lines indicate three chromosomes of the *S. pombe*. The *ade6* locus is present in Chr III, which is the smallest chromosome, where *tRNA*^{GLU} was inserted (as shown in A). The pSRS5 plasmid is represented by a large open circle. This circle carries the second *ade6* allele (*ade6-ΔG1483*). The point mutation is at the 3′ end of *ade6* which is also remote from the point of insertion position of *tRNA*^{GLU}. Gene combined recombination between the plasmid and chromosome allele's with result in *ade6+* recombination. The frequency of producing prototroph will be utilized in measuring the frequency of the recombination process (adapted from Pryce et al., 2009).

3.2.4 Mutant strains construction

The *ade6::tRNA*^{GLU} (pSRS5) strain was used as the basis for creation of de novo mutants. All the strains were created by antibiotic-resistant cassette replacement as founded on the PCR-based gene targeting approach described by Bähler et al. (1998). The single mutant *dcr1*Δ, *tsn1*Δ and the double mutant *dcr1*Δ *tsn1*Δ strains were developed in the investigation and were constructed by the McFarlane group. Nonetheless, before being utilised, they were subjected to verification through PCR checking of relevant loci. Additionally, in this study the single mutant *dcr1*Δ, *tfx1*Δ and the double mutant *dcr1*Δ *tfx1*Δ strains were developed by deleting the genes from parental strains, orientation 1 and 2 (BP1478 and BP1508). Generating the single mutant of *tfx1*Δ in the first orientation (BP3493), the single mutant *tfx1*Δ in the second orientation (BP3491), the single mutant *dcr1*Δ in the first orientation (BP3313), and the single mutant *dcr1*Δ in the second orientation (BP3343). To create a double mutant *tfx1*Δ *dcr1*Δ in the first orientation (BP3496), *tfx1* deletion took place in the background of *dcr1*Δ (BP3313), and in the second orientation (BP3498), *tfx1* deletion took place in the background of *dcr1*Δ (BP3343). The antibiotic *natMX6* and *kanMX6* were used as the replacement cassettes in the deletion of *dcr1* and *tfx1*. For instance, *kanMX6* was used for the single mutant *tfx1*Δ in both orientations (BP3493, BP3491) and the single mutant *dcr1*Δ in orientation 2 (BP3343), whereas *natMX6* was utilised for the single mutant *dcr1*Δ in orientation 1 (BP3313). To verify the correct deletion, candidates of both strains were screened through the PCR (see Figures 3.9, 3.10, and 3.11). Two independent isolates were tested for each construct.

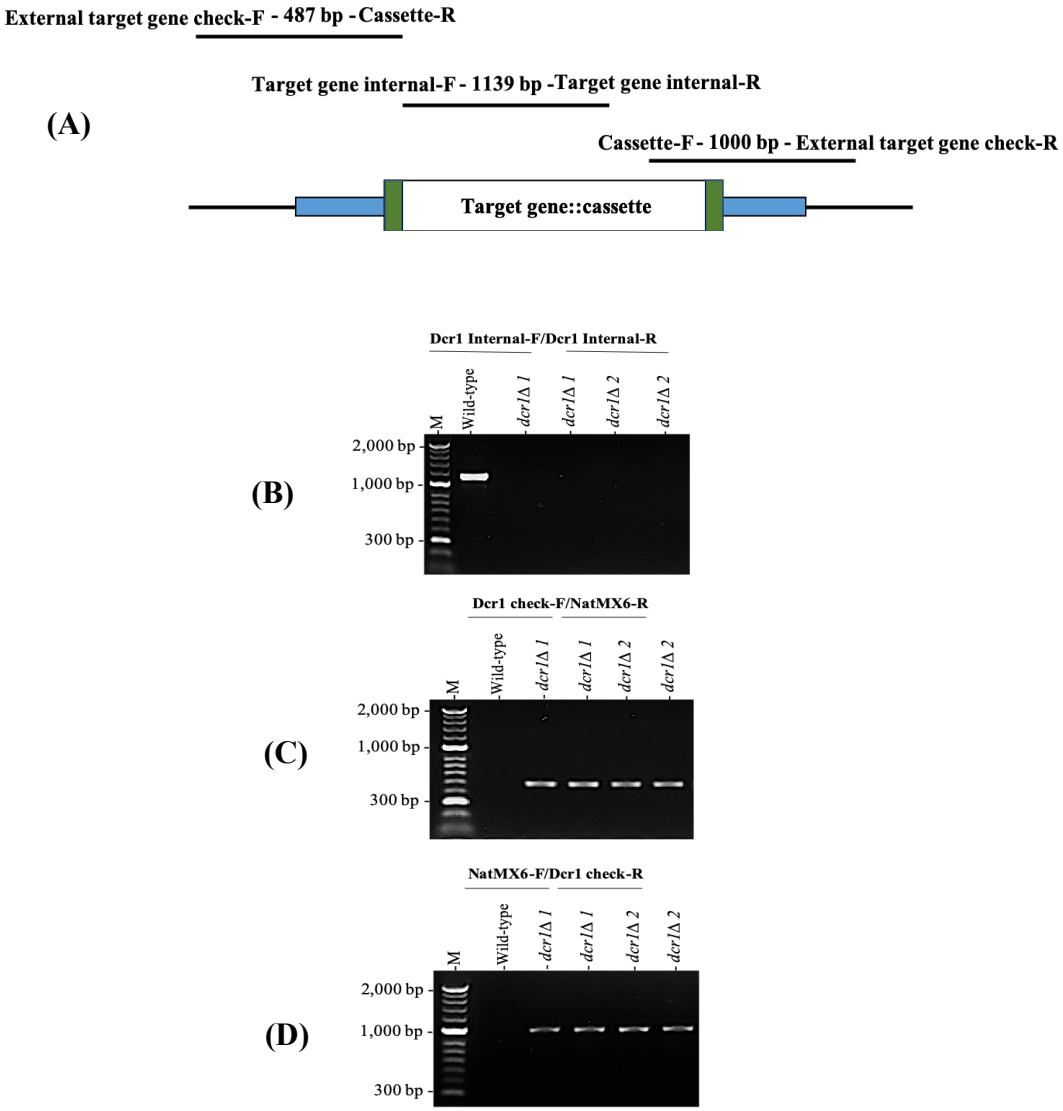

Figure 3.9 Confirmation by PCR screening of successful *dcr1*Δ single mutant knockout.
(A) The genes were deleted and replacement with antibiotic resistant cassettes. To confirm the deletion of the target genes, three sets of primers were used. **(B)** Illustration of agarose gel screening of PCR products for the wild-type strain and *dcr1*Δ single mutant in orientation 1 and 2 respectively. The number after the mutant designation represent the $tRNA^{GLU}$ orientation. The Dcr1-int-F and Dcr1-int-R primers were used, and the gel screening displays no PCR products in the successful *dcr1*Δcandidate strains. The expected sizes of the PCR product in *dcr1*Δ gene was 1139 bp. (**C**) The Dcr1 check-F and KanMX6-R primers were used to generate the PCR products for the wild-type and *dcr1*Δ candidate strains. The PCR products were seen in the *dcr1*Δ strains in both orientations, but not in the wild-type strain and the expected band sizes is 487 bp. **(D)** The wild-type and *dcr1*Δ candidate strains were utilised to amplify by the KanMX6-F and Dcr1 check-R primers and the expected sizes is 1000 bp.

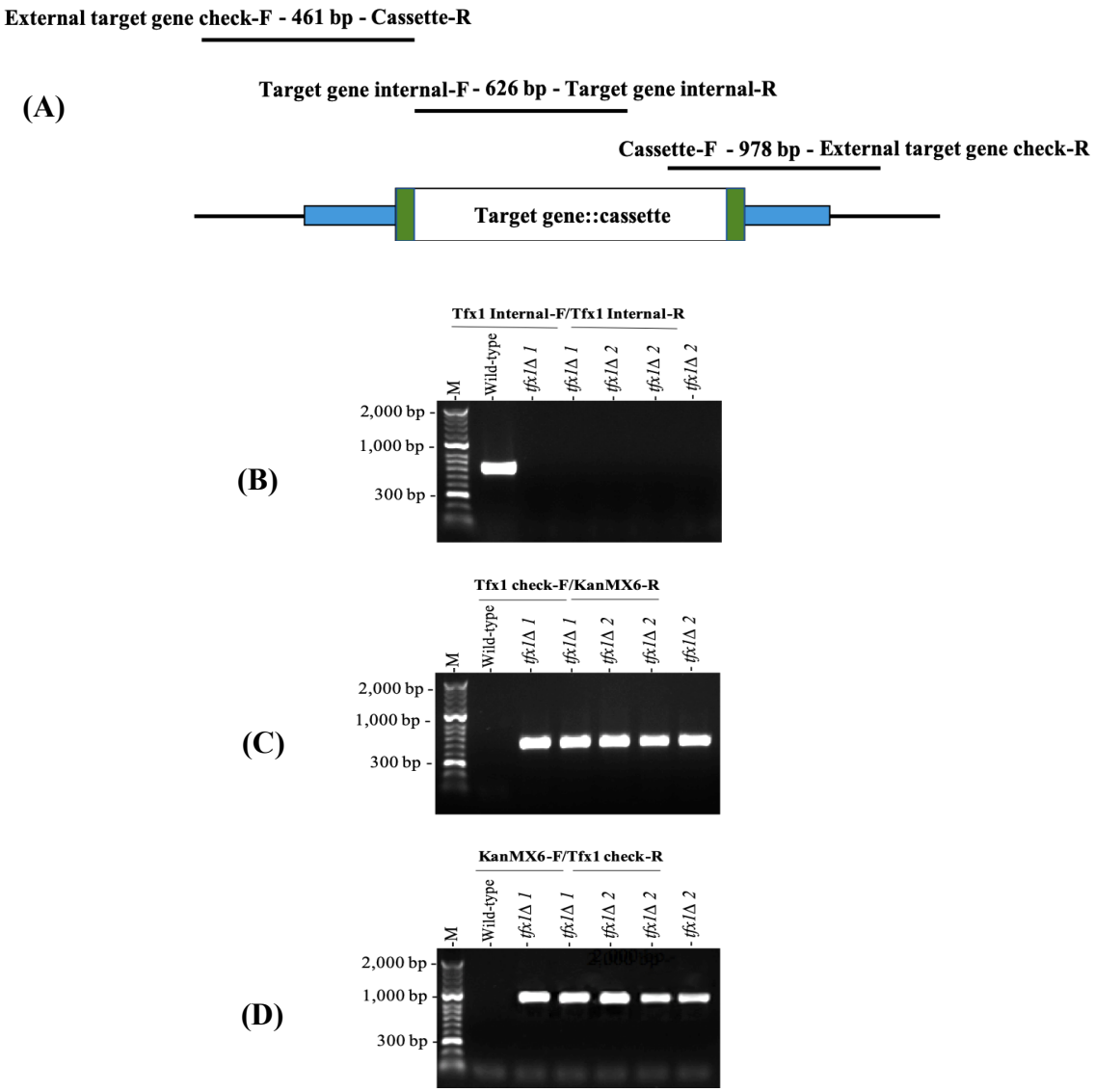

Figure 3.10 Confirmation by PCR screening of successful *tfx1*Δ single mutant knockout.
(A) The genes were deleted and replacement with antibiotic resistant cassettes. To confirm the deletion of the target genes, three sets of primers were used. **(B)** Illustration of agarose gel screening of PCR products for the wild-type strain and *tfx1*Δ single mutant in orientation 1 and 2 respectively. The number after the mutant designation represent the $tRNA^{GLU}$ orientation. The Tfx1-int-F and Tfx1-int-R primers were used, and the gel screening displays no PCR products in the successful *tfx1*Δ candidate strains. The expected sizes of the PCR product in *tfx1* gene was 626 bp. **(C)** The Tfx1 check-F and KanMX6-R primers were used to generate the PCR products for the wild-type and *tfx1*Δ candidate strains. The PCR products were seen in the *tfx1*Δ strains in both orientations, but not in the wild-type strain and the expected band sizes is 461 bp. **(D)** The wild-type and *tfx1*Δ candidate strains were utilised to amplify by the KanMX6-F and Tfx1 check-R primers and the expected sizes is 978 bp.

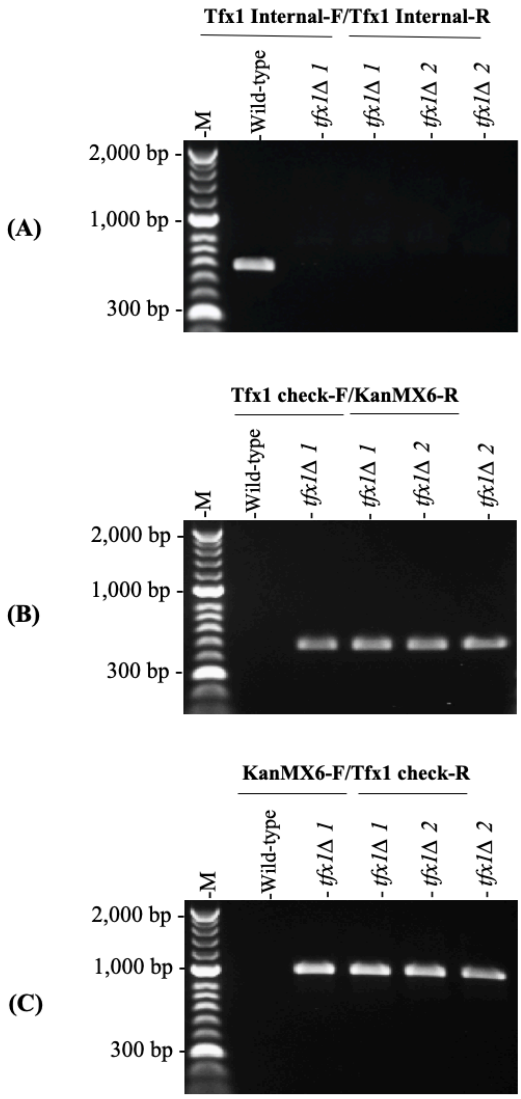

Figure 3.11 Confirmation by PCR screening of successful *tfx1*Δ *dcr1*Δ double mutant knockout.
(A) Illustration of agarose gel screening of PCR products for the wild-type strain and *tfx1*Δ single mutant in orientation 1 and 2 respectively. The number after the mutant designation represent the $tRNA^{GLU}$ orientation. The Tfx1-int-F and Tfx1-int-R primers were used. The gel screening displays no PCR products in the successful *tfx1*Δ candidate strains. The expected sizes of the PCR product in *tfx1* gene was 626 bp. (**B)** The Tfx1 check-F and KanMX6-R primers were used to generate the PCR products for the wild-type and *tfx1*Δ candidate strains. The PCR products were seen in the *tfx1*Δ strains in both orientations, but not in the wild-type strain and the expected band sizes approximately is 461 bp. **(C)** The wild-type and *tfx1*Δ candidate strains were utilised to amplify by the KanMX6-F and Tfx1 check-R primers and the expected sizes is 978 bp.

3.2.5 Sensitivity spot tests for DNA damaging agent and TBZ drug for the newly constructed strains

Data in Section 3.1.1 showed that, the double mutant *dcr1*Δ *tsn1*Δ showed higher sensitivity compared to the single mutant *dcr1*Δ to the microtubule destabilizing TBZ drug, HU and phleomycin. Accordingly, we decided to verify this phenotype in the newly constructed recombination assay strains. Consistent with the data in Section 3.1.1, the double mutant *dcr1Δ tsn1Δ* showed higher sensitivity compared to the *dcr1Δ* single mutant in response to TBZ (Figure 3.12), HU (Figure 3.14) and phleomycin (Figure 3.16). As for the analyses of the previous strains, the *dcr1Δ tfx1Δ* double mutant did exhibit a slight increase in sensitivity to TBZ relative to the *dcr1Δ* single mutant (Figure 3.13). Interestingly, there was a mild increase in sensitivity in the *dcr1Δ tfx1Δ* double mutant relative to the *dcr1Δ* single mutant to both HU and phleomycin, but this was only apparent in orientation 2 and was not as increased as the *dcr1Δ tsn1Δ* double mutant. The reason for this is unclear but it might demonstrate some auxiliary role for Tfx1. Interestingly, in most cases the strains carrying the *dcr1Δ tsn1Δ* double mutants appeared to exhibit slightly more sensitivity in the $tRNA^{GLU}$ orientation 2 background. In this might suggest that $tRNA^{GLU}$ in orientation 2 might present a genomic locus which is more likely to required Tsn1 function in a *dcr1Δ* background under DNA damaging condition. In combination, the two results in different background verify that Tsn1 is needed in the DNA damaging recovery response when Dcr1 is absent. Furthermore, the results verify the ability of these newly constructed strains for testing inter-molecular recombination at a defined locus.

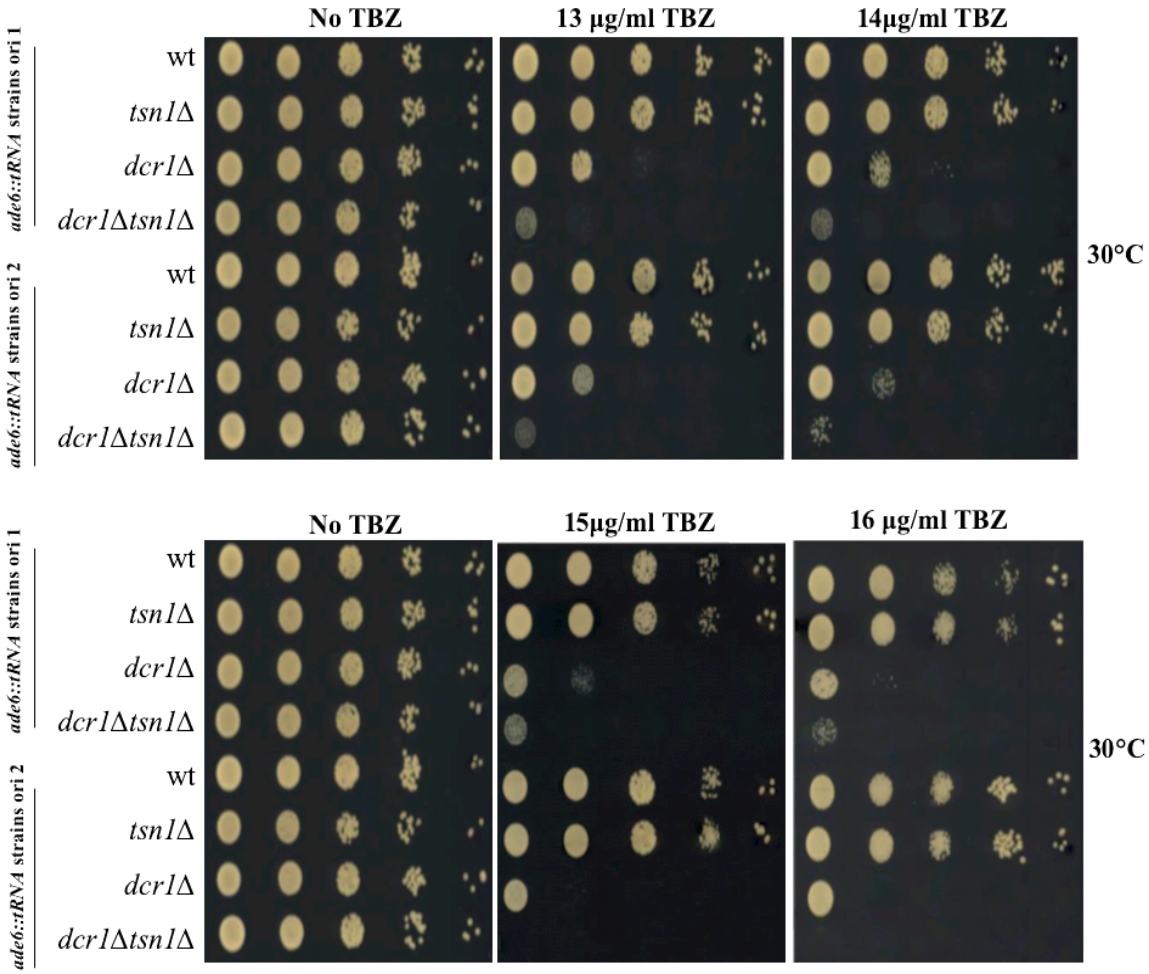

Figure 3.12 Increased the sensitivity of the *dcr1Δ tsn1Δ* cells to the TBZ.
S. pombe mutants were diluted (10-fold serial dilution left to right) and spotted onto YEA media contain different concentration of TBZ. The data displayed, the single mutant *dcr1*Δ show increased sensitivity to TBZ compared with the WT. The hypersensitivity to the TBZ was displayed by the double mutant *dcr1Δ tsn1Δ* compared with the *dcr1*Δ single mutant. In addition, the high sensitivity of the double mutant *dcr1Δ tsn1Δ* and the *dcr1*Δ single mutant increased in the orientation 2 compared with the orientation 1. The plates were incubated 3 days at 30°C.

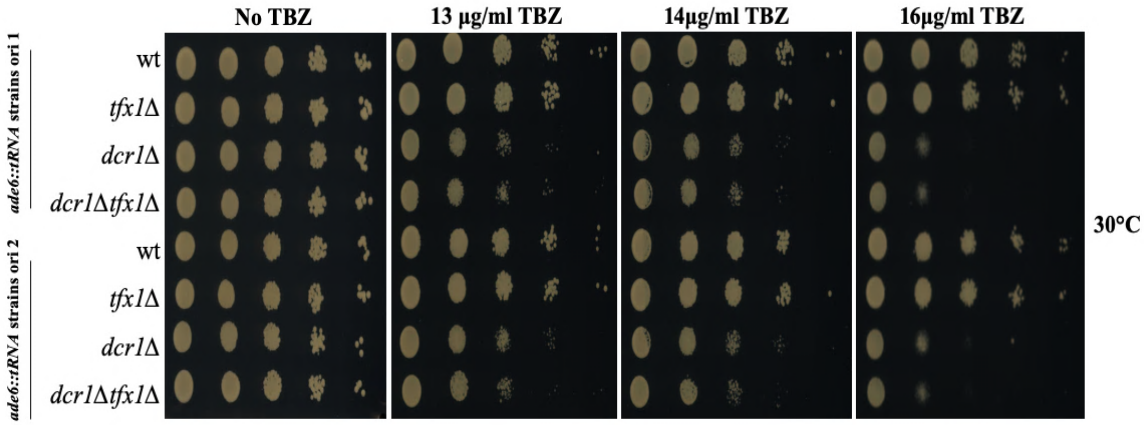

Figure 3.13 Spot test sensitivity of the *dcr1Δ tfx1Δ* to the TBZ.
S. pombe mutants were diluted (10-fold serial dilution left to right) and spotted onto YEA media contain different concentration of TBZ. The data show that, the *dcr1Δ tfx1Δ* double mutant and *dcr1*Δ single mutant displayed similar sensitivity to TBZ compared with the WT in both orientations. The plates were incubated 3 days at 30°C.

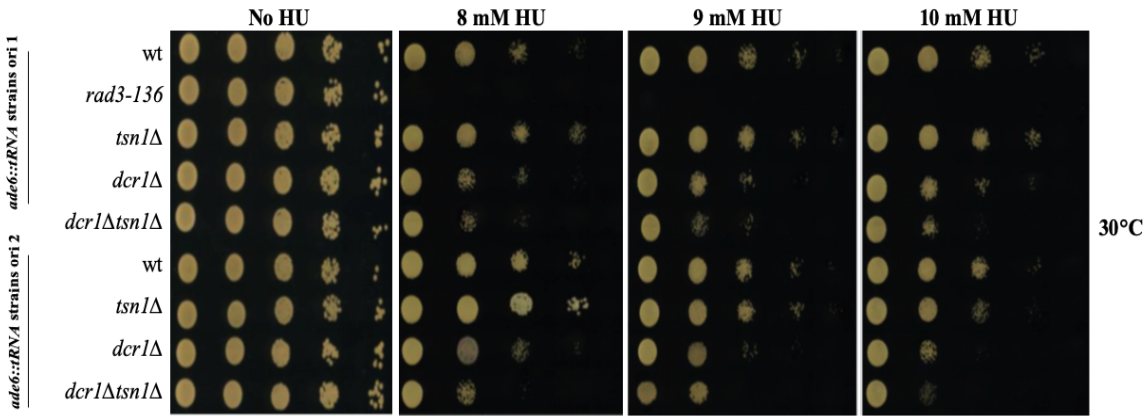

Figure 3.14 Increased the sensitivity of the *dcr1Δ tsn1Δ* to hydroxyurea (HU).
S. pombe mutants were diluted (10-fold serial dilution left to right) and spotted onto YEA media contain different concentration of hydroxyurea (8 mM, 9 mM and 10 mM HU). *rad3-136* was used as a positive control. The *dcr1Δ tsn1Δ* double mutant show increased sensitivity to HU compared with the *dcr1*Δ single mutant. In addition, the high sensitivity of the double mutant *dcr1Δ tsn1Δ* and the *dcr1*Δ single mutant increased in the orientation 2 compared with the orientation 1. The plates were incubated 3 days at 30°C.

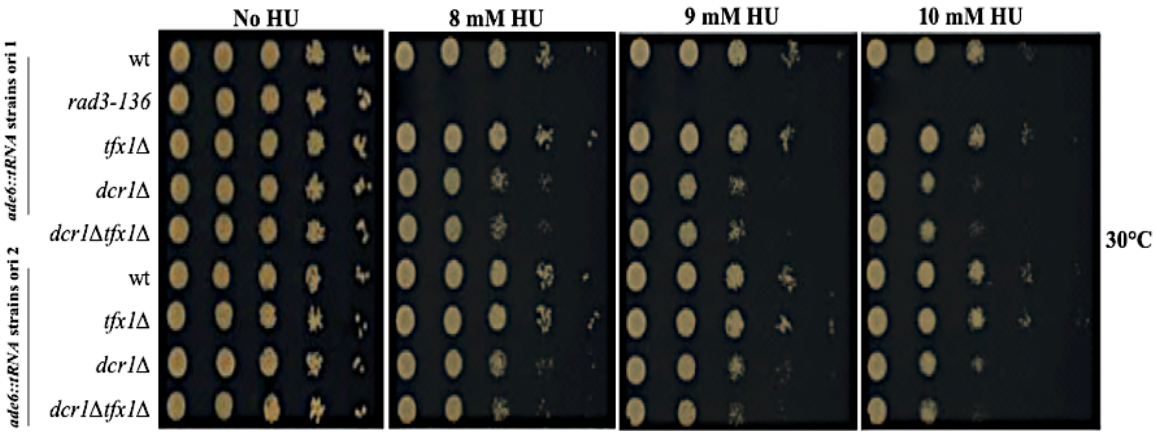

Figure 3.15 Spot test sensitivity of the *dcr1Δ tfx1Δ* to hydroxyurea (HU).
S. pombe mutants were diluted (10-fold serial dilution left to right) and spotted onto YEA media contain different concentration of hydroxyurea (8 mM, 9 mM and 10 mM HU). *rad3-136* was used as a positive control. The *dcr1Δ tfx1Δ* double mutants and *dcr1*Δ single mutant displayed similar sensitivity to HU compared with the WT in both orientations. The plates were incubated for 3 days at 30°C.

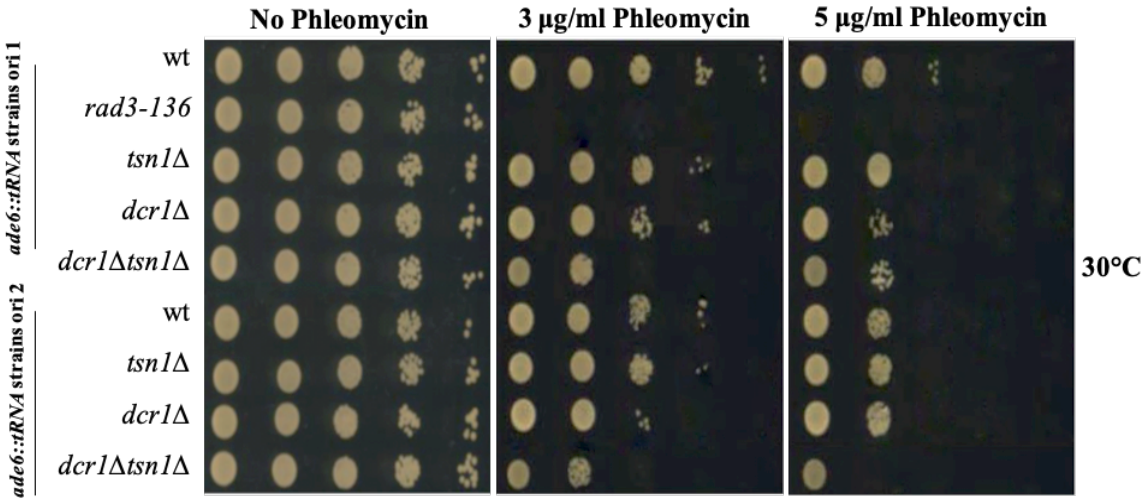

Figure 3.16 Increased the sensitivity of the *dcr1Δ tsn1Δ* to Phleomycin.
S. pombe mutants were diluted (10-fold serial dilution left to right) and spotted onto YEA media contain different concentration of phleomycin drug. *rad3-136* was used as a positive control. The *dcr1Δ tsn1Δ* double mutant show increased sensitivity to phleomycin drug compared with the *dcr1*Δ single mutant. In addition, the high sensitivity of the double mutant *dcr1Δ tsn1Δ* increased in the orientation 2 compared with the orientation 1. The plates were incubated 3 days at 30°C.

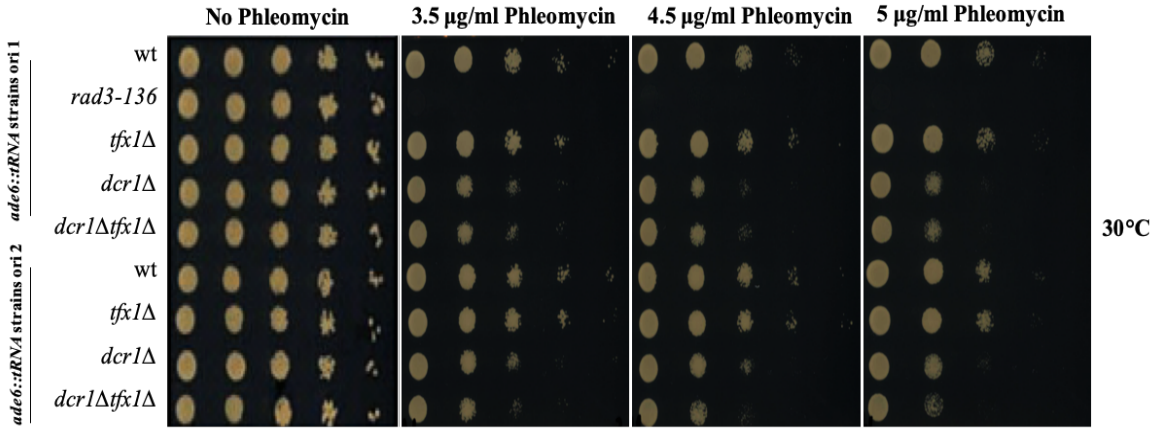

Figure 3.17 Spot test sensitivity of the *dcr1Δ tfx1Δ* to Phleomycin.
S. pombe mutants were diluted (10-fold serial dilution left to right) and spotted onto YEA media contain different concentration of phleomycin drug. *rad3-136* was used as a positive control. The *dcr1Δ tfx1Δ* double mutant and *dcr1*Δ single mutant displayed similar sensitivity to phleomycin drug compared with the WT in both orientations. The plates were incubated 3 days at 30°C.

3.2.6 Recombination frequencies analysis

Fluctuation tests were performed on single mutants *tsn1*Δ*, tfx1*Δ*, dcr1*Δ and the double mutant strains *dcr1*Δ *tsn1*Δ *and dcr1*Δ *tfx1*Δ in combination with the WT strains. In this analysis, the recombination frequency (adenine prototrophs per 10^6 viable cells) was measured using the pSRS5 plasmid. The fluctuation test was utilised to verify whether the high sensitivity of the *dcr1*Δ *tsn1*Δ double mutant to DNA damage agents is associated with increased recombination at a replication fork barrier (RFB). In this analysis, *swi1*Δ was used as a positive control, as this mutant has a high recombination frequency in the assay.

3.2.6.1 The recombination frequencies analysis for *tsn1*Δ*, dcr1*Δ and *dcr1*Δ *tsn1*Δ mutants

The fluctuation analysis on orientation 1 of the *ade6::tRNA*^{GLU} allele, showed no statistically significant elevation in recombination frequency for the single mutant *tsn1*Δ, *dcr1*Δ and the double mutants *dcr1*Δ *tsn1*Δ compared with the WT strain (Figure 3.18). The results of the study illustrate that the single mutant *dcr1*Δ failure to simulate recombinogenic lesions for orientation 1 (Figure 3.18). For orientation 2 of the *ade6::tRNA*^{GLU} insert, the single mutants *tsn1*Δ and *dcr1*Δ showed no significant increase in recombination frequency in comparison to the WT strain (Figure 3.19). A higher level of recombination frequency was observed in the *dcr1*Δ*tsn1*Δ double mutant relative to both WT and *dcr1*Δ single mutant. The increase between the *dcr1*Δ single mutant and the double mutant *dcr1*Δ *tsn1*Δ strain was found to be statistically significant. Based on this result, it is evident that elevated sensitivity to DNA damage agents, as depicted in *dcr1*Δ *tsn1*Δ double mutant in comparison to the *dcr1*Δ single mutant, is associated with orientation-specific increased recombination at a recognized RFB.

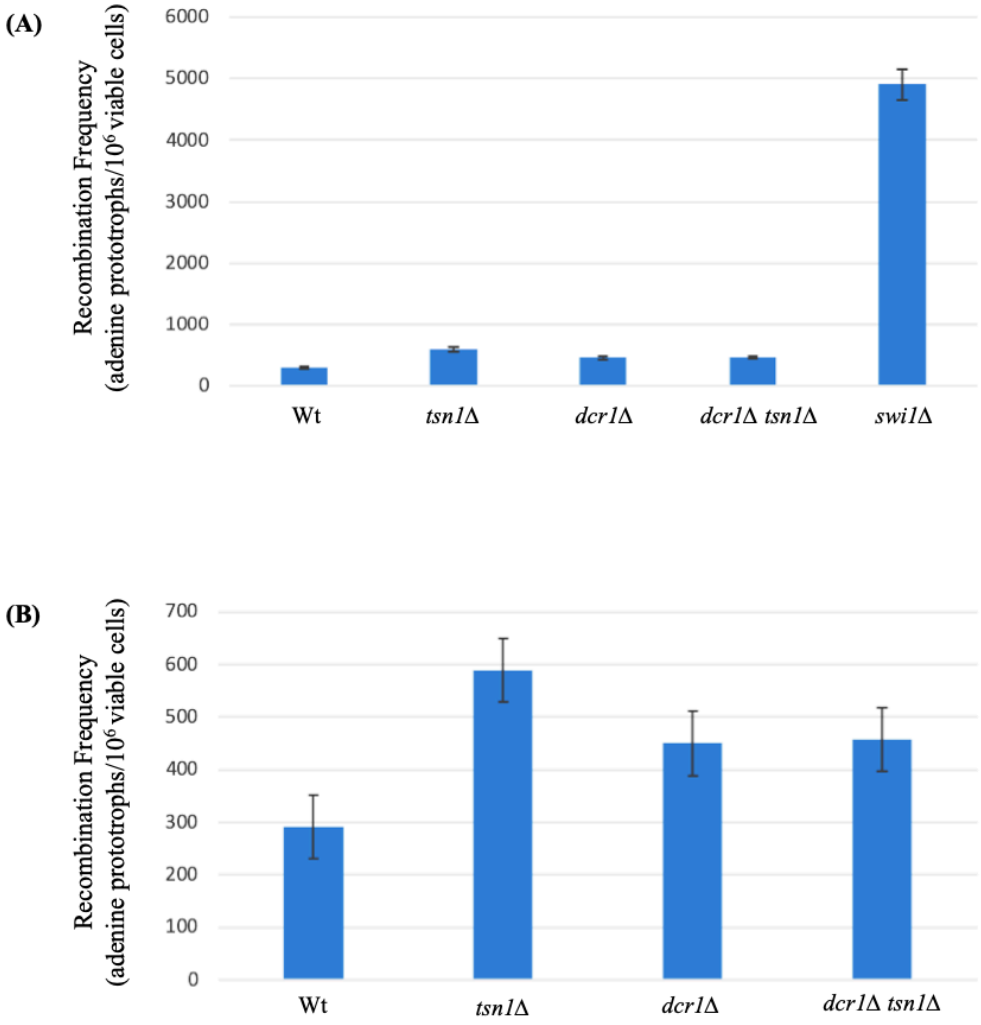

Figure 3.18 The recombination assay for orientation 1 strains.
(A) The plot illustrated that the mean values of three independent median values. The data gained from the fluctuation test for plasmid-by-chromosome intermolecular recombination frequencies. The data display the recombination frequency of *tsn1*Δ and *dcr1*Δ single mutants and *dcr1*Δ *tsn1*Δ double mutant in ori1 showed no statistically significant change relative to the WT strain. The *swi1*Δ mutant was used as a positive control. **(B)** The plot showed the same data but the *swi1*Δ values removed. The error bars show triplicate repeats of the standard error. P-values between WT and the indicated time point have been determined through student T-tests. All p-values were > 0.05 except WT vs. *swi1*Δ, which was < 0.01.

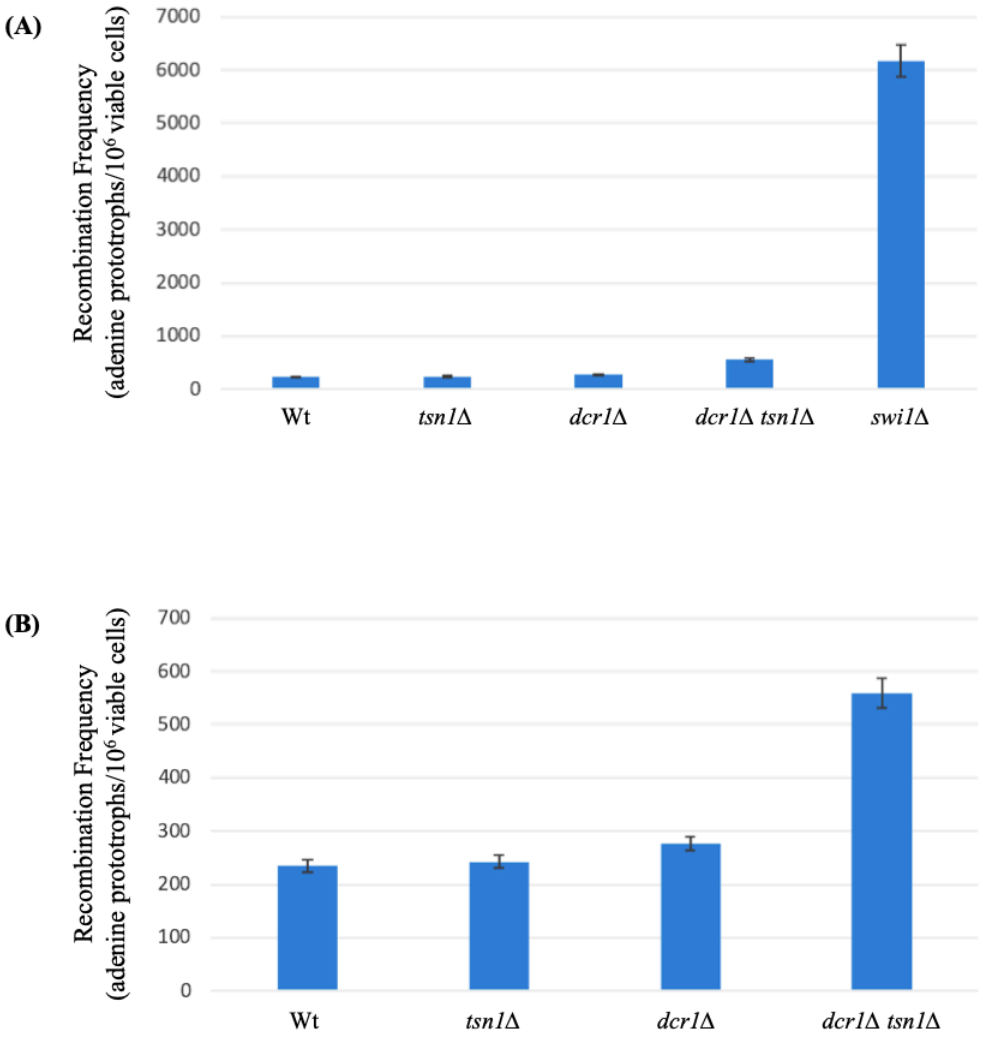

Figure 3.19 The recombination assay for orientation 2 strains.
(A) The plot illustrated that the mean values of three independent median values. The data gained from the fluctuation test for plasmid-by-chromosome intermolecular recombination frequencies. The data display the recombination frequency of *tsn1*Δ and *dcr1*Δ single mutants and *dcr1*Δ *tsn1*Δ double mutant in ori2 showed statistically significant change relative to the WT strain. The *swi1*Δ mutant was used as a positive control**. (B)** The plot showed the same data but the *swi1*Δ values removed. The error bars show triplicate repeats of the standard error. P-values between WT and the indicated time point have been determined through student T-tests. The p-values of WT vs. *tsn1Δ*, $p > 0.05$; WT vs. *dcr1Δ*, $p > 0.05$; *dcr1Δ* vs. *dcr1Δ tsn1*Δ, $p < 0.02$; and WT vs. *dcr1Δ tsn1*Δ, $p < 0.01$.

3.2.6.2 The recombination frequencies analysis for *tfx1*Δ, *dcr1*Δ *and dcr1*Δ *tfx1*Δ mutants at tRNA genes

Analysis of *tfx1*Δ strain and *dcr1*Δ*tfx1*Δ double mutant in both orientation 1 and 2 showed no significant increase relative to the wild-type (Figure 3.20 and 3.21). In these experiments recombination frequency slightly was lower than the *tsn1*Δ experiments (for example, compare wild-type values for both orientation). The reason for this inter experiments difference is unclear, but this was not observed when these experiments were duplicated by other lab members.

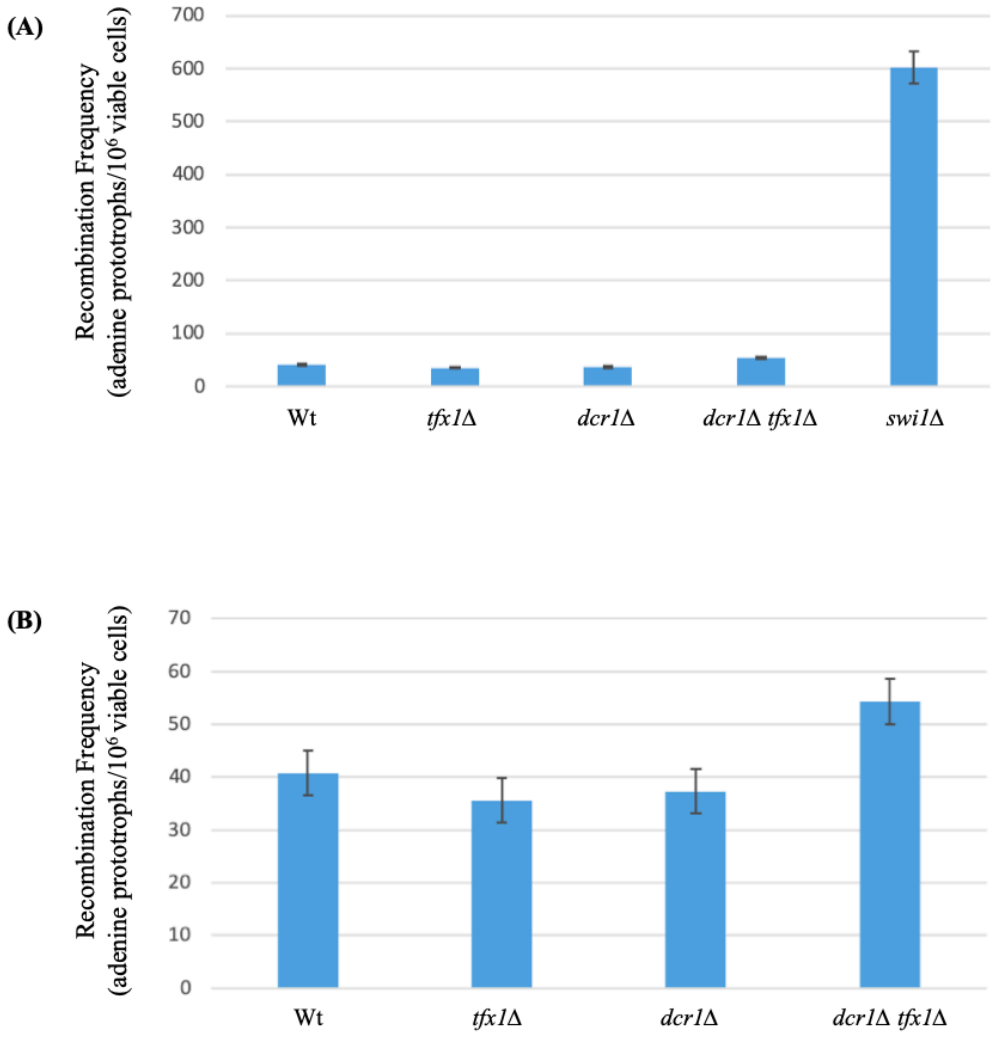

Figure 3.20 The recombination assay for the *ade6::tRNA^{GLU}* –orientation 1 strains.
(A) The plot illustrated that the mean values of three independent median values. The data gained from the fluctuation test for plasmid-by-chromosome intermolecular recombination frequencies. The data display the recombination frequency of *tfx1*Δ, *dcr1*Δ and *dcr1*Δ *tfx1*Δ mutants in ori1 and showed no statistically significant change relative to the WT strain. The *swi1*Δ mutant was used as a positive control. **(B)** The plot showed the same data but the *swi1*Δ values were removed. The error bars show triplicate repeats of the standard error. P-values between WT and the indicated time point have been determined through student T-tests. All p-values were > 0.05 except WT vs. *swi1*Δ, which was < 0.01**.**

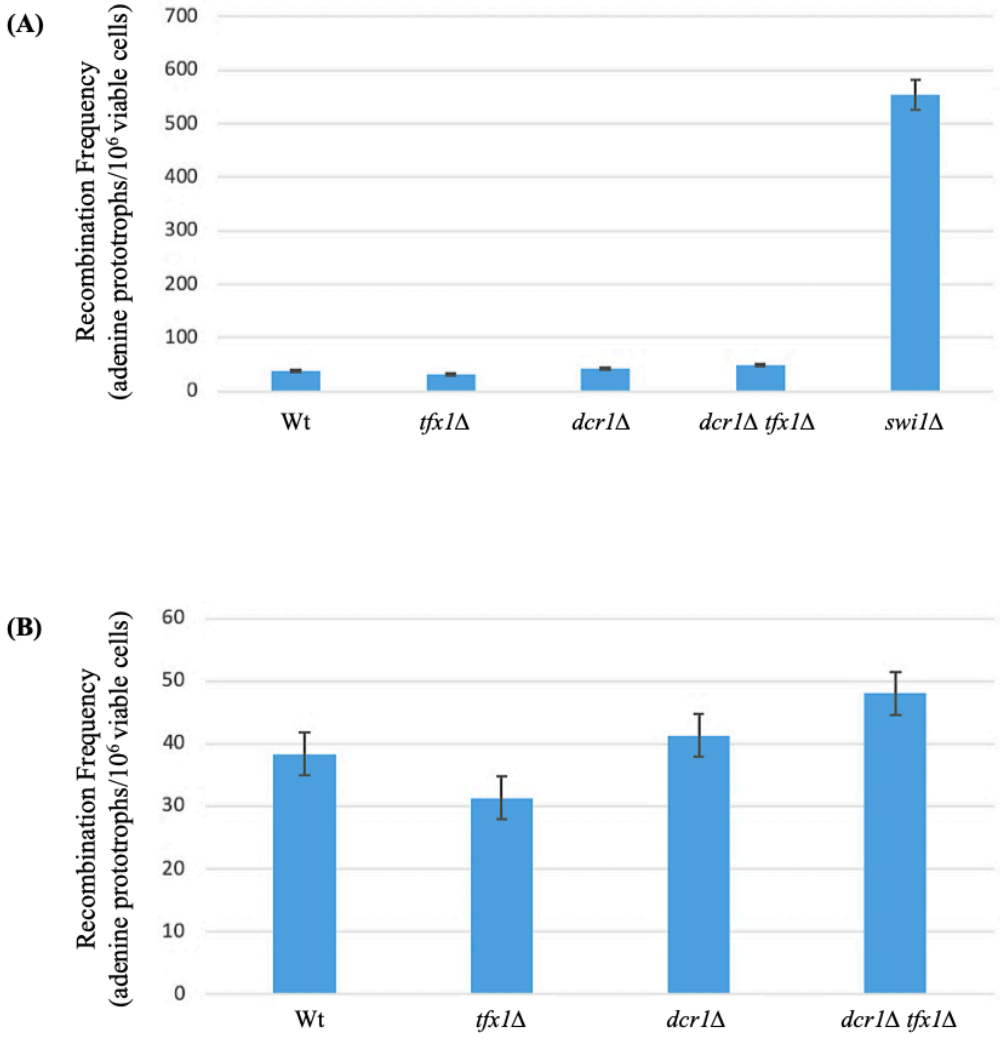

Figure 3.21 The recombination assay for the *ade6::tRNA*^{GLU} orientation 2 strains.
(A) The plot illustrated that the mean values of three independent median values. The data gained from the fluctuation test for plasmid-by-chromosome intermolecular recombination frequencies. The data display the recombination frequency of *tfx1*Δ, *dcr1*Δ and *dcr1*Δ *tfx1*Δ mutants in ori 2 and showed no statistically significant change relative to the WT strain. The *swi1*Δ mutant was used as a positive control. **(B)** The plot showed the same data but the *swi1*Δ values were removed. The error bars show triplicate repeats of the standard error. P-values between WT and the indicated time point have been determined through student T-tests. All p-values were > 0.05 except WT vs. *swi1*Δ, which was < 0.01.

3.3 Discussion

Prior to this work there was little direct evidence that Translin is involved in the recovery from DNA damage, despite the proposal that it is required for chromosomal translocations (Jaendling & McFarlane, 2010). Trax, however, has been demonstrated to be required for proper recruitment of the ATM kinase to DNA double-strand breaks to mediate the DNA repair process, although it is proposed that this function is independent of Translin (Wang et al., 2016). In addition to this, Translin and /Trax have been implicated in the regulation of the RNAi process, although there is no evidence for this in *S. pombe* (Jaendling et al., 2008; Jaendling et al., 2010). One of the lead components of the RNAi pathway, Dicer, has been demonstrated to have RNAi-independent functions in DNA damage avoidance *S. pombe*, where it is proposed it assists the removal of RNA pol II to avoid transcription-replication conflicts which might generate recombinogenic lesions (Castel et al., 2014).

This led our group to assess whether Tsn1 and/or Tfx1 had role in DNA damage recovery/avoidance in the absence of Dcr1 and the data presented here indicate that Tsn1, but not Tfx1, do indeed have a role to play in the recovery from DNA damage for some types of damage, including DNA replicative stress (HU). This is the first evidence for a direct role for Tsn1 in DNA damage recovery in *S. pombe*, and this organism offers a model in which this can be explored further. Interestingly, there does not appear to be a similar requirement for Tfx1. Mammalian Translin can form nucleic acid binding complexes in the absence of Trax, but it remains unclear form our data whether the nucleic acid binding function of Tsn1 is required for DNA damage recovery. Tsn1 and Tfx1 functions have been separated previously in *S. pombe* as it has been demonstrated that they both independently regulate distinct telomere-associated transcripts (Gomez-Escobar et al., 2016). Whether the DNA damage recovery requirement revealed here relates to the regulation of telomeric RNAs, specifically TERRAs, remains to be seen, but TERRAs are known to be required for the DNA damage response (Bettin et al., 2019). The link between Tsn1, genome stability and telomeres will be tested in a later chapter.

A role in recombination suppression? Here we demonstrate that the *tsn1Δ dcr1Δ* double mutant exhibits a slightly higher intermolecular recombination frequency than the wild-type or single mutants in our recombination report system. The same is not true for the *tfx1Δ dcr1Δ* double mutant, which is consistent with the DNA damaging agent responses. Interestingly, this is only observed in one of our two reporter systems, the $tRNA^{GLU}$ orientation 2. This suggests that there is a polarity to the requirement for Tsn1 in the Dcr1 background. Why this might be us unclear, but a possible explanation requires an understanding of the reporter system. The intermolecular recombination in the system being used is thought to be based on the fact that tRNA genes form a barrier to DNA replication (Pryce et al., 2009). This barrier appears to be orientation-independent (Pryce et al., 2009), so the polarity observed here is a surprise. The barrier is also thought to be caused by RNA pol III, which is required to transcribe tRNAs. However, Castel and co-workers (2014) made a remarkable discovery. They demonstrated that not only RNA pol III, but also RNA pol II was actively transcribing at tRNA genes. It is proposed that RNA pol II transcribes the anti-sense strand in the opposite direction to RNA pol III transcription (Castel et al., 2016). This offers some insight into what might be taking place in our experiments. Castel and co-workers additionally demonstrated that Dcr1 was required to remove RNA pol II to prevent transcriptional conflicts with DNA replication. At the *ade6* locus, where our tRNA gene replication barrier is inserted, DNA replication is overwhelmingly unidirectional (Pryce et al., 2009). When the tRNA gene is in orientation 1, this will generate head-to-head conflicts between RNA pol III and the replisome, and head-to-tail conflicts between RNA pol II and the replisome; head-to-head conflicts are thought to be the most likely cause of recombinogenic replication conflicts. In orientation 2 of the tRNA gene the inverse is the case, and now the head-to-head conflict will be between RNA pol II and the replisome. It is orientation 2 which has increased recombination in the absence of both Dcr1 and Tsn1, but not only one. Given that Dcr1 is proposed to be required for preventing RNA pol II-to-replisome conflicts (Castel et al., 2016), then it could be possible that it is RNA pol II-to-replisome blocks that Tsn1 is required to process/prevent in the absence of Dcr1. RNA pol III-to-replisome conflicts are either not as difficult for the replisome to overcome, or their processing/removal does not require Dcr1 and/or Tsn1.

Castel and co-workers demonstrated that in the absence of Dcr1 RNA:DNA hybrid levels became elevated, and it was these structures that were generated by RNA pol II that were the cause of increased genome instability in the absence of Dcr1, although it should be noted that Castel and co-workers did not overexpress and RNA:DNA hybrid processing enzyme, such as RNAse H to demonstrate this could suppress the need for Dcr1. So, it might be the case that in the absence of Dcr1, the processing of RNA:DNA hybrids generated by RNA pol II, and not RNA pol III, require Tsn1, but not Tfx1. This is consistent with the nucleic acid binding and RNAse H capabilities of Tsn1 (Jaendling and McFarlane, 2010), and could account for the need for Translin to avoid oncogenic chromosomal translocation if this Translin function is orthologous in humans. Interestingly, a co-worker in the group has now demonstrated that in the absence of both Dcr1 and Tsn1 elevated chromosomal RNA:DNA hybrids can be observed, although this has not been tested at the *ade6* locus with or without tRNA gene insertions. Interestingly, the observations from the *ade6* locus demonstrate that there is a requirement for Tsn1 at a locus that is non-telomeric. This is the first indication that the genome stability regulation function for Tsn1 is independent of the telomeres. We cannot discount the possibility that telomeric transcripts, such as TERRAs are contributing to non-telomeric loci, but this will be tested elsewhere in this thesis by studying the genome stability phenotypes in strains without telomeres/telomerase.

So, from the work in this chapter we have revealed a role for Tsn1, but not Tfx1, in DNA damage recovery in the absence of Dcr1. We have shown that this function appears to associated with DNA replication and propose a model in which Tsn1 is required to prevent transcription-replication conflicts between the replisome and RNA pol II, possibly via processing RNA:DNA hybrids which occur at sites of conflict.

3.4 Conclusion

1. The *tsn1*or *tfx1* mutations increases the viability of the *dcr1*Δ mutant.

2. In the absence of Dcr1, Tsn1, but not Tfx1, is required in the DNA damage response.

3. The hypersensitivity of the *dcr1*Δ *tsn1*Δ cells to DNA damaging agents is linked to increase in recombination stimulating lesions.

4. Tsn1, but not Tfx1 is required to suppress recombination in the absence of Dcr1 at a specific artificial locus.

Chapter 4: Results

Relationship between Tsn1 and RNase H activities

4.1 Introduction

In chapter 3 we have seen that the *tsn1*Δ *dcr1*Δ double mutant exhibited increase sensitivity to some DNA damaging agents. Therefore, we have revealed a relationship between Tsn1 and Dcr1. This suggests the Tsn1 function potentially relates to Dcr1 RNAi-independent function in removing stalled RNA polymerase II and associated RNA: DNA hybrids from the genome to prevent transcription to replication conflicts (Castel et al., 2014). In the absence of Dcr1 the RNA:DNA hybrid levels became elevated, and it was these structures that were generated by RNA pol II that are the cause of increased genome instability (Castel et al., 2014). It might be the case that in the absence of Dcr1, the processing of RNA:DNA hybrids generated by RNA pol II, and not RNA pol III, require Tsn1, but not Tfx1. This is consistent with the nucleic acid binding and RNAse capabilities of Tsn1 (Jaendling and McFarlane, 2010), and could account for the need for Translin to avoid chromosomal translocation. RNA:DNA hybrids, generated by transcription can cause transcription replication conflicts, which can lead to chromosome instability, resulting diseases such as cancer (Zimmer & Koshland et al., 2016). Two of the major suppressor of RNA:DNA hybrids are RNase H1 and RNase H2 (Amon & Koshland et al., 2016).The RNase H enzymes are two highly conserved ribonucleases and they have ability to remove the RNA:DNA hybrids by degrading the RNA moiety (Cerritelli & Crouch et al., 2009; Amon & Koshland et al., 2016). Therefore, the RNase H activities are important in preventing genome instability (Amon & Koshland et al., 2016). It has been found that one of the RNase H, RNase H2, has an additional function, which is the removal of ribonucleotides misincorporated during DNA replication, or improper Okazaki fragment removal. In *S. pombe* the RNase H activities are important for efficient DSB repair. The deletion of RNase H1 and RNase H2 genes (*rnh1* and *rnh201)* results in different DNA damage recovery, suggesting that the two pathways of RNase H function redundantly in DNA repair (Ohle et al., 2016).

The hypothesis to be tested is that the loss of Tsn1 or/Tfx1 function results in DNA:RNA hybrids causing an assist in DSB repair, or, in the absence of Dcr1 cause increases in DNA replication, transcription collision and led to genome instability. This led us to ask whether Tsn1 or Tfx1 function in concert with known RNAase H activities. To test this hypothesis, *tsn1*, *tfx1* and *dcr1* were mutated in both RNases H pathways.

4.2 Results

4.2.1 Sensitivity spot tests to investigate if Tsn1 functions in one of the RNase H pathways

The data for the response of the *dcr1*Δ *tsn1*Δ double mutant to Phleomycin, Bleomycin and HU agents provoked the question if Tsn1 has function in one of the RNase H pathways. This prompted us to investigate the sensitivity of the *tsn1*Δ *rnh1*Δ and *tsn1*Δ *rnh201*Δ double mutants to DNA damaging agents. The strains employed were constructed by co-workers in the lab, but the strains used in the spot tests shown were subjected to PCR verification of mutation status (Appendix Figures 4 and 6). Spot tests were carried out using a range of DNA damage agents. The DNA damage agents tested in this study included phleomycin and bleomycin, which are responsible for generation of DSBs (Figures 4.1 and 4.2); HU, as a DNA replication inhibitor (Figure 4.3); ultraviolet irradiation (UV), which induces multiple adducts (Figure 4.4); MMS, a DNA alkylating agent (Figure 4.5); mitomycin C, a potent DNA crosslinker (Figure 4.6); CPT, a topoisomerase inhibitor (Figure 4.7) and Aphidicolin, a DNA polymerase inhibitor (Figure 4.8). The data demonstrate that, the *rnh1*Δ*rnh201*Δ double mutant showed high sensitivity to the all DNA damaging agents consistent with previous reports (Ohle et al., 2016; Zhao et al., 2018). The *tsn1*Δ *rnh201*Δ double mutant exhibited hypersensitivity relative to the *rnh1*Δ and *rnh201*Δ single mutants and the *tsn1*Δ *rnh1*Δ double mutant in response to phleomycin, bleomycin and HU. However, the sensitivity of the *tsn1*Δ *rnh201*Δ double mutant was not as extreme as the *rnh1*Δ *rnh201*Δ double mutant. Conversely, the *tsn1*Δ *rnh201*Δ double mutant did not show any sensitivity increase compared with the *rnh1*Δ and *rnh201*Δ single mutants or WT in response to MMC, MMS, UV, CPT and Aphidicolin. These results indicate that Tsn1 is needed in the DNA damage recovery response when Rnh201 is absent, for some types of DNA damage.

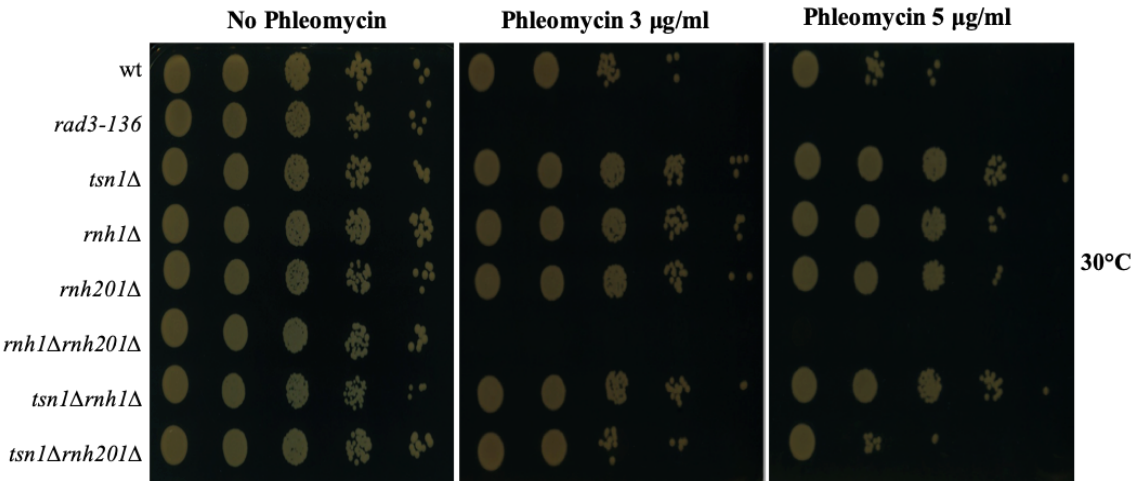

Figure 4.1 Rnh201, but not Rnh1, is required for the response to Phleomycin in the absence of Tsn1.
S. pombe mutants were diluted (10-fold serial dilution left to right) and spotted onto YEA media contain different concentration of Phleomycin. *rad3-136* was used as a positive control. The *rnh1Δ rnh201Δ* double mutant show high sensitivity. The *tsn1Δ rnh201Δ* double mutant show increased sensitivity to Phleomycin compared with the *rnh1*Δ and *rnh201*Δ single mutants, but the *tsn1Δ rnh1Δ* double mutant show no increased sensitivity compared with the single mutants. The plates were incubated 3 days at 30°C.

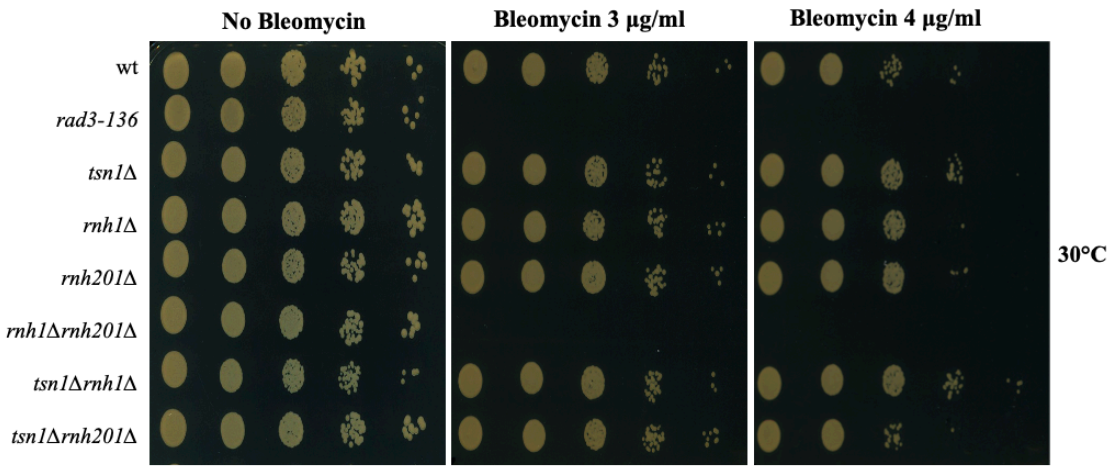

Figure 4.2 Rnh201, but not Rnh1, is required for the response to Bleomycin in the absence of Tsn1.
S. pombe mutants were diluted (10-fold serial dilution left to right) and spotted onto YEA media contain different concentration of Phleomycin. *rad3-136* was used as a positive control. The *rnh1Δ rnh201Δ* double mutant show high sensitivity. The *tsn1Δ rnh201Δ* double mutant showed a mild increase sensitivity to Bleomycin compared with the *rnh1*Δ and *rnh201*Δ single mutants, but the *tsn1Δ rnh1Δ* double mutant show no increased sensitivity compared with the single mutants. The plates were incubated 3 days at 30°C.

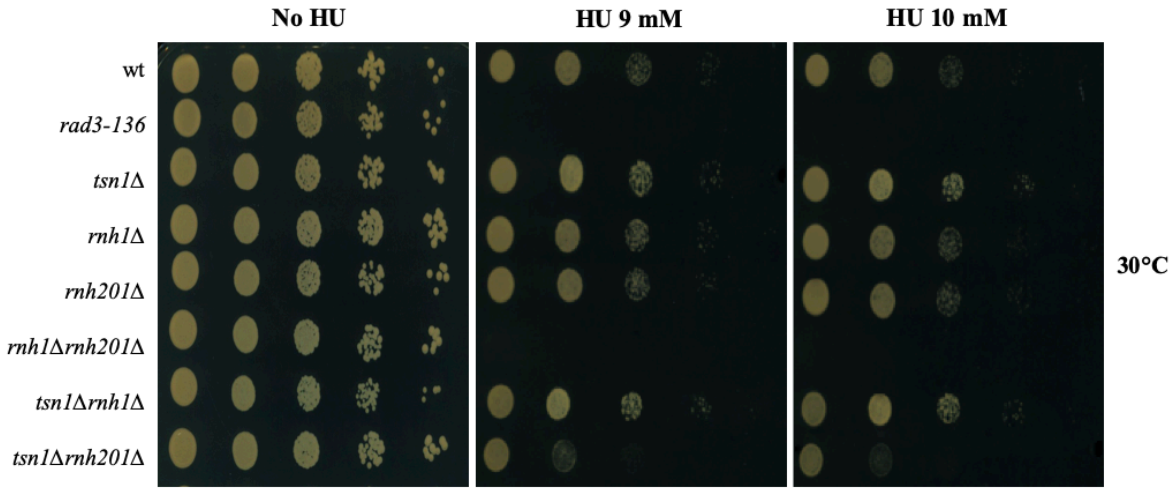

Figure 4.3 Rnh201, but not Rnh1, is required for the response to Hydroxyurea in the absence of Tsn1.
S. pombe mutants were diluted (10-fold serial dilution left to right) and spotted onto YEA media contain different concentration of hydroxyurea (8 mM, 9 mM and 10 mM HU). *rad3-136* was used as a positive control. The *rnh1Δ rnh201Δ* double mutant show high sensitivity. The *tsn1Δ rnh201Δ* double mutant show increased sensitivity to hydroxyurea compared with the *rnh1*Δ and *rnh201*Δ single mutants, but the *tsn1Δ rnh1Δ* double mutant exhibited little/no sensitivity compared with the single mutant. The plates were incubated 3 days at 30°C.

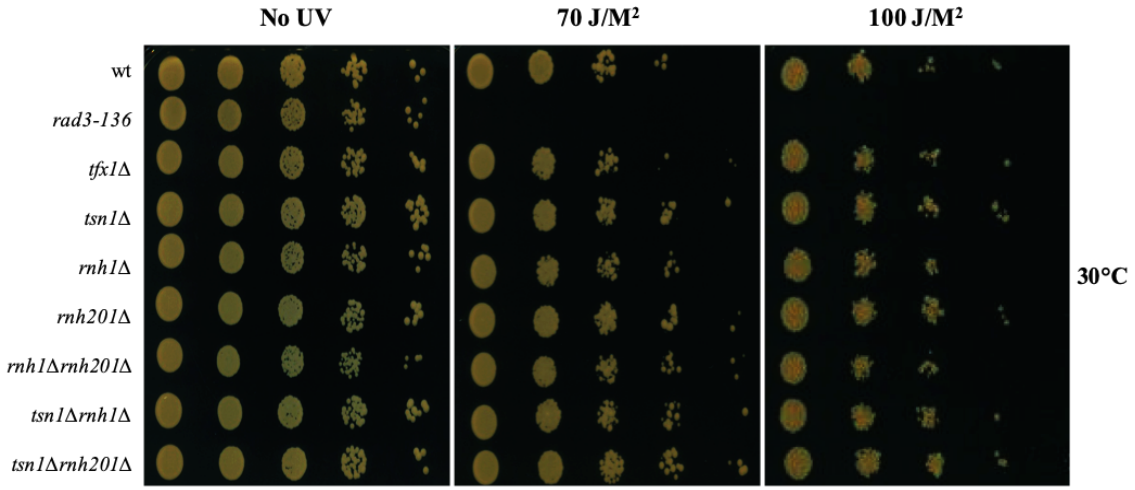

Figure 4.4 Sensitivity spot test of UV irradiation.
S. pombe mutants were diluted (10-fold serial dilution left to right) and spotted onto YEA media and then exposed to different doses of UV irradiation. *rad3-136* was used as a positive control. The *rnh1Δ rnh201Δ* double mutant show slight increase sensitivity, but the *tsn1Δ rnh1Δ* and *tsn1Δ rnh201Δ* double mutants show no sensitivity to UV irradiation compared with the *rnh1*Δ and *rnh201*Δ single mutants or the WT. The plates were incubated 3 days at 30°C.

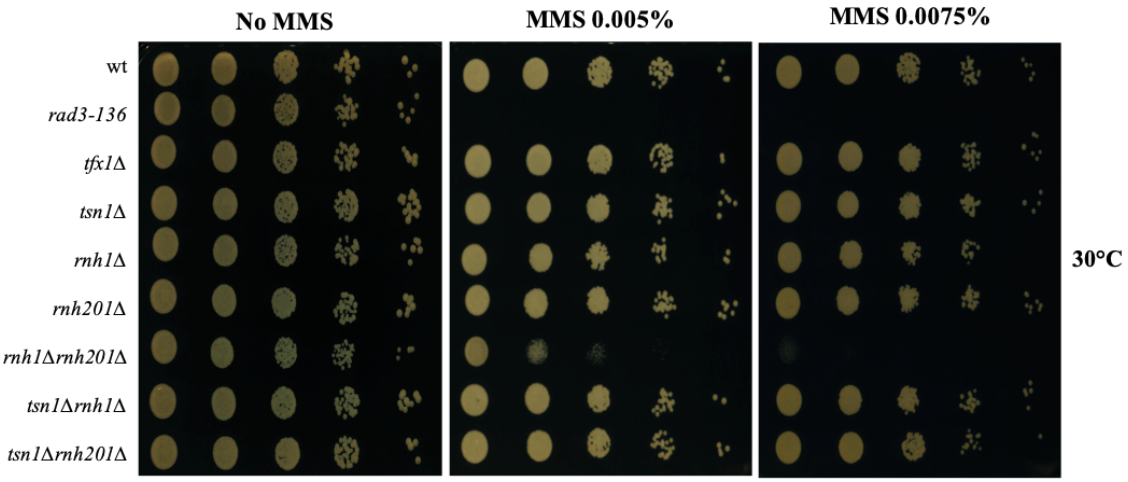

Figure 4.5 Sensitivity spot test of Methyl methane sulfonate (MMS).
S. pombe mutants were diluted (10-fold serial dilution left to right) and spotted onto YEA media contain different concentration of MMS (0.005% and 0.0075% MMS). *rad3-136* was used as a positive control. The *rnh1Δ rnh201Δ* double mutant shows increased sensitivity, but the *tsn1Δ rnh1Δ* and *tsn1Δrnh201Δ* double mutants show no sensitivity to MMS compared with the *rnh1*Δ and *rnh201*Δ single mutants or the WT. The plates were incubated 3 days at 30°C.

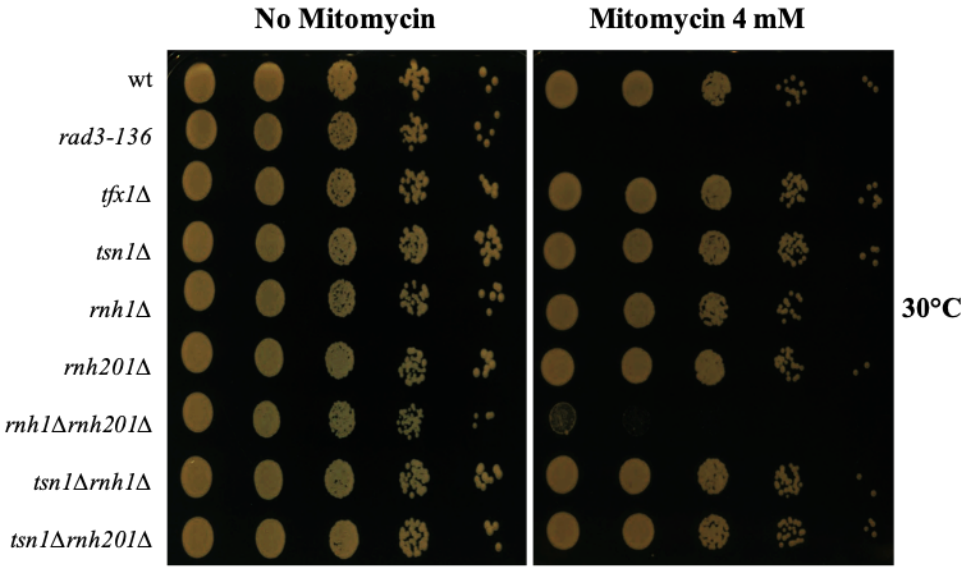

Figure 4.6 Sensitivity spot test of Mitomycin C (MMC).
S. pombe mutants were diluted (10-fold serial dilution left to right) and spotted onto YEA media contain concentration of Mitomycin C (4 mM MMC). *rad3-136* was used as a positive control. The *rnh1Δ rnh201Δ* double mutant shows high sensitivity, but the *tsn1Δ rnh1Δ* and *tsn1Δ rnh201Δ* double mutants show no sensitivity to MMC compared with the *rnh1*Δ and *rnh201*Δ single mutants or the WT. The plates were incubated 3 days at 30°C.

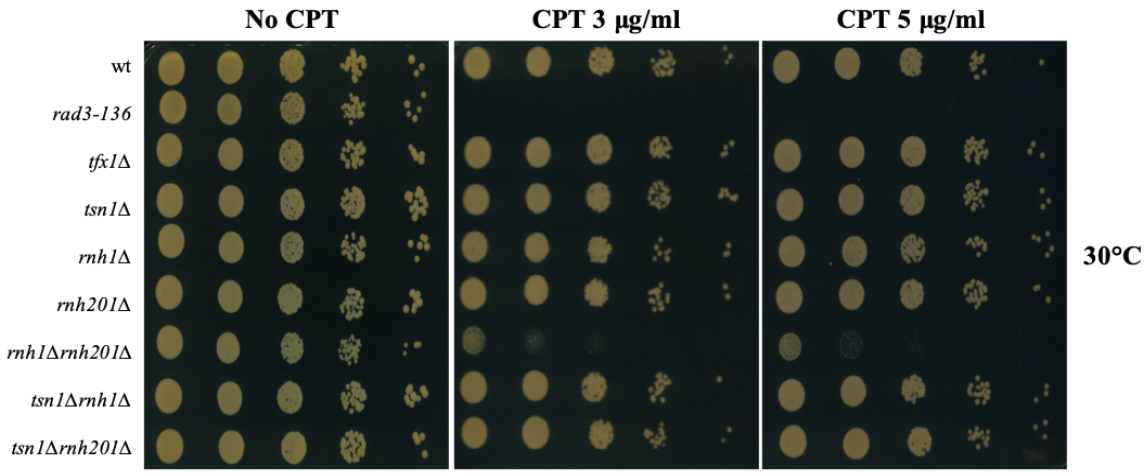

Figure 4.7 Sensitivity spot test of Camptothecin (CPT).
S. pombe mutants were diluted (10-fold serial dilution left to right) and spotted onto YEA media contain different concentration of CPT (3 µg/m and 5 µg/m CPT). *rad3-136* was used as a positive control. The *rnh1Δ rnh201Δ* double mutant shows high sensitivity, but the *tsn1Δ rnh1Δ* and *tsn1Δ rnh201Δ* double mutants show no sensitivity to CPT compared with the *rnh1*Δ and *rnh201*Δ single mutants and the WT. The plates were incubated 3 days at 30°C.

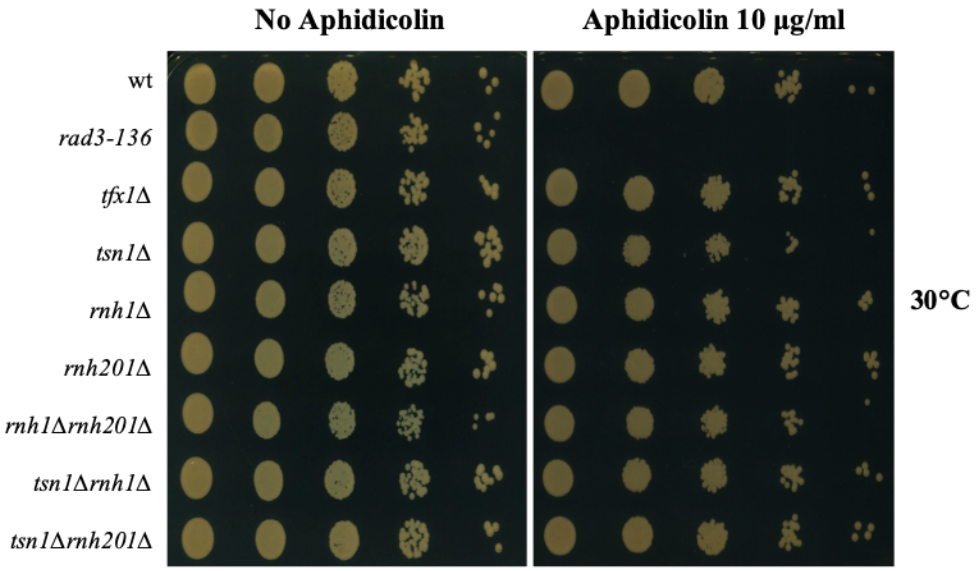

Figure 4.8 Sensitivity spot test of Aphidicolin.
S. pombe mutants were diluted (10-fold serial dilution left to right) and spotted onto YEA media contain concentration of Aphidicolin 10 µg/ml. *rad3-136* was used as a positive control. The *rnh1Δ rnh201Δ,* the *tsn1Δ rnh1Δ* and *tsn1Δ rnh201Δ* double mutants show no sensitivity compared with the *rnh1*Δ and *rnh201*Δ single mutants and the WT. The plates were incubated 3 days at 30°C.

4.2.2 Sensitivity spot tests to investigate if Tfx1 functions in one of the RNases H pathways.

The data for the response of the *tsn1*Δ *rnh201*Δ double mutant to phleomycin, bleomycin and HU agents provoked the question of whether Tfx1 has function in one of the RNase H pathways. This prompted us to investigate the sensitivity of the *tfx1*Δ *rnh1*Δ and *tfx1*Δ *rnh201*Δ double mutants to DNA damaging agents. The strains employed were constructed by co-workers in the lab, but the strains used in the spot tests shown were subjected to PCR verification of mutation status (Appendix Figures 5 and 6). Spot tests were carried out using a range of DNA damage agents. The DNA damage agents tested in this study included phleomycin and bleomycin, which are responsible for generation of DSBs (Figures 4.9 and 4.10); HU, as a DNA replication inhibitor (Figure 4.11); UV, which induces multiple adducts (Figure 4.12); MMS, a DNA alkylating agent (Figure 4.13); mitomycin C, a potent DNA crosslinker (Figure 4.14); CPT, a topoisomerase inhibitor (Figure 4.15) and Aphidicolin, a DNA polymerase inhibitor (Figure 4.16). The data demonstrate that, the *rnh1*Δ *rnh201*Δ double mutant showed high sensitivity to the all DNA damaging agents consistent with previous reports (Ohle et al., 2016; Zhao et al., 2018). However, the *tfx1*Δ *rnh1*Δ and *tfx1*Δ *rnh201*Δ double mutants did not show any sensitivity increase compared with the *rnh1*Δ and *rnh201*Δ single mutants or WT in response to all DNA damaging agents. These results indicate that Tsn1, but not Tfx1 is needed in the DNA damage recovery response when Rnh201 is absent, for some types of DNA damage.

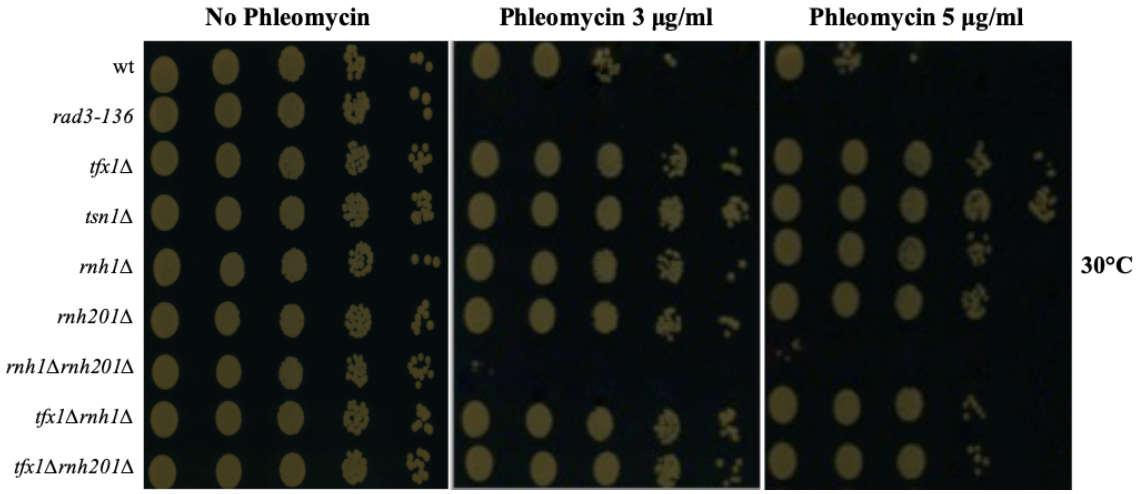

Figure 4.9 Sensitivity spot test of Phleomycin.
S. pombe mutants were diluted (10-fold serial dilution left to right) and spotted onto YEA media contain different concentration of Phleomycin. *rad3-136* was used as a positive control. The *rnh1Δ rnh201Δ* double mutant shows high sensitivity. The *tfx1Δ rnh1Δ* and *tfx1Δ rnh201Δ* double mutants show no increased sensitivity to Phleomycin compared with the *rnh1*Δ and *rnh201*Δ single mutants. The plates were incubated 3 days at 30°C.

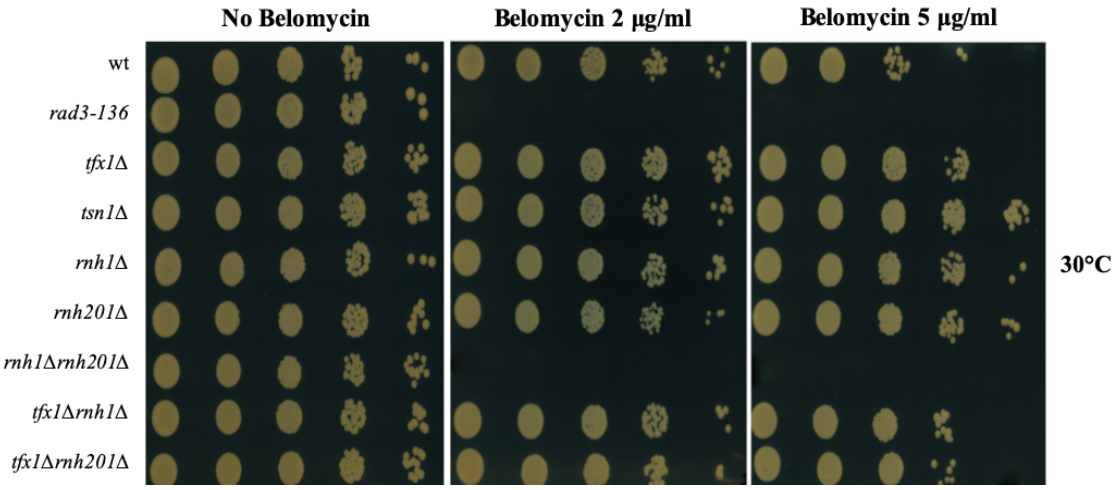

Figure 4.10 Sensitivity spot test of Bleomycin.
S. pombe mutants were diluted (10-fold serial dilution left to right) and spotted onto YEA media contain different concentration of Bleomycin. *rad3-136* was used as a positive control. The *rnh1Δ rnh201Δ* double mutant shows high sensitivity. The *tfx1Δ rnh1Δ* and *tfx1Δ rnh201Δ* double mutants show no increased sensitivity to Bleomycin compared with the *rnh1*Δ and *rnh201*Δ single mutants. The plates were incubated 3 days at 30°C.

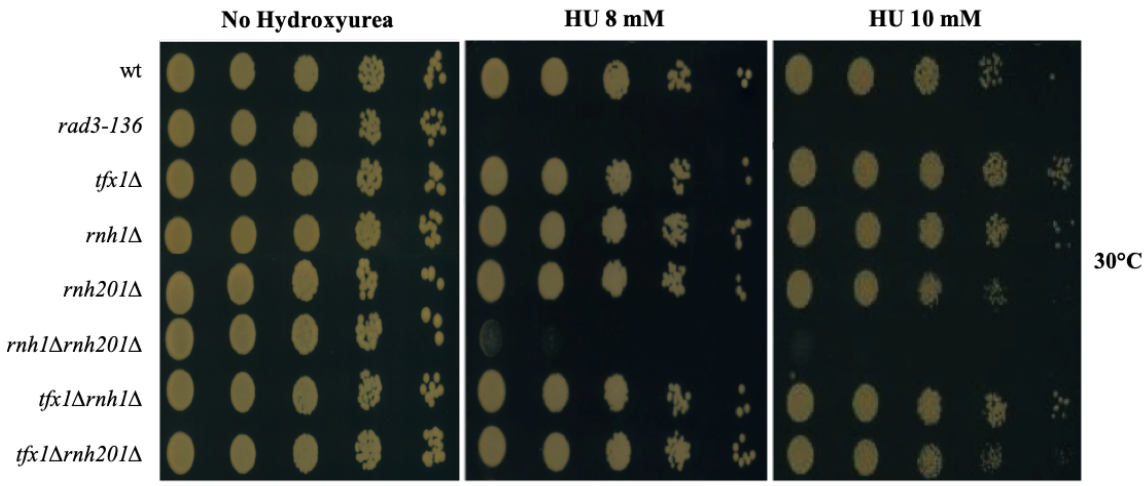

Figure 4.11 Sensitivity spot test of Hydroxyurea.
S. pombe mutants were diluted (10-fold serial dilution left to right) and spotted onto YEA media contain different concentration of hydroxyurea (8 mM and 10 mM HU). *rad3-136* was used as a positive control. The *rnh1Δ rnh201Δ* double mutant shows high sensitivity. The *tfx1Δ rnh1Δ* and *tfx1Δ rnh201Δ* double mutants show no increased sensitivity to hydroxyurea compared with the *rnh1*Δ and *rnh201*Δ single mutants. The plates were incubated 3 days at 30°C.

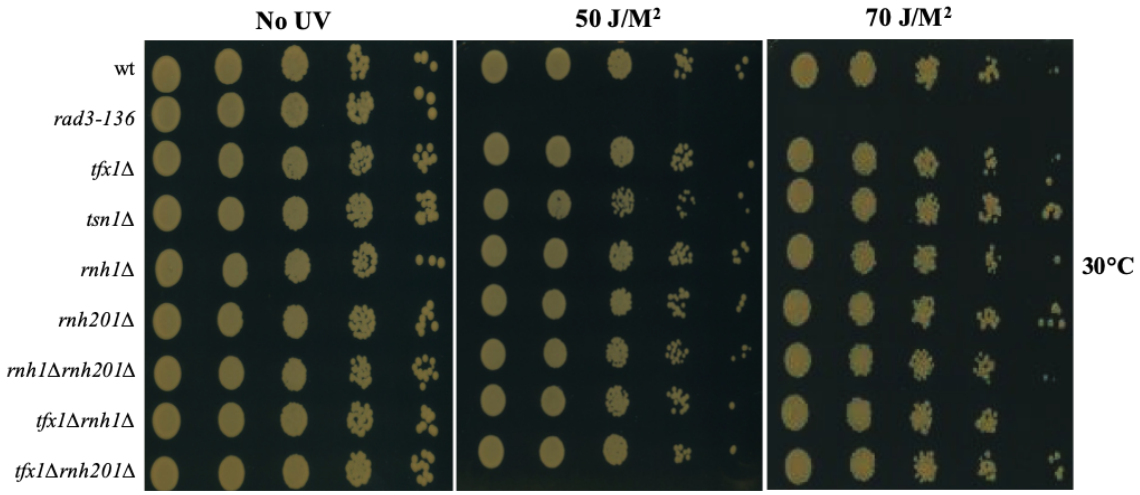

Figure 4.12 Sensitivity spot test of UV irradiation.
S. pombe mutants were diluted (10-fold serial dilution left to right) and spotted onto YEA media and then exposed to different doses of UV irradiation. *rad3-136* was used as a positive control. The *tfx1Δ rnh1Δ* and *tfx1Δ rnh201Δ* double mutants show no increased sensitivity to UV compared with the *rnh1*Δ and *rnh201*Δ single mutants. The plates were incubated 3 days at 30°C.

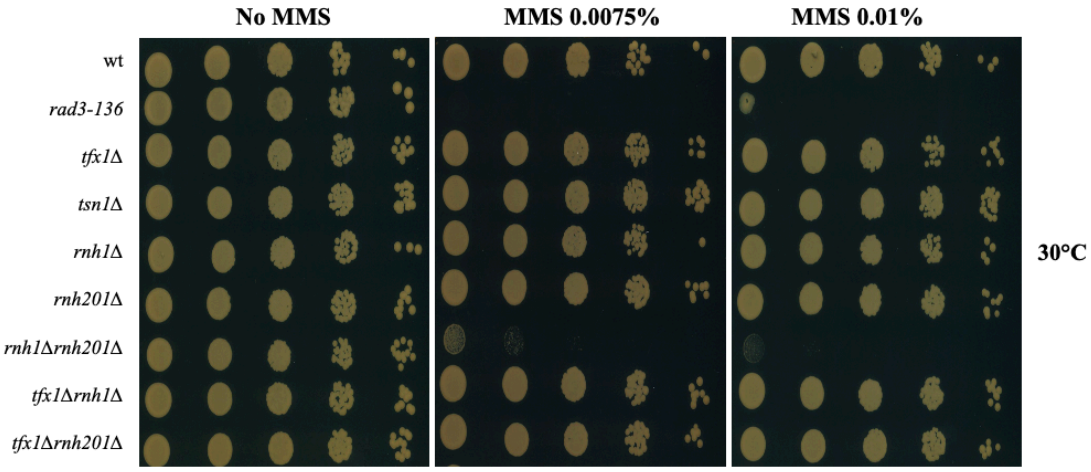

Figure 4.13 Sensitivity spot test of Methyl methane sulfonate (MMS).
S. pombe mutants were diluted (10-fold serial dilution left to right) and spotted onto YEA media contain different concentration of MMS (0.0075% and 0.1% MMS). *rad3-136* was used as a positive control. The *rnh1Δ rnh201Δ* double mutant shows high sensitivity. The *tfx1Δ rnh1Δ* and *tfx1Δ rnh201Δ* double mutants show no increased sensitivity to MMS compared with the *rnh1*Δ and *rnh201*Δ single mutants. The plates were incubated 3 days at 30°C.

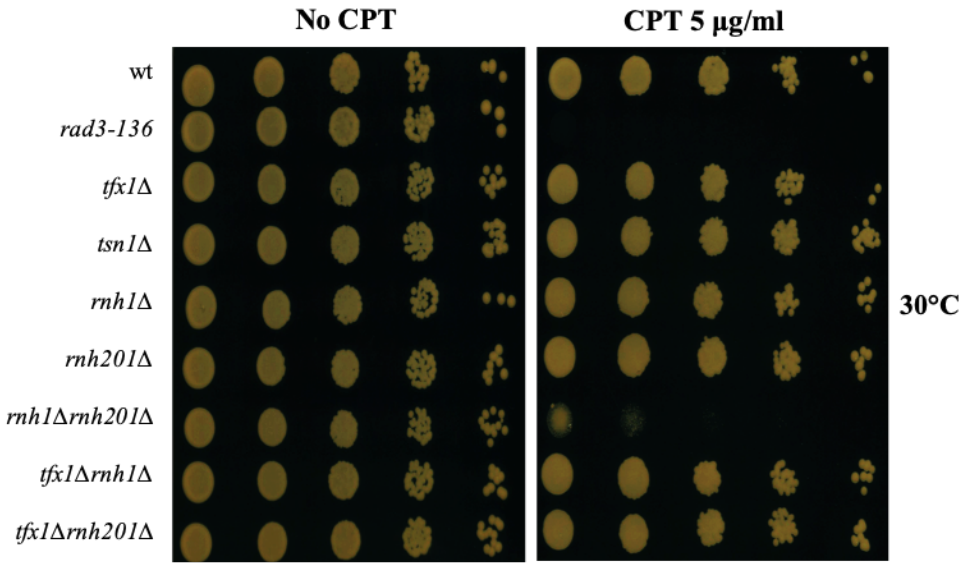

Figure 4.14 Sensitivity spot test of Camptothecin (CPT).
S. pombe mutants were diluted (10-fold serial dilution left to right) and spotted onto YEA media contain concentration of CPT (5 µg/m CPT). *rad3-136* was used as a positive control. The *rnh1Δ rnh201Δ* double mutant showed high sensitivity. The *tfx1Δ rnh1Δ* and *tfx1Δ rnh201Δ* double mutants show no increased sensitivity to CPT compared with the *rnh1*Δ and *rnh201*Δ single mutants. The plates were incubated 3 days at 30°C.

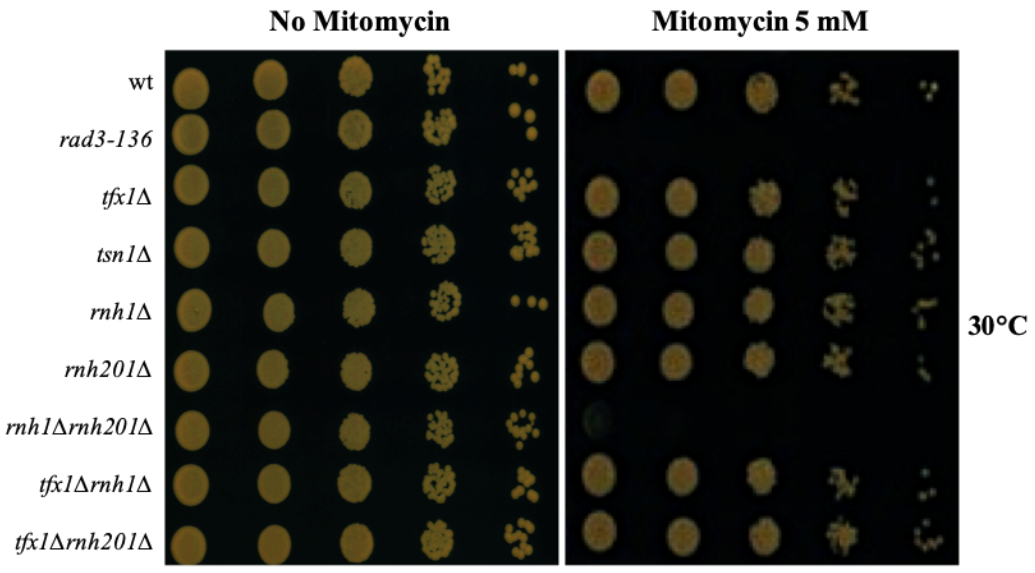

Figure 4.15 Sensitivity spot test of Mitomycin C (MMC).
S. pombe mutants were diluted (10-fold serial dilution left to right) and spotted onto YEA media contain concentration of Mitomycin C (5 mM MMC). *rad3-136* was used as a positive control. The *rnh1Δ rnh201Δ* double mutant shows high sensitivity. The *tfx1Δ rnh1Δ* and *tfx1Δ rnh201Δ* double mutants show no increased sensitivity to MMC. The plates were incubated 3 days at 30°C**.**

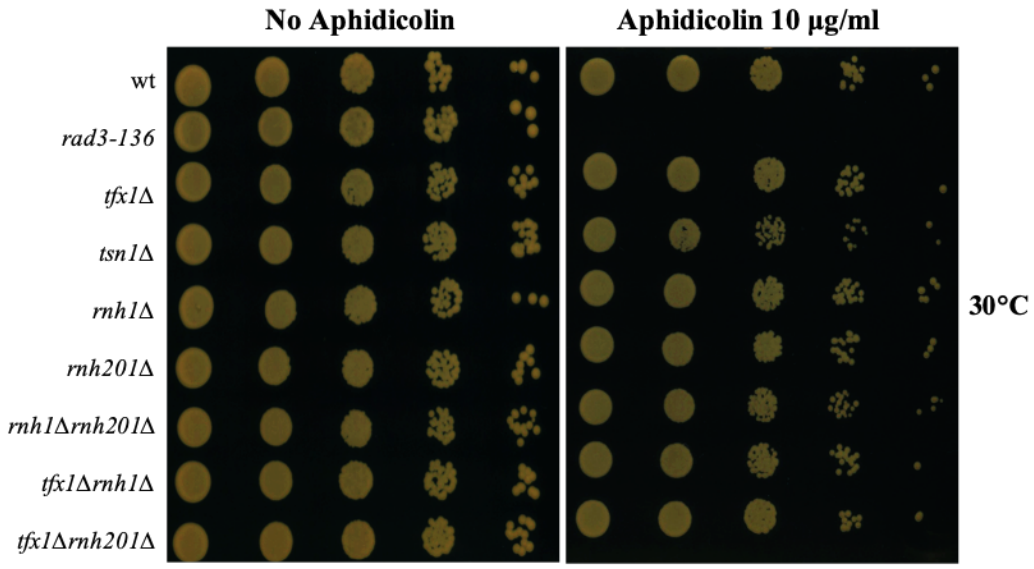

Figure 4.16 Sensitivity spot test of Aphidicolin.
S. pombe mutants were diluted (10-fold serial dilution left to right) and spotted onto YEA media contain concentration of Aphidicolin 10 µg/ml. *rad3-136* was used as a positive control. The *rnh1Δ rnh201Δ* double mutant shows high sensitivity. The *tfx1Δ rnh1Δ* and *tfx1Δ rnh201Δ* double mutants show no increased sensitivity to Aphidicolin. The plates were incubated 3 days at 30°C.

4.2.3 Relationship between Dcr1 and RNase H enzymes

4.2.3.1 Strains construction

The Dcr1 strain was used as the basis for creation of *de novo* mutants. All the strains were created by antibiotic-resistant cassettes replacement as founded on the PCR-based gene targeting approach as described by Bähler et al. (1998). The single mutant *rnh1*Δ and *rnh201*Δ strains were developed in the investigation and were constructed by the McFarlane group. Nonetheless, before being utilised, they were subjected to verification through PCR checking.

Additionally, in this study the double mutant *dcr1*Δ *rnh1*Δ (BP3469), and the double mutant *dcr1*Δ *rnh201*Δ (BP3461), were developed by deleting the genes from the single mutants *rnh1*Δ and *rnh201*Δ (BP3401 and BP3405). The antibiotic *natMX6* was used as the replacement cassettes in the deletion of *dcr1* and amplified by using PCR primers that designed with 80 bp homologous sequences directly flanked upstream and downstream from the *dcr1* ORFs and contained a 20 bp of homologous sequence to the plasmid that carries the *natMX6* gene. To verify the correct deletion, candidates of both strains were screened through the PCR (Figures 4.17 and 4.18). Two or more independent isolates were tested for each construct.

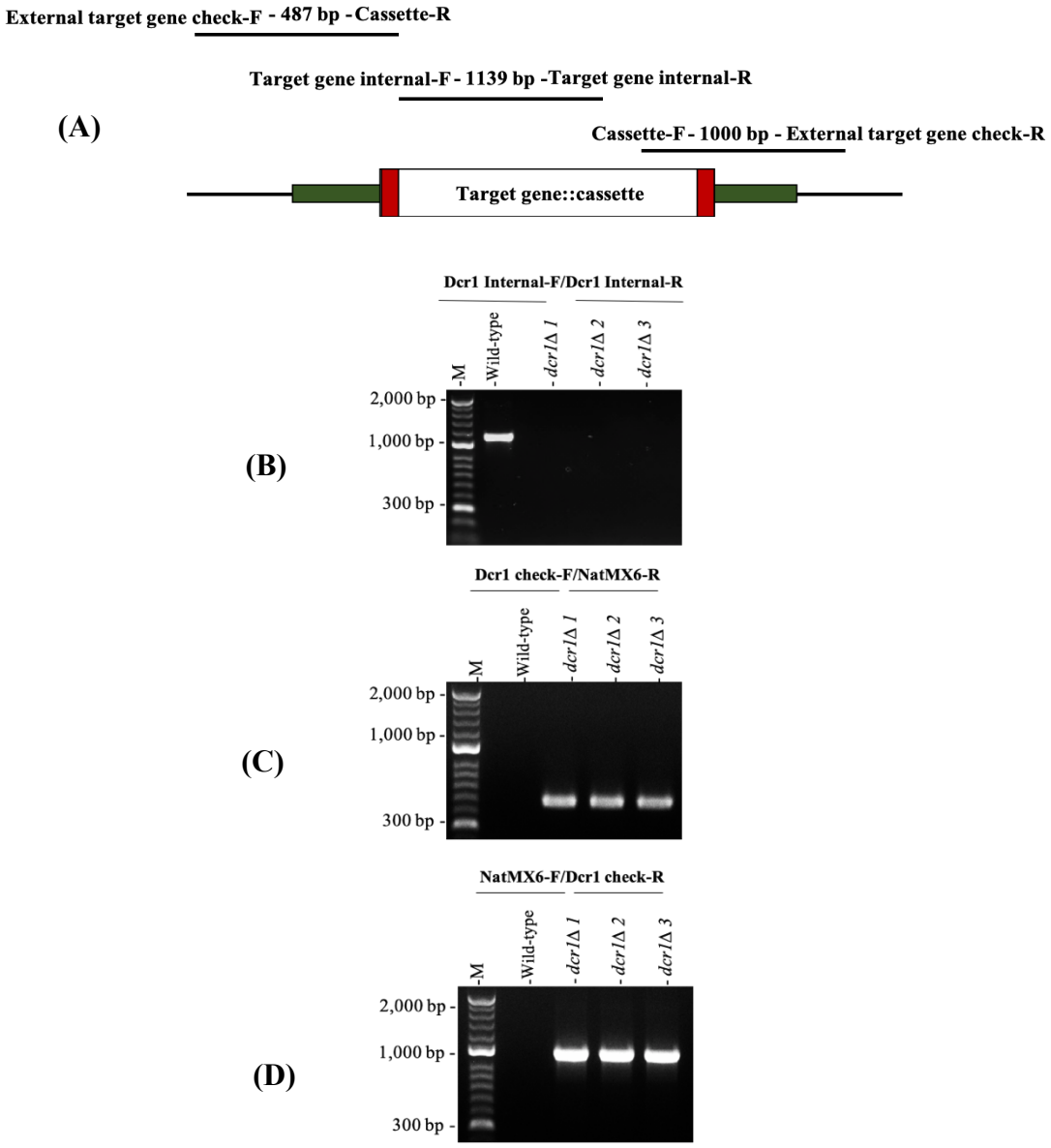

Figure 4.17 Confirmation by PCR screening of successful *dcr1Δrnh1Δ* double mutant knockout. (A) The genes were deleted and replacement with antibiotic resistant cassettes. To confirm the deletion of the target genes, three sets of primers were used. (B) Illustration of agarose gel screening of PCR products for the wild-type strain and *dcr1*Δ single mutant. The Dcr1-int-F and Dcr1-int-R primers were used, and the gel screening displays no PCR products in the successful *dcr1*Δcandidate strains. The expected sizes of the PCR product in *dcr1*Δ gene was 1139 bp. (C) The Dcr1 check-F and NatMX6-R primers were used to generate the PCR products for the wild-type and *dcr1*Δ candidate strains. The PCR products were seen in the *dcr1*Δ strains, but not in the wild-type strain and the expected band size is 487 bp. (D) The wild-type and *dcr1*Δ candidate strains were utilised to amplify by the NatMX6-F and Dcr1 check-R primers and the expected size is 1000 bp**.**

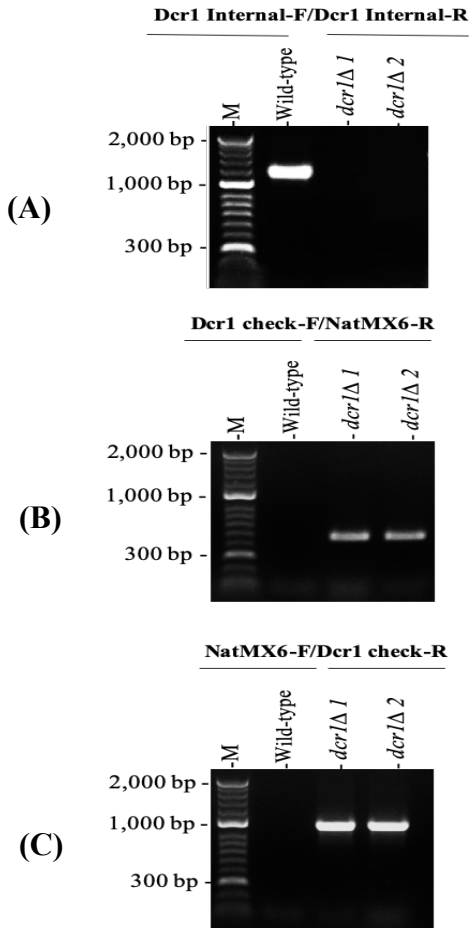

Figure 4.18 Confirmation by PCR screening of successful *dcr1Δrnh201Δ* double mutant knockout.

(A) Illustration of agarose gel screening of PCR products for the wild-type strain and *dcr1*Δ single mutant. The Dcr1-int-F and Dcr1-int-R primers were used, and the gel screening displays no PCR products in the successful *dcr1*Δcandidate strains. The expected sizes of the PCR product in *dcr1*Δ gene was 1139 bp. **(B)** The Dcr1 check-F and NatMX6-R primers were used to generate the PCR products for the wild-type and *dcr1*Δ candidate strains. The PCR products were seen in the *dcr1*Δ strains, but not in the wild-type strain and the expected band size is 487 bp. **(C)** The wild-type and *dcr1*Δ candidate strains were utilised to amplify by the NatMX6-F and Dcr1 check-R primers and the expected size is 1000 bp.

4.2.3.1 Spot test sensitivity to TBZ

Thiabendazole (TBZ), a microtubule-destabilizing drug has been found to play a role to inhibit microtubule function (Ahringer, 2003; Sadeghi et al., 2015). Mutations which causes disruption to distinct aspects of genome maintenance pathways can cause sensitivity to TBZ. In *S. pombe, dcr1*Δ cells are sensitive to the TBZ (Figure 4.19). The sensitivity of *dcr1*Δ cells to TBZ is attributed to chromosome mis-segregation (Volpe et al., 2003; Macrae et al.; 2006).

In addition to an RNAi role in centromere control, Dcr1 has been implicated in the maintenance of genome stability via an RNAi independent pathway (Castel et al., 2014). This prompted us to investigate the sensitivity of the *dcr1*Δ *rnh1*Δ and *dcr1*Δ *rnh201*Δ double mutants were both RNAase H pathways are inhibited to defraying whither Dcr1 functions specifically in one of these two pathways. Spot tests were carried out using the TBZ (Figure 4.19). The results showed that, the *rnh1*Δ*rnh201*Δ double mutants showed high sensitivity to the all agents consistent with previous reports (Ohle et al., 2016). The *rnh1*Δ and *rnh201*Δ single mutants showed no sensitivity increased to TBZ (Figure 4.19). The *dcr1*Δ *rnh1*Δ and *dcr1*Δ *rnh201*Δ double mutants did not show any sensitivity increase in comparison with *dcr1*Δ single mutant. Indeed, at higher concentrations of TBZ loss of either *rnh1* or *rnh201* appear to partly suppress the TBZ sensitivity of the *dcr1*Δ mutant. The reason for this is unclear.

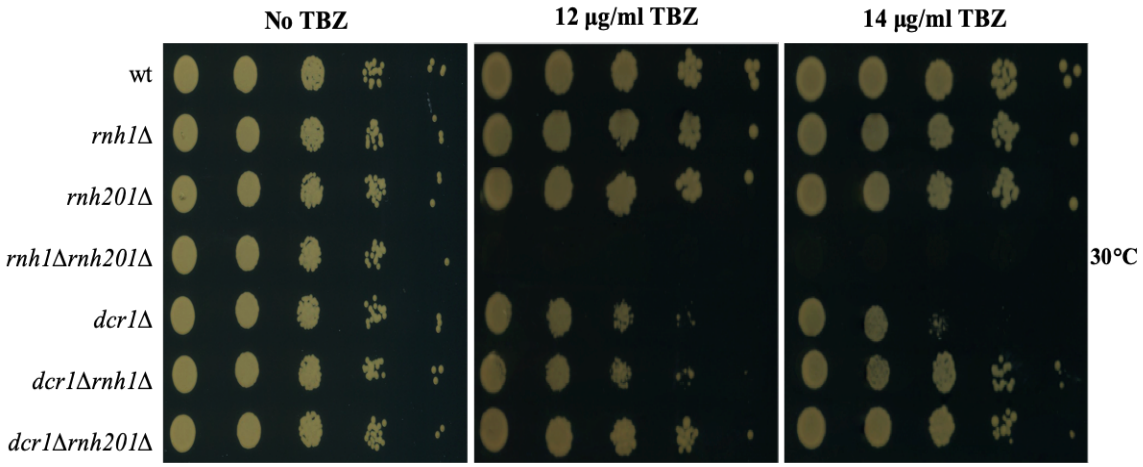

Figure 4.19 Loss of Rnh1 or Rnh201 suppress TBZ sensitivity of absence of a *dcr1*Δ mutant. *S. pombe* mutants were diluted (10-fold serial dilution left to right) and spotted onto YEA media contain different concentration of TBZ. The data displayed, the single mutant *dcr1*Δ showed increased sensitivity to TBZ compared with the WT. In addition, the double mutants *dcr1Δ rnh1Δ* and *dcr1Δ rnh201Δ* showed no increased sensitivity compared with the *dcr1*Δ single mutant. At higher TBZ concentration loss of *rnh1Δ or rnh201Δ* result in suppression of the *dcr1*Δ TBZ sensitivity. The plates were incubated 3 days at 30°C.

4.2.3.2 Sensitivity spot tests to investigate if Dcr1 functions in one of the RNase H pathways

The *dcr1*Δ single mutant showed sensitivity to HU (Castel et al., 2014), and in the absence of Dcr1 RNA:DNA hybrid levels became elevated and that causes barriers to DNA replication procession. This can sensitize *dcr1*Δ cells to DNA replication inhibitors such as HU. This led us to ask the question if Dcr1 is involved in one of the RNase H pathways. This prompted us to test the *dcr1*Δ *rnh1*Δ and *dcr1*Δ *rnh201*Δ double mutants to DNA damaging agents. Spot tests were carried out using a range of DNA damage agents. The DNA damage agents were tested in this study included phleomycin, which is responsible for generation of DNA double-strand breaks (Figures 4.20); UV, which induces multiple adducts (Figure 4.21); HU, as a DNA replication inhibitor (Figure 4.22); MMS, a DNA alkylating agent (Figure 4.23); CPT, a topoisomerase inhibitor (Figure 4.24); mitomycin C, a potent DNA crosslinker (Figure 4.25). The results showed that the *rnh1*Δ *rnh201*Δ double mutant showed high sensitivity to the all agents. The *rnh1*Δ and *rnh201*Δ*,* single mutants showed sensitivity to HU (Figure 4.22), but a little or no notable sensitivity to other agents tested. There was a mild sensitivity to phleomycin and UV in *dcr1*Δ *rnh201*Δ*,* but not *dcr1*Δ *rnh1*Δ double mutant. However, for the *dcr1*Δ *rnh1*Δ and *dcr1*Δ *rnh201*Δ double mutant there was no sensitivity increase to HU relative to the *dcr1*Δ single mutant. The *dcr1*Δ *rnh1*Δ and *dcr1*Δ *rnh201*Δ double mutant did not show any increase sensitivity in comparison with the *rnh1*Δ and *rnh201*Δ single mutants or WT in response to MMC, MMS and CPT.

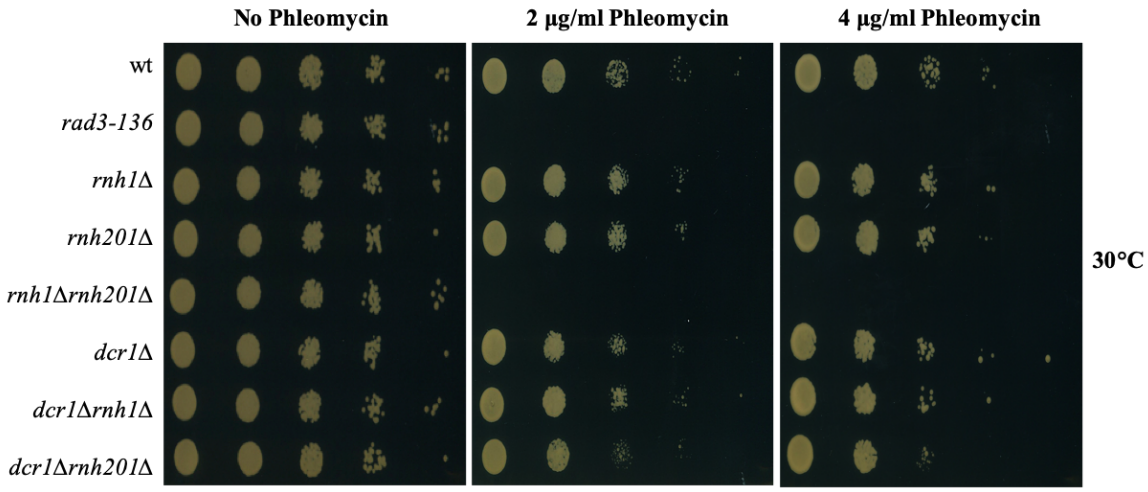

Figure 4.20 Rnh201, but not Rnh1, is required for the response to Phleomycin in the absence of Dcr1.
S. pombe mutants were diluted (10-fold serial dilution left to right) and spotted onto YEA media contain different concentration of Phleomycin. *rad3-136* was used as a positive control. The *rnh1Δ rnh201Δ* double mutant show high sensitivity. The *dcr1Δ rnh201Δ* double mutant show increased sensitivity to Phleomycin compared with the *rnh1*Δ and *rnh201*Δ single mutant, but the *dcr1Δ rnh1Δ* double mutant show no increased sensitivity compared with the single mutants. The plates were incubated 3 days at 30°C.

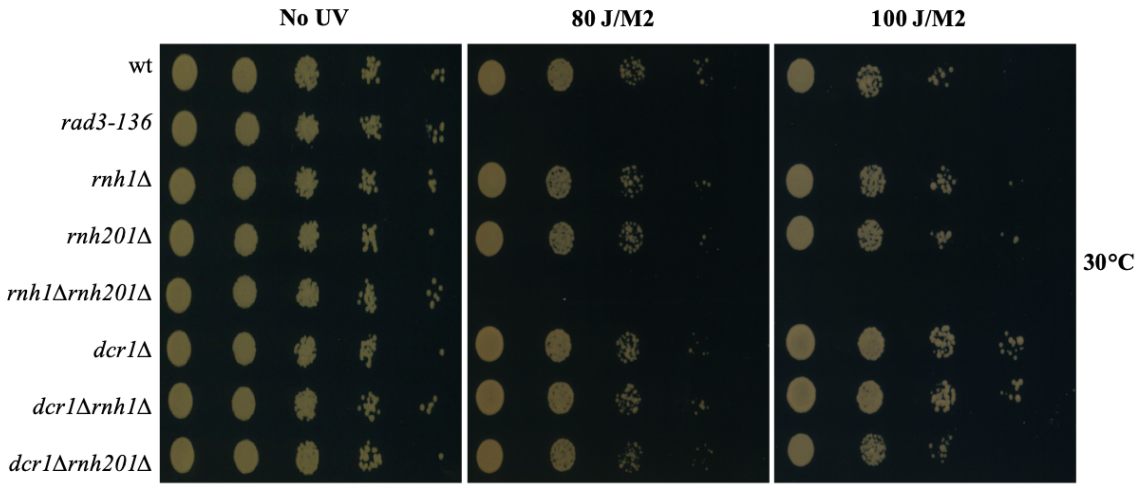

Figure 4.21 Sensitivity spot test of UV irradiation.
S. pombe mutants were diluted (10-fold serial dilution left to right) and spotted onto YEA media and then exposed to different doses of UV irradiation. *rad3-136* was used as a positive control. The *rnh1Δ rnh201Δ* double mutant shows full sensitivity. The double mutant *dcr1Δ rnh201Δ* show increase sensitivity to the UV compared with the *dcr1*Δ single mutant and the *dcr1Δrnh1Δ* double mutant. The plates were incubated 3 days at 30°C. The plates were incubated 3 days at 30°C.

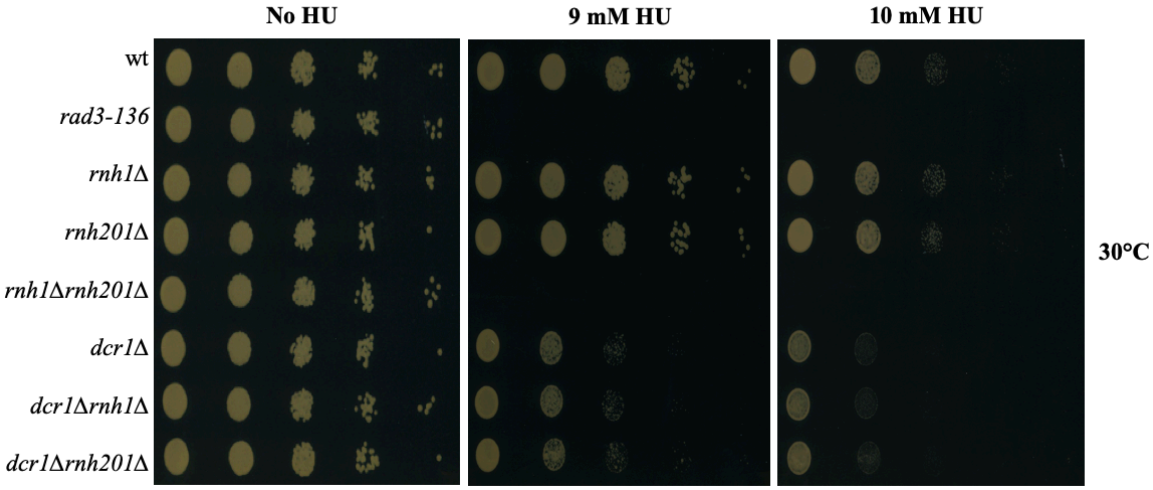

Figure 4.22 Sensitivity spot test of Hydroxyurea.
S. pombe mutants were diluted (10-fold serial dilution left to right) and spotted onto YEA media contain different concentration of hydroxyurea (8 mM, 9 mM and 10 mM HU). *rad3-136* was used as a positive control. The *rnh1Δ rnh201Δ* double mutant shows high sensitivity. The *dcr1Δ rnh1Δ* and *dcr1Δ rnh201Δ* double mutants show similar sensitivity to hydroxyurea compared with the *dcr1Δ* single mutant. The plates were incubated 3 days at 30°C.

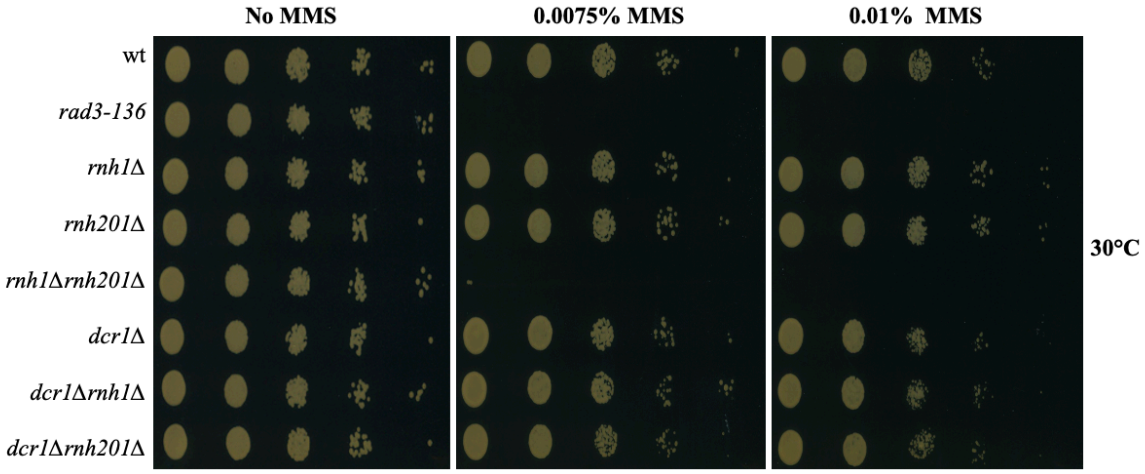

Figure 4.23 Sensitivity spot test of Methyl methane sulfonate (MMS).
S. pombe mutants were diluted (10-fold serial dilution left to right) and spotted onto YEA media contain different concentration of MMS (0.0075% and 0.01% MMS). *rad3-136* was used as a positive control. The *rnh1Δ rnh201Δ* double mutant shows high sensitivity. The *dcr1Δ rnh1Δ* and *dcr1Δ rnh201Δ* double mutants show no sensitivity to MMS compared with the *dcr1Δ* single mutant and the WT. The plates were incubated 3 days at 30°C.

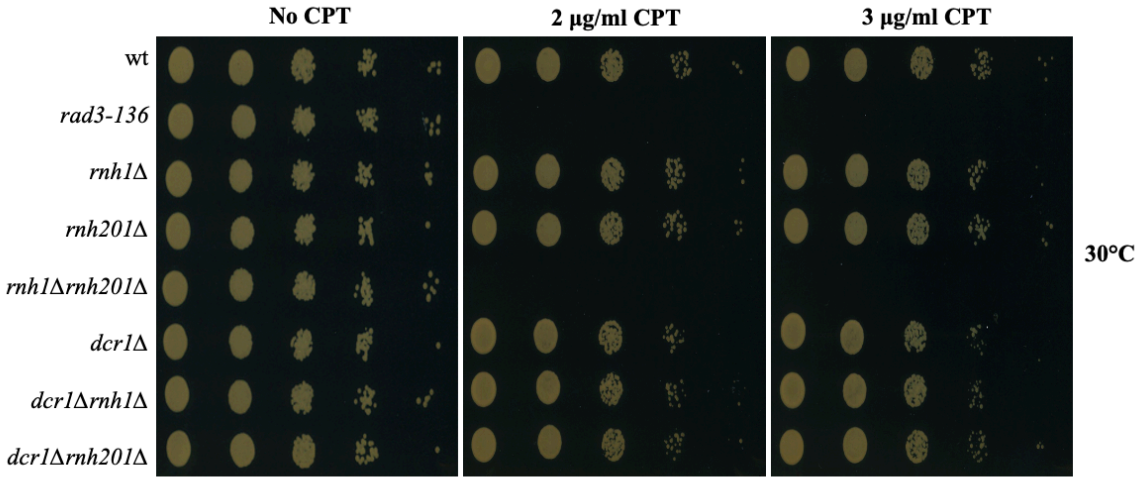

Figure 4.24 Sensitivity spot test of Camptothecin (CPT).
S. pombe mutants were diluted (10-fold serial dilution left to right) and spotted onto YEA media contain different concentration of CPT (2 µg/m and 3 µg/m CPT). *rad3-136* was used as a positive control. The *rnh1Δ rnh201Δ* double mutant shows high sensitivity. The *dcr1Δ rnh1Δ* and *dcr1Δ rnh201Δ* double mutants show no sensitivity to CPT compared with the *dcr1Δ* single mutant and the WT. The plates were incubated 3 days at 30°C.

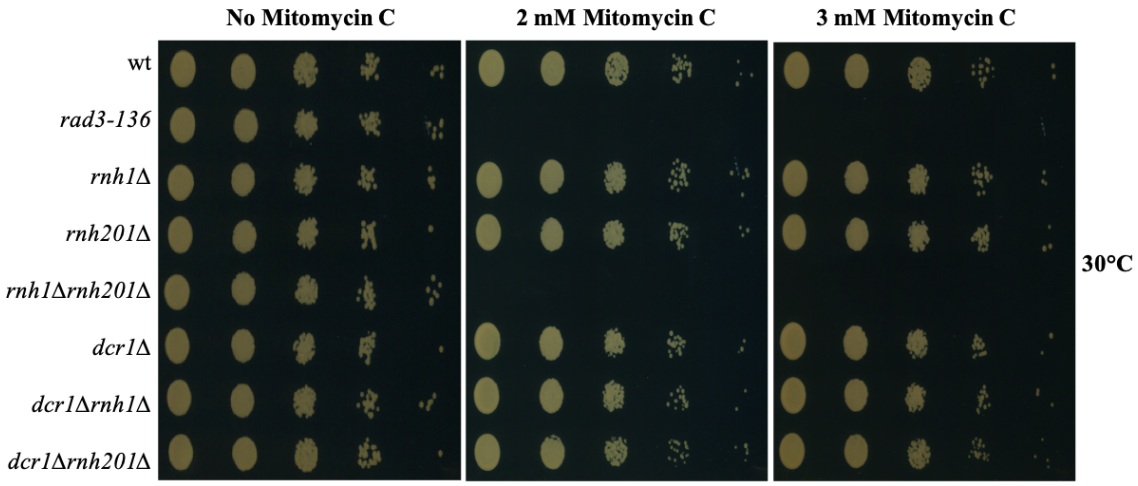

Figure 4.25 Sensitivity spot test of Mitomycin C (MMC).
S. pombe mutants were diluted (10-fold serial dilution left to right) and spotted onto YEA media contain concentration of Mitomycin C (2 mM and 3 mM MMC). *rad3-136* was used as a positive control. The *rnh1Δ rnh201Δ* double mutant show high sensitivity. The *dcr1Δ rnh1Δ* and *dcr1Δ rnh201Δ* double mutants show no sensitivity to MMC compared with the *dcr1Δ* single mutant and the WT. The plates were incubated 3 days at 30°C.

4.2.4 Analysis of Sen1 deficient cells

RNA-DNA hybrids are disrupted by RNA-DNA helicases, such as Sen1 in *S. cerevisiae* (Stuckey et al., 2015). Sen1 function protects the genome from transcription associated recombination by unwinding the RNA:DNA hybrids that formed during transcription (Li et al., 2016). Having determined a relationship between Tsn1 and *S. pombe* RNase H pathway, here we set out to address whether these a sematic relationship between Tsn1 and the *S. pombe* Sen1 orthologue. We set out to make strains defective in Sen1 and Tsn1/Tfx1. The *sen1*Δ strain was used as the basis for creation of *de novo* mutants. All the strains were created by antibiotic-resistant cassettes replacement as founded on the PCR-based gene targeting approach as described by Bähler et al. (1998). The single mutant *sen1*Δ and *tsn1*Δ*sen1*Δ*, tfx1*Δ *sen1*Δ double mutant strains were developed by the McFarlane group. Nonetheless, before being utilised, they were subjected to verification through PCR checking. Additionally, in this study the double mutant *sen1*Δ *rnh201*Δ were developed by deleting the genes from the single mutants *sen1*Δ (BP3448). To create a double mutants *sen1*Δ *rnh201*Δ (BP3480), *rnh201* deletion took place in the background of *sen1*Δ (BP3480). The antibiotic *natMX6* was used as the replacement cassettes in the deletion of *rnh201.* To verify the correct deletion, candidates of both strains were screened through the PCR (Figure 4.26) Two or more independent isolates were tested for each construct.

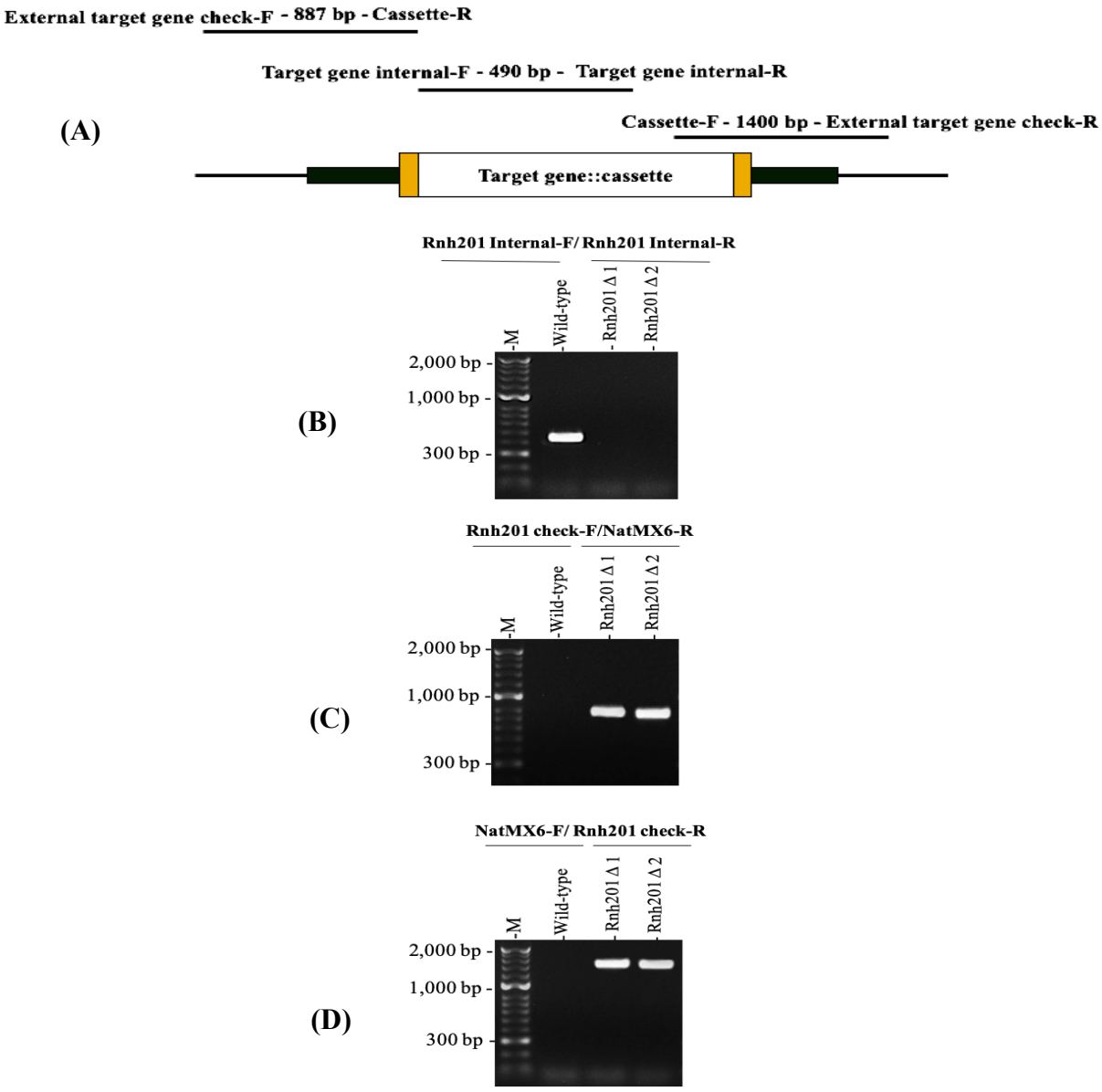

Figure 4.26 Confirmation by PCR screening of successful *sen1Δrnh201Δ* double mutant knockout. **(A)** The genes were deleted and replacement with antibiotic resistant cassettes. To confirm the deletion of the target genes, three sets of primers were used. **(B)** Illustration of agarose gel screening of PCR products for the wild-type strain and *rnh201*Δ single mutant. The Rnh201-int-F and Rnh201-int-R primers were used, and the gel screening displays no PCR products in the successful *rnh201*Δ candidate strains. The expected sizes of the PCR product in *rnh201*Δ gene was 490 bp. **(C)** The Rnh201 check-F and NatMX6-R primers were used to generate the PCR products for the wild-type and *rnh201*Δ candidate strains. The PCR products were seen in the *rnh201*Δ strains, but not in the wild-type strain and the expected band size is 887 bp. **(D)** The wild-type and *rnh201*Δ candidate strains were utilised to amplify by the NatMX6-F and Rnh201 check-R primers and the expected size is 1400 bp.

4.2.4.1 Sensitivity spot tests to investigate the inter-relationship between distinct RNA:DNA hybrid pathways

The data for the response of the *tsn1*Δ *rnh201*Δ double mutant to phleomycin, bleomycin and HU agents provoked the question if the Sen1 helicases was removed do we still see have the same defect observed in *tsn1*Δ *rnh201*Δ strains, as a Sen1 offers a distinct RNA:DNA hybrid removal pathway. This prompted us to investigate the sensitivity of the *sen1*Δ *tsn1*Δ*, sen1*Δ *tfx1*Δ and *sen1*Δ *rnh201*Δ double mutants to DNA damaging agents. Spot tests were carried out using a range of DNA damage agents. The DNA damage agents tested in this study included phleomycin, which is responsible for generation of DNA double-strand breaks (Figures 4.27); as a DNA replication inhibitor (Figure 4.28); UV, which induces multiple adducts (Figure 4.29); MMS, a DNA alkylating agent (Figure 4.30); CPT, a topoisomerase inhibitor (Figure 4.31); mitomycin C, a potent DNA crosslinker (Figure 4.32);. The data demonstrate that, *sen1*Δ *tsn1*Δ*, sen1*Δ *tfx1*Δ and *sen1*Δ *rnh201*Δ double mutants did not show any sensitivity increase compared with the *sen1*Δ, *rnh1*Δ and *rnh201*Δ single mutants or WT in response to most DNA damaging agents. However, the *sen1*Δ *rnh201*Δ double mutant showed a very mild sensitivity to HU relative to other strains (Figure 4.28). This mutant showed no discernible sensitivity to any other agent tested.

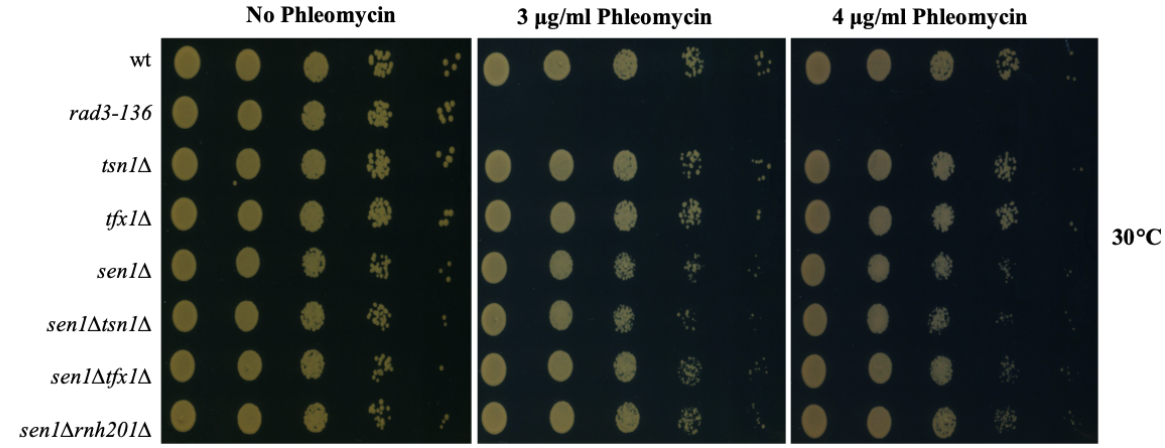

Figure 4.27 Sensitivity spot test of Phleomycin.
S. pombe mutants were diluted (10-fold serial dilution left to right) and spotted onto YEA media contain different concentration of Phleomycin. *rad3-136* was used as a positive control. The *sen1*Δ single mutant and the *sen1Δ tsn1Δ, sen1Δ tfx1Δ and sen1Δ rnh201Δ* double mutants show no increased sensitivity to Phleomycin. The plates were incubated 3 days at 30°C.

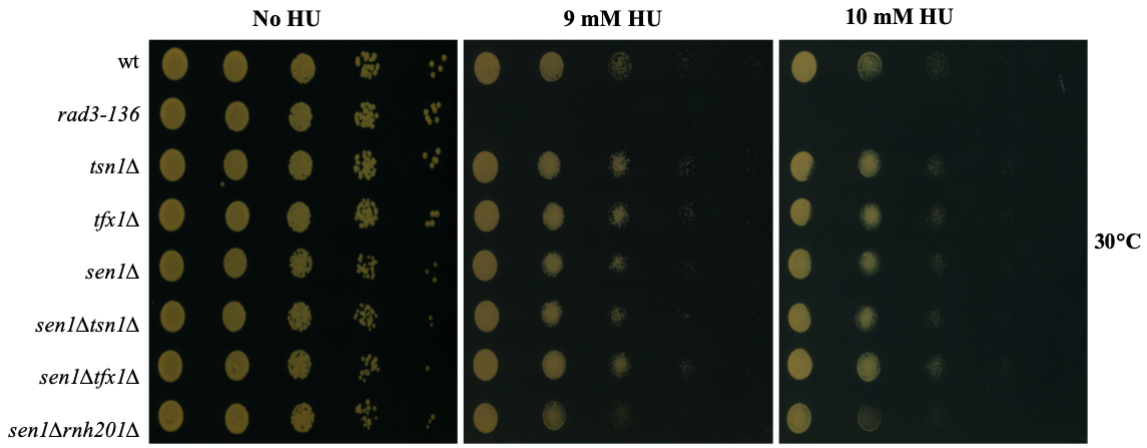

Figure 4.28 Sensitivity spot test of Hydroxyurea.
S. pombe mutants were diluted (10-fold serial dilution left to right) and spotted onto YEA media contain different concentration of Hydroxyurea. *rad3-136* was used as a positive control. The *sen1*Δ single mutant and the *sen1Δ tsn1Δ, sen1Δ tfx1Δ and sen1Δ rnh201Δ* double mutants show no increased sensitivity to Hydroxyurea. The plates were incubated 3 days at 30°C.

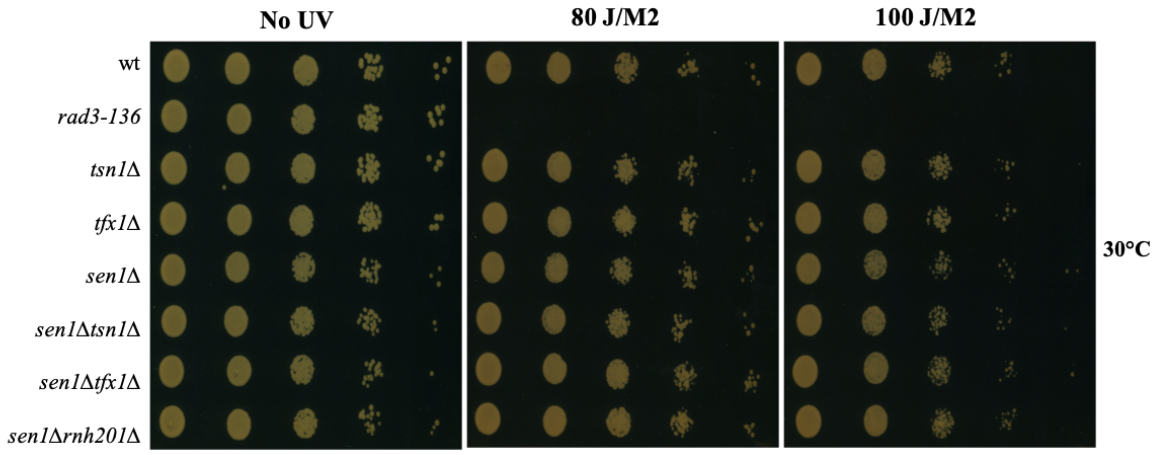

Figure 4.29 Sensitivity spot test of UV irradiation.
S. pombe mutants were diluted (10-fold serial dilution left to right) and spotted onto YEA media and then exposed to different doses of UV irradiation. *rad3-136* was used as a positive control. The *sen1*Δ single mutant and the *sen1Δ tsn1Δ, sen1Δ tfx1Δ and sen1Δ rnh201Δ* double mutants show no increased sensitivity to UV irradiation. The plates were incubated 3 days at 30°C.

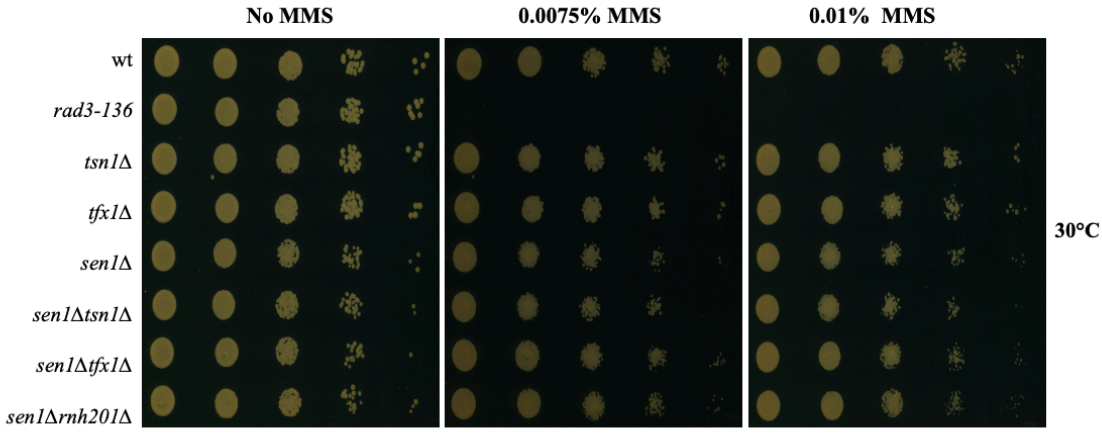

Figure 4.30 Sensitivity spot test of Methyl methane sulfonate (MMS).
S. pombe mutants were diluted (10-fold serial dilution left to right) and spotted onto YEA media contain different concentration of MMS (0.0075% and 0.01% MMS). *rad3-136* was used as a positive control. The *sen1*Δ single mutant and the *sen1 Δtsn1Δ, sen1Δ tfx1Δ and sen1Δ rnh201Δ* double mutants show no increased sensitivity to MMS. The plates were incubated 3 days at 30°C.

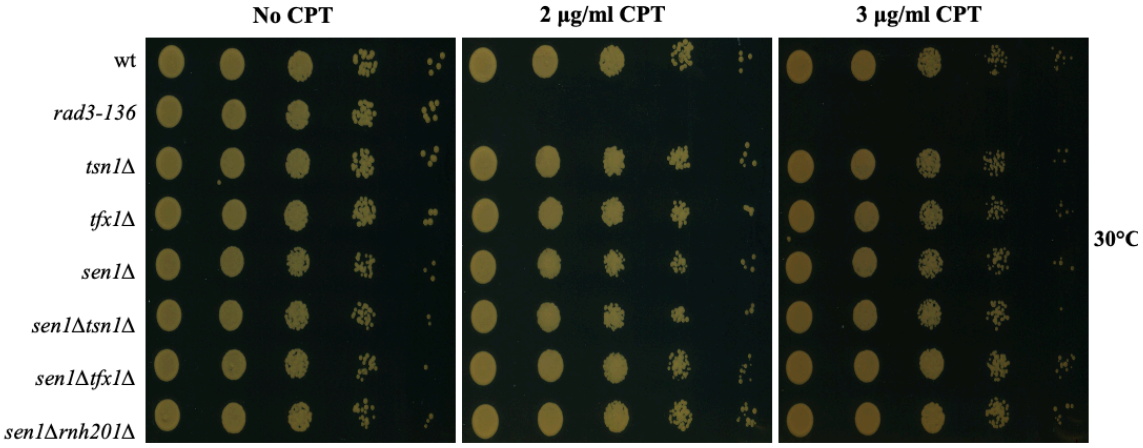

Figure 4.31 Sensitivity spot test of Camptothecin (CPT).
S. pombe mutants were diluted (10-fold serial dilution left to right) and spotted onto YEA media contain different concentration of CPT (2 µg/m and 3 µg/m CPT). *rad3-136* was used as a positive control. The *sen1*Δ single mutant and the *sen1Δ tsn1Δ, sen1Δ tfx1Δ and sen1Δ rnh201Δ* double mutants show no increased sensitivity to CPT. The plates were incubated 3 days at 30°C.

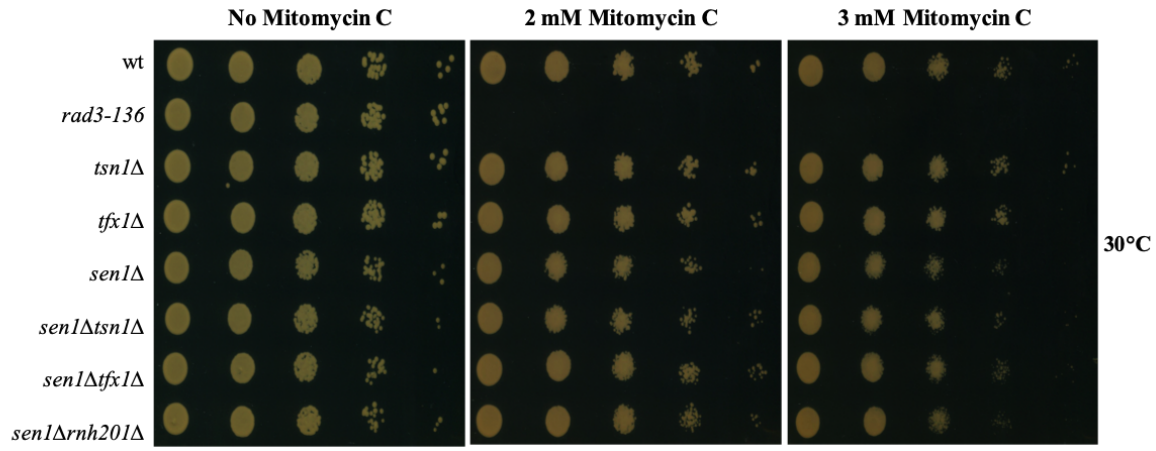

Figure 4.32 Sensitivity spot test of Mitomycin C (MMC).
S. pombe mutants were diluted (10-fold serial dilution left to right) and spotted onto YEA media contain concentration of Mitomycin C (2 mM and 3 mM MMC). *rad3-136* was used as a positive control. The *sen1*Δ single mutant shows no increased sensitivity to MMC. The *sen1Δtsn1Δ, sen1Δ tfx1Δ and sen1Δ rnh201Δ* double mutants show no increased sensitivity to MMC. The plates were incubated 3 days at 30°C.

4.3 Discussion

In order to avoid the formation of the RNA:DNA hybrids, there are two major suppressor of RNA:DNA hybrids which are RNase H1 and RNase H2. The RNase Hs are two highly conserved ribonucleases enzymes and they have ability to remove RNA:DNA hybrids by degrading the RNA moiety Therefore, the RNase Hs are important in preventing genome instability and transcription replication conflicts (Cerritelli & Crouch et al., 2009; Amon & Koshland et al., 2016). RNase H activity is also important for efficient repair of the DSBs. The deletion of both RNase H1 and RNase H2 coding genes results in defects in DNA damage recovery, which results inhibition of HR-mediated DSB repair. This suggesting that the two RNase H pathways are needed redundantly in DSB repair (Ohle et al., 2016), but Zhao and co-workers (2018), however, demonstrated that RNase H is not generally required for efficient DSB repair. The data presented here demonstrated that the *rnh1Δ rnh201Δ* double mutant showed hypersensitivity to all DNA damage agents indicating their importance in the recovery from DNA damage. In addition, prior to this work there was little direct evidence that Translin is also involved in the recovery from DNA damage by possibly control the DNA:RNA hybrid, despite the proposal that it is required for chromosomal translocations (Jaendling & McFarlane, 2010). However, Trax has been demonstrated to be required for proper recruitment of the ATM kinase to DSBs to mediate DNA repair process, although it is proposed that this function is independent of Translin (Wang et al., 2016).

This led our group to assess whether Tsn1 and/or Tfx1 has functions in one of the RNase H pathways and the data presented here indicate that Tsn1, but not Tfx1, does indeed have a role to play in the recovery from DNA damage for several genotoxic and DNA replicative stress agents. The effect of the HU agent is increases in DNA replication stress (Sparks et al., 2012). This mechanism likely explains why *rnh1Δ rnh201Δ* double mutant cells are sensitive to HU. Therefore, likely that increased ribonucleotide incorporation into DNA, coupled with defects in ribonucleotide excision repair (RER), R-loop processing, or RNA primer removal, results in increased sensitivity of the *tsn1Δ rnh201Δ* double mutant to HU (Figure 4.3). However, the *tsn1Δ rnh1Δ* double mutant does not show this sensitivity to HU. Therefore, the loss of the RNase H2, but not the

RNase H1 in combination with loss of Tsn1 results in a stronger genome instability phenotype (Zimmer & Koshland et al., 2016). So, from the work in this chapter we have revealed the role of Tsn1 in DNA damage recovery by possibly destabilising RNA:DNA hybrids in a pathway redundant with Rnh201, and possibly assumed to be the Rnh1 pathway.

Castel and co-workers (2016) demonstrated that the *dcr1*Δ single mutant showed increase sensitivity to HU. In the absence of Dcr1 RNA:DNA hybrid levels became elevated and causes more problem during the DNA replication. So, because there is an increase in RNA:DNA hybrids, when replication occurs the cells become sensitive to slowed DNA replication, for example, by HU. This let us to ask if Dcr1 is also involved in one of the two RNase H pathways, so we mutate *dcr1*Δ in the both backgrounds. Interestingly, the *dcr1*Δ *rnh1*Δ and *dcr1*Δ *rnh201*Δ double mutants did not show any sensitivity increase in response to HU, which suggest Dcr1 is not directly related to these two pathways (Figure 4.22). Castel and co-workers proposed that Dcr1 is involved in the removal of the RNA:DNA hybrids. So, it is clear here this suggestion of the RNase H pathways is not the case and it may be that Dcr1 removes the RNA pol II, and not RNA:DNA hybrids.

The phenotype of the TBZ was different for the *dcr1*Δ *tsn1*Δ and *dcr1*Δ *tfx1*Δ double mutants backgrounds (Chapter 3; Figure 3.1), but this may be because the TBZ mechanism probably relates to centromere and telomere structure control, whereas the HU response is relates to internal region avoidance of transcription- replication conflicts, so different mechanisms are play.

RNA:DNA hybrids can also be removed by unwinding the duplex by Sen1 RNA-DNA helicases in *S. cerevisiae* (Stuckey et al., 2015). The data here demonstrate that *sen1*Δ *tsn1*Δ, *sen1*Δ *tfx1*Δ and *sen1*Δ *rnh201*Δ double mutants did not show any sensitivity increase in response to all DNA damaging agents, although there is a mild sensitivity in the *sen1*Δ *rnh201*Δ double mutant to HU. This suggest that Tsn1 and Tfx1 are not acting in a helicase- associated pathway.

So, from the work in this chapter we have revealed a role for Tsn1, but not Tfx1, with appears to be functionally required in the absence of Rnh201.

4.4 Conclusion

1. The mutation of both RNase H1 and RNase H2 coding genes inhibits DSB repair in *S. pombe.*
2. Tsn1 function is redundant with Rnh201 in replication- associated DNA damage recovery, possible in Rnh1- dependent pathway.
3. Dcr1 and Sen1are not involved in the RNase H pathways.

Chapter 5: Results

Assessment of a role for Tsn1 and/or Tfx1 in DSB repair

5.1 Introduction

In the previous chapter we have seen that the *tsn1*Δ *rnh201*Δ double mutant exhibited increased sensitivity to some DNA damaging agents. Both Tsn1 and Tfx1 suppress RNA:DNA hybrid levels (McFarlane group, unpublished data), but only loss of Tsn1 results in a failure to respond to DNA damage upon loss of RNase function. Ionizing irradiation causes DSBs which can lead to cancer (Chakarov et al., 2014). RNA:DNA hybrids can both promote DSB repair and cause unwanted genomic instability by causing DNA replication-associated damage after DNA polymerase collisions with transcription (Yang & Qi, 2015; Gaillard & Aguilera, 2016). DNA replication disturbance is an oncogenic initiator (Tomasetti & Vogelstein, 2017). Translin has ability to bind to the breakpoint junctions of cancer chromosomal translocations and is required for murine recovery from ionizing irradiation. However, whilst Translin is proposed to have a function recombination repair this has not yet been demonstrated (Aoki et al., 1995; Fukuda et al., 2008; Wang et al., 2016). Prior to this current work, there was little direct evidence that Tsn1 and/or Tfx1 are involved in recovery from DNA damage, despite the proposal that it is required for chromosomal translocations (Jaendling & McFarlane, 2010).

The hypothesis to be tested here is that the loss of Tsn1 and/or Tfx1 function results in increased RNA:DNA hybrids, which assists in DSB repair. Resent work from the Fisher group has demonstrated a positive role of RNA:DNA hybrids in DSB repair (Ohle et al.,2016). This led us to ask if increased RNA:DNA hybrids function to control or protect the genome by stimulating DSB repair in the absence of Tsn1 or/and Tfx1. To test this hypothesis, *tsn1* and *tfx1* were mutated and tested by some agents that cause DSBs.

5.2 Results

5.2.1 Sensitivity spot tests to investigate whether the Tsn1 and Tfx1 have roles in the DSB repair

The hypothesis that loss of Tsn1 and/or Tfx1 might elevate DSB repair efficiently, not only comes from the findings of the Fischer group, but also a fortuitous observation within our lab. Whilst carrying out spot test on phleomycin, we occasionally noticed that *tsn1*Δ and *tfx1*Δ single mutants exhibited more resistance to this agent than the wild-type control (Figures 5.1). This was also the case for bleomycin (Figures 5.1). This effect was not always reproducible and appears to be condition dependent. Whilst we suspect growth strains/conditions to be discrimination, this has not yet been fully elucidated. This resistance was only observed for phleomycin and bleomycin (Figures 5.1), and not for the HU, MMS, UV, CPT or MMC (Figures 5.2 - 5.6).

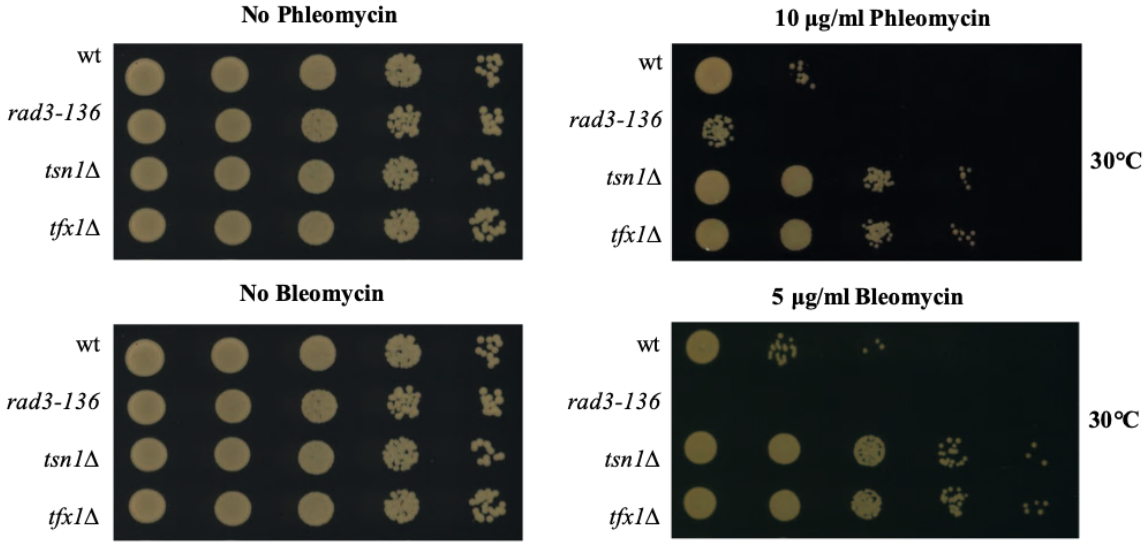

Figure 5.1 Sensitivity spot test of Phleomycin and Bleomycin.
S. pombe mutants were diluted (10-fold serial dilution left to right) and spotted onto YEA media contain different concentration of Phleomycin and Bleomycin. *rad3-136* was used as a positive control. The *tsn1Δ* and *tfx1Δ* single mutants shows hyper resistant to the DSB agent phleomycin and bleomycin. The plates were incubated 3 days at 30°C.

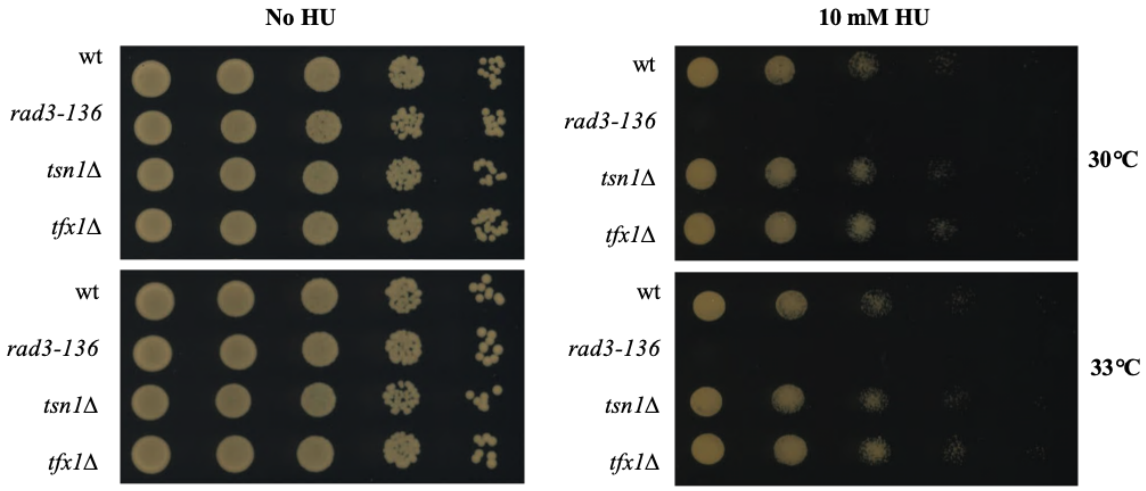

Figure 5.2 Sensitivity spot test of hydroxyurea.
S. pombe mutants were diluted (10-fold serial dilution left to right) and spotted onto YEA media contain 10 mM concentration of hydroxyurea. *rad3-136* was used as a positive control. The *tsn1Δ* and *tfx1Δ* single mutants shows no increase sensitivity to HU compared to the WT. The plates were incubated 3 days at 30°C and 33°C.

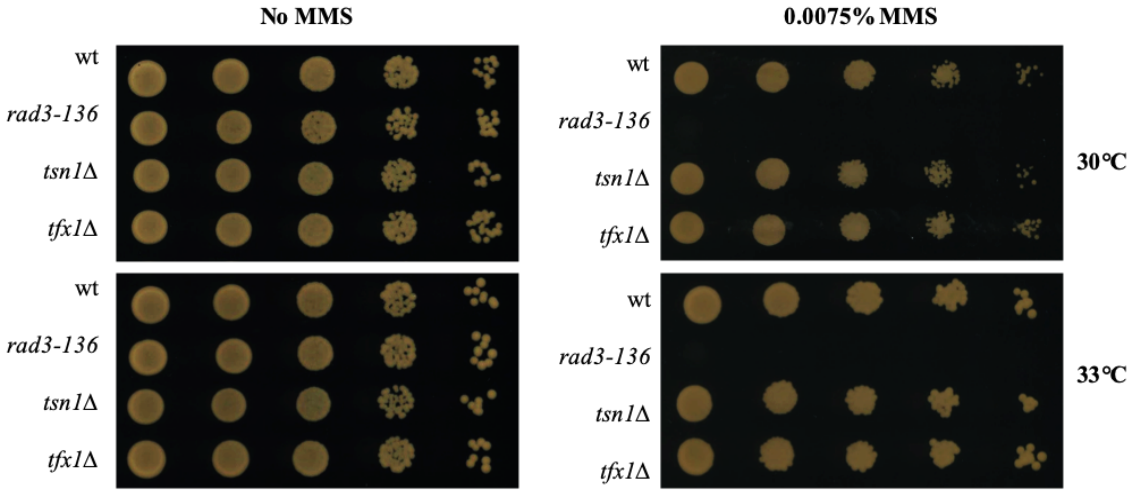

Figure 5.3 Sensitivity spot test of MMS.
S. pombe mutants were diluted (10-fold serial dilution left to right) and spotted onto YEA media contain 0.0100% concentration of MMS. *rad3-136* was used as a positive control. The *tsn1Δ* and *tfx1Δ* single mutants shows no increase sensitivity to MMS compared to the WT. The plates were incubated 3 days at 30°C and 33°C.

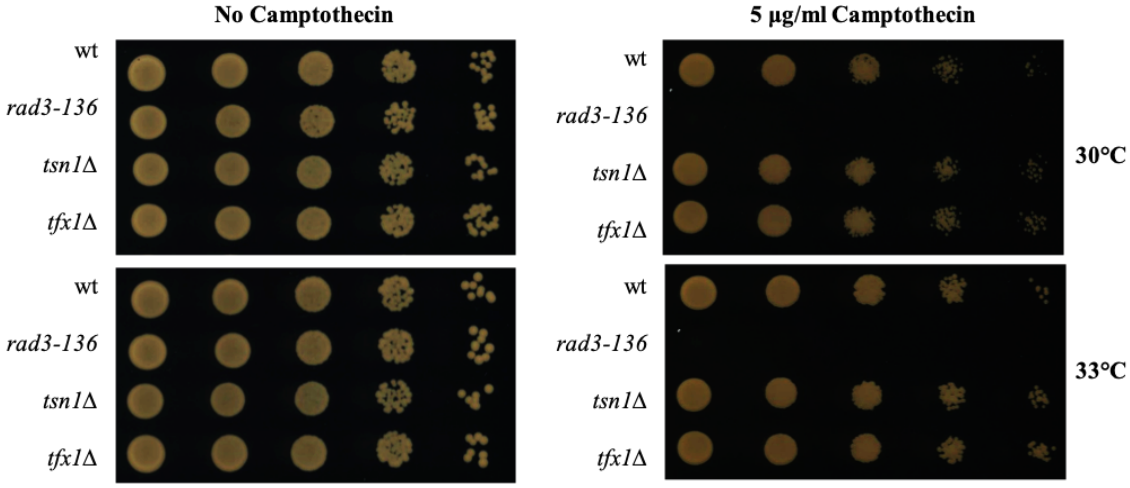

Figure 5.4 Sensitivity spot test of CPT.
S. pombe mutants were diluted (10-fold serial dilution left to right) and spotted onto YEA media contain 5 µg/ml concentration of CPT. *rad3-136* was used as a positive control. The *tsn1Δ* and *tfx1Δ* single mutants shows no increase sensitivity to CPT compared to the WT. The plates were incubated 3 days at 30°C and 33°C.

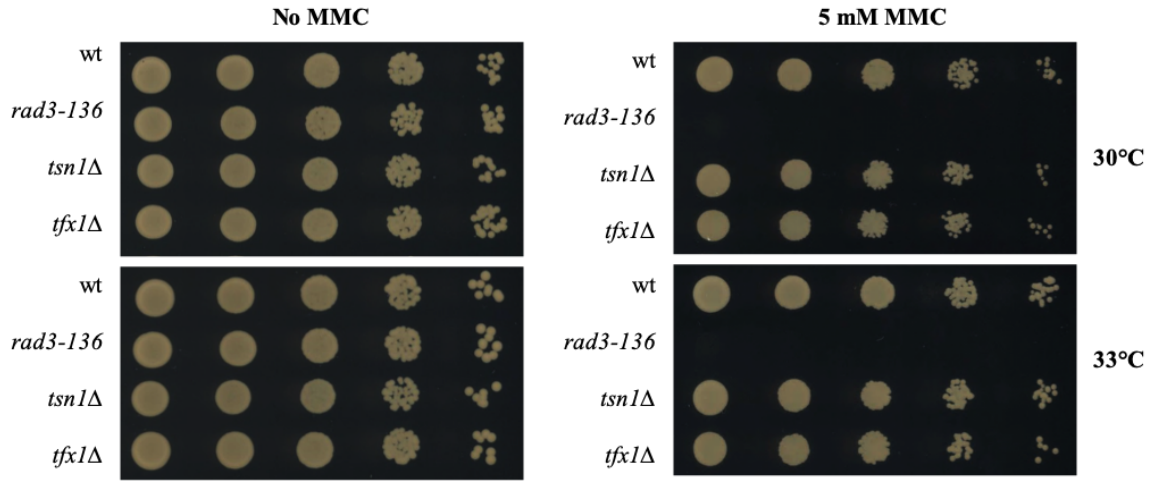

Figure 5.5 Sensitivity spot test of Mitomycin C.
S. pombe mutants were diluted (10-fold serial dilution left to right) and spotted onto YEA media contain 5 mM concentration of MMC. *rad3-136* was used as a positive control. The *tsn1Δ* and *tfx1Δ* single mutants shows no increase sensitivity to MMC compared to the WT. The plates were incubated 3 days at 30°C and 33°C.

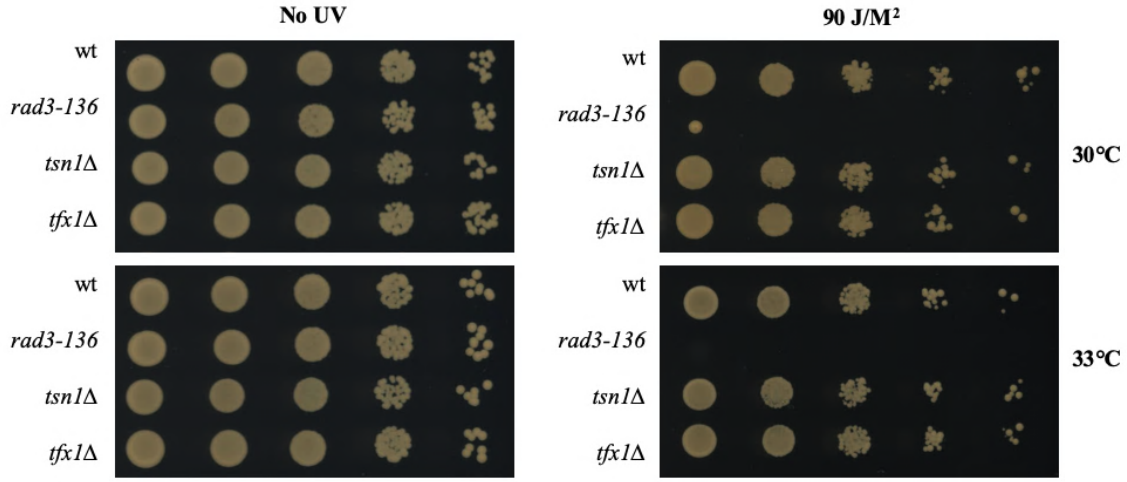

Figure 5.6 Sensitivity spot test of UV irradiation.
S. pombe mutants were diluted (10-fold serial dilution left to right) and spotted onto YEA media and then exposed to 90 J/M^2 dose of UV irradiation. *rad3-136* was used as a positive control. The *tsn1Δ* and *tfx1Δ* single mutants shows no increase sensitivity to UV compared to the WT. The plates were incubated 3 days at 30°C and 33°C.

5.2.2 I-PpoI nuclease induction system

In fission yeast, RNA:DNA hybrids have been shown to assist the repair of DSBs (Ohle et al., 2016; Plosky, 2016). An inducible endonuclease can introduce DSBs at a specific locus (Ohle et al.,2016), and this allows for the measurement of DSB kinetics, repair and RNA:DNA hybrid levels/recruitment/processing/RNA pol II enrichment at one locus. The unexpected observation that *tsn1*Δ and *tfx1*Δ single mutants were more resistant to a DSB agent under certain condition led us to speculate that these mutants were more efficient at DSB repair, not less. To test this, we have obtained the DSB system from the Fischer group which is based on I-PpoI nuclease induction (Ohle et al., 2016). In appropriate mutants, we evaluate DSB repair.

5.2.2.1 I-PpoI Strains construction

The I-PpoI DSB assay strain was used as the basis for creation of *de novo* mutants. All the strains were created by antibiotic-resistant cassettes replacement using the PCR-based gene targeting approach as described by Bähler et al. (1998). The single mutant *tsn1*Δ (BP3377), and the single mutant *tfx1*Δ (BP3380), were developed by deleting the genes from the WT- I-PpoI strains (BP3350). The antibiotic *natMX6* was used as the replacement cassettes in the deletion of *tsn1* and *tfx1* and amplified by using PCR primers that designed with 80 bp homologous sequences directly flanked upstream and downstream from the *dcr1* ORFs and contained a 20 bp of homologous sequence to the plasmid that carries the *natMX6* gene. These strains were developed and constructed by the McFarlane group. Nonetheless, before being utilised, they were subjected to verification through PCR checking (Appendix Figure 3).

5.2.2.2 Analysis of I-PpoI induced site specific system in DSB

In this study we have used system that generating the tetracycline inducible site-specific DSB that used the homing endonuclease I-PpoI. In *S. pombe* there is only one cleavage site of I-PpoI in the rDNA and the rDNA are replicated about 150 times which are separated at the both ends of Chromosome 3 (*chr* III) in two clusters. Therefore, in the fission yeast genome, I-PpoI has about 150 endogenous cleavage sites (Ohle et al., 2016). An artificial cleavage site at Chromosome 2 (*chr* II) to the natural cleavage sites that can led us to follow the cut easily at a specific site (Figure 5.7).

I-PpoI expression was induced for 2 hours by using the tetracycline inducible system in the wild-type, *rnh1Δ rnh201Δ* double mutant, *tsn1 Δ* and *tfx1Δ* single mutant strains. After 2 hours of induction, we have checked the DSB repair process during the recovery periods at 2, 4 and 8 hours. Western blot was used to detect the protein. In all strains, the protein dynamics of turnover after I-PpoI transcription repression were identical (Figures A 5.8 - 5.11). After that, to test the efficiency of DNA repair on the cleavage sites, the genomic DNA has been extracted from the WT and all mutant strains and the repaired DNA strands have been quantified by using qPCR primers covering the cleavage sites (Figures B 5.8 - 5.11). Overall, these results show that the WT, *tsn1Δ* and *tfx1Δ* single mutant cells showed quick repair after I-PpoI-induced DSBs, but the *rnh1Δ rnh201Δ* double mutant was unable to recover after I-PpoI-induced DSBs (Figure 5.9).

Following I-PpoI-induced DSBs, WT cells were able to recover to 95%, while *tsn1Δ* and *tfx1Δ* single mutant cells showed 85% of recovery. However, the *rnh1Δ rnh201Δ* double mutant cells were unable to recover after I-PpoI-induced DSBs (recovery rate 5%) (Figure 5.12). Importantly, these is no evidence that the *tsn1Δ* or *tfx1Δ* cells repair the DSB more rapidly of efficiently than the wild-type.

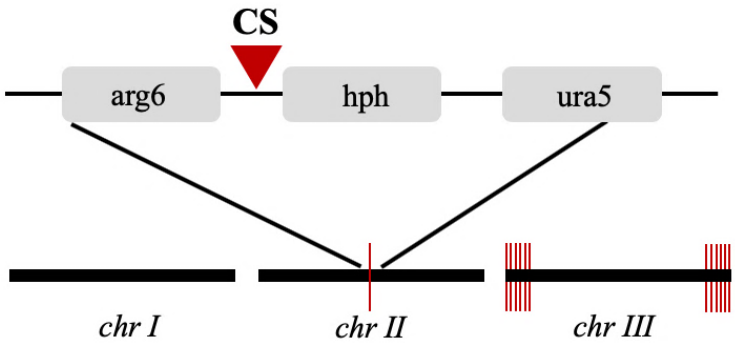

Figure 5.7 Cleavage sites location in *S. pombe* chromosomes.
Schematic demonstrating the three chromosomes of the *S. pombe.* The red lines are the I-PpoI cleavage sites. At *chr III* the endogenous cleavage sites were represented in the rDNA repeats. The artificially cleavage site (CS) and the Hph marker gene were located at *chr II* (adapted form Ohle et al., 2016).

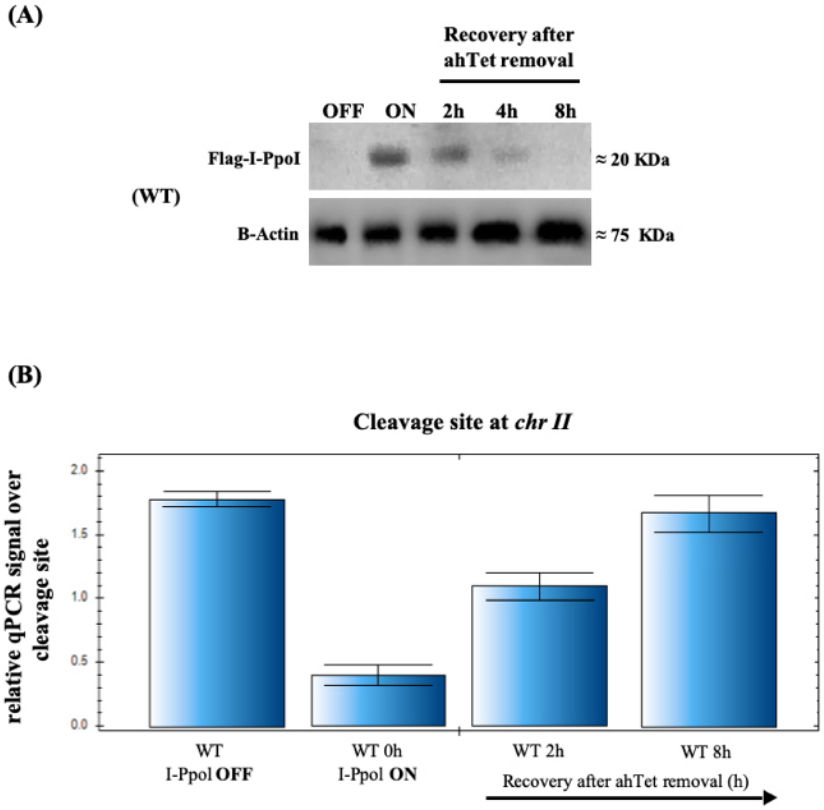

Figure 5.8 I-PpoI DSB induction and repair in wt cells.
(A) Induction of I-PpoI assessed by western blot analysis used the anti-Flag antibody. The anti-Flag antibody, which detects Flag-I-PpoI, and the B-actin antibody was used as control. Flag I-PpoI level was monitored at the specified time point (t=2 h, 4 h and 8 h). **(B)** The plot of the qPCR data is shown as relative qPCR signal in the indicated strains in comparison with the non-cleave sample (pre-I-PpoI induction/ I-PpoI-OFF). The I-PpoI has been inducted for 2 hours I-PpoI-ON (time, t=0 h), then the anhydrotetracycline (ahTET) has been removed by washing the cells to stop the I-PpoI induction. At the indicated time points (time, t= 2 h and t= 8 h), the repair efficiency was measured. The result show that wild-type cells showed quick recovery of the DSB at the (t= 8 h) time point of the I-PpoI cleavage site at *chr II*. The error bars show triplicate repeats of the standard error. P-values between WT and the indicated time point have been determined through student T-tests. All p-values were > 0.05. To analysis this data Bio-RAD CFX Manager was used.

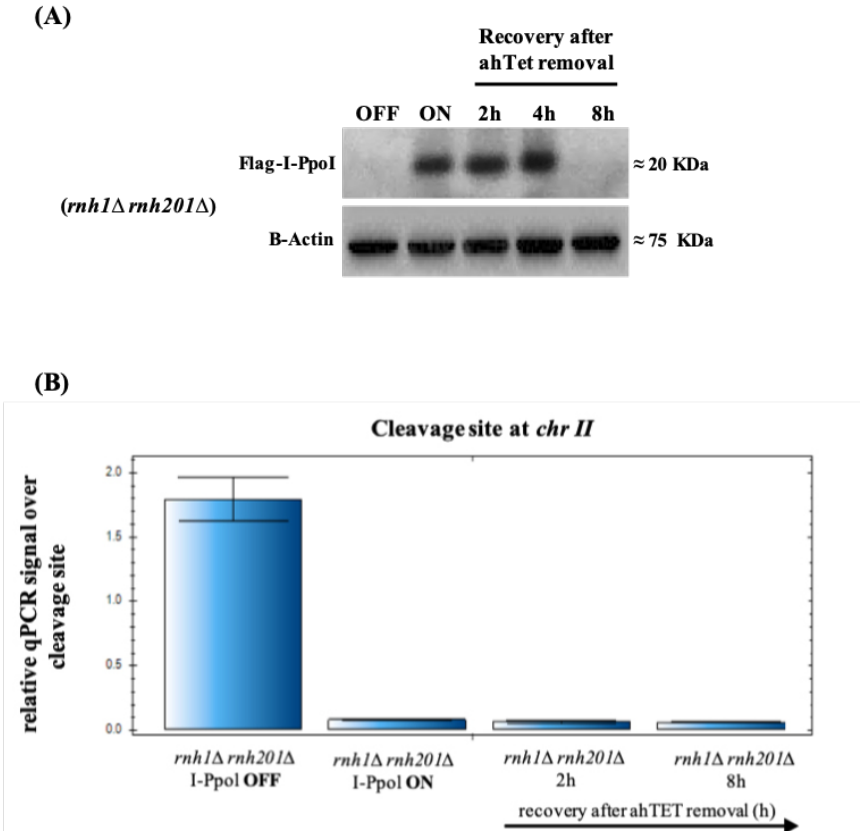

Figure 5.9 I-PpoI DSB induction and repair in *rnh1Δ rnh201Δ* double mutant cells.
(A) Induction of I-PpoI assessed by western blot analysis used the anti-Flag antibody. The anti-Flag antibody, which detects Flag-I-PpoI, and the B-actin antibody was used as control. Flag I-PpoI level was monitored at the specified time point (t=2 h, 4 h and 8 h). **(B)** The plot of the qPCR data is shown as relative qPCR signal in the indicated strains in comparison with the non-cleave sample (pre-I-PpoI induction/ I-PpoI-OFF). The I-PpoI has been inducted for 2 hours I-PpoI-ON (time, t=0 h), then the anhydrotetracycline (ahTET) has been removed by washing the cells to stop the I-PpoI induction. At the indicated time points (time, t= 2 h and t= 8 h), the repair efficiency was measured. The result show that the *rnh1Δ rnh201Δ* double mutant was unable to repair the DSB at the (t= 8 h) time point of the I-PpoI cleavage site at *chr II.* The error bars show triplicate repeats of the standard error. P-values between *rnh1Δ rnh201Δ* and the indicated time point have been determined through student T-tests. All p-values were < 0.01. To analysis this data Bio-RAD CFX Manager was used.

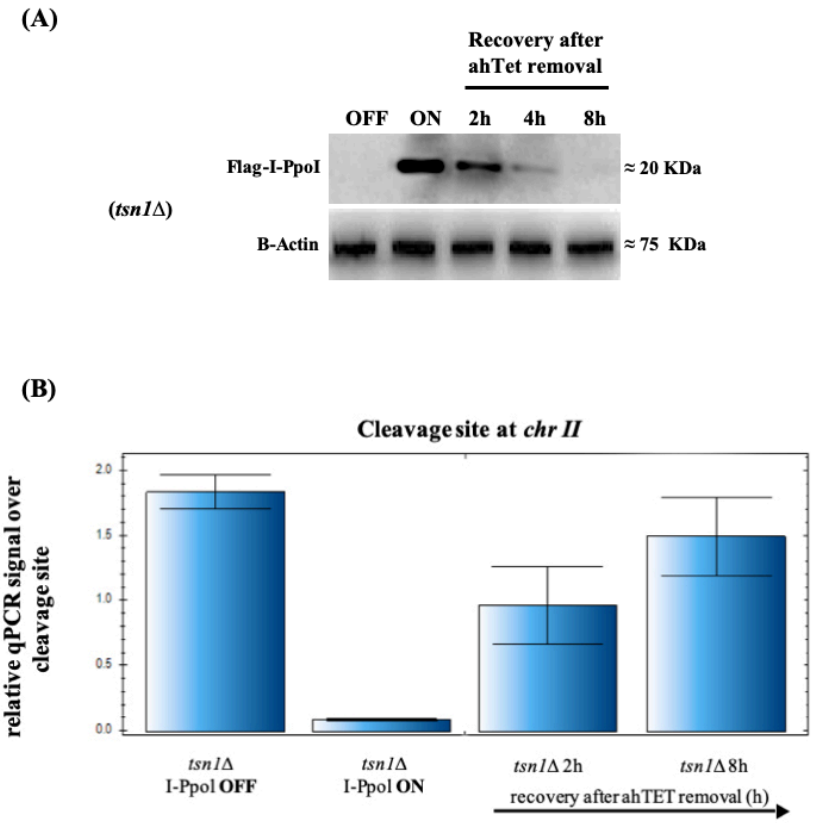

Figure 5.10 I-PpoI DSB induction and repair in *tsn1Δ* cells.
(A) Induction of I-PpoI assessed by western blot analysis used the anti-Flag antibody. The anti-Flag antibody, which detects Flag-I-PpoI, and the B-actin antibody was used as control. Flag I-PpoI level was monitored at the specified time point (t=2 h, 4 h and 8 h). **(B)** The plot of the qPCR data is shown as relative qPCR signal in the indicated strains in comparison with the non-cleave sample (pre-I-PpoI induction/ I-PpoI-OFF). The I-PpoI has been inducted for 2 hours I-PpoI-ON (time, t=0 h), then the anhydrotetracycline (ahTET) has been removed by washing the cells to stop the I-PpoI induction. At the indicated time points (time, t= 2 h and t= 8 h), the repair efficiency was measured. The result show that the *tsn1Δ* cells showed quick recovery of the DSB at the (t= 8 h) time point of the I-PpoI cleavage site at *chr II.* The error bars show triplicate repeats of the standard error. P-values between *tsn1Δ* and the indicated time point have been determined through student T-tests. All p-values were > 0.05. To analysis this data Bio-RAD CFX Manager was used.

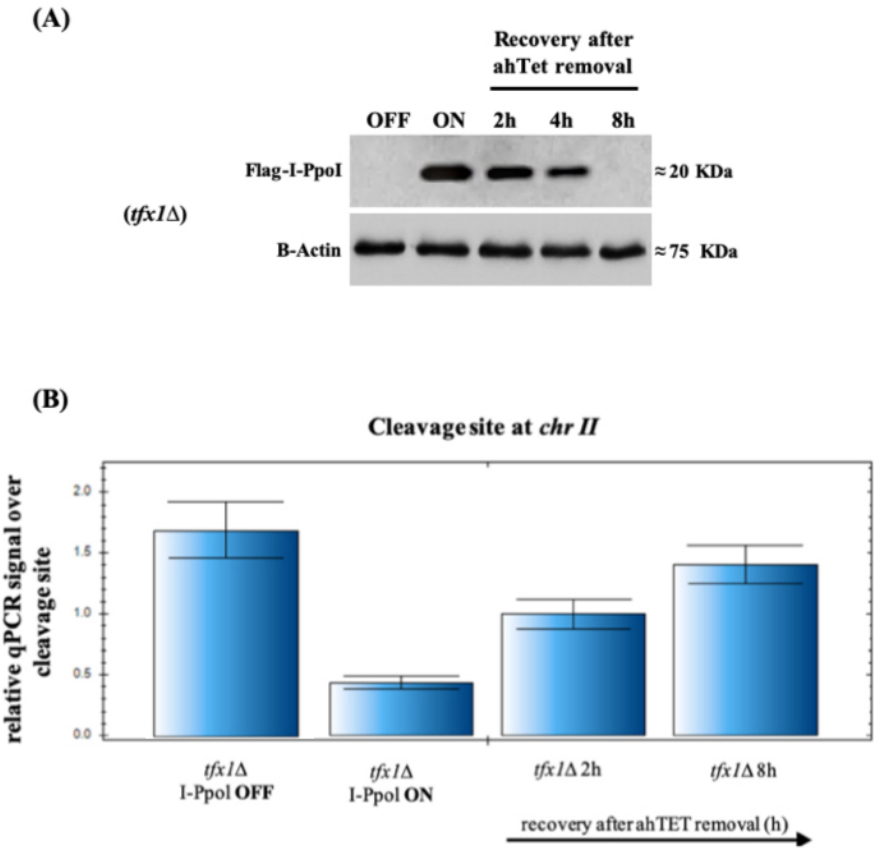

Figure 5.11 I-PpoI DSB induction and repair in *tfx1Δ* cells.
(A) Induction of I-PpoI assessed by western blot analysis used the anti-Flag antibody. The anti-Flag antibody, which detects Flag-I-PpoI, and the B-actin antibody was used as control. Flag I-PpoI level was monitored at the specified time point (t=2 h, 4 h and 8 h). **(B)** The plot of the qPCR data is shown as relative qPCR signal in the indicated strains in comparison with the non-cleave sample (pre-I-PpoI induction/ I-PpoI-OFF). The I-PpoI has been inducted for 2 hours I-PpoI-ON (time, t=0 h), then the anhydrotetracycline (ahTET) has been removed by washing the cells to stop the I-PpoI induction. At the indicated time points (time, t= 2 h and t= 8 h), the repair efficiency was measured. The result show that the *tfx1Δ* cells showed quick recovery of the DSB at the (t= 8 h) time point of the I-PpoI cleavage site at *chr II.* The error bars show triplicate repeats of the standard error. P-values between *tfx1Δ* and the indicated time point have been determined through student T-tests. All p-values were > 0.05. To analysis this data Bio-RAD CFX Manager was used.

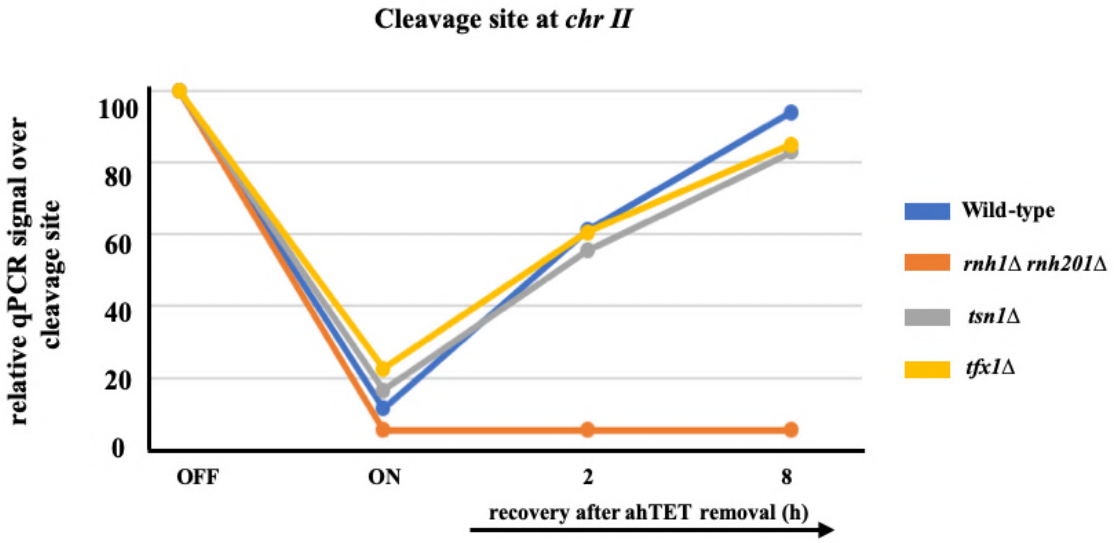

Figure 5.12 DSB repair kinetics at I-PpoI site.
The graph shows the WT cells were able to repair DSBs to 95% after I-PpoI-induction, while *tsn1Δ* and *tfx1Δ* single mutant cells showed 85% of recovery. The *rnh1Δ rnh201Δ* double mutant were unable to recover after I-PpoI-induced DSBs with recovery rate 5%. The rate of DSB repair in while *tsn1Δ* and *tfx1Δ* single mutant was indistinguishable from the WT.

5.2.2.3 Sensitivity spot tests to investigate whether the Tsn1 and/or Tfx1 suppress RNA:DNA hybrids and assist DSB repair

The data for the response of the *tsn1*Δ and *tfx1*Δ single mutants to phleomycin and bleomycin agents provoked the question if Tsn1or/and Tfx1 has function in DNA damage response and suppress RNA:DNA hybrids. This prompted us to investigate the hyper resistant of the *tsn1*Δ and *tfx1*Δ single mutants to the DSB agent by using an appropriate mutant from the Fischer group based on *Ppo*I nuclease induction. Spot tests were carried out using some DNA damaging agents. The DNA damage agents tested in this study were phleomycin and bleomycin, which are responsible for generation of DSBs (Figures 5.13 and 5.14) and UV, which induces multiple adducts (Figure 5.15). The data demonstrate that, the *tsn1*Δ and *tfx1*Δ single mutants showed high resistant to phleomycin and bleomycin compared with the wild-type in the BP90 background. However, we have not seen the same phenotype of *tsn1*Δ and *tfx1*Δ single mutants in response to phleomycin and bleomycin at the I-PpoI background. Indeed, the I-PpoI wild-type background appears to be more resistant to phleomycin than the BP90 wild-type background (Figure 5.13). This either indicates BP90 carries an unknown change (possibly mutation) which renders it more sensitive, or the I-PpoI wild-type strain (which has a complex configuration) may also be more resistant to DSB than the BP90 wild-type. However, this phenotype is not apparent in bleomycin (Figure 5.14), the reason for this are not clear. For UV treatment, whilst the I-PpoI background results in more sensitivity, there is no apparent difference between wild-type and *tsn1*Δ and *tfx1*Δ single mutants.

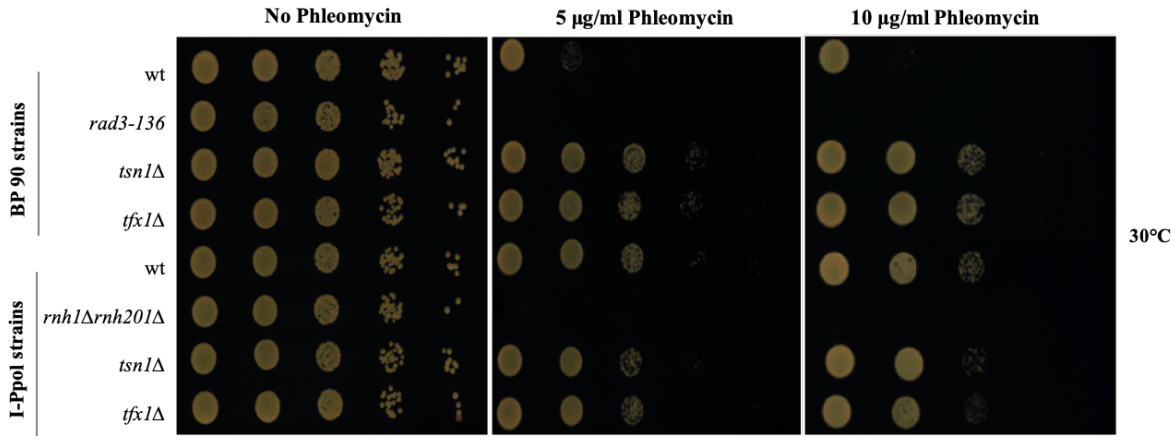

Figure 5.13 Sensitivity spot test of Phleomycin.
S. pombe mutants were diluted (10-fold serial dilution left to right) and spotted onto YEA media contain 5 and 10 µg/ml concentration of Phleomycin. *rad3-136* was used as a positive control. The *tsn1Δ* and *tfx1Δ* single mutants at BP90 background show resistance to Phleomycin compared to the WT. The *rnh11Δ rnh201Δ* double mutant show hypersensitivity to Phleomycin. In I-Ppol background the *tsn1Δ* and *tfx1Δ* single mutants show no resistant to Phleomycin compared to the WT. The plates were incubated 3 days at 30°C.

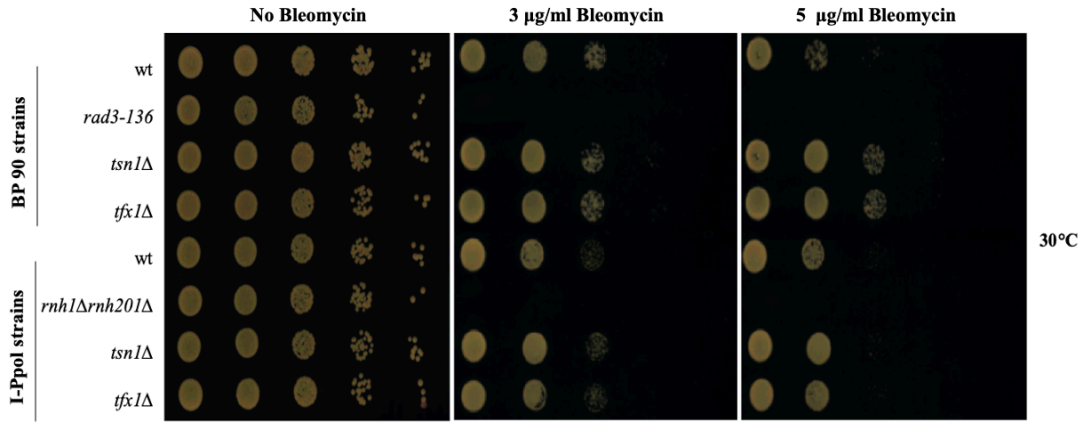

Figure 5.14 Sensitivity spot test of Bleomycin.
S. pombe mutants were diluted (10-fold serial dilution left to right) and spotted onto YEA media contain 3 and 5 µg/ml concentration of bleomycin. *rad3-136* was used as a positive control. The *tsn1Δ* and *tfx1Δ* single mutants in BP90 background show resistance to bleomycin compared to the WT. The *rnh1Δ rnh201Δ* double mutant show hypersensitivity to bleomycin. In I-Ppol background the *tsn1Δ* and *tfx1Δ* single mutants show no resistant to bleomycin compared to the WT. The plates were incubated 3 days at 30°C.

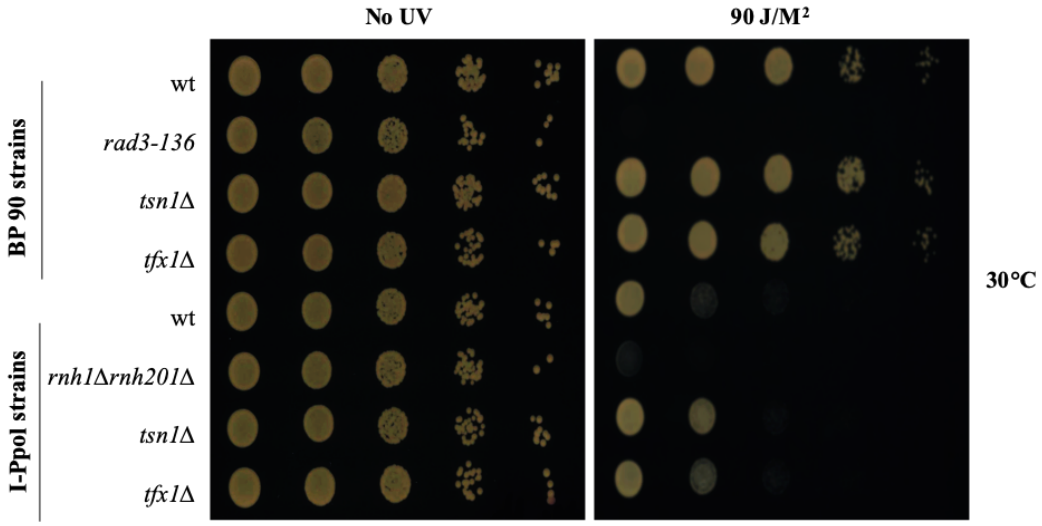

Figure 5.15 Sensitivity spot test of UV irradiation.
S. pombe mutants were diluted (10-fold serial dilution left to right) and spotted onto YEA media and then exposed to 90 J/M^2 dose of UV irradiation. *rad3-136* was used as a positive control. The *tsn1Δ* and *tfx1Δ* single mutants in BP90 background show no resistant to UV compared to the WT. The *rnh1Δrnh201Δ* double mutant show hypersensitivity to UV. In I-Ppol background the *tsn1Δ* and *tfx1Δ* single mutants show no resistant to UV compared to the WT. The plates were incubated 3 days at 30°C.

5.3 Discussion

The accumulation of RNA:DNA hybrid associated with transcription replication collision is a major cause of DNA damage that may impact cell function and genomic stability (Brambati et al., 2015). In *S. pombe* it has been shown that RNA pol II is recruited DSB to make a different type of hybrid which is have an unexpectedly positive role in the DNA repair process that is crucial for maintaining genome stability (Ohle et al., 2016). In this study we have noted that the *tsn1*Δ and *tfx1*Δ single mutants were hyper resistant to ionizing irradiation mimetic agents such as phleomycin and bleomycin, but not to other agents that generate DNA replication-associated recombinogenic lesions, such as camptothecin (CPT) and hydroxyurea (HU). We postulated based on biochemical capabilities of Translin and Trax they were required for inhibiting the formation or accumulation of RNA:DNA hybrid that have a positive effect on DSB repair. If this were the case, this would explain the hyper resistance to the DSB agents of the *tsn1*Δ and *tfx1*Δ single mutants.

This led our group to assess whether the loss of Tsn1 or/and Tfx1 function results in increased RNA:DNA hybrids causing an assist in DSB repair. Co-workers in the McFarlane group, showed that the level of RNA:DNA hybrid become elevated in the absence of Tsn1 and Tfx1. So, loss of Tsn1 or/and Tfx1 could result in the formation of more RNA:DNA hybrid or RNA molecule because it might be not the RNA:DNA hybrid that help in the DSB repair. This elevation is not due to increased transcripts as genome-wide array analysis showed no increased in transcripts in *tsn1*Δ and *tfx1*Δ single mutants (McFarlane lab). Unfortunately, we did not measure increased efficiency of DSB repair at the I-PpoI break in either *tsn1*Δ or *tfx1*Δ single mutant strains.

Given this, there is a mismatch between the drug resistance data, the RNA:DNA hybrid data and the I-PpoI DSB analysis. RNA:DNA hybrid analysis was conducted in distinct strains, and levels were not assessed in the I-PpoI strains. Given that the I-PpoI stains did not exhibit increased resistance to DNA damage, we can draw little conclusion from these data, as this stains background is clearly distinct.

5.4 Conclusion

1.The *tsn1*Δ and *tfx1*Δ single mutants exhibit enhanced resistance to DSB agents such Phleomycin, but not other DNA damaging agent, including HU (although this might be specific to the genetic background).

2. Both Tsn1 and Tfx1 has function to suppress a DSB recovery pathways.

3. Loss of Tsn1 or/and Tfx1 function results in increased RNA:DNA hybrids (this conclusion is drawn from the work of others in the group).

4. In one genetic background at least loss of Tsn1 and Tfx1do not alter DSB repair levels or kinetics.

Chapter 6: Results

Analysis of Tsn1 and Tfx1 function in genome stability regulation in the absence of telomeres.

6.1 Introduction

Instability of chromosomes can be triggered by defects in certain essential processes, such as DNA repair pathways (Fragkos & Naim, 2017). In many cancer cells, telomerase, the enzyme required for synthesizing telomeres, is activated and plays a role in telomere maintenance that is crucial for the extension of DNA at the chromosome ends in proliferating cells (Buhler & Gasser, 2009; Ohlo et al., 2016; Hsu & Lue, 2017; Mizukoshi & Kaneko, 2019).

Previously, the McFarlane group demonstrated that Tsn1 and Tfx1 regulate telomere-associated transcripts (Gomez-Escobar et al., 2016), and have shown that this does not result in increased RNA:DNA hybrids in sub-telomeric regions. We have shown that the *tsn1*Δ *dcr1*Δ double mutant exhibited increase sensitivity to some DNA damaging agents. Therefore, we have revealed a relationship between Tsn1 and Dcr1. Interestingly, a co-worker in the group has now demonstrated that in the absence of both Dcr1 and Tsn1 elevated chromosomal RNA:DNA hybrids can be observed at tRNA genes and the rDNA locus (data not shown, Gomez-Escobar, personal communication), although this has not been tested at the *ade6* locus with or without tRNA gene insertions. Interestingly, the observations from the *ade6* locus demonstrate that there is a requirement for Tsn1 at a locus that is non-telomeric. This is the first indication that the genome stability regulation function for Tsn1 is independent of the telomeres. In the absence of telomere, fission yeast can survive by recombining continuing telomere sequences, which form linear survivors (Jain et al., 2010; Begnis et al., 2018). There are two survivor classes, which are linear and circular telomerase minus survivors. The first one is called HAATI, which is deficient in telomerase and has linear chromosome ends where canonical telomerase-dependent telomeres have been replaced by heterochromatin. HAATI has two subtypes, $HAATI^{rDNA}$ and $HAATI^{STE}$. The second survivor type has circular chromosomes and is called O *trt1*Δ (Jain et al., 2010; Begnis et al., 2018).

We hypothesised a role of Tsn1 and/or Tfx1 to DNA damaging agents in non-telomeric DNA. To further address this hypothesis, we generated a range of mutants to test the DNA damaging agent sensitivity/resistance to confirm that the requirement of Tsn1 and

Tfx1 in DNA damage response is maintained in the absence of canonical telomeres. So, we have used these fission yeast strains that lack of telomeres/telomerase and this will confirm that if Tsn1 and/or Tfx1 are required for non-telomeric DNA repair.

6.2 Results

6.2.1 DNA damage sensitivity analysis for O *trt1*Δ and HAATI *trt1*Δ strains.

loss of Tsn1 and/or Tfx1 might elevate DSB repair efficiently. In spot tests on phleomycin we occasionally noticed that *tsn1*Δ and *tfx1*Δ single mutants exhibited more resistance to this agent than the wild-type control, this was also the case for bleomycin (Chapter 5; Figure 5.1). This resistance was only observed for phleomycin and bleomycin, and not to other DNA damaging agents such as, HU, MMS, UV, CPT or MMC. Given this we have identified a possible direct pathway role for Tsn1 in genome stability. This led us to test the DNA damaging agent resistance to confirm that the requirement of Tsn1/Tfx1 in DNA damage response is maintained in the absence of telomeres.

To test this, we used fission yeast strains that lack telomeres such as O *trt1* and HAATI strains. The spot test result of the O *trt1*Δ strain showed high sensitivity to all the DNA damaging agents (Figures A 6.1-6.5). Whilst O *trt1*Δ fission yeast strain with a telomeric circular chromosomes are viable, they are ultra-sensitive to DNA damaging agents, so are of limited use and we were unable to generate a range of mutants required. Other strains, referred to as HAATI strains, have linear chromosome ends where canonical telomerase-dependent telomeres have been replaced by heterochromatin. HAATI has two subtypes and at their noncanonical chromosome ends there are different repeats. The first subtype is HAATI^{rDNA}, in which the ribosomal DNA (rDNA) has spread to all three chromosomes. Whereas, the second subtype is HAATI^{STE}, called sub-telomeric elements (STEs), are amplified from the subterminal regions of chromosomes I and II to all chromosome, while the rDNA remains at only on Chr III (Jain et al. 2010; Begnis et al., 2018). We have chosen the HAATI^{STE} in this study because we were concerned that HAATI^{rDNA} might require Dcr1 for maintenance of the rDNA telomere replacements and

using this strain background would negate generating *dcr1*Δ *tsn1*Δ double mutant or *dcr1*Δ single mutant to enable testing of DNA damage responses. The spot test result of HAATI^{STE} displayed no sensitivity to DNA damaging agents (Figures B 6.1-6.5). We conclude that the O *trt1*Δ strain is not useful but HAATI^{STE} strain is. This led us to generate a range of mutants from the HAATI^{STE} strain and test them to DNA damaging agents (see Section 6.2.2).

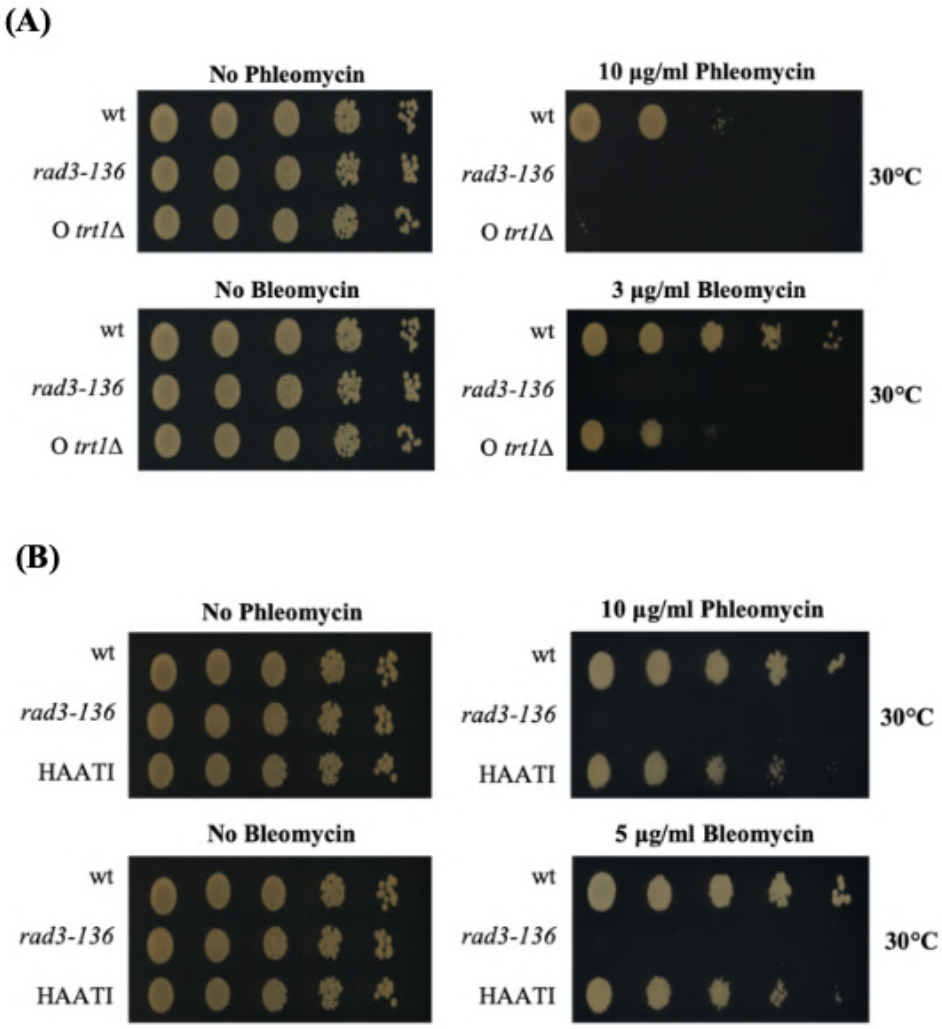

Figure 6.1 Sensitivity spot test of O *trt1Δ* and HAATI^{STE} strains to Phleomycin and Bleomycin. *S. pombe* mutants were diluted (10-fold serial dilution left to right) and spotted onto YEA media contain different concentration of Phleomycin and Bleomycin. *rad3-136* was used as a positive control. **(A)** The O *trt1Δ* single mutant show hypersensitivity to Phleomycin and Bleomycin compared with WT. **(B)** The HAATI strain show no increased sensitivity to Phleomycin and Bleomycin compared with WT. The HAATI background used was HAATI^{STE}. The plates were incubated 3 days at 30°C.

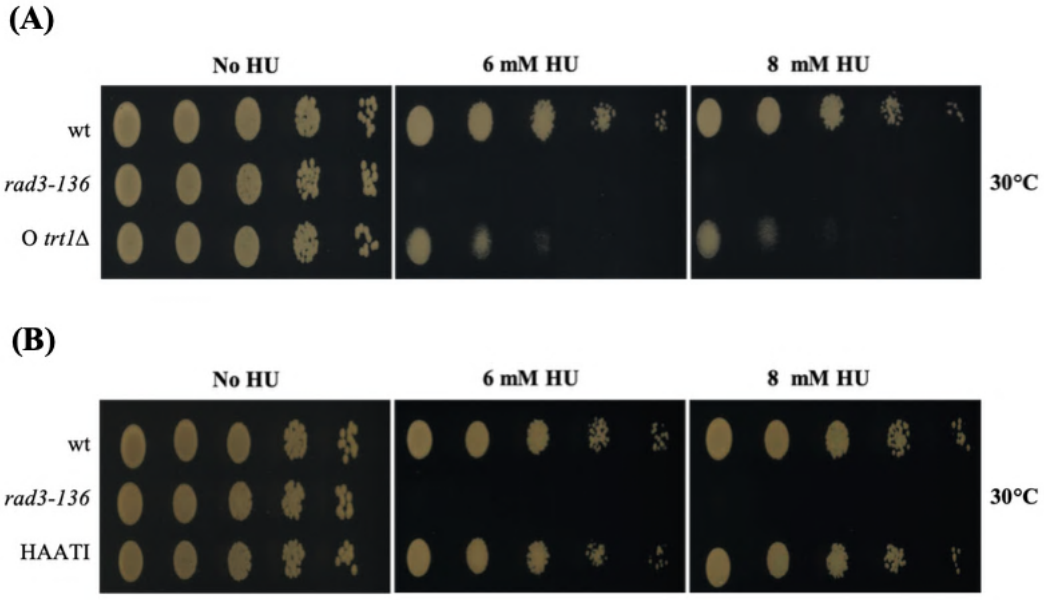

Figure 6.2 Sensitivity spot test of O *trt1Δ* and HAATI^{STE} strains to Hydroxyurea.
S. pombe mutants were diluted (10-fold serial dilution left to right) and spotted onto YEA media contain different concentration of HU. *rad3-136* was used as a positive control. **(A)** The O *trt1Δ* single mutant show hypersensitivity to HU compared with WT. **(B)** The HAATI strain show no increased sensitivity to HU compared with WT. The HAATI background used was HAATI^{STE}. The plates were incubated 3 days at 30°C.

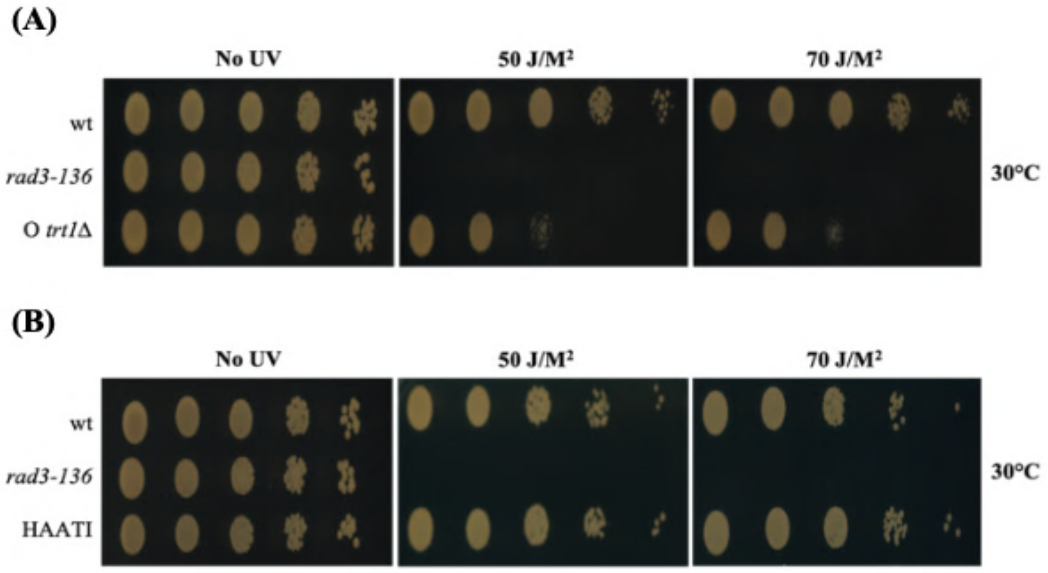

Figure 6.3 Sensitivity spot test of O *trt1Δ* and HAATI^{STE} strains to UV irradiation.
S. pombe mutants were diluted (10-fold serial dilution left to right) and spotted onto YEA media then exposed to different doses of UV irradiation. *rad3-136* was used as a positive control. **(A)** The O *trt1Δ* single mutant show increased sensitivity to UV compared with WT**. (B)** The HAATI strain show no increased sensitivity to UV compared with WT. The HAATI background used was HAATI^{STE}. The plates were incubated 3 days at 30°C.

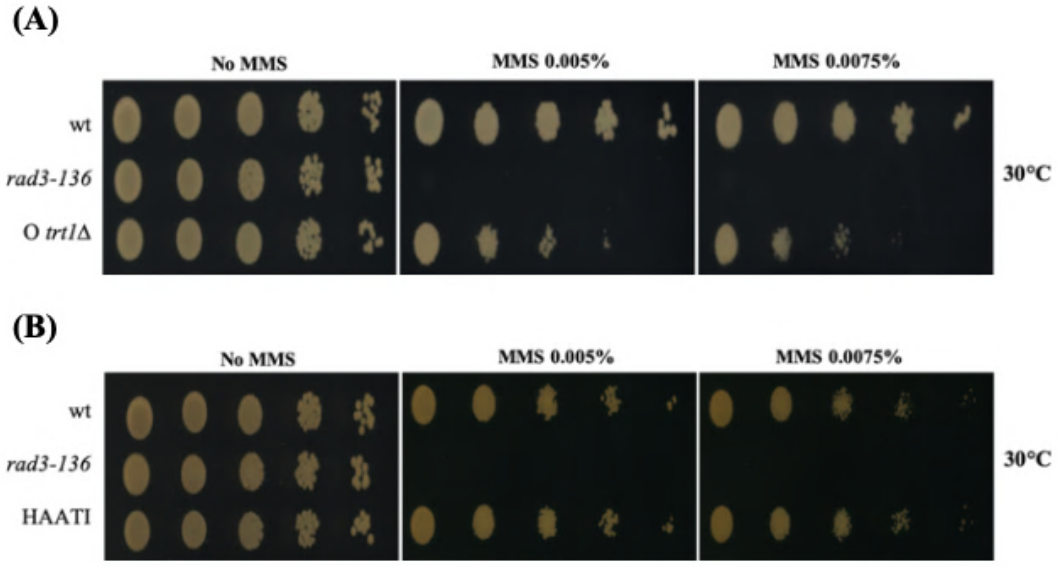

Figure 6.4 Sensitivity spot test of O *trt1Δ* and HAATI^{STE} strains to MMS.
S. pombe mutants were diluted (10-fold serial dilution left to right) and spotted onto YEA media contain different concentration of MMS. *rad3-136* was used as a positive control. **(A)** The O *trt1Δ* single mutant show increased sensitivity to MMS compared with WT. **(B)** The HAATI strain show no increased sensitivity to MMS compared with WT. The HAATI background used was HAATI^{STE}. The plates were incubated 3 days at 30°C.

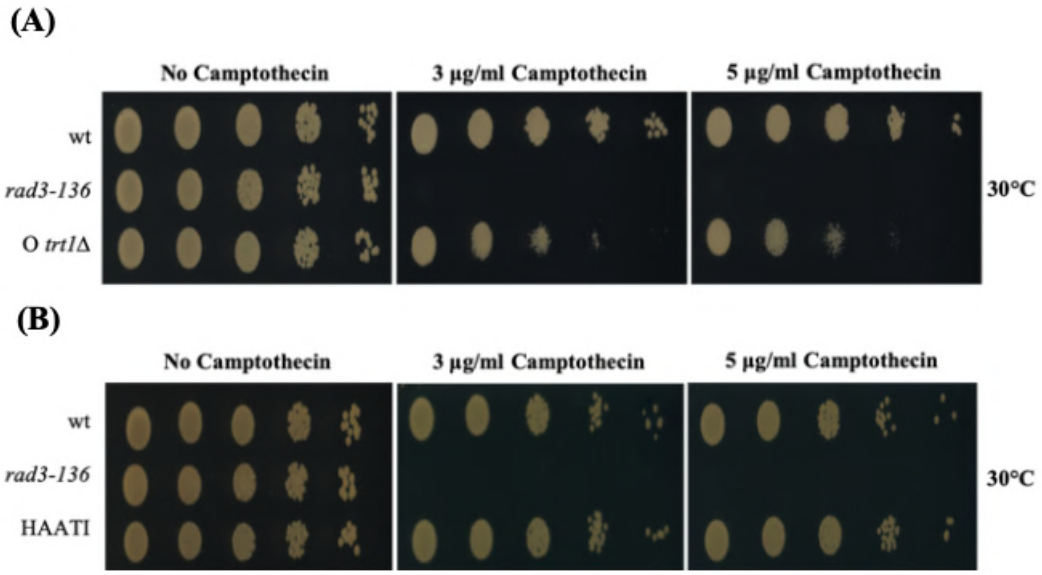

Figure 6.5 Sensitivity spot test of O *trt1Δ* and HAATI^{STE} strains to Camptothecin.
S. pombe mutants were diluted (10-fold serial dilution left to right) and spotted onto YEA media contain different concentration of camptothecin. *rad3-136* was used as a positive control. **(A)** The O *trt1Δ* single mutant show increased sensitivity to camptothecin compared with WT. **(B)** The HAATI strain show no increased sensitivity to camptothecin compared with WT. The HAATI background used was HAATI^{STE}. The plates were incubated 3 days at 30°C.

6.2.2 Roles of Tsn1 and/or Tfx1 in the DSB repair in the absence of telomeres.

6.2.2.1 Construction of Tsn1 and Tfx1 mutant strains in the HAATI^{STE} background.

*tsn1*Δ and *tfx1*Δ mutant were created in the HAATI^{STE} background via *de novo* mutation All the strains were created by antibiotic-resistant cassettes replacement as founded on the PCR-based gene targeting approach as described by Bähler et al. (1998). In this study the single mutants *tsn1*Δ (BP3381) and *tfx1*Δ (BP3384), were developed by deleting the genes from the HAATI^{STE} wild type (BP3305). The antibiotic *kanMX6* was used as the replacement cassettes in the deletion of *tsn1* and *tfx1* and this was amplified by using PCR primers that designed with 80 bp homologous sequences directly flanked upstream and downstream from the of *tsn1* and *tfx1* ORFs, with 20 bp of homologous sequence to the plasmid that carries the *kanMX6* gene. To verify the correct deletion, candidates of both strains were screened through the PCR (Figures 6.6 and 6.7). Two or more independent isolates were tested for each construct.

6.2.2.2 Sensitivity spot tests to investigate if Tsn1 and/or Tfx1 have roles in the DSB repair in the absence of telomeres.

In previous chapter we have showed that loss of Tsn1 and/or Tfx1 might elevate DSB repair efficiently. For the spot tests on phleomycin, we noticed that *tsn1*Δ and *tfx1*Δ single mutants exhibited more resistance to this agent than the wild-type control (Chapter 5; Figure 5.1). This was also the case for bleomycin. This resistance was only observed for phleomycin and bleomycin, and not to other DNA damaging agents such as, HU, MMS, UV, CPT or MMC. This led us to test the DNA damaging agent resistance to confirm that the requirement of Tsn1 and Tfx1 in DNA damage response is maintained in the absence of telomeres. The spot test result of *tsn1*Δ and *tfx1*Δ single mutants in HAATI^{STE} background showed wild-type sensitivity level to all DNA damaging agents (Figures 6.8-6.12). So, we have not seen the same resistance phenotype of *tsn1*Δ and *tfx1*Δ single mutants in response to phleomycin in compered with the wild-type in the HAATI^{STE} background. Indeed, from these experiments it seems as through the genetic background of the wild-type plays a role, as the non HAATI (*trt1*$^{+}$) BP90 wild-type seems to be a little more resistant to phleomycin than the HAATI^{STE} wild-type. This would infer that loss of Tsn1 and/or Tfx1 function mimics loss of telomeres.

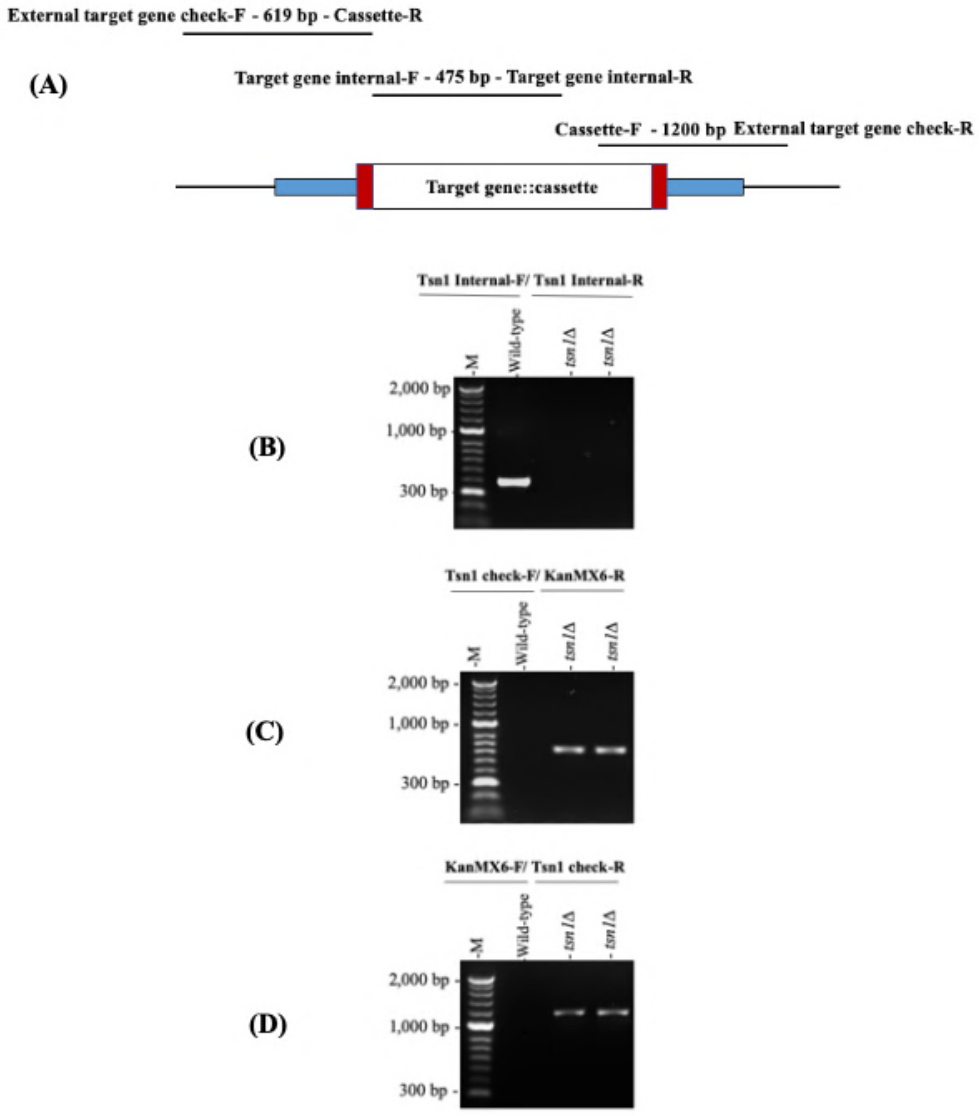

Figure 6.6 Confirmation by PCR screening of successful *tsn1*Δ single mutant knockout.
(A) The genes were deleted and replacement with antibiotic resistant cassettes. To confirm the deletion of the target genes, three sets of primers were used. **(B)** Illustration of agarose gel screening of PCR products for the HAATI^{STE} wild-type strain and *tsn1*Δ single mutant. The Tsn1-int-F and Tsn1-int-R primers were used, and the gel screening displays no PCR products in the successful *tsn1*Δ candidate strains. The expected sizes of the PCR product in *tsn1* gene was 475 bp. **(C)** The Tsn1 check-F and KanMX6-R primers were used to generate the PCR products for the wild-type and *tsn1*Δ candidate strains. The PCR products were seen in the *tsn1*Δ strains, but not in the wild-type strain and the expected band sizes is 619 bp. **(D)** The wild-type and *tsn1*Δ candidate strains were utilised to amplify by the KanMX6-F and Tsn1 check-R primers and the expected sizes is 1200 bp.

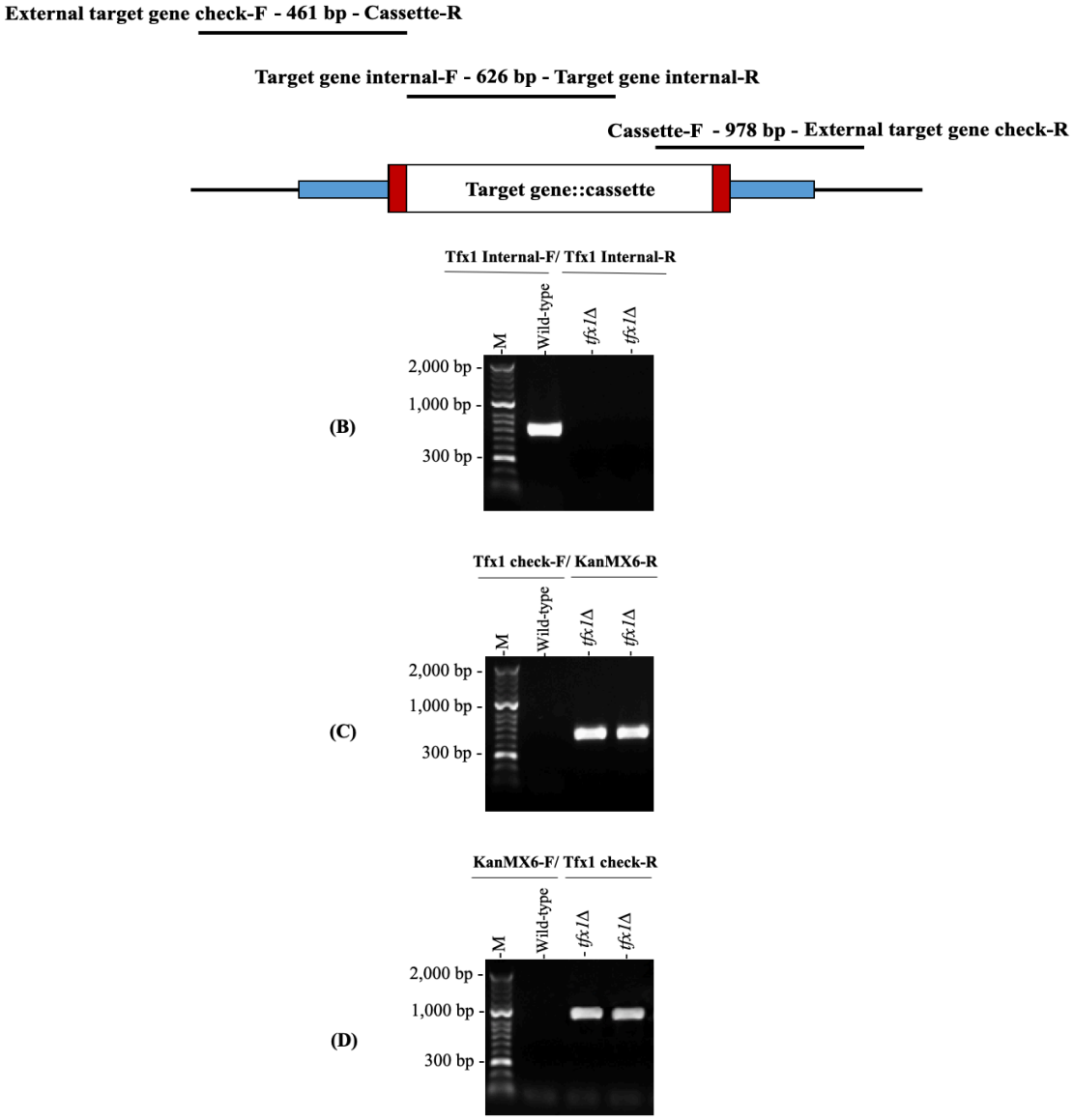

Figure 6.7 Confirmation by PCR screening of successful *tfx1*Δ single mutant knockout.
(A) The genes were deleted and replacement with antibiotic resistant cassettes. To confirm the deletion of the target genes, three sets of primers were used. **(B)** Illustration of agarose gel screening of PCR products for the HAATI^{STE} wild-type strain and *tfx1*Δ single mutant. The Tfx1-int-F and Tfx1-int-R primers were used, and the gel screening displays no PCR products in the successful *tfx1*Δ candidate strains. The expected sizes of the PCR product in *tfx1* gene was 626 bp. **(C)** The Tfx1 check-F and KanMX6-R primers were used to generate the PCR products for the wild-type and *tfx1*Δ candidate strains. The PCR products were seen in the *tfx1*Δ strains, but not in the wild-type strain and the expected band sizes is 461 bp. **(D)** The wild-type and *tfx1*Δ candidate strains were utilised to amplify by the KanMX6-F and Tfx1 check-R primers and the expected sizes is 978 bp.

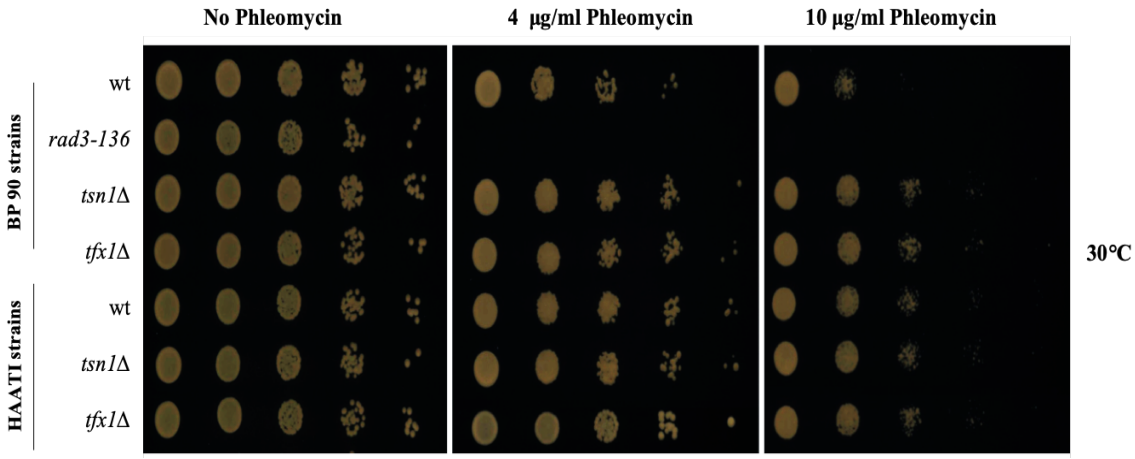

Figure 6.8 Sensitivity spot test for Phleomycin.
S. pombe mutants were diluted (10-fold serial dilution left to right) and spotted onto YEA media containing different concentration of Phleomycin. *rad3-136* was used as a positive control. The *tsn1Δ* and *tfx1Δ* single mutants shows hyper resistant to the DSB agent phleomycin in the BP90 background but shows no resistant in the HAATI^{STE} background. The plates were incubated 3 days at 30°C.

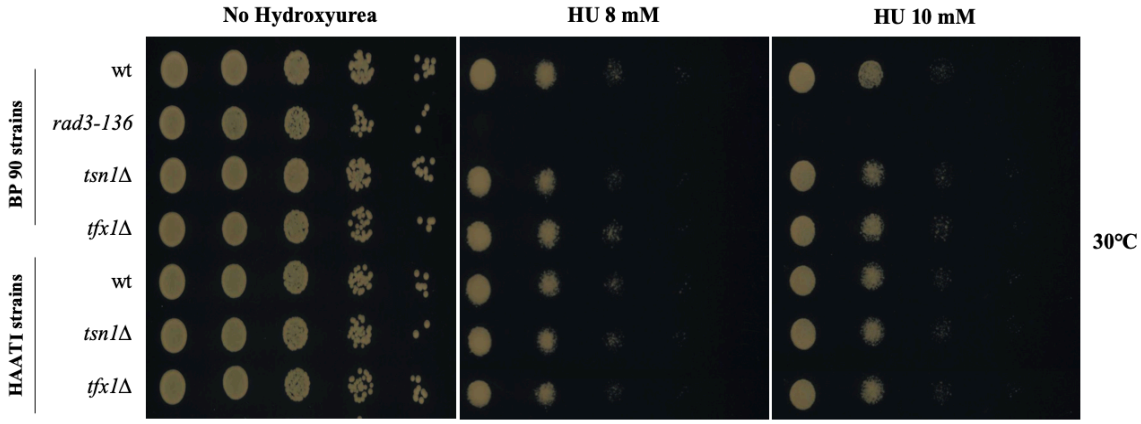

Figure 6.9 Sensitivity spot test of hydroxyurea.
S. pombe mutants were diluted (10-fold serial dilution left to right) and spotted onto YEA media containing 8 mM and 10 mM concentrations of hydroxyurea. *rad3-136* was used as a positive control. The *tsn1Δ* and *tfx1Δ* single mutants shows no increase sensitivity to HU compared to the WT in both backgrounds, BP90 and HAATI^{STE}. The plates were incubated 3 days at 30°C.

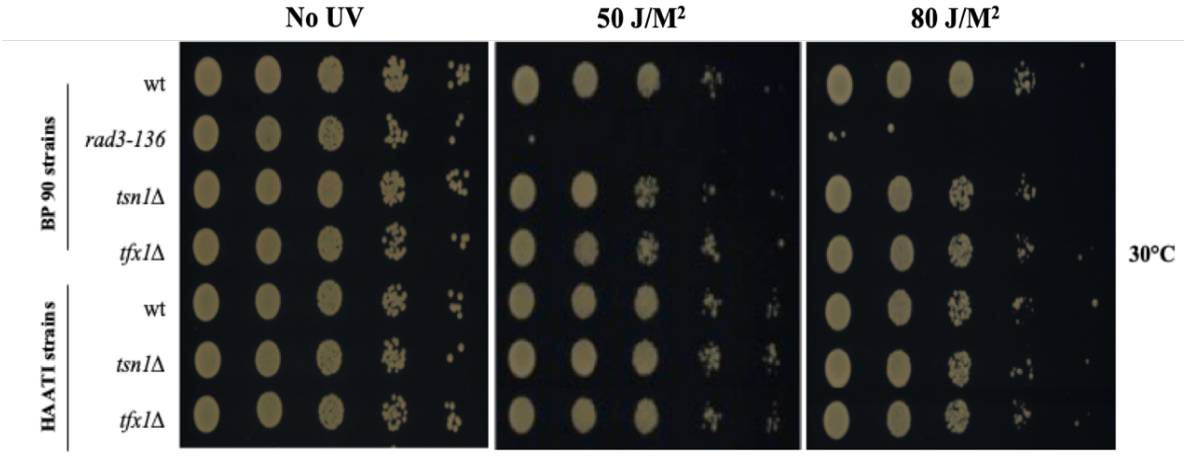

Figure 6.10 Sensitivity spot test of UV irradiation.
S. pombe mutants were diluted (10-fold serial dilution left to right) and spotted onto YEA media and then exposed to 50 J/M^2 and 80 J/M^2 doses of UV irradiation. *rad3-136* was used as a positive control. The *tsn1Δ* and *tfx1Δ* single mutants shows no increase sensitivity to UV compared to the WT in both BP90 and HAATI^{STE} backgrounds. The plates were incubated 3 days at 30°C.

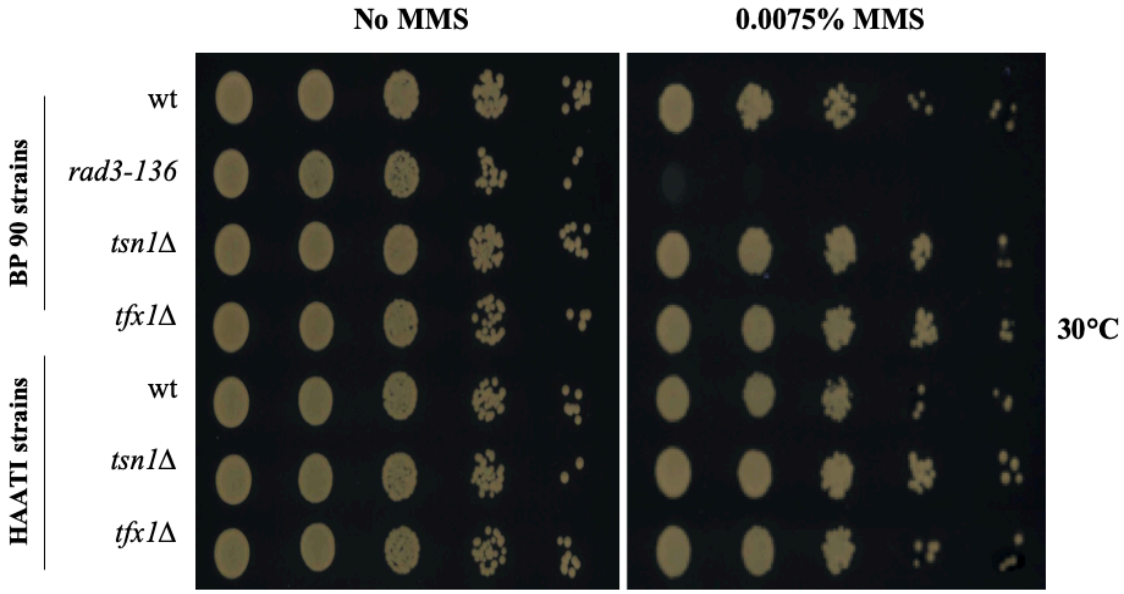

Figure 6.11 Sensitivity spot test of MMS.
S. pombe mutants were diluted (10-fold serial dilution left to right) and spotted onto YEA media containing 0.0075% concentration of MMS. *rad3-136* was used as a positive control. The *tsn1Δ* and *tfx1Δ* single mutants shows no increase sensitivity to MMS compared to the WT in both BP90 and HAATI^{STE} backgrounds. The plates were incubated 3 days at 30°C.

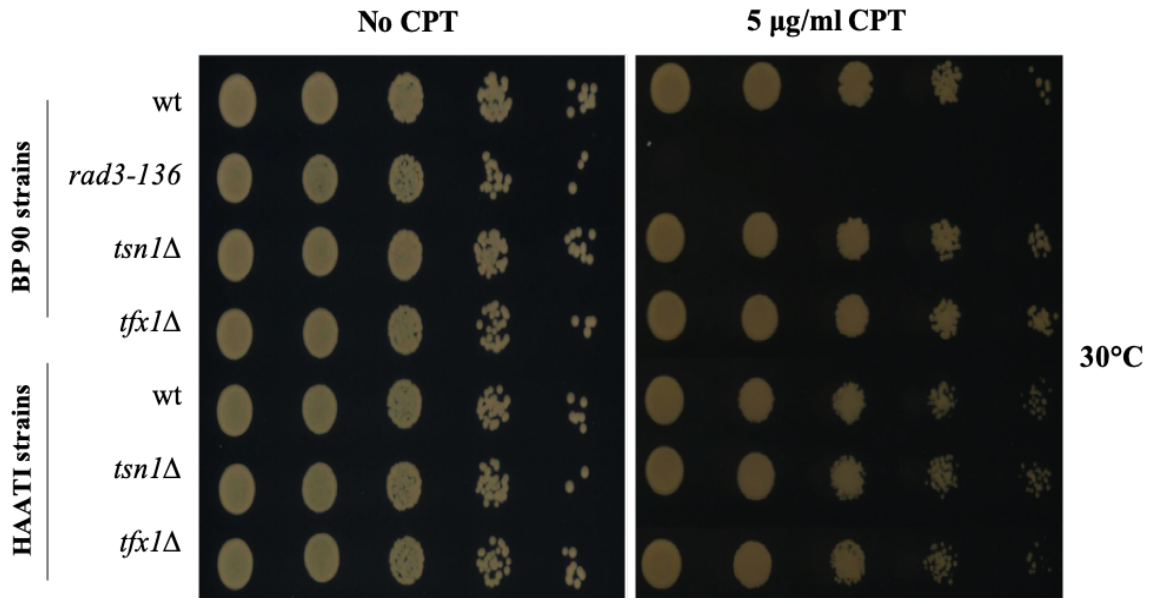

Figure 6.12 Sensitivity spot test of CPT.
S. pombe mutants were diluted (10-fold serial dilution left to right) and spotted onto YEA media containing 5 µg/ml concentration of CPT. *rad3-136* was used as a positive control. The *tsn1Δ* and *tfx1Δ* single mutants shows no increase sensitivity to CPT compared to the WT in both BP90 and HAATI^{STE} backgrounds. The plates were incubated 3 days at 30°C.

6.2.3 Tsn1 functions in one of the RNase H pathways in the absence of telomeres.

6.2.3.1 Construction of mutant strains in the HAATI^{STE} background.

The data for the response of the *dcr1*Δ *tsn1*Δ and the *tsn1*Δ *rnh201*Δ double mutants revealed increased sensitivity to some DNA damaging agents such as, phleomycin, bleomycin and HU relative to single mutants. This prompted us to investigate the sensitivity of the *dcr1*Δ *tsn1*Δ and the *tsn1*Δ *rnh201*Δ double mutants to DNA damaging agents in a telomere-deficient HAATI^{STE} background. However, we cannot test the *dcr1*Δ *tsn1*Δ double mutant strain, we postulate that the HAATI^{STE} telomeres require Dcr1. *tsn1*Δ single mutant was viable. Recently, Cooper and co-workers (2018) demonstrated that HAATI^{STE} viability was not Dcr1 dependent, so the reason for our inability to construct the *dcr1*Δ mutant is unclear.

The *rnh1*Δ and *rnh201*Δ single mutant strains were used as the basis for creation of *de novo* double mutants. All the strains were created by antibiotic-resistant cassettes replacement as founded on the PCR-based gene targeting approach as described by Bähler et al. (1998). In this study the single mutant *rnh1*Δ (BP3454), *rnh201*Δ (BP3453) and the *rnh1*Δ *rnh201*Δ (BP3459), *tsn1*Δ *rnh1*Δ (BP3451) and *tsn1*Δ *rnh201*Δ (BP3450) double mutants, were developed by deleting the genes from the HAATI^{STE} wild type (BP3305). The antibiotic *natMX6* and *kanMX6* were used as the replacement cassettes in the deletion of *rnh1* and *rnh201* and amplified by using PCR primers that designed with 80 bp homologous sequences directly flanked upstream and downstream from the of *rnh1* and *rnh201* ORFs, with 20 bp of homologous sequence to the plasmid that carries the *natMX6* and *kanMX6* genes. To verify the correct deletion, candidates of both strains were screened through the PCR (Figures 6.13; 6.17). Two or more independent isolates were tested for each construct.

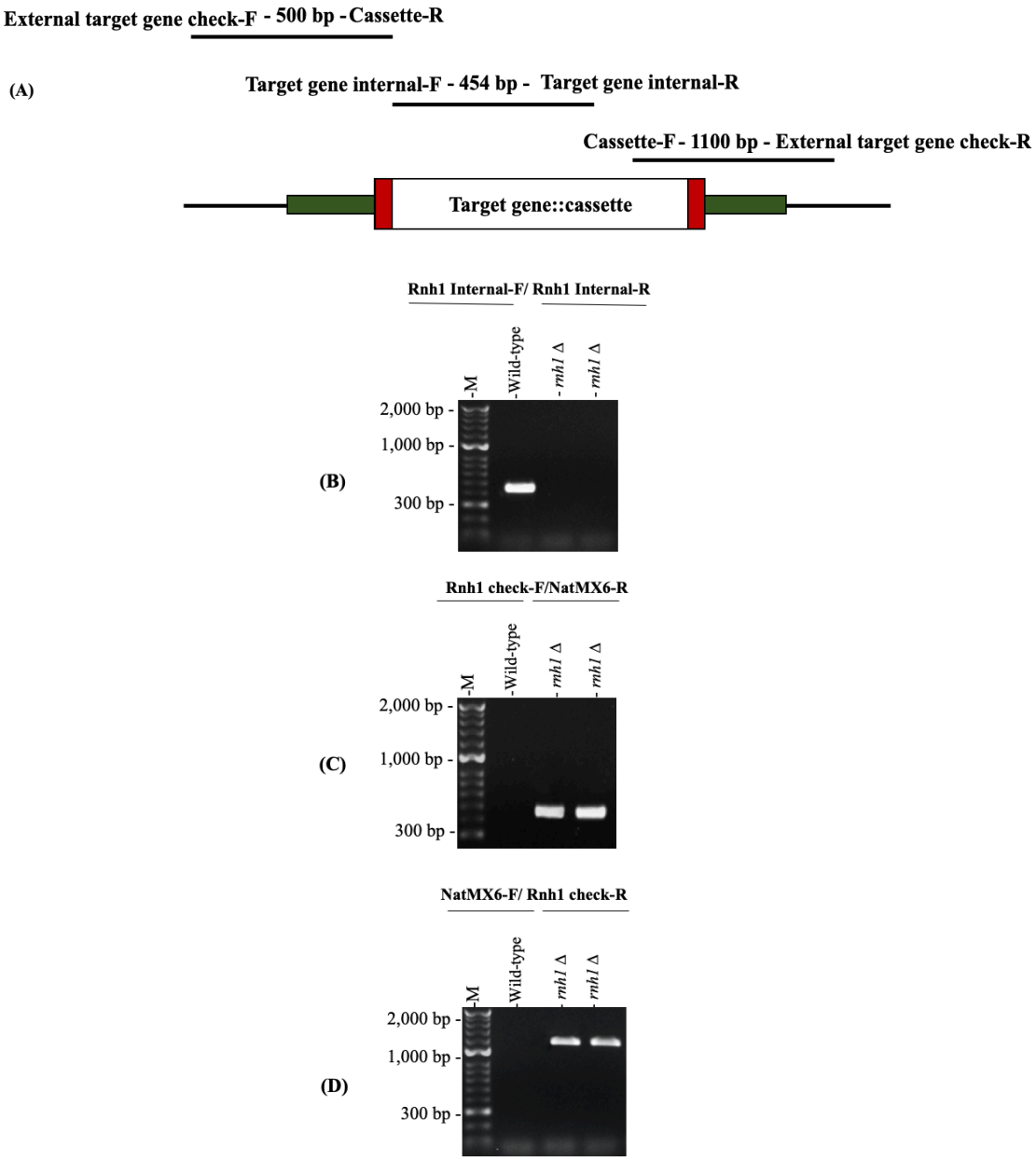

Figure 6.13 Confirmation by PCR screening of successful *rnh1Δ* single mutant knockout from HAATI^{STE} background.

(A) The genes were deleted and replacement with antibiotic resistant cassettes. To confirm the deletion of the target genes, three sets of primers were used. **(B)** Illustration of agarose gel screening of PCR products for the HAATI wild-type strain and *rnh1*Δ single mutant. The Rnh1-int-F and Rnh1-int-R primers were used, and the gel screening displays no PCR products in the successful *rnh1*Δ candidate strains. The expected sizes of the PCR product in *rnh1*Δ gene was 454 bp. **(C)** The Rnh1 check-F and NatMX6-R primers were used to generate the PCR products for the wild-type and *rnh1*Δ candidate strains. The PCR products were seen in the *rnh1*Δ strains, but not in the wild-type strain and the expected band size is 500 bp. **(D)** The wild-type and *rnh1*Δ candidate strains were utilised to amplify by the NatMX6-F and Rnh1 check-R primers and the expected size is 1100 bp.

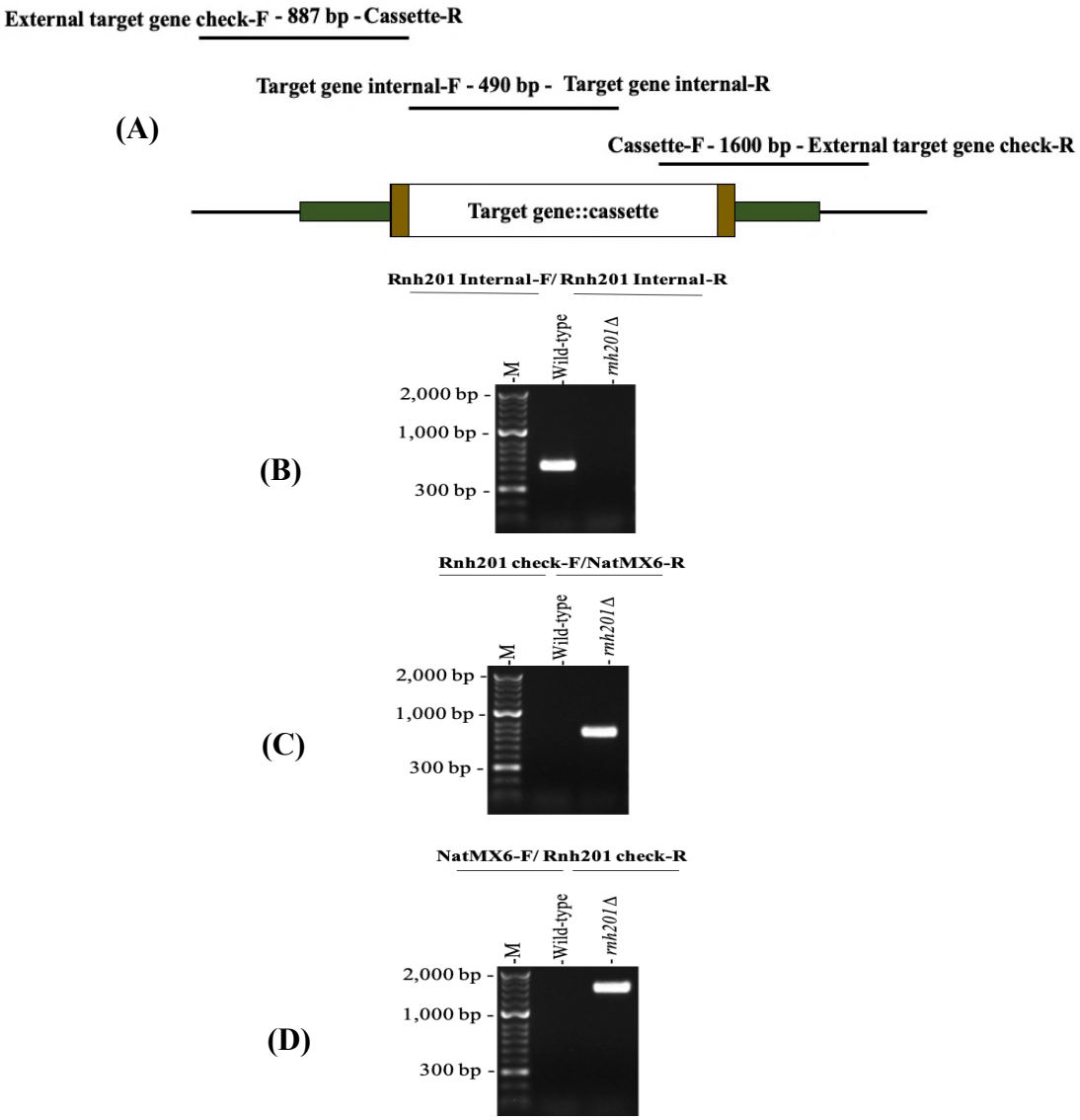

Figure 6.14 Confirmation by PCR screening of successful *rnh201Δ* single mutant knockout from HAATI^{STE} background.

(A) The genes were deleted and replacement with antibiotic resistant cassettes. To confirm the deletion of the target genes, three sets of primers were used. **(B)** Illustration of agarose gel screening of PCR products for the HAATI wild-type strain and *rnh201*Δ single mutant. The Rnh201-int-F and Rnh201-int-R primers were used, and the gel screening displays no PCR products in the successful *rnh201*Δ candidate strains. The expected sizes of the PCR product in *rnh201*Δ gene was 490 bp. **(C)** The Rnh201 check-F and NatMX6-R primers were used to generate the PCR products for the wild-type and *rnh201*Δ candidate strains. The PCR products were seen in the *rnh201*Δ strains, but not in the wild-type strain and the expected band size is 887 bp. **(D)** The wild-type and *rnh201*Δ candidate strains were utilised to amplify by the NatMX6-F and Rnh201 check-R primers and the expected size is 1600 bp.

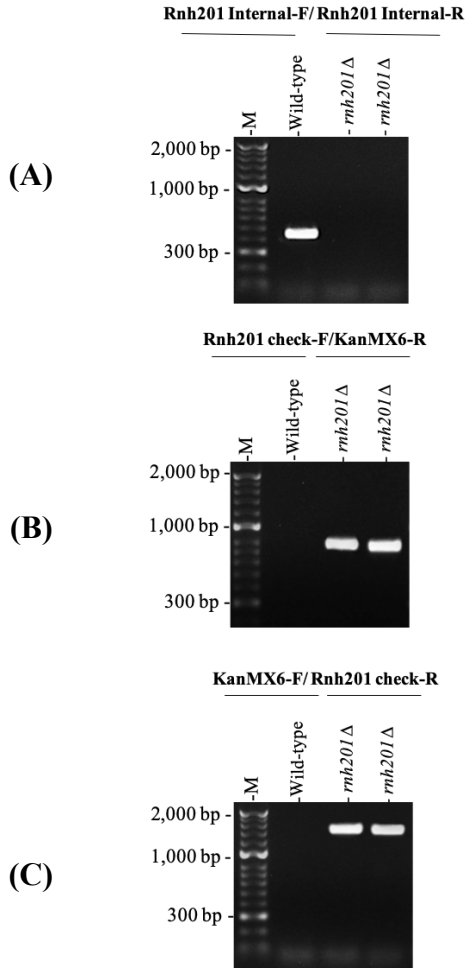

Figure 6.15 Confirmation by PCR screening of successful *rnh1Δ rnh201Δ* double mutant knockout from HAATI^{STE} background.
(A) Illustration of agarose gel screening of PCR products for the HAATI wild-type strain and *rnh201*Δ single mutant. The Rnh201-int-F and Rnh201-int-R primers were used, and the gel screening displays no PCR products in the successful *rnh201*Δ candidate strains. The expected sizes of the PCR product in *rnh201*Δ gene was 490 bp. **(B)** The Rnh201 check-F and KanMX6-R primers were used to generate the PCR products for the wild-type and *rnh201*Δ candidate strains. The PCR products were seen in the *rnh201*Δ strains, but not in the wild-type strain and the expected band size is 887 bp. **(C)** The wild-type and *rnh201*Δ candidate strains were utilised to amplify by the KanMX6-F and Rnh201 check-R primers and the expected size is 1600 bp.

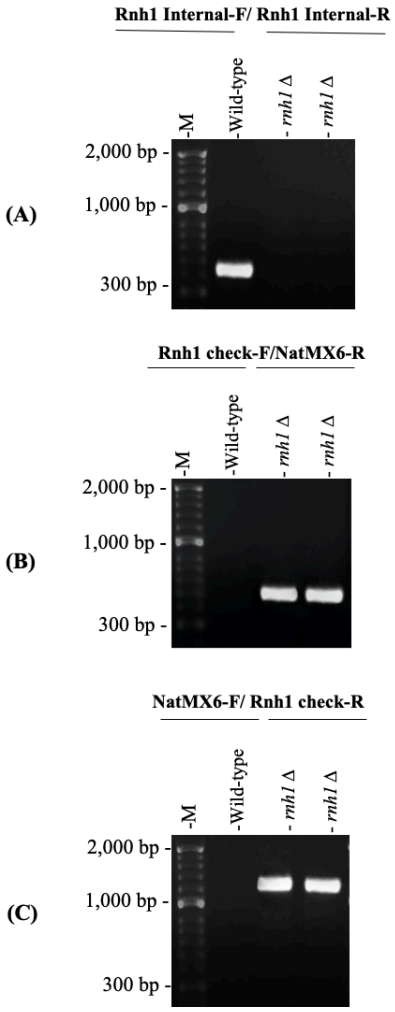

Figure 6.16 Confirmation by PCR screening of successful *tsn1Δ rnh1Δ* double mutant knockout from HAATI^{STE} background.
(A) Illustration of agarose gel screening of PCR products for the HAATI wild-type strain and *rnh1*Δ single mutant. The Rnh1-int-F and Rnh1-int-R primers were used, and the gel screening displays no PCR products in the successful *rnh1*Δ candidate strains. The expected sizes of the PCR product in *rnh1*Δ gene was 454 bp. **(B)** The Rnh1 check-F and NatMX6-R primers were used to generate the PCR products for the wild-type and *rnh1*Δ candidate strains. The PCR products were seen in the *rnh1*Δ strains, but not in the wild-type strain and the expected band size is 500 bp. **(C)** The wild-type and *rnh1*Δ candidate strains were utilised to amplify by the NatMX6-F and Rnh1 check-R primers and the expected size is 1100 bp.

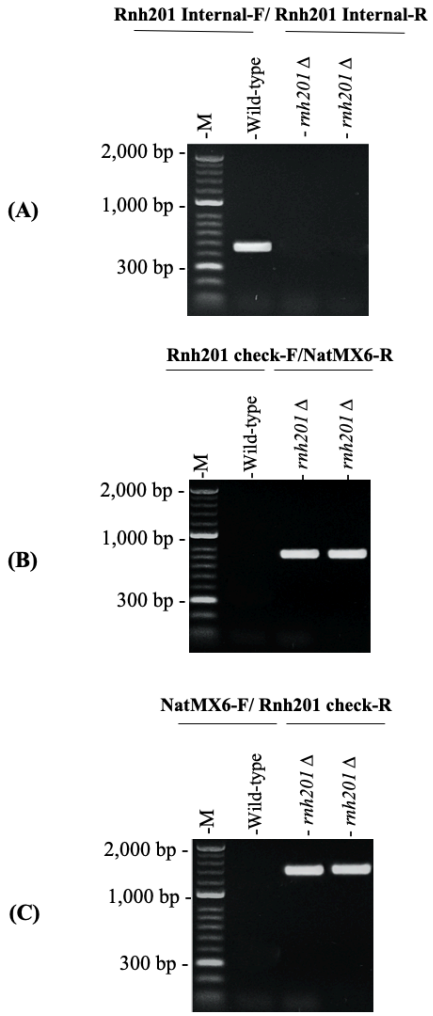

Figure 6.17 Confirmation by PCR screening of successful *tsn1Δ rnh201Δ* double mutant knockout from HAATI^{STE} background.
(A) Illustration of agarose gel screening of PCR products for the HAATI wild-type strain and *rnh201*Δ single mutant. The Rnh201-int-F and Rnh201-int-R primers were used, and the gel screening displays no PCR products in the successful *rnh201*Δ candidate strains. The expected sizes of the PCR product in *rnh201*Δ gene was 490 bp. **(B)** The Rnh201 check-F and NatMX6-R primers were used to generate the PCR products for the wild-type and *rnh201*Δ candidate strains. The PCR products were seen in the *rnh201*Δ strains, but not in the wild-type strain and the expected band size is 887 bp. **(C)** The wild-type and *rnh201*Δ candidate strains were utilised to amplify by the NatMX6-F and Rnh201 check-R primers and the expected size is 1600 bp.

6.2.3.2 Sensitivity spot tests to investigate if Tsn1 has functions in one of the RNase H pathways in the absence of telomeres.

The data for the response of the *tsn1*Δ *rnh201*Δ double mutant to phleomycin, bleomycin and HU agents provoked the question of whether we will see the same phenotype of the *tsn1*Δ *rnh201*Δ double mutant in cells without telomere. This prompted us to investigate the sensitivity of the *tsn1*Δ *rnh1*Δ and *tsn1*Δ *rnh201*Δ double mutants to DNA damaging agents in the HAATI^{STE} background. The DNA damage agents tested in this study included phleomycin, which is responsible for generation of DSBs (Figures 6.18); HU, as a DNA replication inhibitor (Figure 6.19); ultraviolet irradiation (UV), which induces multiple adducts (Figure 6.20); MMS, a DNA alkylating agent (Figure 6.21); CPT, a topoisomerase inhibitor (Figure 6.22) and mitomycin C, a potent DNA crosslinker (Figure 6.23). The data demonstrate that, the *rnh1*Δ *rnh201*Δ double mutant in the HAATI^{STE} background showed high sensitivity to the all DNA damaging agents consistent with previous reports (Ohle et al., 2016; Zhao et al., 2018). The *tsn1*Δ *rnh201*Δ double mutant exhibition hypersensitivity relative to the *rnh1*Δ and *rnh201*Δ single mutants and the *tsn1*Δ *rnh1*Δ double mutant in response to phleomycin, bleomycin and HU the in HAATI^{STE} background. Interestingly, the *tsn1Δ rnh1Δ* double mutant show increased sensitivity to HU compared with the single mutants, which is a different phenotype form the non-HAATI telomere proficient strains. However, the sensitivity of the *tsn1*Δ *rnh201*Δ double mutant was not as extreme as the *rnh1*Δ *rnh201*Δ double mutant. Conversely, the *tsn1*Δ *rnh201*Δ double mutant did not show any sensitivity increase compared with the *rnh1*Δ and *rnh201*Δ single mutants or WT in response to MMC, MMS, UV and CPT. These results indicate that Tsn1 is needed in the DNA damage recovery response when Rnh201 is absent, for some types of DNA damage in non-telomeric region. This confirms that Tsn1 is required for non-telomeric DNA repair.

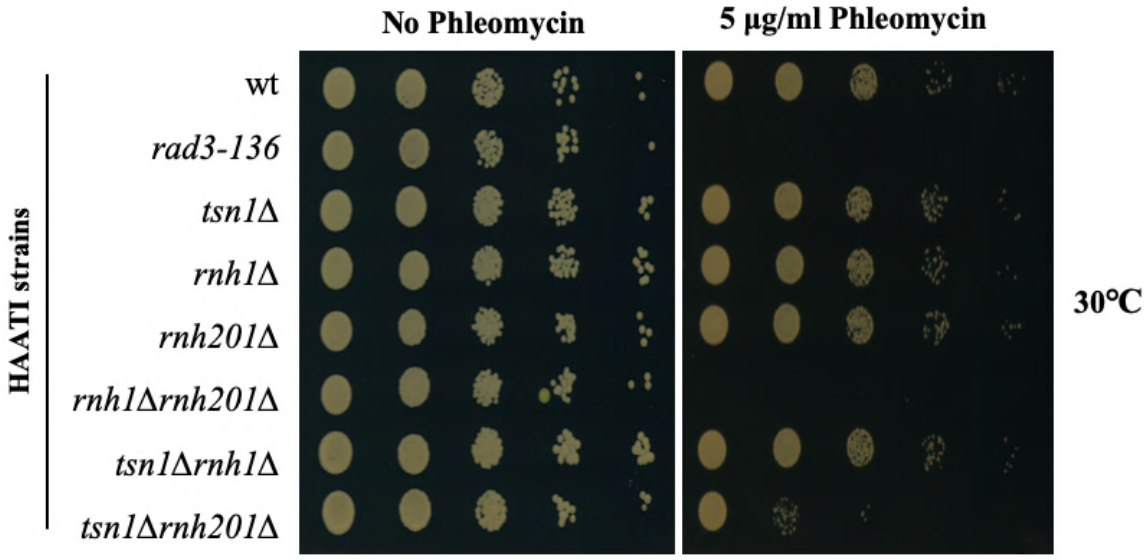

Figure 6.18 Rnh201, but not Rnh1, is required for the response to Phleomycin in the absence of Tsn1 in the HAATI^{STE} background.
S. pombe mutants were diluted (10-fold serial dilution left to right) and spotted onto YEA media contain 5 µg/ml concentration of Phleomycin. *rad3-136* was used as a positive control (Note: this is not a HAATI strain). The *tsn1Δ, rnh1Δ* and *rnh201Δ* single mutants shows no increase sensitivity compared to the WT. The *rnh1Δ rnh201Δ* double mutant show high sensitivity. The *tsn1Δ rnh201Δ* double mutant show increased sensitivity to Phleomycin compared with the *rnh1*Δ and *rnh201*Δ single mutants. The plates were incubated 3 days at 30°C.

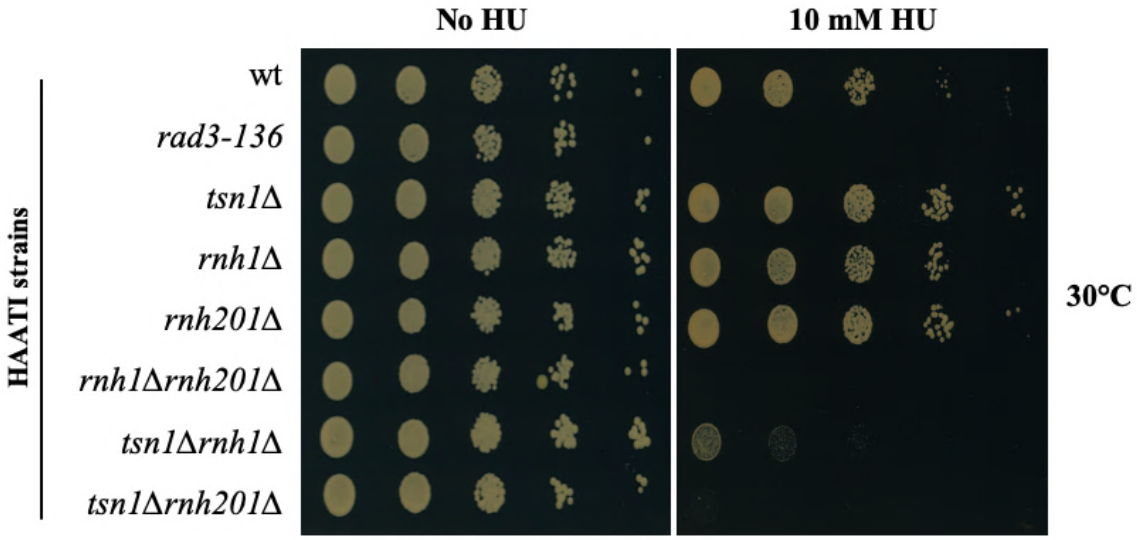

Figure 6.19 Rnh1 and Rnh201, are required for the response to Hydroxyurea in the absence of Tsn1 in the HAATI^{STE} background.
S. pombe mutants were diluted (10-fold serial dilution left to right) and spotted onto YEA media contain 10 mM concentration of hydroxyurea. *rad3-136* was used as a positive control (Note: this is not a HAATI strain). The *tsn1Δ, rnh1Δ* and *rnh201Δ* single mutants shows no increase sensitivity compared to the WT. The *rnh1Δ rnh201Δ* double mutant show hypersensitivity. The *tsn1Δ rnh201Δ* double mutant also showed hypersensitivity to hydroxyurea compared with the *rnh1*Δ and *rnh201*Δ single mutants. The *tsn1Δ rnh1Δ* double mutant exhibited increased sensitivity compared with the single mutants. The plates were incubated 3 days at 30°C.

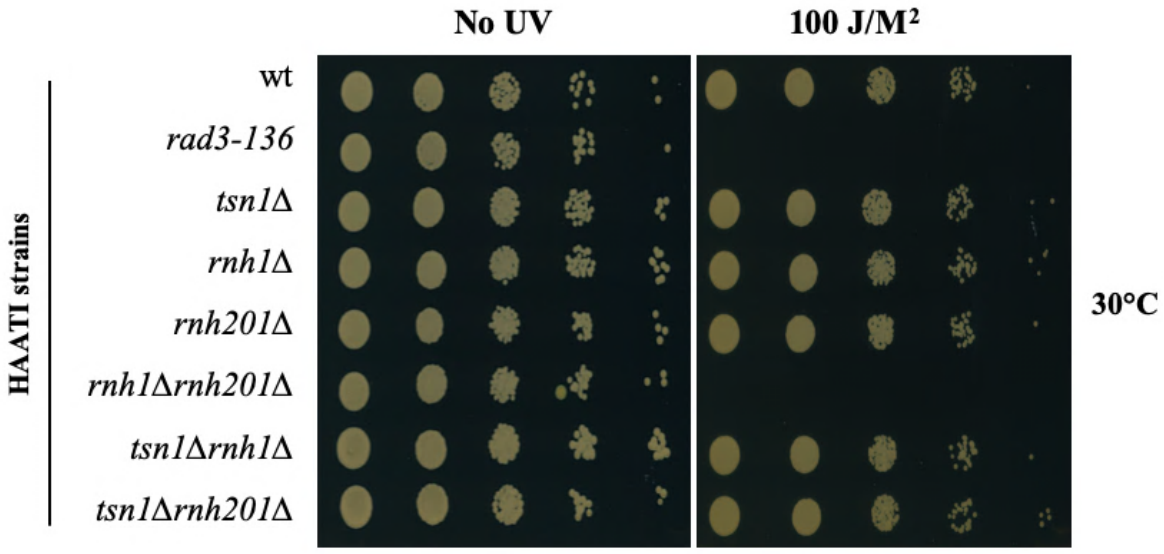

Figure 6.20 Sensitivity spot test of UV irradiation in the HAATI^{STE} background.
S. pombe mutants were diluted (10-fold serial dilution left to right) and spotted onto YEA media and then exposed to 100 J/M^2 dose of UV irradiation. *rad3-136* was used as a positive control (Note: this is not a HAATI strain). The *tsn1Δ, rnh1Δ* and *rnh201Δ* single mutants shows no increase sensitivity compared to the WT. The *rnh1Δ rnh201Δ* double mutant show slight increase sensitivity, but the *tsn1Δ rnh1Δ* and *tsn1Δ rnh201Δ* double mutants show no sensitivity to UV irradiation compared with the *rnh1*Δ and *rnh201*Δ single mutants or the WT. The plates were incubated 3 days at 30°C.

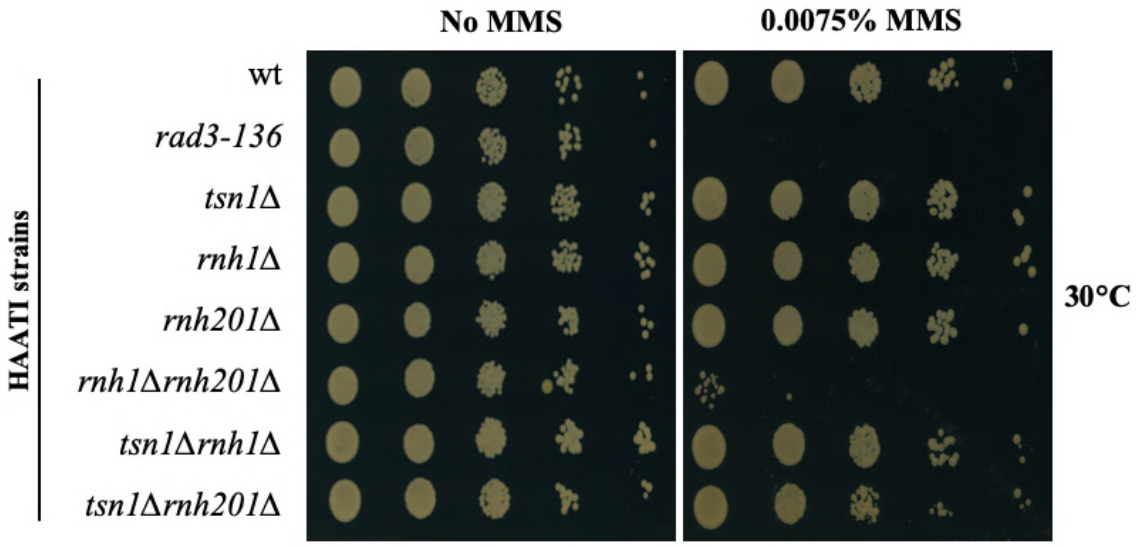

Figure 6.21 Sensitivity spot test of Methyl methane sulfonate (MMS) in the HAATI^{STE} background.

S. pombe mutants were diluted (10-fold serial dilution left to right) and spotted onto YEA media contain 0.0075% concentration of MMS. *rad3-136* was used as a positive control (Note: this is not a HAATI strain). The *tsn1Δ, rnh1Δ* and *rnh201Δ* single mutants shows no increase sensitivity compared to the WT. The *rnh1Δ rnh201Δ* double mutant shows increased sensitivity, but the *tsn1Δ rnh1Δ* and *tsn1Δrnh201Δ* double mutants show no sensitivity to MMS compared with the *rnh1*Δ and *rnh201*Δ single mutants or the WT. The plates were incubated 3 days at 30°C.

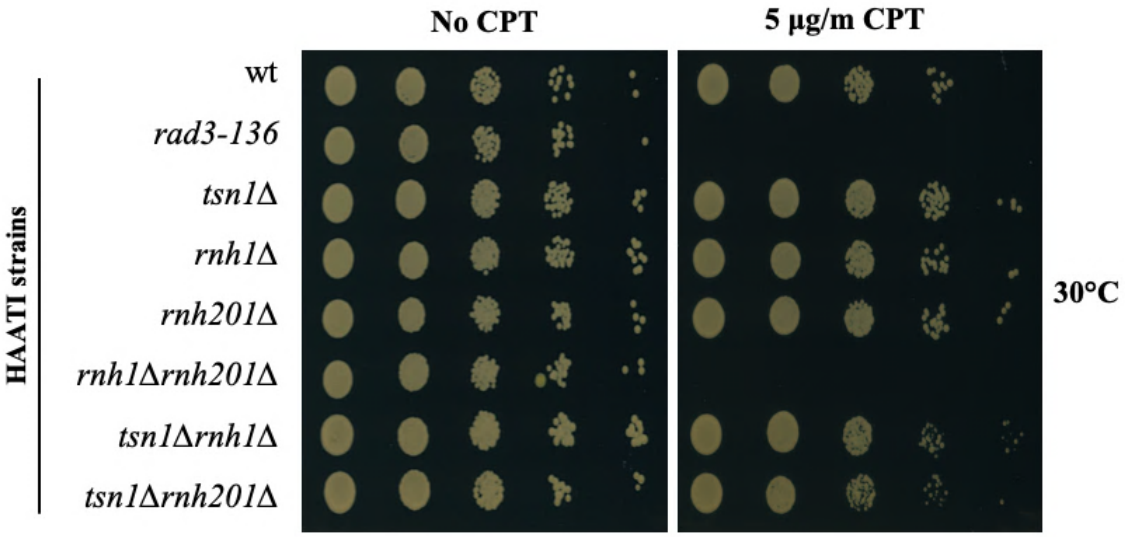

Figure 6.22 Sensitivity spot test of Camptothecin (CPT) in the HAATI^{STE} background.
S. pombe mutants were diluted (10-fold serial dilution left to right) and spotted onto YEA media contain 5 µg/m concentration of CPT. *rad3-136* was used as a positive control (Note: this is not a HAATI strain). The *tsn1Δ, rnh1Δ* and *rnh201Δ* single mutants shows no increase sensitivity compared to the WT. The *rnh1Δ rnh201Δ* double mutant shows high sensitivity, but the *tsn1Δ rnh1Δ* and *tsn1Δ rnh201Δ* double mutants show no sensitivity to CPT compared with the *rnh1*Δ and *rnh201*Δ single mutants and the WT. The plates were incubated 3 days at 30°C.

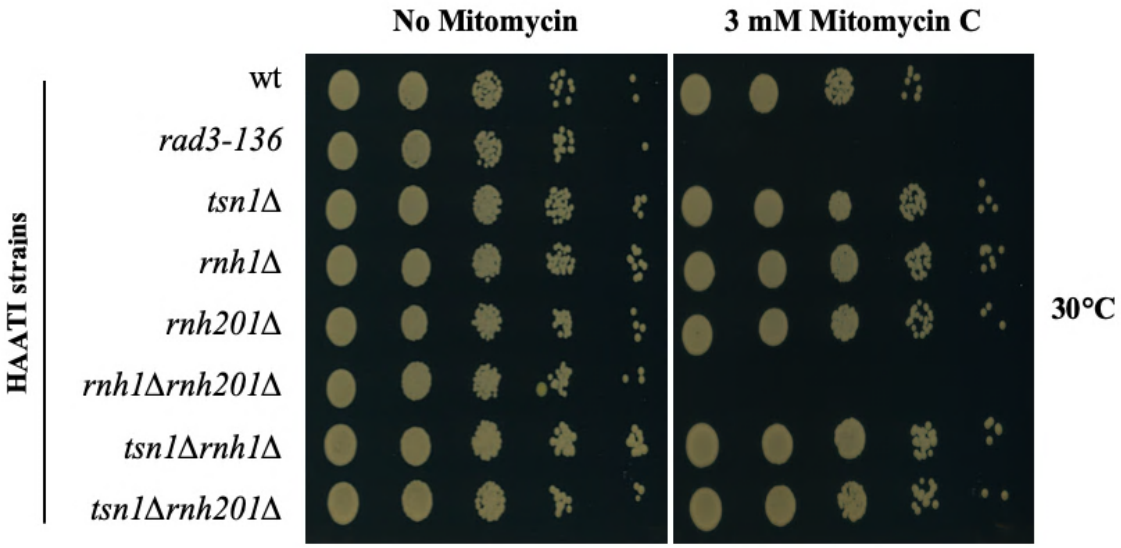

Figure 6.23 Sensitivity spot test of Mitomycin C (MMC) in the HAATI^{STE} background.
S. pombe mutants were diluted (10-fold serial dilution left to right) and spotted onto YEA media contain concentration of Mitomycin C (3 mM MMC). *rad3-136* was used as a positive control (Note: this is not a HAATI strain). The *tsn1Δ, rnh1Δ* and *rnh201Δ* single mutants shows no increase sensitivity compared to the WT. The *rnh1Δ rnh201Δ* double mutant shows high sensitivity, but the *tsn1Δ rnh1Δ* and *tsn1Δ rnh201Δ* double mutants show no sensitivity to MMC compared with the *rnh1*Δ and *rnh201*Δ single mutants or the WT. The plates were incubated 3 days at 30°C.

6.2.4 Role of Tfx1 in one of the RNase H pathways in the absence of telomeres.

6.2.4.1 Construction mutant strains in the HAATI^{STE} background.

The *tfx1*Δ single mutant strains were used as the basis for creation of *de novo* mutants. All the strains were created by antibiotic-resistant cassettes replacement as founded on the PCR-based gene targeting approach as described by Bähler et al. (1998). In this study the double mutants *tfx1*Δ *rnh1*Δ (BP3458) and *tfx1*Δ *rnh201*Δ (BP3456) were developed by deleting the genes from the *tfx1*Δ single mutant (BP3384). The antibiotic *natMX6* was used as the replacement cassettes in the deletion of *rnh1* and *rnh201* and amplified by using PCR primers that designed with 80 bp homologous sequences directly flanked upstream and downstream from the of *rnh1* and *rnh201* ORFs, with 20 bp of homologous sequence to the plasmid that carries the *natMX6* gene. To verify the correct deletion, candidates of strains were screened using PCR (Figures 6.24 and 6.25). Two or more independent isolates were tested for each construct.

6.2.4.2 Sensitivity spot tests to investigate if Tfx1 has functions in one of the RNase H pathways in the absence of telomeres.

The data for the response of the *tsn1*Δ *rnh201*Δ double mutant to phleomycin, bleomycin and HU agents provoked the question of wither Tfx1 has function in one of the RNases H pathways in cells without telomeres. This prompted us to investigate the sensitivity of the *tfx1*Δ *rnh1*Δ and *tfx1*Δ *rnh201*Δ double mutants to DNA damaging agents in HAATI^{STE} background. The DNA damage agents tested in this study included phleomycin, which is responsible for the generation of DSBs (Figures 6.26); HU, as a DNA replication inhibitor (Figure 6.27); ultraviolet irradiation (UV), which induces multiple adducts (Figure 6.28); MMS, a DNA alkylating agent (Figure 6.29); CPT, a topoisomerase inhibitor (Figure 6.30) and mitomycin C, a potent DNA crosslinker (Figure 6.31). The data demonstrate that, the *rnh1*Δ *rnh201*Δ double mutant showed high sensitivity to the all DNA damaging agents consistent with previous reports (Ohle et al., 2016; Zhao et al., 2018). However, the *tfx1*Δ *rnh1*Δ and *tfx1*Δ *rnh201*Δ double mutants did not show any sensitivity increase compared with the *rnh1*Δ and *rnh201*Δ single mutants or WT in response to all DNA damaging agents. Convectively, these results indicate that Tsn1, but not Tfx1 is needed in the DNA damage recovery response when Rnh201 is absent, for some types of DNA damage at non-telomeric region.

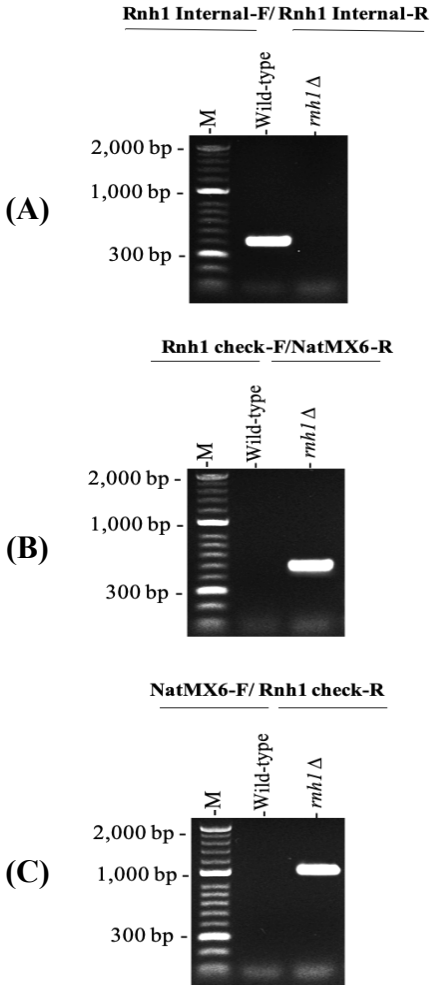

Figure 6.24 Confirmation by PCR screening of successful *tfx1Δ rnh1Δ* double mutant knockout from HAATI^{STE} background.
(A) Illustration of agarose gel screening of PCR products for the HAATI wild-type strain and *rnh1*Δ single mutant. The Rnh1-int-F and Rnh1-int-R primers were used, and the gel screening displays no PCR products in the successful *rnh1*Δ candidate strains. The expected sizes of the PCR product in *rnh1*Δ gene was 454 bp. **(B)** The Rnh1 check-F and NatMX6-R primers were used to generate the PCR products for the wild-type and *rnh1*Δ candidate strains. The PCR products were seen in the *rnh1*Δ strains, but not in the wild-type strain and the expected band size is 500 bp. (C) The wild-type and *rnh1*Δ candidate strains were utilised to amplify by the NatMX6-F and Rnh1 check-R primers and the expected size is 1100 bp.

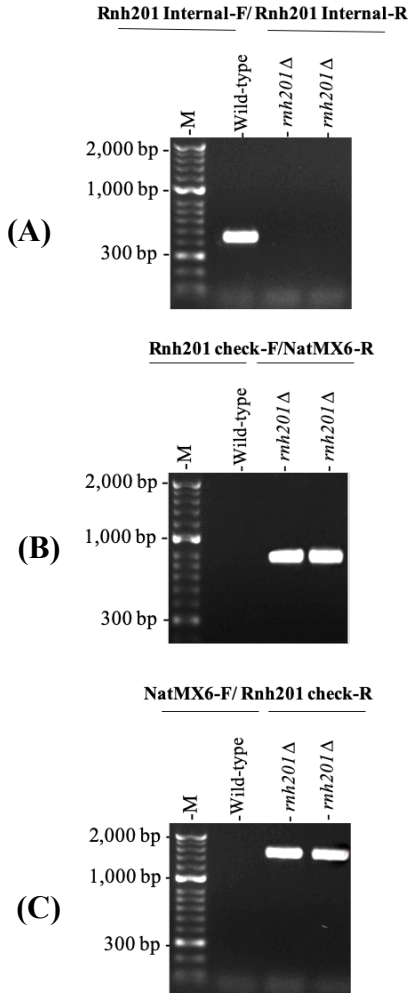

Figure 6.25 Confirmation by PCR screening of successful *tfx1Δ rnh201Δ* double mutant knockout from HAATI^{STE} background.
(A) Illustration of agarose gel screening of PCR products for the HAATI wild-type strain and *rnh201*Δ single mutant. The Rnh201-int-F and Rnh201-int-R primers were used, and the gel screening displays no PCR products in the successful *rnh201*Δ candidate strains. The expected sizes of the PCR product in *rnh201*Δ gene was 490 bp. **(B)** The Rnh201 check-F and NatMX6-R primers were used to generate the PCR products for the wild-type and *rnh201*Δ candidate strains. The PCR products were seen in the *rnh201*Δ strains, but not in the wild-type strain and the expected band size is 887 bp. **(C)** The wild-type and *rnh201*Δ candidate strains were utilised to amplify by the NatMX6-F and Rnh201 check-R primers and the expected size is 1600 bp.

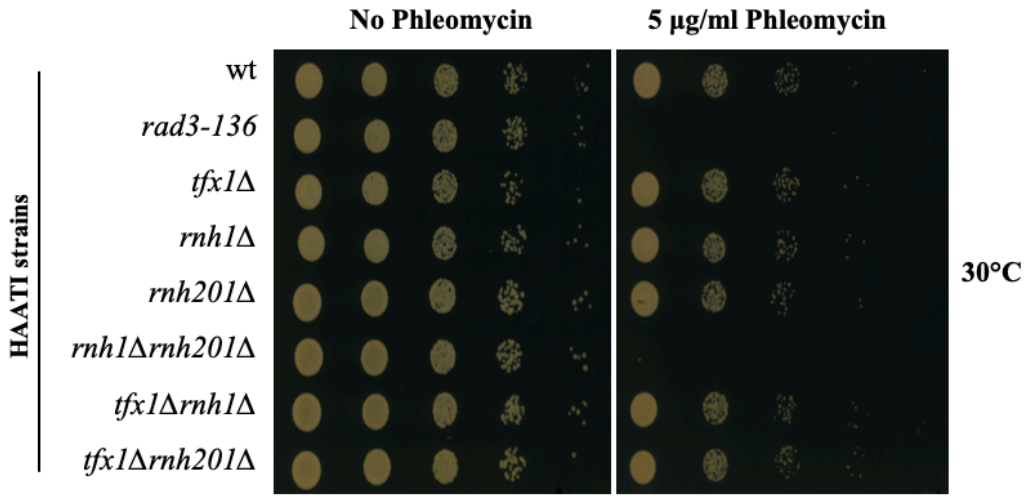

Figure 6.26 Sensitivity spot test of Phleomycin in the HAATI^{STE} background.
S. pombe mutants were diluted (10-fold serial dilution left to right) and spotted onto YEA media containing 5 µg/ml of Phleomycin. *rad3-136* was used as a positive control (Note: this is not a HAATI strain). The *tfx1Δ, rnh1Δ* and *rnh201Δ* single mutants shows no increase sensitivity compared to the WT. The *rnh1Δ rnh201Δ* double mutant shows high sensitivity. The *tfx1Δ rnh1Δ* and *tfx1Δ rnh201Δ* double mutants show no increased sensitivity to Phleomycin compared with the *rnh1*Δ and *rnh201*Δ single mutants. The plates were incubated 3 days at 30°C.

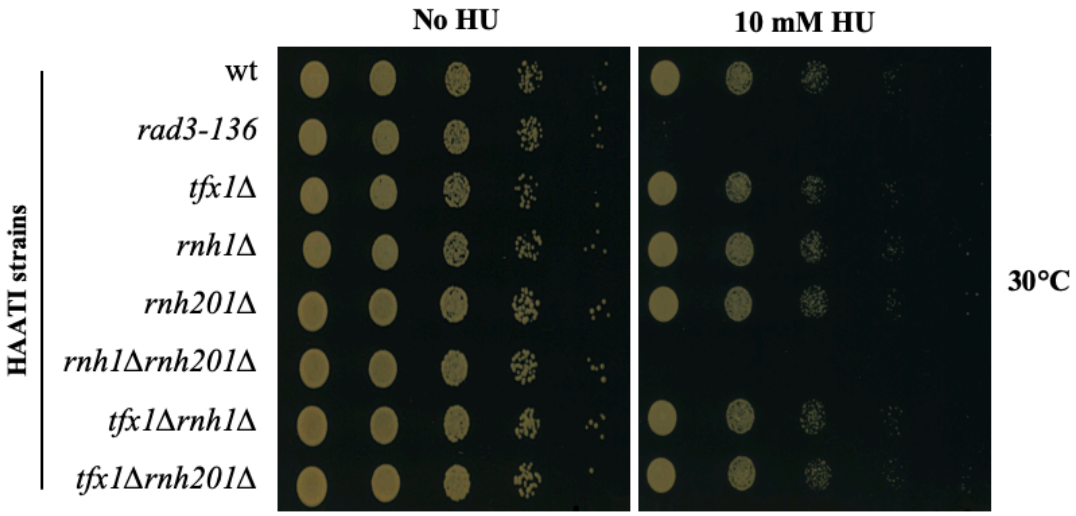

Figure 6.27 Sensitivity spot test of Hydroxyurea in the HAATI^{STE} background.
S. pombe mutants were diluted (10-fold serial dilution left to right) and spotted onto YEA media containing 10 mM of hydroxyurea. *rad3-136* was used as a positive control (Note: this is not a HAATI strain). The *tfx1Δ, rnh1Δ* and *rnh201Δ* single mutants shows no increase sensitivity compared to the WT. The *rnh1Δ rnh201Δ* double mutant shows high sensitivity. The *tfx1Δ rnh1Δ* and *tfx1Δ rnh201Δ* double mutants show no increased sensitivity to hydroxyurea compared with the *rnh1*Δ and *rnh201*Δ single mutants. The plates were incubated 3 days at 30°C.

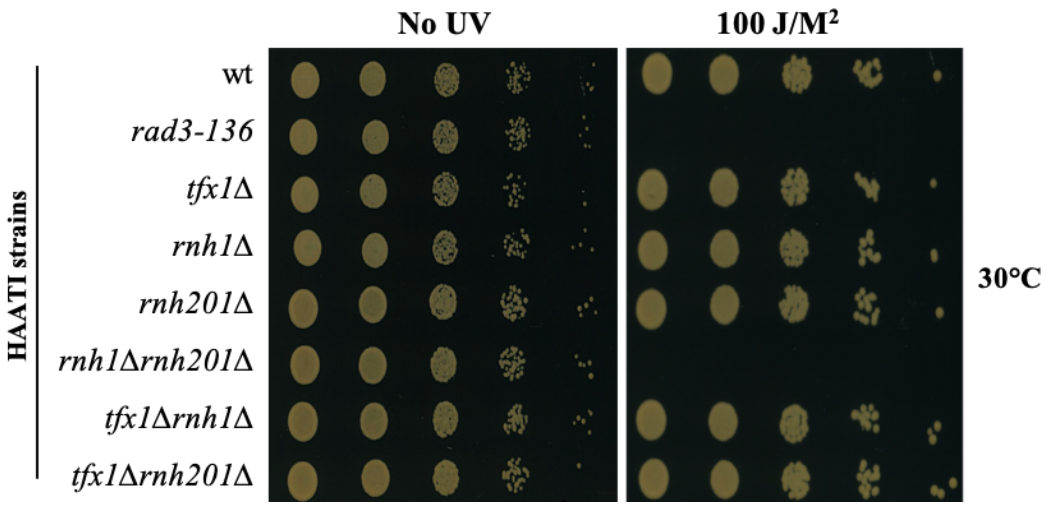

Figure 6.28 Sensitivity spot test of UV irradiation in the HAATI^{STE} background.
S. pombe mutants were diluted (10-fold serial dilution left to right) and spotted onto YEA media and then exposed to 100 J/M^2 doses of UV irradiation. *rad3-136* was used as a positive control (Note: this is not a HAATI strain). The *tfx1Δ, rnh1Δ* and *rnh201Δ* single mutants shows no increase sensitivity compared to the WT. The *tfx1Δ rnh1Δ* and *tfx1Δ rnh201Δ* double mutants show no increased sensitivity to UV compared with the *rnh1*Δ and *rnh201*Δ single mutants. The plates were incubated 3 days at 30°C.

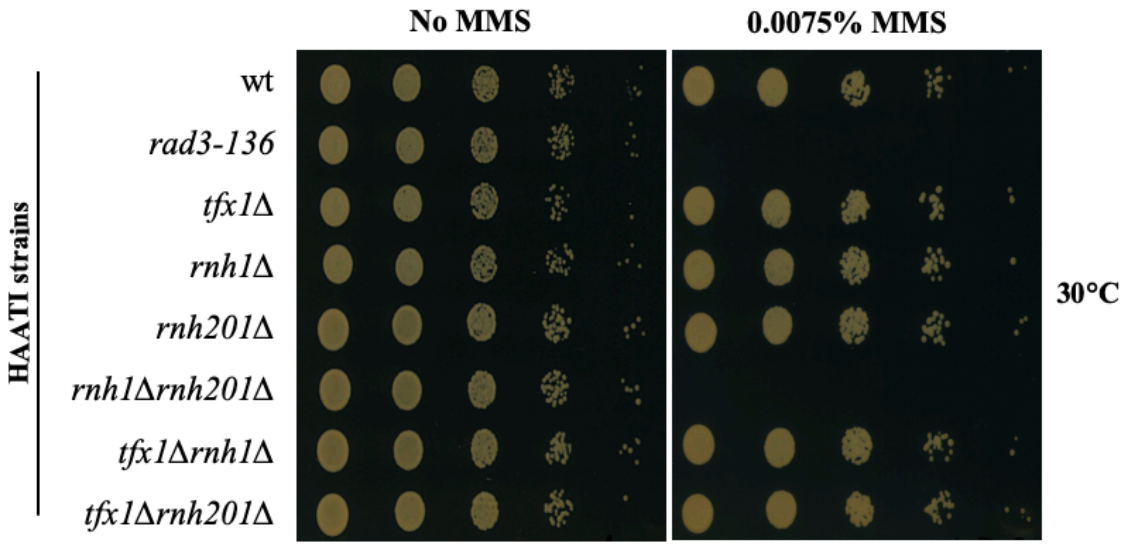

Figure 6.29 Sensitivity spot test of Methyl methane sulfonate (MMS) in the HAATI^{STE} background.

S. pombe mutants were diluted (10-fold serial dilution left to right) and spotted onto YEA media containing 0.0075% of MMS. *rad3-136* was used as a positive control (Note: this is not a HAATI strain). The *tfx1Δ, rnh1Δ* and *rnh201Δ* single mutants shows no increase sensitivity compared to the WT. The *rnh1Δ rnh201Δ* double mutant shows high sensitivity. The *tfx1Δ rnh1Δ* and *tfx1Δ rnh201Δ* double mutants show no increased sensitivity to MMS compared with the *rnh1*Δ and *rnh201*Δ single mutants. The plates were incubated 3 days at 30°C.

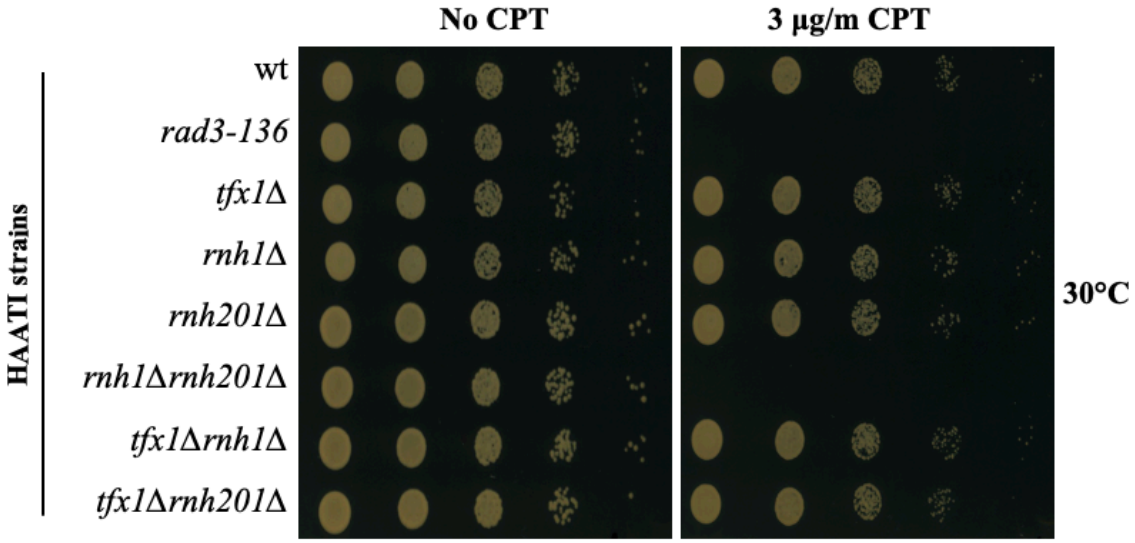

Figure 6.30 Sensitivity spot test of Camptothecin (CPT) in the HAATI^{STE} background.
S. pombe mutants were diluted (10-fold serial dilution left to right) and spotted onto YEA media containing 3 µg/m of CPT. *rad3-136* was used as a positive control (Note: this is not a HAATI strain). The *tfx1Δ, rnh1Δ* and *rnh201Δ* single mutants shows no increase sensitivity compared to the WT. The *rnh1Δ rnh201Δ* double mutant showed high sensitivity. The *tfx1Δ rnh1Δ* and *tfx1Δ rnh201Δ* double mutants show no increased sensitivity to CPT compared with the *rnh1*Δ and *rnh201*Δ single mutants. The plates were incubated 3 days at 30°C.

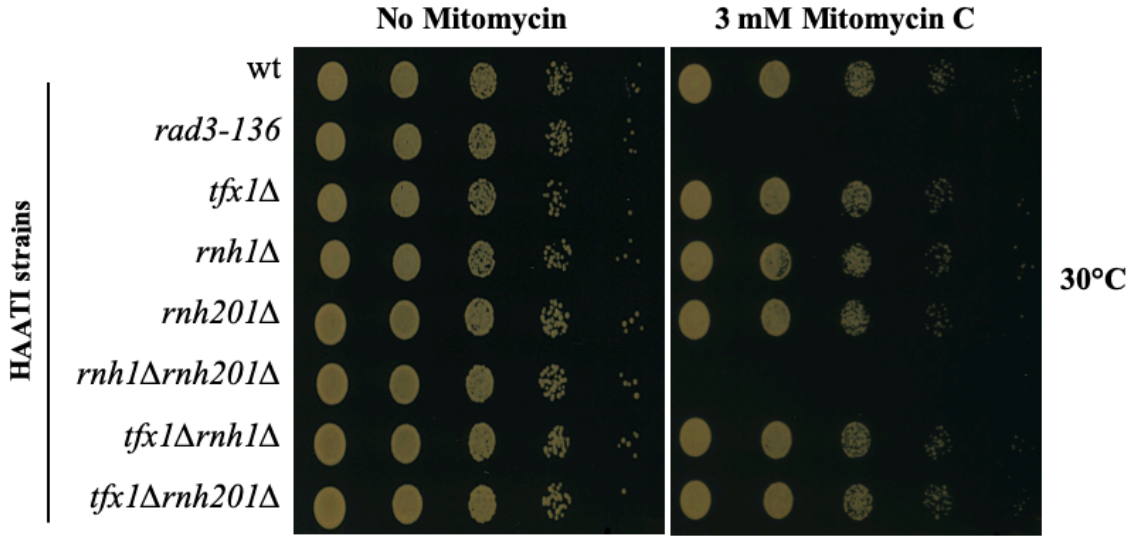

Figure 6.31 Sensitivity spot test of Mitomycin C (MMC) in the HAATI^{STE} background.
S. pombe mutants were diluted (10-fold serial dilution left to right) and spotted onto YEA media contain concentration of Mitomycin C (3 mM MMC). *rad3-136* was used as a positive control (Note: this is not a HAATI strain). The *tfx1Δ, rnh1Δ* and *rnh201Δ* single mutants shows no increase sensitivity compared to the WT. The *rnh1Δ rnh201Δ* double mutant shows high sensitivity. The *tfx1Δ rnh1Δ* and *tfx1Δ rnh201Δ* double mutants show no increased sensitivity to MMC. The plates were incubated 3 days at 30°C.

6.3 Discussion

Telomeres are sequences that are repeated and usually found at the ends of linear chromosomes. One of the purposes of telomeres is to protect the ends of the chromosomes from potential degradation, and telomeres ensure the ends of chromosomes are not be recognized as DSBs (Vancevska et al., 2017). Previously our group initially showed that Tsn1/Tfx1, which regulates telomere-associated transcripts (Gomes-Escobar et al., 2016). The regulation does not contribute to increases in RNA:DNA hybrids that are found in the sub-telomeric regions (Gomes-Escobar, personal commination, data not shown). We hypothesized that RNA:DNA hybrid-induced recombination, has an impact in non-telomeric regions. This led us to test this by using fission strains that do not have telomeres, which is referred to as HAATI strains.

The current study has shown that mutants of *tsn1* and *tfx1* are hyper resistant to the DSB agent phleomycin in the BP90 background but not in the HAATI^{STE} background. We speculate that this would be interpreted in one of three ways. Firstly, loss of telomeres confers some resistance to phleomycin, as the HAATI^{STE} wild-type strain was more resistant to phleomycin than the BP90 wild-type. If this is correct, it might suggest that loss of Tsn1 and/or Tfx1from the BP90 background mimics the loss of telomeres, as the *tsn1Δ* and *tfx1Δ* single mutants also show increased resistance to phleomycin. Secondly, it might suggest there is genetic or epigenetic difference between the BP90 and HAATI^{STE} background which is unknown and unrelated to telomeres, and it is this which causes distinct phleomycin sensitivity, and it is suppressed wither *tsn1* and *tfx1* are mutated. Thirdly, the HAATI strain contains blocks of STE heterochromatin throughout the genome which could influence DNA repair and sensitivity to damage.

Previously in Chapter 3, the *dcr1*Δ *tsn1*Δ double mutant shows increased sensitivity to damaging agents relative to the *dcr1*Δ single mutant. To test if this is related to non-telomeric DNA damage recovery, generation of *dcr1*Δ single mutant and *dcr1*Δ *tsn1*Δ double mutant from HAATI strain would be needed. For instance, if *dcr1*Δ single mutant and *dcr1*Δ *tsn1*Δ double mutant shows a similar phenotype sensitivity to the DNA damaging agents, this will refer to a telomere specificity effect for Tsn1. Here we used

the HAATI^{STE}, but not HAATI^{rDNA} because we suspected Dcr1 might require for maintenance of the rDNA telomere replacements (Begnis et al., 2018). However, in this current study we were unable to generate a single *dcr1*Δ and *dcr1*Δ *tsn1*Δ double mutant from HAATI strain to test this requirement. The reasons for this may that Dcr1 is required to maintain HAATI^{STE} viably. Julie Cooper's group have recently shown that HAATI^{rDNA} can be maintained in the *dcr1*Δ background and they also show Dcr1 is needed to suppress formation of HAATI^{STE}, but they do not specify if HAATI^{STE} require Dcr1 for maintenance. So, this remains a possible reason for the future to generate HAATI^{STE} *dcr1*Δ strains (Begnis et al., 2018).

Central to our hypothesis, loss of Tsn1/Tfx1 function results in non-telomeric RNA:DNA hybrids causing a Goldilocks effect (too much is BAD, too little is BAD), that can assist in DSB repair. In addition, RNase H activity is crucial in DSBs repair. However, the removal of both RNase H1 and RNase H2 coding genes contributed to the DNA damage recovery, which results inhibition of HR-mediated DSB repair. This suggesting that the two RNase H pathways are needed redundantly in DSB repair (Ohle et al., 2016). This led us to generate the single and double mutants in *tsn1*Δ and *tfx1*Δ with the RNAse H gene mutants *rnh1*Δ and *rnh201*Δ, to delineate whether Tsn1 and Tfx1 function in concert with known RNAse H activities in non-telomeric DNA in strains without telomeres/telomerase. The experiment presented in this chapter shows similar sensitivities to DNA-damaging reagents in the HAATI^{STE} background as we have shown in the BP90 background, and this indicates that Tsn1, but not Tfx1, does indeed have a role to play in the recovery from DNA damage for several genotoxic and DNA replicative stress agents in non-telomeric DNA repair. Surprisingly, the *tsn1*Δ *rnh1*Δ and *tsn1*Δ *rnh201*Δ both were considerably more sensitive to HU than is apparent in the non-HAATI strains where the *tsn1*Δ *rnh1*Δ double mutant showed no sensitivity. The reason for this may be because the HAATI^{STE} strains have many STE repeats internally within the genome. Julie Cooper's group state this as these arise due to a retro transposition-like mechanism, and the added RNAse H phenotype might reflect transcripts in this region.

So, from the work in this chapter we have revealed a role for Tsn1, but not Tfx1, with appears to be functionally required in the absence of Rnh201, and that this is not related to the function of Tsn1 in regulating telomeric RNA manuscripts in canonical telomeres.

6.4 Conclusion

Tsn1, but not Tfx1 is required for non-telomeric DNA repair.

7. Final Discussion

7. Final Discussion

7.1 Introduction

Translin is a highly conserved DNA and RNA binding protein that abounds in the testis, brain and some malignancies in human (Gupta et al., 2019). Initially, Translin human protein was identified for its capacity to bind to the breakpoint junctions of lymphoid malignancy chromosomal translocations (Aoki et al., 1995). Subsequently, it was shown to bind to translocation break point junctions in many other genetic diseases and cancer (Jaendling & McFarlane, 2010). Previous studies on human, *Drosophila*, mice, and *S. pombe* showed that Translin can form an octameric ring. Translin is a typical a cytoplasmic protein but can translocate into the nucleus when subjected to genotoxic stress (Jaendling & McFarlane, 2010; Guptaet al., 2019). Translin, and its binding partner TRAX, are highly conserved from the fission yeast to human cells suggesting and important conserved function, although the budding yeast does not have orthologues (Li et al., 2008; Jaendling &McFarlane, 2010). These two proteins create a heteromeric complex and play important roles in various biological processes such as RNA interference, the degradation of microRNA during oncogenesis, neuronal regulation, spermatogenesis, and tRNA processing (Wang et al., 2004; Laufman et al., 2005; Gomez-Escobar et al., 2016).

Notably, the Translin and TRAX complex has RNase activity and binds to nucleic acids *in vitro* with a bias towards RNA (Jaendling et al., 2008; Li et al., 2012; Jaendling &McFarlane, 2010). The loss of the functions of TRAX and Translin does not cause major phenotypic abnormalities. Essentially, losing these two proteins has no as yet measured negative consequences on fission yeast cells (Jaendling et al., 2008), which implies that the proteins may function in secondary or redundant pathways (Jaendling &McFarlane, 2010). In addition, preferences for binding of specific sequences informs the proposition that Translin could function in telomere regulation despite lack of current evidence of this (Jacob et al., 2004).

Recent studies have shown that Trax plays a crucial role in responding to damage of murine DNA through associating with the ATM pathway (Wang et al., 2015). However, research has not established a role for Translin in this response (Fukuda et al., 2008). Translin and TRAX complex is also known as C3PO (component 3 promoter of RISC) in human and *Drosophila* cells. C3PO facilitate efficient RNA interference (RNAi), that plays a crucial role in removal of passenger strands from the small interfering RNAs that are involved in the process of Argonaute-dependent RNAi and its induced form of transcriptional silencing (Holoch & Moazed, 2015).

Recent studies have highlighted a role for Translin and Trax in oncogenesis for cancers possessing haploinsufficient traits for the RNAs III Dicer (Asada et al., 2014). These seminal works showed that Dicer in reduced levels triggers the exposure of pre-miRNAs to an alternative ribonuclease activity that is mediated by the C3PO complex formed by Trax and Translin (Asada et al., 2014). Loss of pre-miRNA results in a failure to mature tumour suppressing miRNA, driving the oncogenic process. An extension of this process revealed that Trax and Translin inhibition facilitates the reduced level of Dicer to restore the pre-miRNAs processing, which helps to re-establish the levels of tumour-suppressing miRNA. Consequently, researchers examined whether Translin and Trax could function as oncological therapeutic target (Asada et al., 2014).

At the beginning of this study a crucial question relating to Translin and Trax remains- what, if any, is the requirement from one, or both of these proteins in the DNA damage response and, or chromosomal translocation, and how does this related to the other known function of this conserved protein pair?

7.2 Tsn1, but not Tfx1, suppresses genome instability in the absence of Dcr1.

Previous studies resulted in the postulate the Translin might be required for chromosomal translocations, although there remains little evidence that it is involved in the DNA damage recovery (Jaendling & McFarlane, 2010). However, Trax has been demonstrated to be required for proper recruitment of the ATM kinase to DNA DSBs to mediate the DNA repair process, although it is proposed that this function is independent of Translin

(Wang et al., 2016). Previous analyses in *S. pombe* demonstrate that Tsn1 and Tfx1 have no principal role during recombination and other associated processes, including the recovery from DNA damage (Jaendling et al., 2008). In addition to this, Translin and /or Trax have been implicated in the regulation of the RNAi process, although there is no evidence for this in *S. pombe* (Jaendling et al., 2008; Jaendling et al., 2010). One of the lead components of the RNAi pathway, Dicer, has been demonstrated to have RNAi-independent functions in DNA damage avoidance in *S. pombe*, where it is proposed it assists the removal of RNA pol II to avoid transcription-replication conflicts which might generate recombinogenic lesions (Castel et al., 2014). Consequently, we found out that the sensitivity of the *dcr1Δ* mutant to some DNA damaging agents increased with the additional mutation of *tsn1*, but not *tfx1*. These significant results show a link between Tsn1 and recovery response to DNA damage in the absence of Drc1, which provides the first association between this critical conserved protein to genomic instability, an oncogenic driver. Interestingly, there does not appear to be a similar requirement for Tfx1.

Mammalian Translin can form nucleic acid binding complexes in the absence of Trax, but it remains unclear from our data whether the nucleic acid binding function of Tsn1 is required for DNA damage recovery. Castel and co-workers demonstrated that in the absence of Dcr1 RNA:DNA hybrid levels became elevated, and it was these structures that were generated by RNA pol II that are the cause of increased genome instability in the absence of Dcr1; although it should be noted that Castel and co-workers did not overexpress and RNA:DNA hybrid processing enzyme, such as RNAse H to demonstrate this could suppress the need for Dcr1. Our findings suggest that a secondary role of Tsn1 to Dcr1 in reducing the stability of RNA:DNA hybrids throughout the genome, which suppress transcription-DNA replication-associated recombination when Dcr1 is absent, resulting chromosomal stability. So, it might be the case that in the absence of Dcr1, the processing of RNA:DNA hybrids generated by RNA pol II requires Tsn1, but not Tfx1. Interestingly, a co-worker in our group has now demonstrated that in the absence of both Dcr1 and Tsn1 elevated chromosomal RNA:DNA hybrids can be observed by using DNA:RNA immunoprecipitation (DRIP) at different genomic loci, including the rDNA

and tRNA genes (Gomez-Escobar, unpublished data) (Figure 7.1). Surprisingly, both *tsn1Δ* and *tfx1Δ* mutants have RNA:DNA hybrids elevated to levels similar to those seen in the *dcr1Δ* single mutant. If elevated RNA:DNA hybrids levels alone were sufficient to confer disruptive replicative stress, and therefore sensitivity to replicative stress agents, such as HU, then we would expect *tsn1Δ* and *tfx1Δ* single mutants to exhibit HU sensitivity, which they do not. This finding refers an important point. Firstly, whilst loss of Tsn1 and Tfx1 result in increased DNA:RNA hybrids, the cellular mechanisms which enable the cell to cope with these levels remains intact in the absence of Tsn1 and Tfx1. However, when Dcr1 is lost, this collaborates with an inability to fully cope with these higher level of DNA:RNA hybrids, suggesting a role for Dicer in their processing, as proposed by Castel et al. However. We must be cautions as Castel et al. (2014) did not demonstrate they could suppress *dcr1Δ* phenotype by over expressing RNAase H, so the *dcr1Δ* sensitivity to DNA damaging agents might not directly relate to the increased hybrid levels seen in this mutant. Indeed, Dicer is an RNAse III enzyme, which digests dsRNA. In addition, Dicer catalytic dead mutants behave like wild-type indicating RNAase activity of Dicer appears not to be required for DNA repair.

Further studies using DRIP-seq on the entire genome could be used to confirm these results as well as assessing whether the role of Tsn1 in RNA:DNA hybrid removal extends to other genomic loci.

Our study suggested that *dcr1Δ tsn1Δ* hypersensitivity to DNA damaging agents rather than *dcr1Δ tfx1Δ* cells, is associated with the elevated formation of recombination stimulating lesions. That puts forward a hypothesis that Tsn1 is suppressing replication-associated recombination and has a conventional mechanistic function in the absence of Dcr1. This interesting proposal may address the outstanding question of why Translin is associated with the formation of chromosomal translocation in human cancers. This study will form the basis for future studies in human cells to examine whether human Translin (TSN), like *S. pombe Tsn1,* is associated with the initiation or regulation of recombination in Dicer-deficient cells.

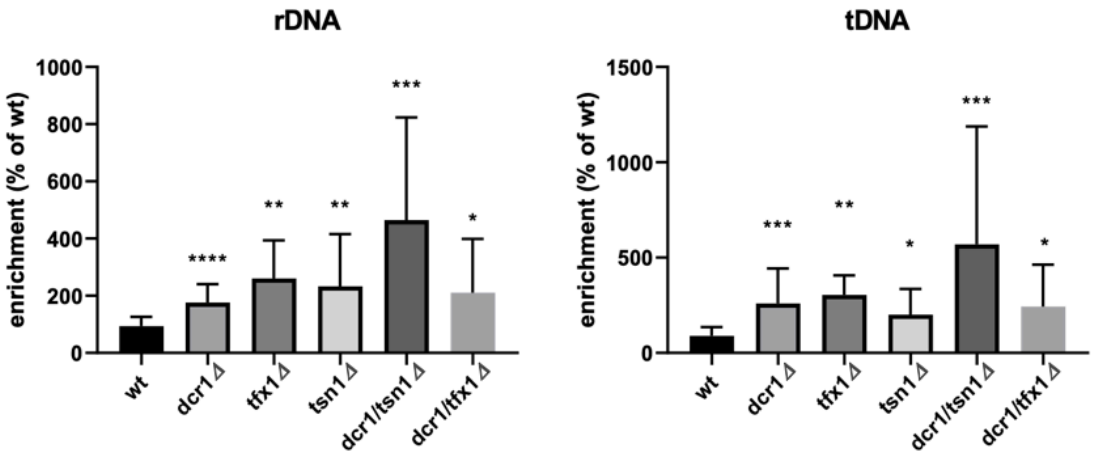

Figure 7.1 Analysis of the DNA:RNA levels by DNA:RNA immunoprecipitation (DRIP). The plot demonstrated that the *tsn1Δ dcr1Δ* double mutant and all mutants showed elevated level of DNA:RNA hybrids at two different genomic loci, the rDNA and tRNA genes. Error bars represent standard error of the mean; * $P < 0.05$, ** $P < 0.01$, *** $P < 0.001$.**** $P < 0.0001$ [$n \geq 5$ in all cases; T- test]. Data shown are one set of a minimum of three independent repeats (adapted from Dr Natalia Gomez-Escobar, unpublished data).

7.3 Tsn1, but not Tfx1, has functions in one of the RNase H pathways

Translin and TRAX are implicated in different biological functions that seem to require the regulation of RNA molecules rather than DNA. In the absence of Dcr1, the processing of RNA:DNA hybrids generated by RNA pol II, appears to be associated with a requirement for Tsn1, but not Tfx1. This is consistent with the nucleic acid binding and RNAse capabilities of Tsn1 (Jaendling and McFarlane, 2010), and this could account for the need for Translin to avoid chromosomal translocation. RNA:DNA hybrids, generated by transcription, can cause transcription replication conflicts, which can lead to chromosome instability, resulting in diseases such as cancer (Zimmer & Koshland et al., 2016). To deter the formation of stable RNA:DNA hybrids, there is two dominant suppressors of RNA:DNA hybrids which are RNase H1 and RNase H2. The RNase Hs are two highly conserved ribonucleases enzymes, and they can remove RNA:DNA hybrids by degrading the RNA moiety (García-Muse & Aguilera, 2019). Importantly, RNase Hs are crucial in preventing genome instability and occurrence of genome replication conflicts (Cerritelli & Crouch et al., 2009; Amon & Koshland et al., 2016; Lockhart et al., 2019). RNases H action is also essential for the for efficient repair of the DSBs. The deletion of both RNase H1 and H2 coding genes together results in defects in DNA damage recovery, which results in the prevention of DSB repair mediated through HR. Thus, this suggests the pathways of the RNase H are needed redundantly in repair of the DSB (Ohle et al., 2016). It also indicates removals of RNA:DNA hybrids is required for DSB repair. On other hand, recent study demonstrated that, the accumulation of RNA:DNA hybrids in the yeast cells lacking of RNase H1 and H2 that trigger replication fork collapse, but RNase H1 and H2 are not generally required for efficient DSB repair (Zhao et al., 2019).

Here, we show that Tsn1 but not Tfx1, may has functions in one of the RNase H pathways. Our finding indicates that Tsn1, but not Tfx1, does indeed have a role to play in the recovery from DNA damage for several genotoxic and DNA replicative stress agents. Loss of RNase H2, but not RNase H1, combined with loss of Tsn1 results in a stronger genome instability phenotype (Zimmer & Koshland et al., 2016). Indeed, this confirms a function of Tsn1 in DNA damage recovery. The study of Zimmer and

Koshland, show that the enzymes RNase H1 and H2 regulate the cell cycle and cell stress linked to R-loops. Their observations as they hypothesised that, the RNase H2 provides most of the RNase H activity in the cell and it was weakly associated with chromatin as tested by ChIP. The difficulties to ChIP RNase H2 as they suggested, it may be because associated with chromatin only at certain cell cycle phases. On the other hand, RNase H1, was able to associate with multiple R-loops along the chromatin, but it was not processing most of the RNase H activity (Lockhart et al., 2019).

There will be follow-up studies to test this, firstly by explore the levels of RNA:DNA hybrids throughout the fission yeast genome to determine regional/transcript specificity. This will include developing DRIP techniques to execute DRIP-seq for the whole fission yeast genome in wild-type and single/double mutant cells, including double mutants in *tsn1Δ /tfx1Δ* with the RNAse H gene mutants (*rnh1Δ /rnh201Δ*), to delineate whether Tsn1 and Tfx1 function in concert with known RNAse H activities. Also we can execute RNA pol II and RNA pol III chromatin immunoprecipitation (ChIP) to determine whether RNA pol II and RNA pol III occupancy levels fluctuate or correlate to changes seen in RNA:DNA hybrids; this will provide mechanistic insight into hybrid formation dynamics.

7.4 Tsn1, but not Tfx1 is required for non-telomeric DNA repair.

In many cancer cells, telomerase, the enzyme required for synthesizing telomeres, is activated and plays a role in telomere maintenance that is crucial for the extension of DNA at the chromosome ends in proliferating cells (Ohlo et al., 2016; Mizukoshi & Kaneko, 2019). Previously, our group showed that Tsn1/Tfx1, regulate telomere-associated transcripts in *S. pombe* (Gomes-Escobar et al., 2016). The regulation does not contribute to increases in RNA:DNA hybrids that are found in the sub-telomeric regions (Gomes-Escobar, personal commination). Telomere transcripts (TERRAs) are needed for DNA damage, so they might influence DNA repair in *tsn1Δ* cells as *tsn1Δ* cells have greatly elevated TERRA levels. Telomere deficient cells would not have TERRAs. We hypothesized that RNA:DNA hybrid-induced recombination, has an impact in non-

telomeric regions. In this study we used fission strains that do not have telomeres. These strains retained a need for Tsn1 in damage recovery.

So, loss of Tsn1 function results in non-telomeric RNA:DNA hybrids that may assist in DSB repair. In addition, RNase H activity is crucial in DSBs repair. However, the removal of both RNase H1 and RNase H2 coding genes contributed to the damage to DNA recovery, which results inhibition of HR-mediated DSB repair. The data presented in this study shows similar phenotype of sensitivities to the DNA-damaging reagents in the HAATI^{STE} background as we have shown in the BP90 background, and this indicate that Tsn1, but not Tfx1, does indeed have a role to play in the recovery from DNA damage for several genotoxic and DNA replicative stress agents in non-telomeric DNA repair. From the results in this study we have revealed a role for Tsn1, but not Tfx1, with appears to be functionally required in the absence of Rnh201, and that this is not related to the function of Tsn1 in regulating telomeric RNA transcripts in canonical telomeres.

7.5 Closing remarks

Since Translin and Trax were initially discovered over 20 years ago, several functions have been associated with them and it has been proposed that these are specific functions in distinct tissues based on nucleic-acid metabolic activities. To date, nearly all studies, which have identified Translin and Trax, indicate that the conserved proteins share an intimate functional relationship. Furthermore, because fission yeast demonstrates distinct roles for Translin and Trax, doubt is cast to their widely accepted intimate functional relationship. Firstly, in the absence of Dcr1, the DNA damage recovery response requires Tsn1, rather than Tfx1. There is evidence proposing another important function of Tsn1 in suppressing replication –associated recombination without Dcr1, which could explain its initial proposed function in producing translocation of chromosomes among human cancers. Secondly, Tsn1, but not Tfx1, functions in one of the RNase H pathways, the finding indicated that Tsn1 rather than Tfx1 is involved in DNA damage recovery for several DNA and genotoxic replicative agents of stress. We suggest that Tsn1 is involved

in the recovery of damaged DNA by destabilising RNA:DNA hybrids in the Rnh201 redundant pathway, and possibly considered as the Rnh1 pathway. Finally, Tsn1, but not Tfx1 has function in genome stability regulation in the absence of telomeres and they are required for non-telomeric DNA repair. In addition to the fact that Translin and Trax are oncogenic drug targets and are associated with different important biological functions, we now provide new insights into the complex nature of drug targeting and basic biological functions of these highly conserved proteins.

8. References

ABBAS, T., KEATON, M.A. and DUTTA, A., 2013. Genomic instability in cancer. *Cold Spring Harbor perspectives in biology,* **5**(3), pp. a012914.

AGRAWAL, N., DASARADHI, P., MOHMMED, A., MALHOTRA, P., BHATNAGAR, R.K. and MUKHERJEE, S.K., 2003. RNA interference: biology, mechanism, and applications. *Microbiol.Mol.Biol.Rev.,* **67**(4), pp. 657-685.

AGUILERA, A. and GARCÍA-MUSE, T., 2013. Causes of genome instability. *Annual Review of Genetics,* **47**, pp. 1-32.

AGUILERA, A. and GÓMEZ-GONZÁLEZ, B., 2017. DNA–RNA hybrids: the risks of DNA breakage during transcription. *Nature structural & molecular biology,* **24**(5), pp. 439.

AGUILERA, A. and GÓMEZ-GONZÁLEZ, B., 2008. Genome instability: a mechanistic view of its causes and consequences. *Nature Reviews Genetics,* **9**(3), pp. 204.

AHRINGER, J., 2003. Control of cell polarity and mitotic spindle positioning in animal cells. *Current opinion in cell biology,* **15**(1), pp. 73-81.

ALLSHIRE, R.C. and EKWALL, K., 2015. Epigenetic regulation of chromatin states in *Schizosaccharomyces pombe*. *Cold Spring Harbor perspectives in biology,* **7**(7), pp. a018770.

ALPER, B.J., LOWE, B.R. and PARTRIDGE, J.F., 2012. Centromeric heterochromatin assembly in fission yeast—balancing transcription, RNA interference and chromatin modification. *Chromosome research,* **20**(5), pp. 521-534.

AMON, J.D. and KOSHLAND, D., 2016. RNase H enables efficient repair of R-loop induced DNA damage. *Elife,* **5**, pp. e20533.

AOKI, K., ISHIDA, R. and KASAI, M., 1997. Isolation and characterization of a cDNA encoding a Translin-like protein, TRAX. *FEBS letters,* **401**(2-3), pp. 109-112.

AOKI, K., SUZUKI, K., ISHIDA, R. and KASAI, M., 1999. The DNA binding activity of Translin is mediated by a basic region in the ring-shaped structure conserved in evolution. *FEBS letters,* **443**(3), pp. 363-366.

ARMSTRONG, C.A., PEARSON, S.R., AMELINA, H., MOISEEVA, V. and TOMITA, K., 2014. Telomerase activation after recruitment in fission yeast. *Current Biology,* **24**(17), pp. 2006-2011.

ARNOULT, N. and KARLSEDER, J., 2015. Complex interactions between the DNA-damage response and mammalian telomeres. *Nature structural & molecular biology,* **22**(11), pp. 859.

ARONICA, L., KASPAREK, T., RUCHMAN, D., MARQUEZ, Y., CIPAK, L., CIPAKOVA, I., ANRATHER, D., MIKOLASKOVA, B., RADTKE, M. and SARKAR, S., 2015. The spliceosome-associated protein Nrl1 suppresses homologous recombination-dependent R-loop formation in fission yeast. *Nucleic acids research,* **44**(4), pp. 1703-1717.

ASADA, K., CANESTRARI, E. & Paroo, Z. 2016. A druggable target for rescuing microRNA defects. *Bioorganic &Medicinal Chemistry Letters.* 26 (20). pp. 4942-4946.

ASADA, K., CANESTRARI, E., FU, X., LI, Z., MAKOWSKI, E., WU, Y., MITO, J.K., KIRSCH, D.G., BARABAN, J. and PAROO, Z., 2014. Rescuing dicer defects via inhibition of an anti-dicing nuclease. *Cell reports,* **9**(4), pp. 1471-1481.

BARABAN, J.M., SHAH, A. and FU, X., 2018. Multiple pathways mediate microRNA degradation: focus on the translin/trax RNase complex. *Advances in Pharmacology.* Elsevier, pp. 1-20.

BARBER, L.J., YOUDS, J.L., WARD, J.D., MCILWRAITH, M.J., O'NEIL, N.J., PETALCORIN, M.I., MARTIN, J.S., COLLIS, S.J., CANTOR, S.B. and AUCLAIR, M., 2008. RTEL1 maintains genomic stability by suppressing homologous recombination. *Cell,* **135**(2), pp. 261-271.

BATTÉ, A., BROCAS, C., BORDELET, H., HOCHER, A., RUAULT, M., ADJIRI, A., TADDEI, A. and DUBRANA, K., 2017. Recombination at subtelomeres is regulated by physical distance, double-strand break resection and chromatin status. *The EMBO journal,* **36**(17), pp. 2609-2625.

BEGNIS, M., APTE, M.S., MASUDA, H., JAIN, D., WHEELER, D.L. and COOPER, J.P., 2018. RNAi drives nonreciprocal translocations at eroding chromosome ends to establish telomere-free linear chromosomes. *Genes & development,* **32**(7-8), pp. 537-554.

BELL, S.P. and DUTTA, A., 2002. DNA replication in eukaryotic cells. *Annual Review of Biochemistry,* **71**(1), pp. 333-374.

BERMEJO, R., LAI, M.S. and FOIANI, M., 2012. Preventing replication stress to maintain genome stability: resolving conflicts between replication and transcription. *Molecular cell,* **45**(6), pp. 710-718.

BERTI, M. and VINDIGNI, A., 2016. Replication stress: getting back on track. *Nature structural & molecular biology,* **23**(2), pp. 103.

BETTIN, N., OSS PEGORAR, C. and CUSANELLI, E., 2019. The emerging roles of TERRA in telomere maintenance and genome stability. *Cells,* **8**(3), pp. 246.

BHATTACHARJEE, S., ROCHE, B. and MARTIENSSEN, R.A., 2019. RNA-induced initiation of transcriptional silencing (RITS) complex structure and function. *RNA biology,* , pp. 1-14.

BIEHS, R., STEINLAGE, M., BARTON, O., JUHÁSZ, S., KÜNZEL, J., SPIES, J., SHIBATA, A., JEGGO, P.A. and LÖBRICH, M., 2017. DNA double-strand break resection occurs during non-homologous end joining in G1 but is distinct from resection during homologous recombination. *Molecular cell,* **65**(4), pp. 671-684. e5.

BOBOILA, C., ALT, F.W. and SCHWER, B., 2012. Classical and alternative end-joining pathways for repair of lymphocyte-specific and general DNA double-strand breaks. *Advances in immunology.* Elsevier, pp. 1-49.

BRAMBATI, A., COLOSIO, A., ZARDONI, L., GALANTI, L. and LIBERI, G., 2015. Replication and transcription on a collision course: eukaryotic regulation mechanisms and implications for DNA stability. *Frontiers in genetics,* **6**, pp. 166.

BRIEÑO-ENRÍQUEZ, M.A., MOAK, S.L., ABUD-FLORES, A. and COHEN, P.E., 2018. Characterization of telomeric repeat-containing RNA (TERRA) localization and protein interactions in primordial germ cells of the mouse. *Biology of reproduction,* **100**(4), pp. 950-962.

BRUGMANS, L., KANAAR, R. and ESSERS, J., 2007. Analysis of DNA double-strand break repair pathways in mice. *Mutation Research/Fundamental and Molecular Mechanisms of Mutagenesis,* **614**(1-2), pp. 95-108.

BÜHLER, M. and GASSER, S.M., 2009. Silent chromatin at the middle and ends: lessons from yeasts. *The EMBO journal,* **28**(15), pp. 2149-2161.

BURGERS, P.M. and KUNKEL, T.A., 2017. Eukaryotic DNA replication fork. *Annual Review of Biochemistry,* **86**, pp. 417-438.

BURMAN, B., ZHANG, Z.Z., PEGORARO, G., LIEB, J.D. and MISTELI, T., 2015. Histone modifications predispose genome regions to breakage and translocation. *Genes & development,* **29**(13), pp. 1393-1402.

CALASANZ, M.J. and CIGUDOSA, J.C., 2008. Molecular cytogenetics in translational oncology: when chromosomes meet genomics. *Clinical and Translational Oncology,* **10**(1), pp. 20-29.

CALZADA, A., HODGSON, B., KANEMAKI, M., BUENO, A. and LABIB, K., 2005. Molecular anatomy and regulation of a stable replisome at a paused eukaryotic DNA replication fork. *Genes & development,* **19**(16), pp. 1905-1919.

CARLBERG, C. and MOLNÁR, F., 2018. The Structure of Chromatin. *Human Epigenomics.* Springer, pp. 41-56.

CASTEL, S.E. and MARTIENSSEN, R.A., 2013. RNA interference in the nucleus: roles for small RNAs in transcription, epigenetics and beyond. *Nature Reviews Genetics,* **14**(2), pp. 100.

CASTEL, S.E., REN, J., BHATTACHARJEE, S., CHANG, A., SÁNCHEZ, M., VALBUENA, A., ANTEQUERA, F. and MARTIENSSEN, R.A., 2014. Dicer promotes transcription termination at sites of replication stress to maintain genome stability. *Cell,* **159**(3), pp. 572-583.

CERRITELLI, S.M. and CROUCH, R.J., 2009. Ribonuclease H: the enzymes in eukaryotes. *The FEBS journal,* **276**(6), pp. 1494-1505.

CHAKAROV, S., PETKOVA, R., RUSSEV, G.C. and ZHELEV, N., 2014. DNA damage and mutation. Types of DNA damage. *BioDiscovery,* **11**, pp. e8957.

CHALK, J.G., BARR, F.G. and MITCHELL, C.D., 1997. Translin recognition site sequences flank chromosome translocation breakpoints in alveolar rhabdomyosarcoma cell lines. *Oncogene,* **15**(10), pp. 1199.

CHAN, F.L. and WONG, L.H., 2012. Transcription in the maintenance of centromere chromatin identity. *Nucleic acids research,* **40**(22), pp. 11178-11188.

CHANG, E. and STIRLING, P., 2017. Replication fork protection factors controlling R-loop bypass and suppression. *Genes,* **8**(1), pp. 33.

CHANG, H.H., PANNUNZIO, N.R., ADACHI, N. and LIEBER, M.R., 2017. Non-homologous DNA end joining and alternative pathways to double-strand break repair. *Nature reviews Molecular cell biology,* **18**(8), pp. 495.

CHANG, Y., WANG, P., LI, W.H., CHEN, L., CHANG, C., SUNG, P., YANG, M., CHENG, L., LAI, Y. and CHENG, Y., 2013. Balanced and unbalanced reciprocal translocation: an overview of a 30-year experience in a single tertiary medical center in Taiwan. *Journal of the Chinese Medical Association,* **76**(3), pp. 153-157.

CHATTERJEE, S., 2017. Telomeres in health and disease. *Journal of oral and maxillofacial pathology: JOMFP,* **21**(1), pp. 87.

CHEN, C., LIM, H.H., SHI, J., TAMURA, S., MAESHIMA, K., SURANA, U. and GAN, L., 2016. Budding yeast chromatin is dispersed in a crowded nucleoplasm in vivo. *Molecular biology of the cell,* **27**(21), pp. 3357-3368.

CHEN, H., LISBY, M. and SYMINGTON, L.S., 2013. RPA coordinates DNA end resection and prevents formation of DNA hairpins. *Molecular cell,* **50**(4), pp. 589-600.

CHEN, R. and WOLD, M.S., 2014. Replication protein A: single-stranded DNA's first responder: dynamic DNA-interactions allow replication protein A to direct single-strand DNA intermediates into different pathways for synthesis or repair. *Bioessays,* **36**(12), pp. 1156-1161.

CHENNATHUKUZHI, V.M., KURIHARA, Y., BRAY, J.D. and HECHT, N.B., 2001. Trax (translin-associated factor X), a primarily cytoplasmic protein, inhibits the binding of TB-RBP (translin) to RNA. *Journal of Biological Chemistry,* **276**(16), pp. 13256-13263.

CHERN, Y., CHIEN, T., FU, X., SHAH, A.P., ABEL, T. and BARABAN, J.M., 2019. Trax: a versatile signaling protein plays key roles in synaptic plasticity and DNA repair. *Neurobiology of learning and memory,* **159**, pp. 46-51.

CHIARUTTINI, C., Vicario, A., Li, Z., Baj, G., Braiuca, P., Wu, Y., Lee, F.S., Gardossi, L., Baraban, J.M. & Tongiorgi, E. 2009. Dendritic trafficking of BDNF mRNA is mediated by translin and blocked by the G196A (Val66Met) mutation. *Proceedings of the National Academy of Sciences of the United States of America.* 106 (38). pp. 16481-16486.

CHO, Y.S., CHENNATHUKUZHI, V.M., HANDEL, M.A., EPPIG, J. and HECHT, N.B., 2004. The relative levels of translin-associated factor X (TRAX) and testis brain RNA-binding protein determine their nucleocytoplasmic distribution in male germ cells. *Journal of Biological Chemistry,* **279**(30), pp. 31514-31523.

CHOI, J.D. and LEE, J., 2013. Interplay between epigenetics and genetics in cancer. *Genomics & informatics,* **11**(4), pp. 164.

COOPER, J.P., NIMMO, E.R., ALLSHIRE, R.C. and CECH, T.R., 1997. Regulation of telomere length and function by a Myb-domain protein in fission yeast. *Nature,* **385**(6618), pp. 744.

CORTEZ, D., 2019. Replication-Coupled DNA Repair. *Molecular cell,* **74**(5), pp. 866-876.

COX, M.M., 2001. Recombinational DNA repair of damaged replication forks in Escherichia coli: questions. *Annual Review of Genetics,* **35**(1), pp. 53-82.

CREAMER, K.M. and PARTRIDGE, J.F., 2011. RITS—connecting transcription, RNA interference, and heterochromatin assembly in fission yeast. *Wiley Interdisciplinary Reviews: RNA,* **2**(5), pp. 632-646.

CUSANELLI, E. and CHARTRAND, P., 2015. Telomeric repeat-containing RNA TERRA: a noncoding RNA connecting telomere biology to genome integrity. *Frontiers in genetics,* **6**, pp. 143.

DAVIS, A.J., CHEN, B.P. and CHEN, D.J., 2014. DNA-PK: a dynamic enzyme in a versatile DSB repair pathway. *DNA repair,* **17**, pp. 21-29.

DAVIS, A.J. and CHEN, D.J., 2013. DNA double strand break repair via non-homologous end-joining. *Translational cancer research,* **2**(3), pp. 130.

DE LANGE, T., 2018. How telomeres solve the chromosome end-protection problem. *The FASEB Journal,* **32**(1_supplement), pp. 472.1.

DEEGAN, T.D. and DIFFLEY, J.F., 2016. MCM: one ring to rule them all. *Current opinion in structural biology,* **37**, pp. 145-151.

DENG, S.K., CHEN, H. and SYMINGTON, L.S., 2015. Replication protein A prevents promiscuous annealing between short sequence homologies: Implications for genome integrity. *Bioessays,* **37**(3), pp. 305-313.

DILLEY, R.L., VERMA, P., CHO, N.W., WINTERS, H.D., WONDISFORD, A.R. and GREENBERG, R.A., 2016. Break-induced telomere synthesis underlies alternative telomere maintenance. *Nature,* **539**(7627), pp. 54.

EBERHARD, S., VALUCHOVA, S., RAVAT, J., FULNEČEK, J., JOLIVET, P., BUJALDON, S., LEMAIRE, S.D., WOLLMAN, F., TEIXEIRA, M.T. and RIHA, K., 2019. Molecular characterization of Chlamydomonas reinhardtii telomeres and telomerase mutants. *Life science alliance,* **2**(3), pp. e201900315.

EKWALL, K., CRANSTON, G. and ALLSHIRE, R.C., 1999. Fission yeast mutants that alleviate transcriptional silencing in centromeric flanking repeats and disrupt chromosome segregation. *Genetics,* **153**(3), pp. 1153-1169.

ELIAHOO, E., LITOVCO, P., YOSEF, R.B., BENDALAK, K., ZIV, T. and MANOR, H., 2014. Identification of proteins that form specific complexes with the highly conserved protein Translin in Schizosaccharomyces pombe. *Biochimica et Biophysica Acta (BBA)-Proteins and Proteomics,* **1844**(4), pp. 767-777.

ERDEMIR, T., BILICAN, B., ONCEL, D., GODING, C.R. and YAVUZER, U., 2002. DNA damage-dependent interaction of the nuclear matrix protein C1D with translin-associated factor X (TRAX). *Journal of cell science,* **115**(1), pp. 207-216.

ERRICO, A. and COSTANZO, V., 2010. Differences in the DNA replication of unicellular eukaryotes and metazoans: known unknowns. *EMBO reports,* **11**(4), pp. 270-278.

ESPEJEL, S., FRANCO, S., RODRÍGUEZ-PERALES, S., BOUFFLER, S.D., CIGUDOSA, J.C. and BLASCO, M.A., 2002. Mammalian Ku86 mediates chromosomal fusions and apoptosis caused by critically short telomeres. *The EMBO journal,* **21**(9), pp. 2207-2219.

ESSANI, K., GLIEDER, A. and GEIER, M., 2015. Combinatorial pathway assembly in yeast. *AIMS Bioengineering,* **2**, pp. 423-436.

FELIPE-ABRIO, I., LAFUENTE-BARQUERO, J., GARCÍA-RUBIO, M.L. and AGUILERA, A., 2015. RNA polymerase II contributes to preventing transcription-mediated replication fork stalls. *The EMBO journal,* **34**(2), pp. 236-250.

FERETZAKI, M. and LINGNER, J., 2017. A practical qPCR approach to detect TERRA, the elusive telomeric repeat-containing RNA. *Methods,* **114**, pp. 39-45.

FINKENSTADT, P.M., KANG, W., JEON, M., TAIRA, E., TANG, W. and BARABAN, J.M., 2000. Somatodendritic localization of Translin, a component of the Translin/Trax RNA binding complex. *Journal of neurochemistry,* **75**(4), pp. 1754-1762.

FORSBURG, S.L., 2007. The yeasts Saccharomyces cerevisiae and Schizosaccharomyces pombe: models for cell biology research. *Gravitational and Space Research,* **18**(2),.

FRAGKOS, M. & NAIM, V. 2017. Rescue from replication stress during mitosis. Cell Cycle. 16 (7). pp. 613-633.

FU, X., SHAH, A. and BARABAN, J.M., 2016. Rapid reversal of translational silencing: Emerging role of microRNA degradation pathways in neuronal plasticity. *Neurobiology of learning and memory,* **133**, pp. 225-232.

FUKUDA, Y., ISHIDA, R., AOKI, K., NAKAHARA, K., TAKASHI, T., MOCHIDA, K., SUZUKI, O., MATSUDA, J. and KASAI, M., 2008. Contribution of Translin to hematopoietic regeneration after sublethal ionizing irradiation. *Biological and Pharmaceutical Bulletin,* **31**(2), pp. 207-211.

GADALETA, M. and NOGUCHI, E., 2017. Regulation of DNA replication through natural impediments in the eukaryotic genome. *Genes,* **8**(3), pp. 98.

GAILLARD, H. and AGUILERA, A., 2016. Transcription as a threat to genome integrity. *Annual Review of Biochemistry,* **85**, pp. 291-317.

GAJECKA, M., GLOTZBACH, C.D. and SHAFFER, L.G., 2006. Characterization of a complex rearrangement with interstitial deletions and inversion on human chromosome 1. *Chromosome Research,* **14**(3), pp. 277-282.

GAJECKA, M., PAVLICEK, A., GLOTZBACH, C.D., BALLIF, B.C., JARMUZ, M., JURKA, J. and SHAFFER, L.G., 2006. Identification of sequence motifs at the breakpoint junctions in three t (1; 9)(p36. 3; q34) and delineation of mechanisms involved in generating balanced translocations. *Human genetics,* **120**(4), pp. 519-526.

GARCÍA-RUBIO, M., BARROSO, S.I. and AGUILERA, A., 2018. Detection of DNA-RNA hybrids in vivo. *Genome Instability.* Springer, pp. 347-361.

GARCÍA-MUSE, T., & Aguilera, A. (2019). R loops: from physiological to pathological roles. *Cell*.

GERACE, E.L., HALIC, M. and MOAZED, D., 2010. The methyltransferase activity of Clr4Suv39h triggers RNAi independently of histone H3K9 methylation. *Molecular cell,* **39**(3), pp. 360-372.

GHOSH, R., DAS, D. and FRANCO, S., 2018. The Role for the DSB Response Pathway in Regulating Chromosome Translocations. *Chromosome Translocation.* Springer, pp. 65-87.

GOMES, L., MENCK, C. and LEANDRO, G., 2017. Autophagy roles in the modulation of DNA repair pathways. *International journal of molecular sciences,* **18**(11), pp. 2351.

GOMEZ-ESCOBAR, N., ALMOBADEL, N., ALZAHRANI, O., FEICHTINGER, J., PLANELLS-PALOP, V., ALSHEHRI, Z., THALLINGER, G.G., WAKEMAN, J.A. and MCFARLANE, R.J., 2016. Translin and Trax differentially regulate telomere-associated transcript homeostasis. *Oncotarget,* **7**(23), pp. 33809.

GÓMEZ-GONZÁLEZ, B. and AGUILERA, A., 2019. Transcription-mediated replication hindrance: a major driver of genome instability. *Genes & development,* .

GOTO, D.B. and NAKAYAMA, J., 2012. RNA and epigenetic silencing: insight from fission yeast. *Development, growth & differentiation,* **54**(1), pp. 129-141.

GROS, J., KUMAR, C., LYNCH, G., YADAV, T., WHITEHOUSE, I. and REMUS, D., 2015. Post-licensing specification of eukaryotic replication origins by facilitated Mcm2-7 sliding along DNA. *Molecular cell,* **60**(5), pp. 797-807.

GULYAEVA, L.F. and KUSHLINSKIY, N.E., 2016. Regulatory mechanisms of microRNA expression. *Journal of translational medicine,* **14**(1), pp. 143.

GUPTA, A., PILLAI, V.S. and CHITTELA, R.K., 2019. Translin: A multifunctional protein involved in nucleic acid metabolism. *Journal of Biosciences,* **44**(6), pp. 139.

GUPTA, G.D. and KUMAR, V., 2012. Identification of nucleic acid binding sites on translin-associated factor X (TRAX) protein. *PloS one,* **7**(3), pp. e33035.

GURTNER, A., Falcone, E., Garibaldi, F. & Piaggio, G. 2016. Dysregulation of microRNA biogenesis in cancer: the impact of mutant p53 on Drosha complex activity. *Journal of Experimental & Clinical Cancer Research.* 35 (1). pp. 45.

HAMMOND, C.M., STRØMME, C.B., HUANG, H., PATEL, D.J. and GROTH, A., 2017. Histone chaperone networks shaping chromatin function. *Nature reviews Molecular cell biology,* **18**(3), pp. 141.

HAN, J., Gu, W. & Hecht, N.B. 1995. Testis-brain RNA-binding protein, a testicular translational regulatory RNA-binding protein, is present in the brain and binds to the 3′ untranslated regions of transported brain mRNAs. *Biology of Reproduction.* 53 (3). pp. 707- 717.

HAREWOOD, L. and FRASER, P., 2014. The impact of chromosomal rearrangements on regulation of gene expression. *Human molecular genetics,* **23**(R1), pp. R76-R82.

HARRIS, C., 2019. Investigating the Effects of Cancer Mutations on the MRN Complex Using Yeast.

HARSHMAN, S.W., YOUNG, N.L., PARTHUN, M.R. and FREITAS, M.A., 2013. H1 histones: current perspectives and challenges. *Nucleic acids research,* **41**(21), pp. 9593-9609.

HASEGAWA, T., HENGYI, X., HAMAJIMA, F. and ISOBE, K., 2000. Interaction between DNA-damage protein GADD34 and a new member of the Hsp40 family of heat shock proteins that is induced by a DNA-damaging reagent. *Biochemical Journal,* **352**(3), pp. 795-800.

HASEGAWA, T. and ISOBE, K., 1999. Evidence for the interaction between Translin and GADD34 in mammalian cells. *Biochimica et Biophysica Acta (BBA)-General Subjects,* **1428**(2-3), pp. 161-168.

HAYLES, J. and NURSE, P., 2018. Introduction to fission yeast as a model system. *Cold Spring Harbor Protocols,* **2018**(5), pp. pdb. top079749.

HER, J. and BUNTING, S.F., 2018. How cells ensure correct repair of DNA double-strand breaks. *Journal of Biological Chemistry,* **293**(27), pp. 10502-10511.

HIGUCHI, K., KATAYAMA, T., IWAI, S., HIDAKA, M., HORIUCHI, T. and MAKI, H., 2003. Fate of DNA replication fork encountering a single DNA lesion during oriC plasmid DNA replication in vitro. *Genes to Cells,* **8**(5), pp. 437-449.

HOLOCH, D. and MOAZED, D., 2015. RNA-mediated epigenetic regulation of gene expression. *Nature Reviews Genetics,* **16**(2), pp. 71-84.

HSU, M. and LUE, N.F., 2017. Analysis of Yeast Telomerase by Primer Extension Assays. *Telomeres and Telomerase.* Springer, pp. 83-93.

HUERTAS, P. and JACKSON, S.P., 2009. Human CtIP mediates cell cycle control of DNA end resection and double strand break repair. Journal of Biological Chemistry, 284(14), pp.9558-9565.

HUSTEDT, N. and DUROCHER, D., 2017. The control of DNA repair by the cell cycle. *Nature cell biology,* **19**(1), pp. 1.

ISHIDA, R., OKADO, H., SATO, H., SHIONOIRI, C., AOKI, K. & KASAI, M. 2002. A role for the octameric ring protein, Translin, in mitotic cell division. *FEBS letters.* 525 (1-3). pp. 105-110.

IKEUCHI, Y., IMANISHI, A., SUDO, K., FUKUNAGA, T., YOKOI, A., MATSUBARA, L., GOTO, C., FUKUOKA, T., KURONUMA, K. and KONO, R., 2018. Translin modulates mesenchymal cell proliferation and differentiation in mice. *Biochemical and biophysical research communications,* **504**(1), pp. 115-122.

JACKSON, R.A., WU, J.S. and CHEN, E.S., 2016. C1D family proteins in coordinating RNA processing, chromosome condensation and DNA damage response. *Cell division,* **11**(1), pp. 2.

JACOB, E., PUCSHANSKY, L., ZERUYA, E., BARAN, N. and MANOR, H., 2004. The human protein translin specifically binds single-stranded microsatellite repeats, d (GT) n, and G-strand telomeric repeats, d (TTAGGG) n: a study of the binding parameters. *Journal of Molecular Biology,* **344**(4), pp. 939-950.

JAENDLING, A. and MCFARLANE, R.J., 2010. Biological roles of translin and translin-associated factor-X: RNA metabolism comes to the fore. *Biochemical Journal,* **429**(2), pp. 225-234.

JAENDLING, A., RAMAYAH, S., PRYCE, D.W. and MCFARLANE, R.J., 2008. Functional characterisation of the Schizosaccharomyces pombe homologue of the leukaemia-associated translocation breakpoint binding protein translin and its binding partner, TRAX. *Biochimica et Biophysica Acta (BBA)-Molecular Cell Research,* **1783**(2), pp. 203-213.

JAIN, D., HEBDEN, A.K., NAKAMURA, T.M., MILLER, K.M. and COOPER, J.P., 2010. HAATI survivors replace canonical telomeres with blocks of generic heterochromatin. *Nature,* **467**(7312), pp. 223.

JAZAYERI, A., & JACKSON, S. P. (2002). Screening the yeast genome for new DNA-repair genes. *Genome biology*, *3*(4), reviews1009-1.

JETTE, N. and LEES-MILLER, S.P., 2015. The DNA-dependent protein kinase: A multifunctional protein kinase with roles in DNA double strand break repair and mitosis. *Progress in biophysics and molecular biology,* **117**(2-3), pp. 194-205.

JOGA, M.R., ZOTTI, M.J., SMAGGHE, G. and CHRISTIAENS, O., 2016. RNAi efficiency, systemic properties, and novel delivery methods for pest insect control: what we know so far. *Frontiers in physiology,* **7**, pp. 553.

JONAS, S. and IZAURRALDE, E., 2015. Towards a molecular understanding of microRNA-mediated gene silencing. *Nature Reviews Genetics,* **16**(7), pp. 421.

JONES, R.M. and PETERMANN, E., 2012. Replication fork dynamics and the DNA damage response. *Biochemical Journal,* **443**(1), pp. 13-26.

KALANTARI, R., Chiang, C.M. & Corey, D.R. 2016. Regulation of mammalian transcription and splicing by Nuclear RNAi. *Nucleic acids research.* 44 (2). pp. 524-537.

KANG, S., KANG, M., RYU, E. and MYUNG, K., 2018. Eukaryotic DNA replication: Orchestrated action of multi-subunit protein complexes. *Mutation Research/Fundamental and Molecular Mechanisms of Mutagenesis,* **809**, pp. 58-69.

KANOE, H., NAKAYAMA, T., HOSAKA, T., MURAKAMI, H., YAMAMOTO, H., NAKASHIMA, Y., TSUBOYAMA, T., NAKAMURA, T., RON, D. and SASAKI, M.S., 1999. Characteristics of genomic breakpoints in TLS-CHOP translocations in liposarcomas suggest the involvement of Translin and topoisomerase II in the process of translocation. *Oncogene,* **18**(3), pp. 721.

KANOH, J., SADAIE, M., URANO, T. and ISHIKAWA, F., 2005. Telomere binding protein Taz1 establishes Swi6 heterochromatin independently of RNAi at telomeres. *Current biology,* **15**(20), pp. 1808-1819.

KASAI, M., MATSUZAKI, T., KATAYANAGI, K., OMORI, A., MAZIARZ, R.T., STROMINGER, J.L., AOKI, K. and SUZUKI, K., 1997. The translin ring specifically recognizes DNA ends at recombination hot spots in the human genome. *Journal of Biological Chemistry,* **272**(17), pp. 11402-11407.

KASPAREK, T.R. and HUMPHREY, T.C., 2011. DNA double-strand break repair pathways, chromosomal rearrangements and cancer, *Seminars in cell & developmental biology* 2011, Elsevier, pp. 886-897.

KEEFE, D.L., 2019. Telomeres and genomic instability during early development. *European journal of medical genetics,* .

KIM, H.S., HROMAS, R. and LEE, S., 2013. Emerging features of DNA double-strand break repair in humans. *New Research Directions in DNA Repair.* IntechOpen, .

KOREN, A., SOIFER, I. and BARKAI, N., 2010. MRC1-dependent scaling of the budding yeast DNA replication timing program. *Genome research,* **20**(6), pp. 781-790.

KOYAMA, M., NAGAKURA, W., TANAKA, H., KUJIRAI, T., CHIKASHIGE, Y., HARAGUCHI, T., HIRAOKA, Y. and KURUMIZAKA, H., 2017. In vitro reconstitution and biochemical analyses of the Schizosaccharomyces pombe nucleosome. *Biochemical and biophysical research communications,* **482**(4), pp. 896-901.

KRAMARA, J., OSIA, B. and MALKOVA, A., 2018. Break-induced replication: the where, the why, and the how. *Trends in Genetics,* **34**(7), pp. 518-531.

KROGH, B.O. and SYMINGTON, L.S., 2004. Recombination proteins in yeast. *Annu.Rev.Genet.,* **38**, pp. 233-271.

KUCIŃSKI, J., KMERA, A., ROWLEY, M.J., KHURANA, P., NOWOTNY, M. and WIERZBICKI, A.T., 2019. Functional characterization of RNase H1 proteins in Arabidopsis thaliana. *bioRxiv,* , pp. 662080.

KUROSE, A., TANAKA, T., HUANG, X., TRAGANOS, F., DAI, W. and DARZYNKIEWICZ, Z., 2006. Effects of hydroxyurea and aphidicolin on phosphorylation of ataxia telangiectasia mutated on Ser 1981 and histone H2AX on Ser 139 in relation to cell cycle phase and induction of apoptosis. *Cytometry Part A,* **69**(4), pp. 212-221.

KUSEVIC, D., KUDITHIPUDI, S., IGLESIAS, N., MOAZED, D. and JELTSCH, A., 2017. Clr4 specificity and catalytic activity beyond H3K9 methylation. *Biochimie,* **135**, pp. 83-88.

LABIB, K., 2010. How do Cdc7 and cyclin-dependent kinases trigger the initiation of chromosome replication in eukaryotic cells? *Genes & development,* **24**(12), pp. 1208-1219.

LAI, D., VISSER-GRIEVE, S. and YANG, X., 2012. Tumour suppressor genes in chemotherapeutic drug response. *Bioscience reports,* **32**(4), pp. 361-374.

LANGSTON, L.D., INDIANI, C. and O'DONNELL, M., 2009. Whither the replisome: emerging perspectives on the dynamic nature of the DNA replication machinery. *Cell Cycle,* **8**(17), pp. 2686-2691.

LANS, H., MARTEIJN, J.A. and VERMEULEN, W., 2012. ATP-dependent chromatin remodeling in the DNA-damage response. *Epigenetics & chromatin,* **5**(1), pp. 4.

LAUFMAN, O., YOSEF, R.B., ADIR, N. and MANOR, H., 2005. Cloning and characterization of the Schizosaccharomyces pombe homologs of the human protein Translin and the Translin-associated protein TRAX. *Nucleic acids research,* **33**(13), pp. 4128-4139.

LEE, S.Y., ROZENZHAK, S. and RUSSELL, P., 2013. γH2A-binding protein Brc1 affects centromere function in fission yeast. *Molecular and cellular biology,* **33**(7), pp. 1410-1416.

LEMAN, A. and NOGUCHI, E., 2013. The replication fork: understanding the eukaryotic replication machinery and the challenges to genome duplication. *Genes,* **4**(1), pp. 1-32.

LEÓN-ORTIZ, A.M., PANIER, S., SAREK, G., VANNIER, J., PATEL, H., CAMPBELL, P.J. and BOULTON, S.J., 2018. A distinct class of genome rearrangements driven by heterologous recombination. *Molecular cell,* **69**(2), pp. 292-305. e6.

LI, H. and O'DONNELL, M.E., 2019. DNA replication from two different worlds. *Science,* **363**(6429), pp. 814-815.

LI, J. and XU, X., 2016. DNA double-strand break repair: a tale of pathway choices. *Acta biochimica et biophysica Sinica,* **48**(7), pp. 641-646.

LI, L., GU, W., LIANG, C., LIU, Q., MELLO, C.C. and LIU, Y., 2012. The translin–TRAX complex (C3PO) is a ribonuclease in tRNA processing. *Nature structural & molecular biology,* **19**(8), pp. 824.

LI, Q. and ZHANG, Z., 2012. Linking DNA replication to heterochromatin silencing and epigenetic inheritance. *Acta Biochim Biophys Sin,* **44**(1), pp. 3-13.

LI, W., SELVAM, K., RAHMAN, S.A. and LI, S., 2016. Sen1, the yeast homolog of human senataxin, plays a more direct role than Rad26 in transcription coupled DNA repair. *Nucleic acids research,* **44**(14), pp. 6794-6802.

LI, X. and HEYER, W., 2008. Homologous recombination in DNA repair and DNA damage tolerance. *Cell research,* **18**(1), pp. 99.

LI, Z., WU, Y. and BARABAN, J.M., 2008. The Translin/Trax RNA binding complex: clues to function in the nervous system. *Biochimica et Biophysica Acta (BBA)-Gene Regulatory Mechanisms,* **1779**(8), pp. 479-485.

LIEBER, M.R., 2016. Mechanisms of human lymphoid chromosomal translocations. *Nature Reviews Cancer,* **16**(6), pp. 387.

LIEBER, M.R., 2010. The mechanism of double-strand DNA break repair by the nonhomologous DNA end-joining pathway. *Annual Review of Biochemistry,* **79**, pp. 181-211.

LIN, Y. and PASERO, P., 2012. Interference between DNA replication and transcription as a cause of genomic instability. *Current Genomics,* **13**(1), pp. 65-73.

LIU, Y., YE, X., JIANG, F., LIANG, C., CHEN, D., PENG, J., KINCH, L.N., GRISHIN, N.V. and LIU, Q., 2009. C3PO, an endoribonuclease that promotes RNAi by facilitating RISC activation. *Science,* **325**(5941), pp. 750-753.

LIU, Y., FANG, Y., LIU, Y., WANG, Z., LYU, B., HU, Y. and ZHOU, X., 2018. Opposite effects of Drosophila C3PO on gene silencing mediated by esi-2.1 and miRNA-bantam. *Acta biochimica et biophysica Sinica,* **51**(2), pp. 131-138.

LLUIS, M., HOE, W., SCHLEIT, J. and ROBERTUS, J., 2010. Analysis of nucleic acid binding by a recombinant translin–trax complex. *Biochemical and biophysical research communications,* **396**(3), pp. 709-713.

LOCKHART, A., PIRES, V.B., BENTO, F., KELLNER, V., LUKE-GLASER, S., YAKOUB, G., ULRICH, H.D. and LUKE, B., 2019. RNase H1 and H2 Are Differentially Regulated to Process RNA-DNA Hybrids. *Cell reports,* **29**(9), pp. 2890-2900. e5.

LOPES, M., COTTA-RAMUSINO, C., PELLICIOLI, A., LIBERI, G., PLEVANI, P., MUZI-FALCONI, M., NEWLON, C.S. and FOIANI, M., 2001. The DNA replication checkpoint response stabilizes stalled replication forks. *Nature,* **412**(6846), pp. 557.

LORD, C.J. and ASHWORTH, A., 2016. BRCAness revisited. *Nature Reviews Cancer,* **16**(2), pp. 110.

LORD, C.J. and ASHWORTH, A., 2012. The DNA damage response and cancer therapy. *Nature,* **481**(7381), pp. 287.

LORENZI, L.E., BAH, A., WISCHNEWSKI, H., SHCHEPACHEV, V., SONESON, C., SANTAGOSTINO, M. and AZZALIN, C.M., 2015. Fission yeast Cactin restricts telomere transcription and elongation by controlling Rap1 levels. *The EMBO journal,* **34**(1), pp. 115-129.

LUGER, K., DECHASSA, M.L. and TREMETHICK, D.J., 2012. New insights into nucleosome and chromatin structure: an ordered state or a disordered affair? *Nature reviews Molecular cell biology,* **13**(7), pp. 436.

LUJAN, S.A., WILLIAMS, J.S. and KUNKEL, T.A., 2016. DNA polymerases divide the labor of genome replication. *Trends in cell biology,* **26**(9), pp. 640-654.

LUSETTI, S.L. and COX, M.M., 2002. The bacterial RecA protein and the recombinational DNA repair of stalled replication forks. *Annual Review of Biochemistry,* **71**(1), pp. 71-100.

MACRAE, I.J., LI, F., ZHOU, K., CANDE, W.Z. and DOUDNA, J.A., 2006. Structure of Dicer and mechanistic implications for RNAi, *Cold Spring Harbor symposia on quantitative biology* 2006, Cold Spring Harbor Laboratory Press, pp. 73-80.

MAESHIMA, K., IMAI, R., TAMURA, S. and NOZAKI, T., 2014. Chromatin as dynamic 10-nm fibers. *Chromosoma,* **123**(3), pp. 225-237.

MAESTRONI, L., MATMATI, S. and COULON, S., 2017. Solving the telomere replication problem. *Genes,* **8**(2), pp. 55.

MALKOVA, A. and IRA, G., 2013. Break-induced replication: functions and molecular mechanism. *Current opinion in genetics & development,* **23**(3), pp. 271-279.

MARTIENSSEN, R. and MOAZED, D., 2015. RNAi and heterochromatin assembly. *Cold Spring Harbor perspectives in biology,* **7**(8), pp. a019323.

MCEACHERN, M.J. and HABER, J.E., 2006. Break-induced replication and recombinational telomere elongation in yeast. *Annu.Rev.Biochem.,* **75**, pp. 111-135.

MCFARLANE, R.J., AL-ZEER, K. and DALGAARD, J.Z., 2011. Eukaryote DNA replication and recombination: an intimate association. *DNA replication: current advances.Intech, Croatia,* , pp. 347-388.

MCFARLANE, R.J. and HUMPHREY, T.C., 2010. A role for recombination in centromere function. *Trends in genetics,* **26**(5), pp. 209-213.

MCFARLANE, R.J. and WHITEHALL, S.K., 2009. tRNA genes in eukaryotic genome organization and reorganization. *Cell Cycle,* **8**(19), pp. 3102-3106.

MCKENNA, M.J., ROBINSON, E., TAYLOR, L., TOMPKINS, C., CORNFORTH, M.N., SIMON, S.L. and BAILEY, S.M., 2019. Chromosome Translocations, Inversions and Telomere Length for Retrospective Biodosimetry on Exposed US Atomic Veterans. *Radiation research,* **191**(4), pp. 311-322.

MÉCHALI, M., 2010. Eukaryotic DNA replication origins: many choices for appropriate answers. *Nature reviews Molecular cell biology,* **11**(10), pp. 728.

MEHTA, A. and HABER, J.E., 2014. Sources of DNA double-strand breaks and models of recombinational DNA repair. *Cold Spring Harbor perspectives in biology,* **6**(9), pp. a016428.

MIRKIN, E.V. and MIRKIN, S.M., 2007. Replication fork stalling at natural impediments. *Microbiol.Mol.Biol.Rev.,* **71**(1), pp. 13-35.

MITELMAN, F., JOHANSSON, B., MERTENS, F., SCHYMAN, T. and MANDAHL, N., 2019. Cancer chromosome breakpoints cluster in gene-rich genomic regions. *Genes, Chromosomes and Cancer,* **58**(3), pp. 149-154.

MIYOSHI, T., KANOH, J., SAITO, M. and ISHIKAWA, F., 2008. Fission yeast Pot1-Tpp1 protects telomeres and regulates telomere length. *Science,* **320**(5881), pp. 1341-1344.

MIZUKOSHI, E. and KANEKO, S., 2019. Telomerase-Targeted Cancer Immunotherapy. *International journal of molecular sciences,* **20**(8), pp. 1823.

MLADENOV, E. and ILIAKIS, G., 2011. Induction and repair of DNA double strand breaks: the increasing spectrum of non-homologous end joining pathways. *Mutation Research/Fundamental and Molecular Mechanisms of Mutagenesis,* **711**(1-2), pp. 61-72.

MOAZED, D., 2009. Small RNAs in transcriptional gene silencing and genome defence. *Nature,* **457**(7228), pp. 413.

MORAES, M.C., NETO, J.B. and MENCK, C.F., 2012. DNA repair mechanisms protect our genome from carcinogenesis. *Front Biosci,* **17**, pp. 1362-1388.

MORENO-MORENO, O., TORRAS-LLORT, M. and AZORÍN, F., 2017. Variations on a nucleosome theme: The structural basis of centromere function. *Bioessays,* **39**(4), pp. 1600241.

MULDER, K.W., WINKLER, G.S. and TIMMERS, H.T.M., 2005. DNA damage and replication stress induced transcription of RNR genes is dependent on the Ccr4–Not complex. *Nucleic acids research,* **33**(19), pp. 6384-6392.

NAMBIAR, M. and RAGHAVAN, S.C., 2011. How does DNA break during chromosomal translocations? *Nucleic acids research,* **39**(14), pp. 5813-5825.

NEGRINI, S., GORGOULIS, V.G. and HALAZONETIS, T.D., 2010. Genomic instability—an evolving hallmark of cancer. *Nature reviews Molecular cell biology,* **11**(3), pp. 220.

NIKOLOV, I. and TADDEI, A., 2016. Linking replication stress with heterochromatin formation. *Chromosoma,* **125**(3), pp. 523-533.

NOVO, C.L. and LONDONO-VALLEJO, J.A., 2013. Telomeres and the nucleus, *Seminars in cancer biology* 2013, Elsevier, pp. 116-124.

NURSE, P., 2002. Cyclin dependent kinases and cell cycle control (nobel lecture). *Chembiochem,* **3**(7), pp. 596-603.

O'CONNOR, C., 2008. Human chromosome translocations and cancer. *Nat Educ,* **1**.

OESTERGAARD, V.H. and LISBY, M., 2017. Transcription-replication conflicts at chromosomal fragile sites—consequences in M phase and beyond. *Chromosoma,* **126**(2), pp. 213-222.

OHLE, C., TESORERO, R., SCHERMANN, G., DOBREV, N., SINNING, I. and FISCHER, T., 2016. Transient RNA-DNA hybrids are required for efficient double-strand break repair. *Cell,* **167**(4), pp. 1001-1013. e7.

OKITA, A.K., ZAFAR, F., SU, J., WEERASEKARA, D., KAJITANI, T., TAKAHASHI, T.S., KIMURA, H., MURAKAMI, Y., MASUKATA, H. and NAKAGAWA, T., 2019. Heterochromatin suppresses gross chromosomal rearrangements at centromeres by repressing Tfs1/TFIIS-dependent transcription. *Communications biology,* **2**(1), pp. 17.

OLSSON, I. and BJERLING, P., 2011. Advancing our understanding of functional genome organisation through studies in the fission yeast. *Current genetics,* **57**(1), pp. 1-12.

ONUFRIEV, A.V. and SCHIESSEL, H., 2019. The nucleosome: from structure to function through physics. *Current opinion in structural biology,* **56**, pp. 119-130.

PANNUNZIO, N.R., WATANABE, G. and LIEBER, M.R., 2018. Nonhomologous DNA end-joining for repair of DNA double-strand breaks. *Journal of Biological Chemistry,* **293**(27), pp. 10512-10523.

PARIZOTTO, E.A., LOWE, E.D. and PARKER, J.S., 2013. Structural basis for duplex RNA recognition and cleavage by Archaeoglobus fulgidus C3PO. *Nature structural & molecular biology,* **20**(3), pp. 380.

PASERO, P. and TOURRIÈRE, H., 2019. Overexpression of the Fork Protection Complex: a strategy to tolerate oncogene-induced replication stress in cancer cells. *Molecular & cellular oncology,* **6**(4), pp. 1607455.

PENG, G. and LIN, S., 2011. Exploiting the homologous recombination DNA repair network for targeted cancer therapy. *World journal of clinical oncology,* **2**(2), pp. 73.

PETROVA, B., DEHLER, S., KRUITWAGEN, T., HÉRICHÉ, J., MIURA, K. and HAERING, C.H., 2013. Quantitative analysis of chromosome condensation in fission yeast. *Molecular and cellular biology,* **33**(5), pp. 984-998.

PIDOUX, A.L. and ALLSHIRE, R.C., 2004. Kinetochore and heterochromatin domains of the fission yeast centromere. *Chromosome Research,* **12**(6), pp. 521-534.

PLOSKY, B.S., 2016. The good and bad of RNA: DNA hybrids in double-strand break repair. *Molecular cell,* **64**(4), pp. 643-644.

PRESTON, B.D., ALBERTSON, T.M. and HERR, A.J., 2010. DNA replication fidelity and cancer, *Seminars in cancer biology* 2010, Elsevier, pp. 281-293.

PRYCE, D.W., RAMAYAH, S., JAENDLING, A. and MCFARLANE, R.J., 2009. Recombination at DNA replication fork barriers is not universal and is differentially regulated by Swi1. *Proceedings of the National Academy of Sciences,* **106**(12), pp. 4770-4775.

PUSHPAVALLI, S.N., Bag, I., Pal-Bhadra, M. & Bhadra, U. 2012. Drosophila Argonaute-1 is critical for transcriptional cosuppression and heterochromatin formation. *Chromosome Research.* 20 (3). pp. 333-351.

RABBITTS, T.H. and STOCKS, M.R., 2003. Chromosomal translocation products engender new intracellular therapeutic technologies. *Nature medicine,* **9**(4), pp. 383.

RASS, E., GRABARZ, A., BERTRAND, P. and LOPEZ, B.S., 2012. Double strand break repair, one mechanism can hide another: alternative non-homologous end joining. *Cancer radiothérapie: journal de la Société française de radiothérapie oncologique,* **16**(1), pp. 1-10.

REINHARDT, H.C. and SCHUMACHER, B., 2012. The p53 network: cellular and systemic DNA damage responses in aging and cancer. *Trends in Genetics,* **28**(3), pp. 128-136.

REN, J., CASTEL, S.E. and MARTIENSSEN, R.A., 2015. Dicer in action at replication-transcription collisions. *Molecular & cellular oncology,* **2**(3), pp. e991224.

REYES-TURCU, F.E. and GREWAL, S.I., 2012. Different means, same end—heterochromatin formation by RNAi and RNAi-independent RNA processing factors in fission yeast. *Current opinion in genetics & development,* **22**(2), pp. 156-163.

ROTHSTEIN, R.J. and BARLOW, J., 2010. Timing is everything: cell cycle control of Rad52.

ROUKOS, V. and MISTELI, T., 2014. The biogenesis of chromosome translocations. *Nature cell biology,* **16**(4), pp. 293.

SABATINOS, S.A., 2010. Replication fork stalling and the fork protection complex. *Nature Education,* **3**(9), pp. 40.

SABATINOS, S.A. and FORSBURG, S.L., 2010. Molecular genetics of Schizosaccharomyces pombe. *Methods in enzymology.* Elsevier, pp. 759-795.

SADEGHI, L., PRASAD, P., EKWALL, K., COHEN, A. and SVENSSON, J.P., 2015. The Paf1 complex factors Leo1 and Paf1 promote local histone turnover to modulate chromatin states in fission yeast. *EMBO reports,* **16**(12), pp. 1673-1687.

SAINI, N., RAMAKRISHNAN, S., ELANGO, R., AYYAR, S., ZHANG, Y., DEEM, A., IRA, G., HABER, J.E., LOBACHEV, K.S. and MALKOVA, A., 2013. Migrating bubble during break-induced replication drives conservative DNA synthesis. *Nature,* **502**(7471), pp. 389.

SAKOFSKY, C.J. and MALKOVA, A., 2017. Break induced replication in eukaryotes: mechanisms, functions, and consequences. *Critical reviews in biochemistry and molecular biology,* **52**(4), pp. 395-413.

SAKOFSKY, C., AYYAR, S. and MALKOVA, A., 2012. Break-induced replication and genome stability. *Biomolecules,* **2**(4), pp. 483-504.

SANTAGUIDA, S. and AMON, A., 2015. Short-and long-term effects of chromosome mis-segregation and aneuploidy. *Nature reviews Molecular cell biology,* **16**(8), pp. 473.

SAREK, G., MARZEC, P., MARGALEF, P. and BOULTON, S.J., 2015. Molecular basis of telomere dysfunction in human genetic diseases. *Nature structural & molecular biology,* **22**(11), pp. 867.

SCHOEFTNER, S. and BLASCO, M.A., 2008. Developmentally regulated transcription of mammalian telomeres by DNA-dependent RNA polymerase II. *Nature cell biology,* **10**(2), pp. 228.

SHANKARANARAYANA, G.D., MOTAMEDI, M.R., MOAZED, D. and GREWAL, S.I., 2003. Sir2 regulates histone H3 lysine 9 methylation and heterochromatin assembly in fission yeast. *Current Biology,* **13**(14), pp. 1240-1246.

SHANMUGANATHAN, R., EDISON, THOMAS NESAKUMAR JEBAKUMAR IMMANUEL, LEWISOSCAR, F., PONNUCHAMY, K., SHANMUGAM, S. and PUGAZHENDHI, A., 2019. Chitosan nanopolymers: an overview of drug delivery against cancer. *International journal of biological macromolecules, .*

SMIRNOVA, J.B. and MCFARLANE, R.J., 2002. The Unique Centromeric Chromatin Structure ofSchizosaccharomyces pombe Is Maintained during Meiosis. *Journal of Biological Chemistry,* **277**(22), pp. 19817-19822.

SMITH, C.E., LLORENTE, B. and SYMINGTON, L.S., 2007. Template switching during break-induced replication. *Nature,* **447**(7140), pp. 102.

SO, A., LE GUEN, T., LOPEZ, B.S. and GUIROUILH-BARBAT, J., 2017. Genomic rearrangements induced by unscheduled DNA double strand breaks in somatic mammalian cells. *The FEBS journal,* **284**(15), pp. 2324-2344.

SON, M.Y. and HASTY, P., 2019. Homologous recombination defects and how they affect replication fork maintenance.

SPARKS, J.L., CHON, H., CERRITELLI, S.M., KUNKEL, T.A., JOHANSSON, E., CROUCH, R.J. and BURGERS, P.M., 2012. RNase H2-initiated ribonucleotide excision repair. *Molecular cell,* **47**(6), pp. 980-986.

STEFANACHI, A., LEONETTI, F., NICOLOTTI, O., CATTO, M., PISANI, L., CELLAMARE, S., ALTOMARE, C. and CAROTTI, A., 2012. New strategies in the chemotherapy of leukemia: eradicating cancer stem cells in chronic myeloid leukemia. *Current cancer drug targets,* **12**(5), pp. 571-596.

STILLMAN, B., 2008. DNA polymerases at the replication fork in eukaryotes. *Molecular cell,* **30**(3), pp. 259-260.

STUCKEY, R., GARCÍA-RODRÍGUEZ, N., AGUILERA, A. and WELLINGER, R.E., 2015. Role for RNA: DNA hybrids in origin-independent replication priming in a eukaryotic system. *Proceedings of the National Academy of Sciences,* **112**(18), pp. 5779-5784.

SUWAKI, N., KLARE, K. and TARSOUNAS, M., 2011. RAD51 paralogs: roles in DNA damage signalling, recombinational repair and tumorigenesis, *Seminars in cell & developmental biology*2011, Elsevier, pp. 898-905.

TABARESTANI, S. and MOVAFAGH, A., 2016. New developments in chronic myeloid leukemia: Implications for therapy. *Iranian journal of cancer prevention,* **9**(1),.

TADEO, X., WANG, J., KALLGREN, S.P., LIU, J., REDDY, B.D., QIAO, F. and JIA, S., 2013. Elimination of shelterin components bypasses RNAi for pericentric heterochromatin assembly. *Genes & development,* **27**(22), pp. 2489-2499.

TALENS, F., JALVING, M., GIETEMA, J.A. and VAN VUGT, M.A., 2017. Therapeutic targeting and patient selection for cancers with homologous recombination defects. *Expert opinion on drug discovery,* **12**(6), pp. 565-581.

THAKUR, J., TALBERT, P.B. and HENIKOFF, S., 2015. Inner kinetochore protein interactions with regional centromeres of fission yeast. *Genetics,* **201**(2), pp. 543-561.

TIAN, H., GAO, Z., LI, H., ZHANG, B., WANG, G., ZHANG, Q., PEI, D. and ZHENG, J., 2015. DNA damage response–a double-edged sword in cancer prevention and cancer therapy. *Cancer letters,* **358**(1), pp. 8-16.

TIAN, Y., SIMANSHU, D.K., ASCANO, M., DIAZ-AVALOS, R., PARK, A.Y., JURANEK, S.A., RICE, W.J., YIN, Q., ROBINSON, C.V. and TUSCHL, T., 2011. Multimeric assembly and biochemical characterization of the Trax–translin endonuclease complex. *Nature structural & molecular biology,* **18**(6), pp. 658.

TIMSINA, R. and QIU, X., 2019. Histone Tail-DNA Interactions: Charge Regulation and Sequence Specificity. *Biophysical journal,* **116**(3), pp. 73a.

TOMASETTI, C., LI, L. and VOGELSTEIN, B., 2017. Stem cell divisions, somatic mutations, cancer etiology, and cancer prevention. *Science,* **355**(6331), pp. 1330-1334.

TRAKSELIS, M.A., SEIDMAN, M.M. and BROSH JR, R.M., 2017. Mechanistic insights into how CMG helicase facilitates replication past DNA roadblocks. *DNA repair,* **55**, pp. 76-82.

TUBBS, A. and NUSSENZWEIG, A., 2017. Endogenous DNA damage as a source of genomic instability in cancer. *Cell,* **168**(4), pp. 644-656.

TUCKER, J.D., 2010. Chromosome translocations and assessing human exposure to adverse environmental agents. *Environmental and molecular mutagenesis,* **51**(8-9), pp. 815-824.

UCKELMANN, M. and SIXMA, T.K., 2017. Histone ubiquitination in the DNA damage response. *DNA repair,* **56**, pp. 92-101.

VAN EMDEN, T.S., FORN, M., FORNÉ, I., SARKADI, Z., CAPELLA, M., CABALLERO, L.M., FISCHER-BURKART, S., BRÖNNER, C., SIMONETTA, M. and TOCZYSKI, D., 2019. Shelterin and subtelomeric DNA sequences control nucleosome maintenance and genome stability. *EMBO reports,* **20**(1),.

VANCEVSKA, A., DOUGLASS, K.M., PFEIFFER, V., MANLEY, S. and LINGNER, J., 2017. The telomeric DNA damage response occurs in the absence of chromatin decompaction. *Genes & development,* **31**(6), pp. 567-577.

VOLPE, T.A., KIDNER, C., HALL, I.M., TENG, G., GREWAL, S.I. and MARTIENSSEN, R.A., 2002. Regulation of heterochromatic silencing and histone H3 lysine-9 methylation by RNAi. *Science,* **297**(5588), pp. 1833-1837.

VOLPE, T., SCHRAMKE, V., HAMILTON, G.L., WHITE, S.A., TENG, G., MARTIENSSEN, R.A. and ALLSHIRE, R.C., 2003. RNA interference is required for normal centromere function infission yeast. *Chromosome Research,* **11**(2), pp. 137-146.

WAHBA, L., GORE, S.K. and KOSHLAND, D., 2013. The homologous recombination machinery modulates the formation of RNA–DNA hybrids and associated chromosome instability. *Elife,* **2**, pp. e00505.

WANG, C., ZHAO, L. and LU, S., 2015. Role of TERRA in the regulation of telomere length. *International journal of biological sciences,* **11**(3), pp. 316.

WANG, J., Boja, E.S., Oubrahim, H. & Chock, P.B. 2004. Testis brain ribonucleic acid-binding protein/translin possesses both single-stranded and double-stranded ribonuclease activities. *Biochemistry.* 43 (42). pp. 13424-13431

WANG, J.Y., CHEN, S.Y., SUN, C.N., CHIEN, T. and CHERN, Y., 2016. A central role of TRAX in the ATM-mediated DNA repair. *Oncogene,* **35**(13), pp. 1657.

WANG, J., COHEN, A.L., LETIAN, A., TADEO, X., MORESCO, J.J., LIU, J., YATES, J.R., QIAO, F. and JIA, S., 2016. The proper connection between shelterin components is required for telomeric heterochromatin assembly. *Genes & development,* **30**(7), pp. 827-839.

Wang, H., Shi, L.Z., Wong, C.C., Han, X., Hwang, P.Y.H., Truong, L.N., Zhu, Q., Shao, Z., Chen, D.J., Berns, M.W. and Yates III, J.R., 2013. The interaction of CtIP and Nbs1 connects CDK and ATM to regulate HR–mediated double-strand break repair. *PLoS genetics*, *9*(2).

WEBERPALS, J.I., KOTI, M. and SQUIRE, J.A., 2011. Targeting genetic and epigenetic alterations in the treatment of serous ovarian cancer. *Cancer genetics,* **204**(10), pp. 525-535.

WESTHORPE, F.G. and STRAIGHT, A.F., 2015. The centromere: epigenetic control of chromosome segregation during mitosis. *Cold Spring Harbor perspectives in biology,* **7**(1), pp. a015818.

WESTHORPE, F.G. and STRAIGHT, A.F., 2013. Functions of the centromere and kinetochore in chromosome segregation. *Current opinion in cell biology,* **25**(3), pp. 334-340.

WILCH, E.S. and MORTON, C.C., 2018. Historical and clinical perspectives on chromosomal translocations. *Chromosome Translocation.* Springer, pp. 1-14.

WILLMAN, C.L. and HROMAS, R.A., 2006. Genomic alterations and chromosomal aberrations in human cancer. *Cancer medicine,* **7**, pp. 104-154.

WOOD, V., GWILLIAM, R., RAJANDREAM, M., LYNE, M., LYNE, R., STEWART, A., SGOUROS, J., PEAT, N., HAYLES, J. and BAKER, S., 2002. The genome sequence of Schizosaccharomyces pombe. *Nature,* **415**(6874), pp. 871.

WRIGHT, W.D., SHAH, S.S. and HEYER, W., 2018. Homologous recombination and the repair of DNA double-strand breaks. *Journal of Biological Chemistry,* **293**(27), pp. 10524-10535.

WU, X., GU, W., MENG, X. and HECHT, N.B., 1997. The RNA-binding protein, TB-RBP, is the mouse homologue of translin, a recombination protein associated with chromosomal translocations. *Proceedings of the National Academy of Sciences,* **94**(11), pp. 5640-5645.

YANG, K., GUO, R. and XU, D., 2016. Non-homologous end joining: advances and frontiers. *Acta biochimica et biophysica Sinica,* **48**(7), pp. 632-640.

YANG, S. and HECHT, N.B., 2004. Translin associated protein X is essential for cellular proliferation. *FEBS letters,* **576**(1-2), pp. 221-225.

YANG, Y. and QI, Y., 2015. RNA-directed repair of DNA double-strand breaks. *DNA repair,* **32**, pp. 82-85.

YAO, Y. and DAI, W., 2014. Genomic instability and cancer. *Journal of carcinogenesis & mutagenesis,* **5**.

YAVUZER, U., SMITH, G.C., BLISS, T., WERNER, D. and JACKSON, S.P., 1998. DNA end-independent activation of DNA-PK mediated via association with the DNA-binding protein C1D. *Genes & development,* **12**(14), pp. 2188-2199.

YE, X., HUANG, N., LIU, Y., PAROO, Z., HUERTA, C., LI, P., CHEN, S., LIU, Q. and ZHANG, H., 2011. Structure of C3PO and mechanism of human RISC activation. *Nature structural & molecular biology,* **18**(6), pp. 650.

YEUNG, D.T. and HUGHES, T.P., 2012. Therapeutic targeting of BCR-ABL: prognostic markers of response and resistance mechanism in chronic myeloid leukaemia. *Critical Reviews™ in Oncogenesis,* **17**(1),.

YOUDS, J.L., METS, D.G., MCILWRAITH, M.J., MARTIN, J.S., WARD, J.D., ONEIL, N.J., ROSE, A.M., WEST, S.C., MEYER, B.J. and BOULTON, S.J., 2010. RTEL-1 enforces meiotic crossover interference and homeostasis. *Science,* **327**(5970), pp. 1254-1258.

Yu, Z., & Hecht, N. B. (2008). The DNA/RNA-binding protein, translin, bindsmicroRNA122a and increases its in vivo stability. *Journal of Andrology*, *29*(5), 572.

ZABOIKIN, M., ZABOIKINA, T., FRETER, C. and SRINIVASAKUMAR, N., 2017. Non-homologous end joining and homology directed DNA repair frequency of double-stranded breaks introduced by genome editing reagents. *PloS one,* **12**(1), pp. e0169931.

ZAMORE, P.D., HUTVAGNER, G., SCHWARZ, D., TANG, G. and HALEY, B., 2017. No title. *Compositions for RNA interference and methods of use thereof,* .

ZHANG, J., LIU, H., YAO, Q., YU, X., CHEN, Y., CUI, R., WU, B., ZHENG, L., ZUO, J. and HUANG, Z., 2016. Structural basis for single-stranded RNA recognition and cleavage by C3PO. *Nucleic acids research,* **44**(19), pp. 9494-9504.

ZHANG, Y., GOSTISSA, M., HILDEBRAND, D.G., BECKER, M.S., BOBOILA, C., CHIARLE, R., LEWIS, S. and ALT, F.W., 2010. The role of mechanistic factors in promoting chromosomal translocations found in lymphoid and other cancers. *Advances in immunology.* Elsevier, pp. 93-133.

ZHAO, H., ZHU, M., LIMBO, O. and RUSSELL, P., 2018. RNase H eliminates R-loops that disrupt DNA replication but is nonessential for efficient DSB repair. *EMBO reports,* **19**(5),.

ZHAO, X., WEI, C., LI, J., XING, P., LI, J., ZHENG, S. and CHEN, X., 2017. Cell cycle-dependent control of homologous recombination. *Acta biochimica et biophysica Sinica,* **49**(8), pp. 655-668.

ZHENG, J., 2013. Oncogenic chromosomal translocations and human cancer. *Oncology reports,* **30**(5), pp. 2011-2019.

ZIMMER, A.D. and KOSHLAND, D., 2016. Differential roles of the RNases H in preventing chromosome instability. *Proceedings of the National Academy of Sciences,* **113**(43), pp. 12220-12225.

ZOCCO, M., MARASOVIC, M., PISACANE, P., BILOKAPIC, S. and HALIC, M., 2016. The Chp1 chromodomain binds the H3K9me tail and the nucleosome core to assemble heterochromatin. *Cell discovery,* **2**, pp. 16004.

9. Appendices

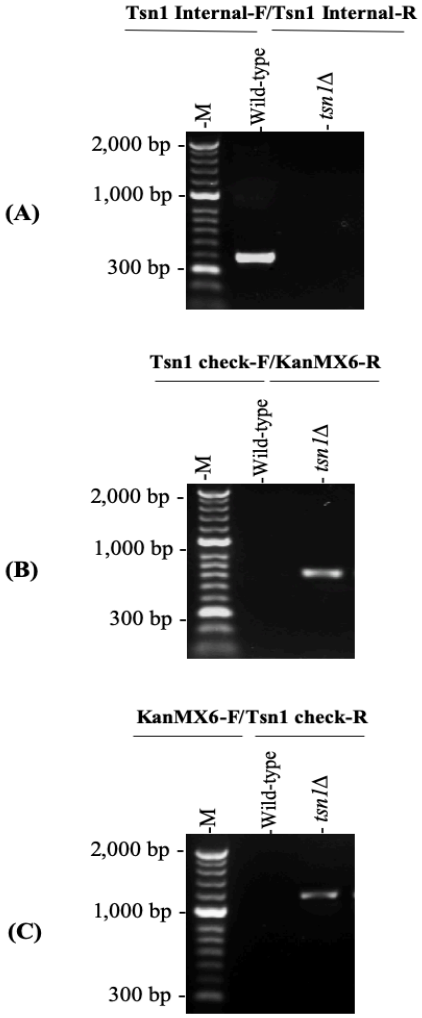

Appendix 1Confirmation by PCR screening of successful *tsn1*Δ single mutant knockout.
(A) Illustration of agarose gel screening of PCR products for the wild-type strain and *tsn1*Δ single mutant. The Tsn1-int-F and Tsn1-int-R primers were used, and the gel screening displays no PCR products in the successful *tsn1*Δ candidate strains. The expected sizes of the PCR product in *tsn1* gene was 475 bp. **(B)** The Tsn1 check-F and KanMX6-R primers were used to generate the PCR products for the wild-type and *tsn1*Δ candidate strains. The PCR products were seen in the *tsn1*Δ strains, but not in the wild-type strain and the expected band sizes is 619 bp. (**C)** The wild-type and *tsn1*Δ candidate strains were utilised to amplify by the KanMX6-F and Tsn1 check-R primers and the expected sizes is 1200 bp.

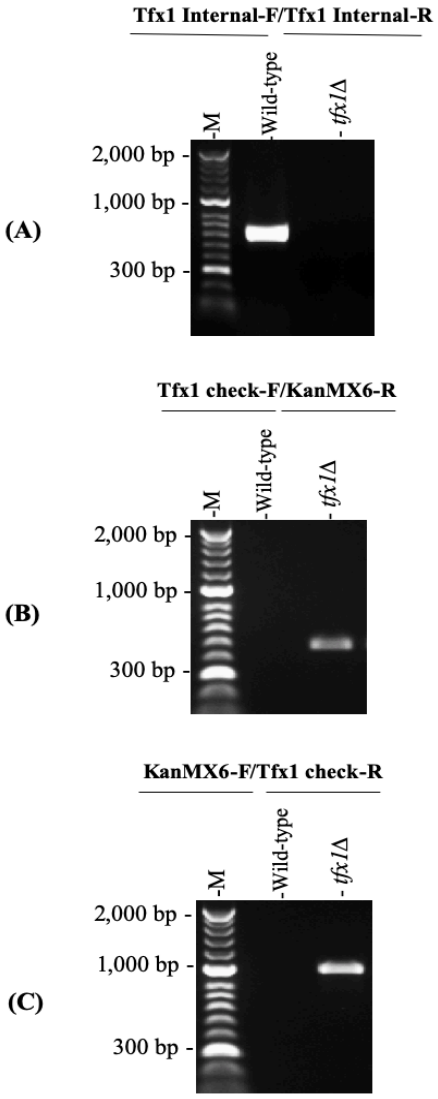

Appendix 2 Confirmation by PCR screening of successful *tfx1*Δ single mutant knockout.
(A) Illustration of agarose gel screening of PCR products for the wild-type strain and *tfx1*Δ single mutant. The Tfx1-int-F and Tfx1-int-R primers were used, and the gel screening displays no PCR products in the successful *tfx1*Δ candidate strains. The expected sizes of the PCR product in *tfx1* gene was 626 bp. **(B)** The Tfx1 check-F and KanMX6-R primers were used to generate the PCR products for the wild-type and *tfx1*Δ candidate strains. The PCR products were seen in the *tfx1*Δ strains, but not in the wild-type strain and the expected band sizes is 461 bp. **(C)** The wild-type and *tfx1*Δ candidate strains were utilised to amplify by the KanMX6-F and Tfx1 check-R primers and the expected sizes is 978 bp.

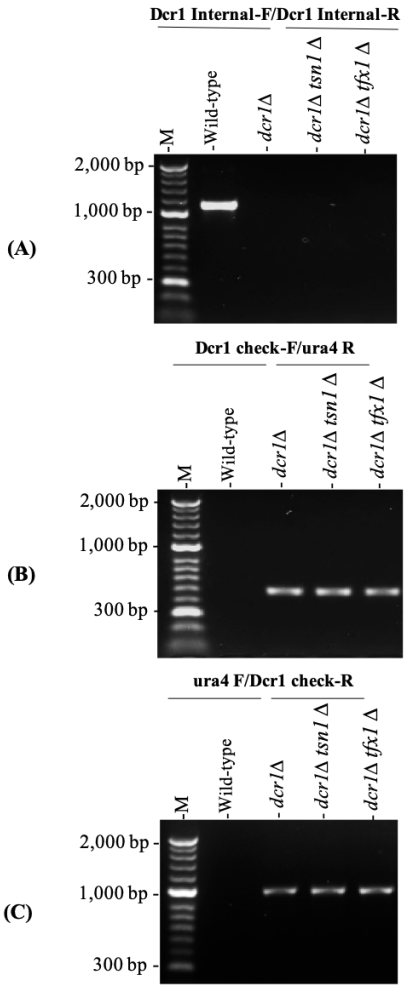

Appendix 3 Confirmation by PCR screening of successful *dcr1Δ* single mutant, *dcr1Δtsn1Δ* and *dcr1Δtfx1Δ* double mutants knockout.

(A) Illustration of agarose gel screening of PCR products for the wild-type strain and *dcr1*Δ single mutant, *dcr1Δtsn1Δ* and *dcr1Δtfx1Δ* double mutant. The Dcr1-int-F and Dcr1-int-R primers were used, and the gel screening displays no PCR products in the successful *dcr1*Δcandidate strains. The expected sizes of the PCR product in *dcr1*Δ gene was 1139 bp. **(B)** The Dcr1 check-F and ura4-R primers were used to generate the PCR products for the wild-type and *dcr1*Δ candidate strains. The PCR products were seen in the *dcr1*Δ strains, but not in the wild-type strain and the expected band size is 487 bp. **(C)** The wild-type and *dcr1*Δ candidate strains were utilised to amplify by the ura4-F and Dcr1 check-R primers and the expected size is 1000 bp.

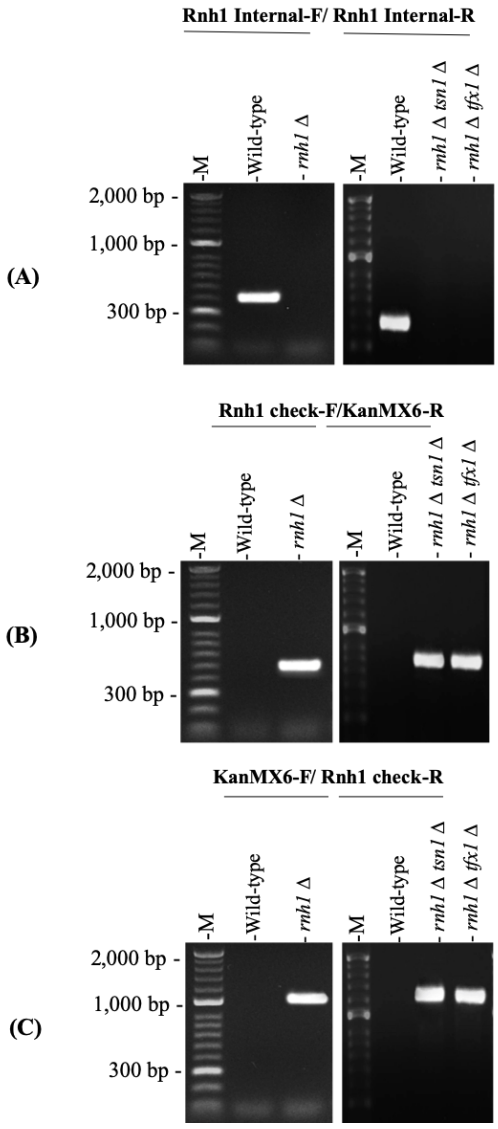

Appendix 4 Confirmation by PCR screening of successful *rnh1Δ* single mutant, *tsn1Δ rnh1Δ* and *tfx1Δ rnh1Δ* double mutants knockout.

(A) Illustration of agarose gel screening of PCR products for the wild-type strain and *rnh1*Δ mutant. The Rnh1-int-F and Rnh1-int-R primers were used, and the gel screening displays no PCR products in the successful *rnh1*Δ candidate strains. The expected sizes of the PCR product in *rnh1*Δ gene was 454 bp. **(B)** The Rnh1 check-F and KanMX6-R primers were used to generate the PCR products for the wild-type and *rnh1*Δ candidate strains. The PCR products were seen in the *rnh1*Δ strains, but not in the wild-type strain and the expected band size is 500 bp. **(C)** The wild-type and *rnh1*Δ candidate strains were utilised to amplify by the KanMX6-F and Rnh1 check-R primers and the expected size is 1100 bp.

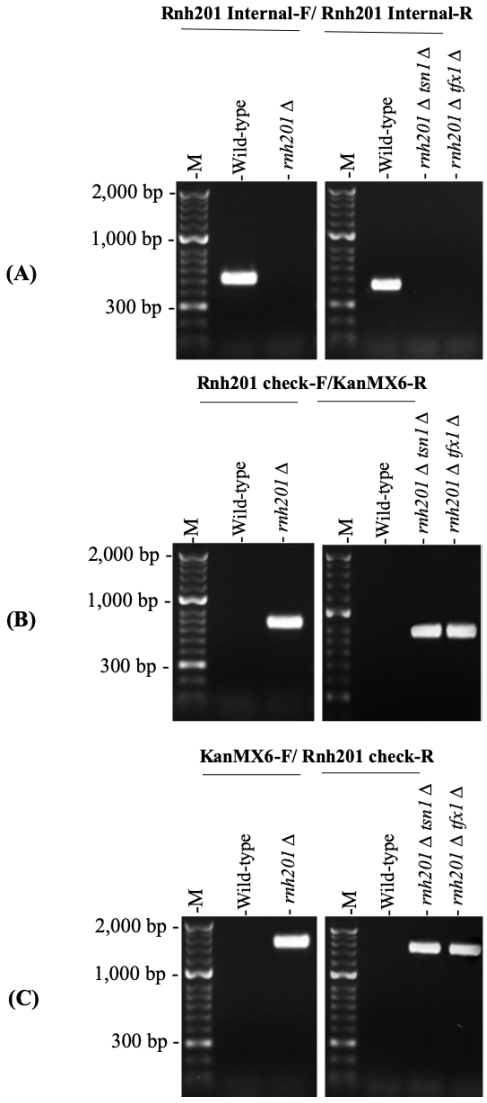

Appendix 5 Confirmation by PCR screening of successful *rnh201Δ* single mutant, *tsn1Δ rnh201Δ* and *tfx1Δ rnh201Δ* double mutants knockout.

(A) Illustration of agarose gel screening of PCR products for the wild-type strain and *rnh201*Δ mutant. The Rnh201-int-F and Rnh201-int-R primers were used, and the gel screening displays no PCR products in the successful *rnh201*Δ candidate strains. The expected sizes of the PCR product in *rnh201*Δ gene was 490 bp. **(B)** The Rnh201 check-F and KanMX6-R primers were used to generate the PCR products for the wild-type and *rnh201*Δ candidate strains. The PCR products were seen in the *rnh201*Δ strains, but not in the wild-type strain and the expected band size is 887 bp. **(C)** The wild-type and *rnh201*Δ candidate strains were utilised to amplify by the KanMX6-F and Rnh201 check-R primers and the expected size is 1600 bp.

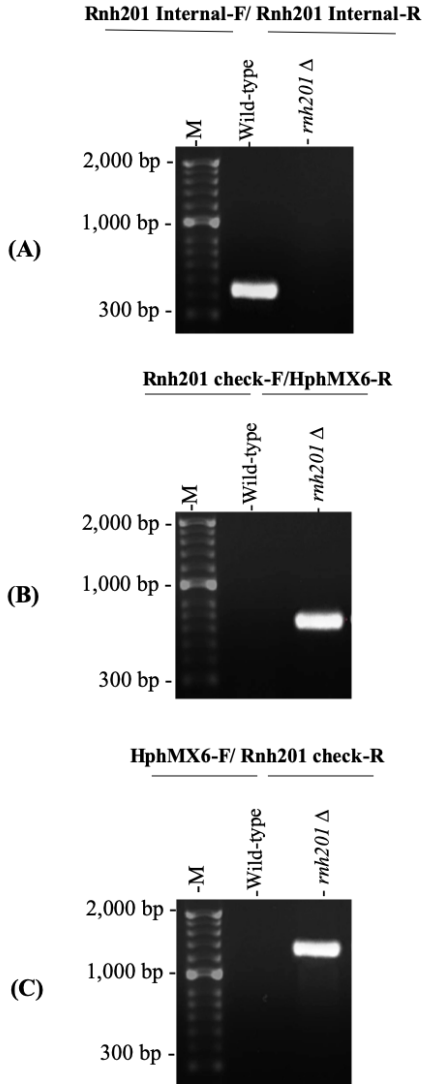

Appendix 6 Confirmation by PCR screening of successful *rnh1Δ rnh201Δ* double mutant knockout.

(A) Illustration of agarose gel screening of PCR products for the wild-type strain and *rnh201*Δ single mutant. The Rnh201-int-F and Rnh201-int-R primers were used, and the gel screening displays no PCR products in the successful *rnh201*Δ candidate strains. The expected sizes of the PCR product in *rnh201*Δ gene was 490 bp. **(B)** The Rnh201 check-F and HphMX6-R primers were used to generate the PCR products for the wild-type and *rnh201*Δ candidate strains. The PCR products were seen in the *rnh201*Δ strains, but not in the wild-type strain and the expected band size is 887 bp. **(C)** The wild-type and *rnh201*Δ candidate strains were utilised to amplify by the HphMX6-F and Rnh201 check-R primers and the expected size is 1600 bp.